



UNIVERSITÀ DEGLI STUDI DI MILANO

PhD COURSE

Integrated Biomedical Research - XXXIII cycle
Department of Biomedical Sciences for Health

PhD THESIS

**GAIN OF TOXIC FUNCTION OF
CHAPERONE ASSISTED SELECTIVE AUTOPHAGY MEMBERS
IN NEUROMUSCULAR DISEASES:
A CHARACTERIZATION OF DISEASE-RELATED MUTANTS**

R23

BARBARA TEDESCO

Matr: R11989

Supervisor: Chiar.mo Prof. ANGELO POLETTI

Co-supervisor: Dr. VALERIA CRIPPA

Coordinator: Chiar.ma Prof. CHIARELLA SFORZA

Academic Year 2019/2020

生き甲斐

[ikigai]

*a reason for being,
the thing that gets you up in the morning.*

Abstract

Proteostasis alteration characterizes several diseases affecting muscle and neuronal cells and can be caused by protein misfolding and aggregation and/or mutations in Protein Quality Control system members. For instance, mutations in the Chaperone Assisted Selective Autophagy (CASA) members are causative of neuropathies/myopathies. The CASA complex mainly acts in muscles and neurons, by facilitating the disposal of misfolding and aggregating proteins. This occurs through substrate recognition by the chaperone HSPB8, which interacts with the HSP70 co-chaperone BAG3. If substrates cannot be refolded by HSP70, they are ubiquitinated by the E3 ubiquitin ligase CHIP. Substrates are then routed and compartmentalized into perinuclear deposits of aggregates, or aggresomes, for subsequent autophagic-lysosomal disposal.

In the first part of my studies, I showed results on neuropathies/myopathies related P209S/L/Q BAG3 mutants. By overexpressing BAG3 mutants in cells, I observed that all BAG3-P209 mutants are characterized by decreased solubility. The decreased solubility determines BAG3-P209 mutants aggregation and relocation with the other CASA members at the aggresome, resulting in an impairment of CASA activity against misfolded clients. In addition, I demonstrated that BAG3-P209 mutants are preferentially degraded through autophagy. Thus, I showed that boosting autophagy using trehalose, proven to favour the clearance of aggregating proteins related to neurodegenerative diseases, determined BAG3-P209 aggregates disposal, representing a valuable therapeutic approach in BAG3-P209 diseases.

In the second part, I firstly showed results on HSPB8 variants S9P, P41S and S181C found in Amyotrophic Lateral Sclerosis (ALS) patients. Using a motoneuron-like cell model overexpressing HSPB8 variants, I observed no differences in HSPB8 variants biochemical behaviour with respect to HSPB8 wildtype (WT), except for the S181C variant, characterized by a structural alteration. However, no differences in HSPB8 variants activity were observed. Instead, I obtained promising results on myopathies/neuropathies-related frameshift mutants pPro173Serfs*43, pGln170Glyfs*45, and pThr194Serfs*23. I found that these mutants present the same C-terminal modification and/or an identical elongated C-terminal tail, predicted to affect protein solubility. Indeed, I observed insolubility and aggregation of these mutants, when overexpressed in cells. Similar to BAG3-P209 mutants, HSPB8 mutants co-segregate with CASA members and associate to an increase in ubiquitinated proteins, suggesting CASA impairment. Again, trehalose-mediated autophagic enhancement favoured the clearance of these aggregating HSPB8 mutants.

In the third part, I characterized isogenic iPSCs-derived motoneurons as new cell models to study TDP-43-related proteinopathies. These cell lines were previously gene-edited, to express WT or the ALS-A315T mutated TDP-43, tagged with the DENDRA2 reporter. Using a small molecules-based protocol, I differentiated these iPSCs obtaining a mixed population of neurons and motoneurons. Model validation showed that under untreated conditions all WT and A315T-mutated cell lines are not characterized by TDP-43 misbehaviour, since no hallmark of pathogenic TDP-43 was observed; instead, upon proteasome inhibition, all cell lines showed TDP-43 cleavage, phosphorylation, and aggregation, correlating with activated cleaved caspase-3, in line with the current literature.

With my work, I determined shared biochemical and functional alterations between BAG3 and HSPB8 mutants, suggesting that a common therapeutic strategy might be beneficial in the related neuromuscular diseases. In addition, I defined TDP-43-DENDRA2-derived motoneurons as a valuable tool to study TDP-43-related proteinopathies.

Table of Contents

List of Figures	vii
List of Abbreviations.....	ix
1. Introduction	1
1.1 The Protein Quality Control system in proteostasis maintenance	1
1.1.1 The Protein Quality Control system	2
1.2 The co-chaperone BAG3 and the BAG family.....	9
1.2.1 Insights into BAG3 mutations and related diseases.....	12
1.2.2 A brief description of the other members of the BAG family	13
1.3 The small Heat Shock protein HSPB8 and the other HSPBs	16
1.3.1 Insights into HSPB8 mutations and related diseases	19
1.3.2 A brief description of the other HSPBs.....	22
1.4 HSPB8-BAG3 functions	31
1.4.1 Chaperone-Assisted Selective Autophagy (CASA).....	31
1.4.2 The other members of CASA complex	32
1.4.3 CASA complex dynamics	34
1.4.4 Granulostasis.....	37
1.4.5 Cell division	38
1.5 A focused overview on diseases that affect motoneurons and muscle cells.....	40
1.5.1 When motoneurons are affected by disease.....	40
1.5.2 Neuropathies with sensory involvement	49
1.5.3 When muscle cells are affected by disease.....	49
2. Characterization and role of BAG3 mutants in neuromuscular diseases	52
2.1 BACKGROUND AND AIMS	53
2.2 Materials and Methods.....	55
2.3 RESULTS.....	61
2.3.1 P209 substitutions in the IPV domain cause BAG3 aggregation and decreased solubility	61
2.3.2 Aggregation propensity of BAG3 P209 mutants is confirmed in motoneuronal and muscle cells models	65

2.3.3 In silico analysis of BAG3 mutants by CamSol method reveals a decreased intrinsic solubility profile of P209 mutants	67
2.3.4 BAG3 aggregates are in the cytoplasm and adhere to the nuclear envelope	69
2.3.5 Nuclear envelope-associated aggregates are aggresomes	71
2.3.6 Interaction and colocalization of BAG3 mutants with CASA-complex members.....	73
2.3.7 BAG3 P209 mutants cause the failure of CASA activity	75
2.3.8 The degradation of the BAG3 mutants occurs mainly through autophagy	77
2.3.9 The autophagic stimulator trehalose favours the clearance of BAG3 P209L mutant aggregates	79
2.4 Discussion	81
3. Characterization and role of HSPB8 variants and mutants in neuromuscular diseases	84
3.1 BACKGROUND AND AIMS	85
3.2 Materials and Methods	87
3.3 Results	91
3.3.1 ALS-related variants in HSPB8 do not affect protein levels, solubility and localization .	91
3.3.2 Analysis of the biochemical behaviour of ALS-related variants of HSPB8	94
3.3.3 Focus on frameshift mutants of HSPB8: sequences analyses reveal a common elongated C-terminal tail with decreased solubility profile	97
3.3.4 Frameshift mutants of HSPB8 form insoluble species and cytoplasmic aggregates	99
3.3.5 Frameshift mutants of HSPB8 co-segregate with wildtype HSPB8, BAG3 and SQSTM1/P62 along with ubiquitinated proteins.....	101
3.3.6 BAG3 co-aggregation with the frameshift mutants is mediated through its IPV motifs	103
3.3.7 HSPB8 frameshift mutant aggregation is only partially diminished upon BAG3 depletion	105
3.3.8 Trehalose as a therapeutic strategy to remove HSPB8 frameshift mutant aggregates	107
3.4 Discussion	109
4. Differentiation of induced Pluripotent Stem Cells to Motoneurons to generate a model to study TDP-43 pathology	113
4.1 BACKGROUND	114
4.1.1 TAR DNA binding protein - 43	114

4.2 AIM	116
4.3 Materials and methods	117
4.4 Results	120
4.4.1 iPSCs differentiation to MNPs	120
4.4.2 Differentiated TDP-43 DENDRA2 cell lines are positive for neuronal markers.....	123
4.4.3 TDP-43 DENDRA2 MNs characterization.....	125
4.5 Discussion	130
5. Conclusions.....	132
References.....	135

List of Figures

Figure 1. 1 Proteins from synthesis to misfolding and aggregation.....	2
Figure 1. 2 Chaperones classified based on the molecular weight.....	3
Figure 1. 3 The UPS relies on substrate ubiquitination and proteasomal degradation.....	5
Figure 1. 4 Autophagy divides in three main branches.....	7
Figure 1. 5 The PQC system is a network of factors and pathways that assure proteostasis.....	8
Figure 1. 6 Role of the BAG domain as NEF of HSP70/HSPA.....	9
Figure 1. 7 The human BAG family (BAG1-6).	10
Figure 1. 8 Schematic representation of BAG3 domains and interacting partners.	12
Figure 1. 9 BAG1/BAG3 switch.	15
Figure 1. 10 Schematic structure and oligomerization of HSPBs.	18
.....	28
Figure 1. 11 List of HSPBs and schematic representation of oligomerization.	28
Figure 1. 12 Alignment of the hHSPBs.....	29
Figure 1. 13 Alternative alignment of HSPBs sequences.	30
Figure 1. 14 HSPB8 and BAG3 functions in CASA.	36
Figure 1. 15 Role of HSPB8-BAG3 and HSP70 in SGs.....	38
Figure 1. 16 Schematic representation of UMNs and LMNs localization and projection and list of typical UMNs and LMNs signs.	41
Figure 1. 17 Examples of genetic overlap in diseases that affect UMNs, LMNs or both (MIXED)...	48
Figure 1. 18 Examples of genetic overlap among MNDs and myopathies.....	51
Figure 2. 1 P209 substitutions in the IPV domain cause BAG3 aggregation and decreased solubility.	63
.....	63
Figure 2. 2 Evaluation of mutation-phenotype relationship using models of neuronal and muscle cells.....	66
Figure 2. 3 In silico analysis of BAG3 mutants by CamSol method reveals a decreased intrinsic solubility profile of P209 mutants.	68
Figure 2. 4 BAG3 aggregates are in the cytoplasm and adhere to the nuclear envelope.....	70
Figure 2. 5 Nuclear envelope-associated aggregates are aggresomes.	72
Figure 2. 6 Interaction and colocalization of BAG3 mutants with CASA-complex members.....	74
Figure 2. 7 BAG3 P209 mutants cause the failure of CASA activity.	76
Figure 2. 8 BAG3 P209 mutant degradation occurs mainly through autophagy.	78
Figure 2. 9 The autophagic stimulator trehalose favours the clearance of BAG3 P209L mutant aggregates.	80

Figure 3. 1 ALS-related variants in HSPB8 do not affect protein levels, solubility, and localization.	93
Figure 3. 2 Analysis of the biochemical behaviour of ALS-related variants of HSPB8.	96
Figure 3. 3 Focus on frameshift mutants of HSPB8: sequences analyses reveal a common elongated C-terminal tail with decreased solubility profile.	98
Figure 3. 4 Frameshift mutants of HSPB8 form insoluble species and cytoplasmic aggregates....	100
Figure 3. 5 Frameshift mutants of HSPB8 co-segregates with wildtype HSPB8, BAG3 and SQSTM1/P62 along with ubiquitinated proteins.	102
Figure 3. 6 BAG3 co-aggregation with the frameshift mutants is mediated through its IPV motifs.	104
Figure 3. 7 HSPB8 frameshift mutant aggregation is only partially diminished upon BAG3 depletion.	106
Figure 3. 8 Trehalose as a therapeutic strategy to remove HSPB8 frameshift mutants aggregates.	108
Figure 4. 1 Differentiation of iPSCs to MNs.....	121
Figure 4. 2 MNPs derived from W80 and A5 iPSC lines.	122
Figure 4. 3 Differentiated TDP-43 DENDRA2 cell lines are positive for neuronal markers.....	124
Figure 4. 4 TDP-43 fragmentation and solubility upon proteasome and/or autophagic inhibition.	127
Figure 4. 5 Proteasome and/or autophagic inhibition effect on TDP-43 localization.....	128
Figure 4. 6 Proteasome but not autophagic inhibition correlates to CC3 activation.....	129

List of Abbreviations

ACD	Alpha-Crystallin Domain
AD	Alzheimer Disease
ALS	Amyotrophic Lateral Sclerosis
Asp	Aspartic Acid
AVM	Autophagic Vacuolar Myopathies
BAGs	Bcl-2 Associated Athanogenes
BICD2	Bicaudal D homologue 2
BSCL2	Berardinelli-Seip Congenital Lipodystrophy type 2
CASA	Chaperone-Assisted Selective Autophagy
CHIP	Carboxy-terminus of HSC70 Interacting Protein
CMA	Chaperone-Mediated Autophagy
CMT	Charcot-Marie-Tooth disease
CTD	C-Terminal Domain
CTFs	C-Terminal Fragments
DCM	Dilated Cardiomyopathy
DCTN1	p150 subunit of dynactin 1
Des	Desmin
dHMNs	distal Hereditary Motor Neuropathies
DPRs	Dipeptide Repeats
DRiPs	Defective Ribosomal Products
DUBs	Deubiquitinating enzymes
DYNC1H1	Dynein Cytoplasmic 1 Heavy Chain 1
EHNA	Erythro-9-(2-hydroxy-3-nonyl)adenine)
ER	Endoplasmic Reticulum
ERAD	Endoplasmic Reticulum-Associated Degradation
FAK	Focal Adhesion Kinase
FHL1	Four-and-a-half LIM domain protein 1
FLoIT	Flow cytometric analysis of Inclusions and Trafficking
FRA	Filter Retardation Assay
FTD	Frontotemporal Dementia
FUS	Fused In Sarcoma
GARS	Glycyl-tRNA synthetase
HD	Huntington Disease
HECT	Homologous to the E6-AP Carboxyl Terminus

HMW	High Molecular Weight
HREs	Heat Shock Response Elements
HSF1	Heat Shock Factor 1
HSC70	Heat Shock Cognate 70
HSP70/HSPAs	Heat Shock Proteins 70
HSPs	Heat Shock Proteins
IBM	Inclusion Body Myositis
IPV	Isoleucine-Proline-Valine
IRES	Internal Ribosome Entry Site
JDPs	J-domain proteins
KD	Knock-Down
KI	Knock-In
KO	Knock-out
KIF5A	Kinesin Heavy Chain isoform 5A
LAMP2A	Lysosomal-Associated Membrane Protein 2A
LIR	LC3-interacting region
LLPS	Liquid-Liquid Phase Separation
LMNA	Lamin A/C
LMNs	Lower Motoneurons
Lys	Lysine
MAP1LC3B/LC3	Microtubule-Associated Proteins 1A/1B Light Chain 3B
MFM	Myofibrillary myopathy
MNDs	Motoneuron Diseases
MNs	Motoneurons
MSP	Multiple System Proteinopathy
MTOC	Microtubule Organizing Center
MYOT	Myotilin
NBD	Nucleotide Binding Domain
NDs	Neurodegenerative Diseases
NEF	Nucleotide Exchange Factor
NES	Nuclear Export Signal
NF- κ B	Nuclear Factor-kappa-light-chain-enhancer of activated B cells
NLS	Nuclear Localization Signal
Nrf2	Nuclear factor erythroid 2–related factor 2
NTD	N-Terminal Domain
OPTN	Optineurin

PD	Parkinson Disease
PE	Phosphatidylethanolamine
PKC δ	Protein kinase C delta
PLC γ	Phospholipase C gamma
PolyQ-AR	Polyglutamine-Androgen Receptor
PolyQ-Htt	Polyglutamine-Huntingtin
polyUb	PolyUbiquitin
PQC	Protein Quality Control
PTMs	Post Translational Modifications
PxxP	Proline-rich region
RAN	Repeat-associated non-ATG translation
RBPs	RNA binding proteins
RING	Really Interesting New Gene
RRG	Arginine-Glycine-Glycine
RRM	RNA binding motif
SBD	Substrate Binding Domain
SBMA	Spinal Bulbar Muscular Atrophy
SCA	Spinocerebellar Ataxia
Ser	Serine
SETX	Senataxin
SGs	Stress granules
sHSPs/HSPBs	Small Heat Shock Proteins
SMA	Spinal Muscular Atrophy
SMN	Survival Motor Neuron
snRNPs	Small nuclear ribonucleoproteins
SOD1	Superoxide Dismutase 1
SPAST	Spastin
SQSTM1/P62	Sequestosome-1/P62
SYNPO2	Synaptopodin-2
TDP-43	TAR DNA Binding Protein-43
TFEB	Transcription Factor EB
Thr	Threonine
TNF	Tumor Necrosis Factor
TPRs	Tetratricopeptide Repeats
TRPV4	Transient Receptor Vallanoid 4
TSC1	Tuberous Sclerosis 1

UBA domain	Ubiquitin-Associated domain
UBL	Ubiquitin-like domain
UBQLN2	Ubiquilin-2
UMNs	Upper Motoneurons
UPR	Unfolded Protein Response
UPS	Ubiquitin Proteasome System
VAPB	Vesicle-Associated Membrane Protein
VCP	Valosin-Containing Protein
VPS	Vacuolar Protein Sorting
WW	Tryptophan-Tryptophan domain

Chapter I

1. Introduction

1.1 The Protein Quality Control system in proteostasis maintenance

Proteostasis, or protein homeostasis, is the maintenance of an intact and functional proteome. To assure proteostasis, cells possess a wide variety of molecular mechanisms and players which, altogether, constitute the Protein Quality Control (PQC) system. The PQC system acts at all levels of proteins lifetime, from synthesis to degradation, assuring the correct folding or disposal. Although neosynthesized proteins reach their native conformation based on the amino acids sequence, the folding process of a given protein is helped and supervised by specific members of the PQC system, such as chaperones (Balchin et al., 2016). Moreover, stochastic errors occurring during mRNA transcription, maturation, or translation, which may lead to the synthesis of misfolded or aberrant products, are not uncommon and require a fast action of the PQC for the disposal of these products. Indeed, it has been estimated that approximately 30% of newly synthesized proteins are defective ribosomal products (DRiPs) and about 20% of newly synthesized proteins are immediately degraded through the intracellular degradative systems (Schubert et al., 2000; Wickner et al., 1999). Even when a newly synthesized protein reaches its native and functional conformation, it might undergo several stress conditions, such as oxidative, mechanical, or thermal stresses, capable to induce protein damage and misfolding. Also, mutations or the presence of intrinsically disordered domain in proteins often enhance their misfolding propensity. In any case, unfolded or misfolded proteins must be recognized by members of the PQC system for refolding or degradation to prevent undesired proteins interactions. Indeed, misfolded proteins tend to expose hydrophobic amino acids sequences that are usually buried in their native structures, and these aberrantly generated regions interact forming oligomers and/or inclusions (**Fig. 1.1**). If not removed from cells, these oligomers and inclusions may become toxic and/or interfere with essential cellular pathways; this may occur either by physical aberrant interaction with cell structures or by sequestering key factors involved in cell responses and in the proteostasis network. Presently, the role of cell inclusions and aggregates is still largely debated. The current opinion, supported by several experimental evidences, suggests that the toxic activity is carried out by the small insoluble oligomers of misfolded proteins; these oligomers may be freely distributed in the cell environment exposing a higher interaction surface which

increases the possibilities of aberrant interactions (Chiti & Dobson, 2017). Instead, big inclusions or aggregates are the result of an active and controlled misfolded proteins/oligomers transport into spatially defined deposits inside the nucleus (e.g., nuclear aggresomes) or in specific regions of the cytoplasm (cytoplasmic juxtannuclear aggresomes); these structures are regulated by PQC members (Kopito, 2000; Latonen, 2019). In this scenario, the compartmentalization of misfolded species into aggregates could be considered as a protective response of the cell, which limits potentially toxic interactions and promotes their subsequent disaggregation and degradation. Proteotoxicity appearing as a consequence of mutations of members of the PQC system or to accumulation of mutated or even wildtype proteins that are prone to misfold, is at the basis of several diseases, including neurodegenerative disease (NDs), emphasizing the importance of proteostasis maintenance in cells (Klaips et al., 2018).

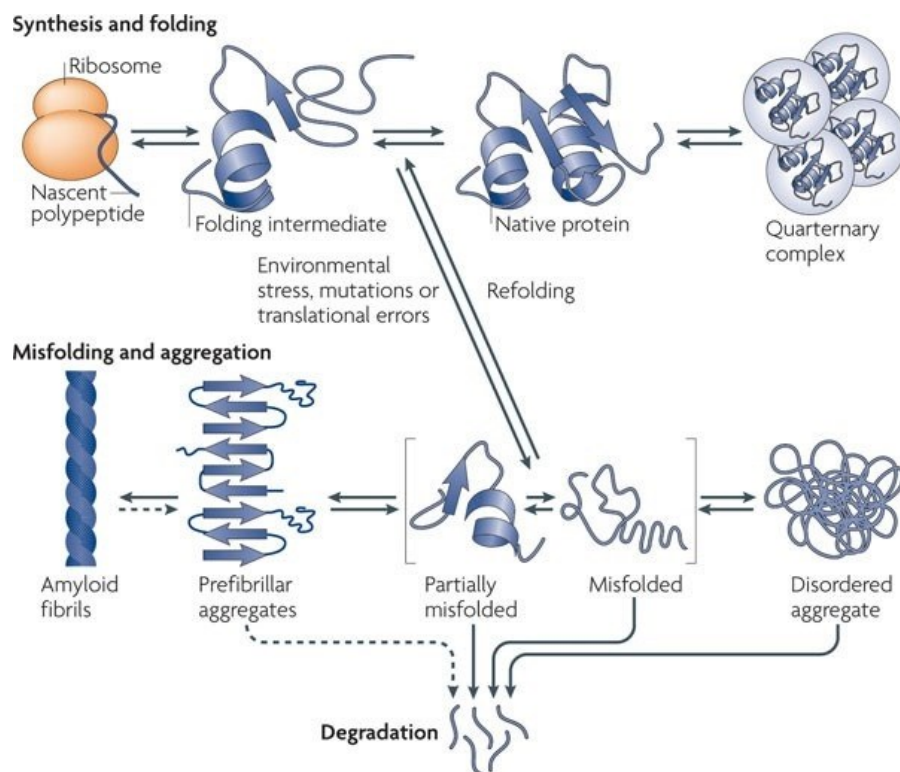


Figure 1. 1 Proteins from synthesis to misfolding and aggregation. When synthesized, proteins reach their native structure in a process called “folding”. Stressors, mutations or stochastic errors during translation and post-translational events can result in protein misfolding. The PQC system acts by promoting substrate refolding or degradation. Accumulation of misfolded substrates results in their aggregation. (From Tyedmers, J et al., 2010).

1.1.1 The Protein Quality Control system

As previously mentioned, the PQC system consists in all pathways and members that act in the maintenance of cell proteostasis. It has been estimated that the PQC system is made up of approximately 2000 factors. PQC members can be divided into three main classes:

the chaperones and the two main degradative systems, which are the autophagic process and the ubiquitin-proteasome system (UPS).

Chaperones are defined as factors that act in the folding, assembly or conformational maintenance of another protein, without being a part of its final structure and are usually assisted by factors named co-chaperones (Hartl, 1996). Thus, chaperones and co-chaperones represent a network of proteins that serve to reach and maintain the correct conformation of a given substrate; when the substrate cannot achieve its native conformation, chaperones favour its routing to the degradative systems. Some chaperones are also known as Heat Shock Proteins (HSPs), as several members were initially identified upregulated in response to heat shock. Indeed, even if several chaperones are constitutively expressed, many others are induced upon stress conditions to counteract a likely increase of misfolded and damaged proteins.

Chaperones were initially classified according to the molecular weight: HSP40s, HSP60s, HSP70s, HSP90s, HSP100s and small HSPs (sHSPs) (Hartl et al., 2011) (**Fig. 1.2**). Recently, a new nomenclature has been proposed in response to ambiguities in denominating human HSPs. For instance, HSPA, HSPB, HSPC, HSPH, DNAJ, HSPD/E families correspond to HSP70s, sHSPs, HSP90s, HSP100s, HSP40s and HSP60s/HSP10s, respectively (Kampinga et al., 2009). HSPA, the Bcl-2 Associated Athanogenes (BAGs) co-chaperones and the HSPBs will be deeply described in the following sections.

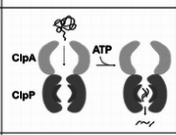
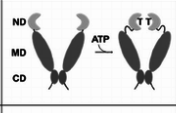
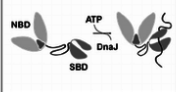
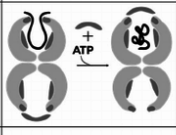
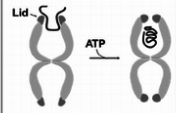
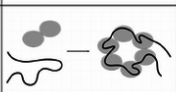
Chaperone Family	Topology of Binding	Co-chaperone	Known Function
Hsp100		CipP, SspB, Hsp70, Hsp40	<ul style="list-style-type: none"> • Works with DnaK in ATP-dependent disaggregation and proteolysis • Prevents aggregation, degradation and turnover of unassembled mitochondrial proteins • Reactivates heat-damaged proteins • Establishes and maintains prion phenotype in yeast
Hsp90		Hop, Hip, Hsp70, Immunophilins, Grp78	<ul style="list-style-type: none"> • Refolds proteins in stressed cells. Probable secretory chaperone in prokaryotes • Major cytosolic chaperone in eukaryotes. • Cytoprotection and intracellular signaling • In ER, controls protein homeostasis, folding and assembly of secretory proteins
Hsp70		Hsp40, GrpE	<ul style="list-style-type: none"> • Ubiquitous Principal folding chaperone • Works with CipB as disaggregase • Folding of newly synthesized proteins • Protein transport into ER and mitochondria
Hsp60 (Group I)		Hsp10	<ul style="list-style-type: none"> • Major chaperone for protein folding in prokaryotes • Stabilizes proteins during heat stress • Promotes folding of over-produced proteins • Major chaperone in mitochondria and chloroplast
Hsp60 (Group II)		Prefoldin/GimC	<ul style="list-style-type: none"> • Promotes folding of a cytosolic proteins in eukaryotes • Refolding of unfolded polypeptides in vitro
sHsps		-	<ul style="list-style-type: none"> • Stabilizes unfolded polypeptides • Prevents aggregation • Works with Hsp70 in protein refolding • Structural protein of eye lens

Figure 1. 2 Chaperones classified based on the molecular weight. Schematic representation of HSPs structure, co-chaperones and functions. (From C. M. Kumar, Mande, & Mahajan, 2015).

When proteins fail to fold or refold, they are targeted to degradation, which can be operated by the UPS or the autophagic pathway. The **UPS (Fig. 1.3)** represents the degradative pathway for short-lived, misfolded and damaged proteins. The UPS also acts in the regulation of other cellular pathways, such as cell cycle progression, cell proliferation or apoptosis (Ciechanover, 1994). The UPS begins with ubiquitination, which consists in the targeting of a substrate with a chain of polyubiquitin (polyUb). Ubiquitin is a conserved protein of 76 amino acids which is covalently bound to amino groups in lysine (Lys) residues of the substrate, and it can be ubiquitinated itself forming the polyUb chains. PolyUb chains are added to the substrate through the action of three class of enzymes: E1 enzymes, which are encoded by two genes, are also known as ubiquitin-activating enzymes; E2 enzymes, encoded by approximately 40 genes, are also known as ubiquitin-carrier or ubiquitin-conjugating enzymes; E3 enzymes, encoded by approximately 800 genes, are called ubiquitin-ligases. The process of ubiquitination (**Fig. 1.3**) requires the ATP-dependent activation of ubiquitin at the glycine residue at position 76. Then, the activated ubiquitin is transferred and conjugated to an E2 enzyme. Through the formation of a complex consisting of the E2 enzyme carrying the ubiquitin moiety and E3 enzyme interacting with the substrate, the ubiquitin is conjugated to the target. The ubiquitin moiety is directly conjugated to a Lys residue of the substrate if the E3 enzyme belongs to the Really Interesting New Gene (RING)-finger class, while it is firstly conjugated to a cysteine residue of the E3 enzyme when this belongs to the Homologous to the E6-AP Carboxyl Terminus (HECT)-domain class, and then transferred to the substrate. By adding other ubiquitin moieties to the substrate-conjugated ubiquitin, a polyUb chain is formed and this is performed through the intervention of E4 enzymes, also known as ubiquitin-chain elongation factors. PolyUb chains represent a signal for both proteasomal and autophagic degradation.

The proteasome 26S is a multicatalytic ATP-dependent protease made up of two complexes: i) the 20S proteasome, which is the barrel-shaped core particle, and ii) the 19S proteasome, a regulatory particle attached to one or both end of the core particle. The regulatory particle consists of a base and a lid, which permit the recognition of ubiquitinated substrates and their insertion into the core particle. In particular, the regulatory particle is made up by several subunits which serve as ubiquitin receptors, ATPases for substrates unfolding and translocation inside the 20S core particle, and deubiquitinating enzymes for ubiquitin recycle. Instead, the core particle is made up of two external α -rings and two internal β -rings. The two internal β -rings consist of β -subunits: β 1, β 2 and β 5 subunits possess caspase-like, trypsin-like and chymotrypsin-like activities, respectively, and are responsible for substrate proteolysis (Budenholzer et al., 2017). Proteasomes localize in

both the nucleus and the cytoplasm. Moreover, their composition, abundance and specialized functions are dynamic and regulated by transcriptional activity, post-translational modifications (PTMs) and their degradation (proteaphagy).

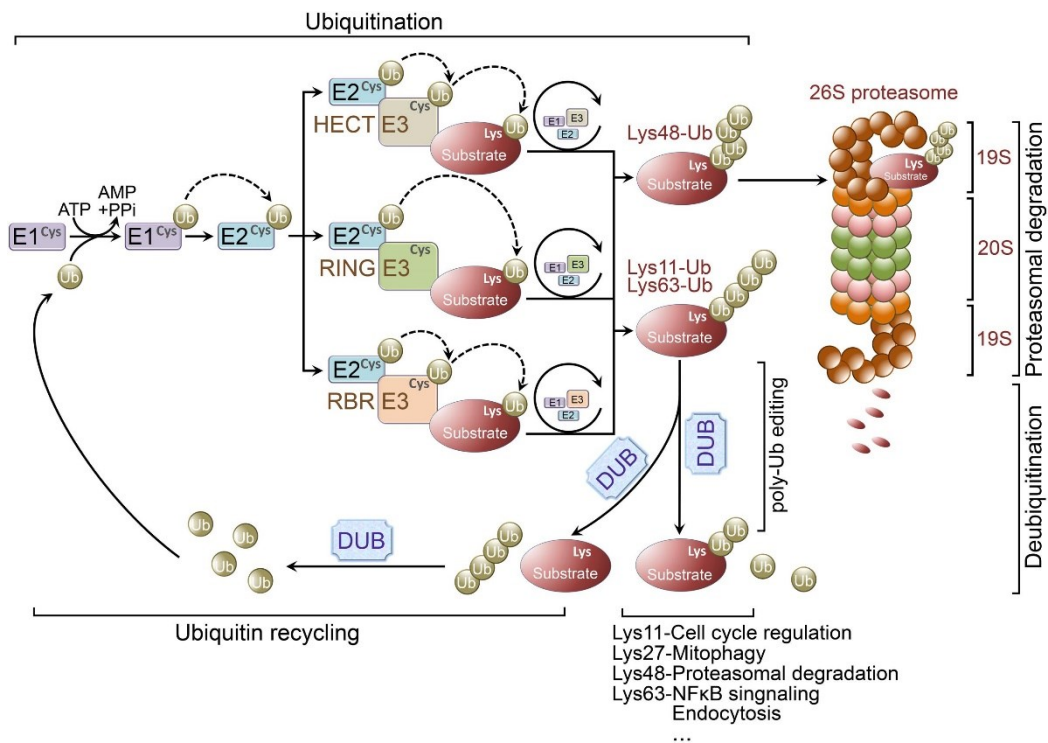


Figure 1.3 The UPS relies on substrate ubiquitination and proteasomal degradation.

Ubiquitination is a multi-step process, which starts with the conjugation of ubiquitin to the ubiquitin-activating E1 enzyme. Then, the activated ubiquitin is transferred to the ubiquitin-conjugating E2 enzyme, which, by interacting with the ubiquitin-ligase E3 enzyme, transfers ubiquitin to the substrate. An iterative process of ubiquitination determines the formation of a polyubiquitin chain. Polyubiquitinated substrates are then recognized and degraded by the 26S proteasome, made up by one or two regulatory particles (19S proteasome) and a barrel-shaped core particle (20S proteasome). Deubiquitinating enzymes (DUBs) remove ubiquitin moieties from substrates, which can be recycled. (From Zheng et al., 2016).

The other main degradative system in cells is **autophagy** (from the Greek, “self-eating”) (**Fig. 1.4**), which has been often counterposed to the UPS as a route for aspecific degradation of long-lived proteins, large multimeric assemblies, aggregates and organelles. Autophagy is a cytoplasmic route for substrates degradation and divides in three main branches: macroautophagy, microautophagy and chaperone-mediated autophagy (CMA), which all end in the lysosomal degradation of substrates. **Macroautophagy** (referred as autophagy herein) begins with the engulfment of cytoplasmic material by the phagophore, a double-membrane structure which rounds up and closes, forming the autophagosome (Lamb et al., 2013). Then, by fusion between the autophagosome and the lysosome, the content is degraded by lysosomal hydrolases. **Microautophagy**, instead, consists in the engulfment of cytoplasmic content by direct invagination of the lysosomal membrane and subsequent degradation (W. W. Li et al., 2012). Finally, **CMA** is a route for degradation of proteins carrying KFERQ or KFERQ-like motifs. These short sequences are recognized by

the Heat Shock Cognate 70 (HSC70, or HSPA8), which routes the substrate to the lysosome. Lysosomal degradation of the substrate needs the binding of HSC70 to the lysosomal-associated membrane protein 2A (LAMP2A) which oligomerizes to form a channel for substrate translocation in the lumen of the lysosome (Kaushik & Cuervo, 2012). As anticipated, autophagy has been considered an aspecific nonselective process for cell components recycle in response to starvation and stresses. However, it is now clear that several forms of selective autophagy exist. For instance, names as Endoplasmic Reticulum (ER)-phagy, mitophagy, aggrephagy, lysophagy and xenophagy have been coined to describe specialized types of autophagy-mediated selective degradation of intracellular structures or microbes (Anding & Baehrecke, 2017). Selective autophagy requires the presence of specialized autophagic receptors which bridge the cargo to proteins located in the autophagosomal membrane, such as the phosphatidylethanolamine (PE)-lipidated microtubule-associated proteins 1A/1B light chain 3B (MAP1LC3B), or simply LC3. An example of autophagic receptor is sequestosome-1/p62 (SQSTM1/P62), which acts as an adaptor protein by interacting with ubiquitinated targets through its ubiquitin-associated UBA domain and with autophagosome membrane-inserted protein LC3 through its LC3-interacting region (LIR). Thus, SQSTM1/P62 promotes the autophagic clearance of selected ubiquitin-tagged substrates (Lamark et al., 2017). An example of selective autophagy is the Chaperone-Assisted Selective Autophagy (CASA), which relies on the HSP70/HSPA, BAG3, HSPB8 and the carboxy-terminus of HSC70 interacting protein (CHIP) protein complex formation for the degradation of damaged and misfolded proteins. Although the UPS and the autophagic pathway are two different degradative systems, they intersect and cooperate at various levels. First, it has been already mentioned the role of ubiquitin as a common degradation signal, or degron, in both UPS and autophagy. It has been shown that ubiquitin moieties link substrates to proteasomal or autophagic degradation based on the Lys residue used in polyubiquitination. For instance, Lys48 linkage, but also Lys11 and Lys29, represent proteasomal degrons. Instead, ubiquitin Lys63 linkage represents an autophagic degron. However, it is worthy to note that ubiquitination can occur at different Lys residues of a substrate and ubiquitin chain polymerization originates distinct types of polyUb chains, characterized by different linkages and branching, complicating the understanding of the ubiquitin code in relation to the degradative systems (Ji & Kwon, 2017). As both the degradative systems use ubiquitin as a common degron, it is clear that the machinery of enzymes responsible for ubiquitination are not only related to the UPS. For example, the E3 ubiquitin ligase CHIP (see below) interacts with HSP70/HSPA and ubiquitinates its bound misfolded substrate promoting the degradation, which can occur both through the proteasome and through autophagy. Indeed, misfolded substrates are

firstly routed to the proteasome for degradation. However, when the proteasome is overwhelmed or when the misfolded substrates deposit into large aggregates, which cannot be processed in the tight hole of the proteasome, autophagy comes into play for their clearance (Minoia et al., 2014). *Vice versa*, blocking the routing of misfolded substrates to autophagosome promotes proteasomal degradation (Cristofani et al., 2017). Autophagy-proteasome switch will be later described as dependent on the ratio between HSP70/HSPA-co-chaperones BAG1/BAG3 (Gamerding, Carra, et al., 2011; Rusmini et al., 2017). This example of compensatory activity reflects the integrated response of the PQC system to overcome proteotoxic stress (**Fig. 1.5**).

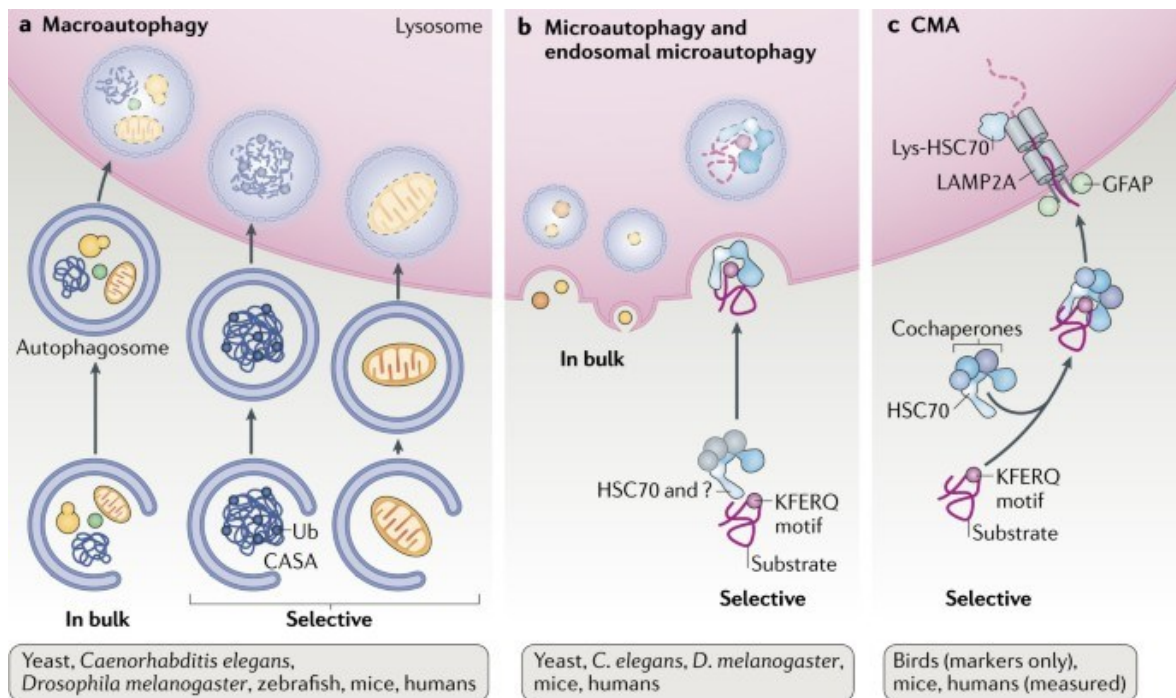


Figure 1. 4 Autophagy divides in three main branches.

a. Macroautophagy consists in the aspecific (*in bulk*) or selective engulfment of cytosolic material in an autophagosome, a double-membrane vesicle. Autophagosomes then fuse with lysosomes, which degrade the engulfed content. **b.** Microautophagy is based on the direct invagination of the lysosomal membrane and subsequent degradation of the substrates by lysosomal enzymes. **c.** CMA consists in the degradation of substrates that possess a KFERQ motif. This motif is recognized by the chaperone HSC70, which carries the substrate to the lysosomal receptor LAMP2A. The substrate is then translocated into the lysosome for degradation. (From Kaushik & Cuervo, 2018).

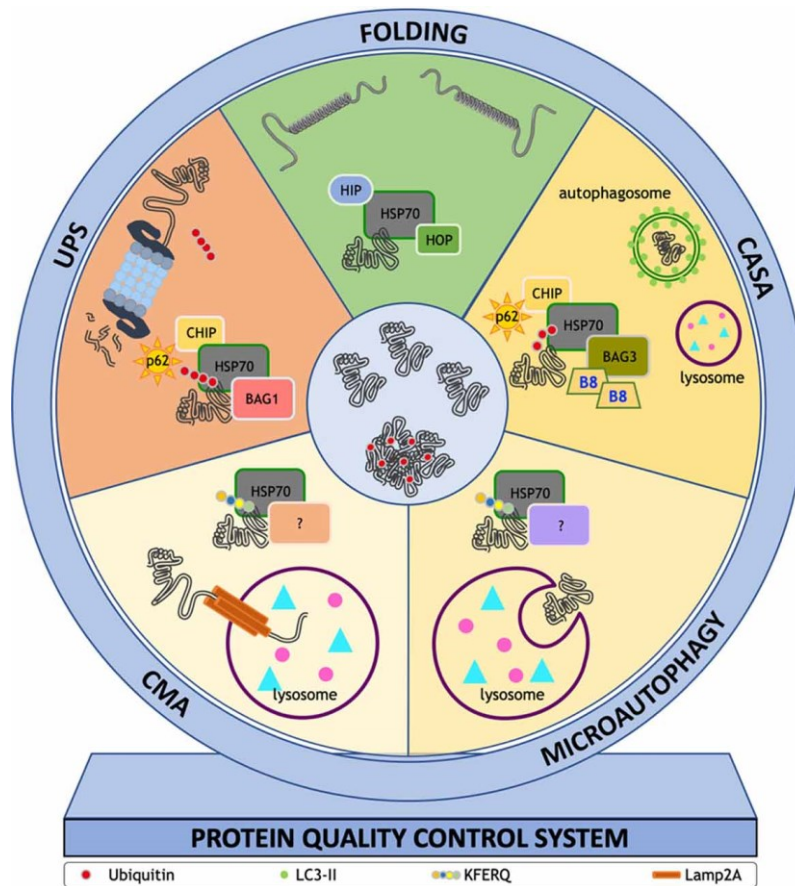


Figure 1. 5 The PQC system is a network of factors and pathways that assure proteostasis. Chaperone and co-chaperones lead the misfolded substrates to their fate, which is folding or degradation through the autophagic pathways (CMA, microautophagy or selective autophagy-CASA) or the proteasome. (From Cristofani et al., 2020).

1.2 The co-chaperone BAG3 and the BAG family

BAG3 is a co-chaperone, belonging to the BAG family. The BAG family includes six members (BAG 1-6), all possessing a BAG domain. The name BAG, which stands for **Bcl-2-Associated Athanogenes**, originates from the identification of BAG proteins as interactors of the anti-apoptotic protein Bcl-2. Functional analyses on the first BAG identified, BAG1, revealed shared anti-apoptotic functions with Bcl-2, condensed in the word Athanogene (from Greek *Athàntos* = against death) (Takayama et al., 1995). Actually, the other BAG members of the family were later identified through a two-hybrid screen assay as interactors of the ATPase domain of HSP70/HSPA chaperone. The BAG domain comprises 78-120 amino acids and is present in one copy in all BAG members, except for BAG5, which contains four putative BAG domains (Doong et al., 2002; Rosati et al., 2007; Takayama et al., 1999). BAG proteins are described as nucleotide exchange factors (**NEFs**), as their BAG domain, interacting with the ATPase domain of **HSP70/HSPA**, favours the ATP-ADP cycle and the release of the substrate (**Fig. 1.6**). Structural analyses revealed that the BAG domain consists of helices with a length of 30-40 amino acids, with the second and third helices binding the ATPase domain of HSP70/HSPA (Briknarová et al., 2001; Brive et al., 2001; Sondermann et al., 2002; Sondermann et al., 2001; Takayama et al., 1999).

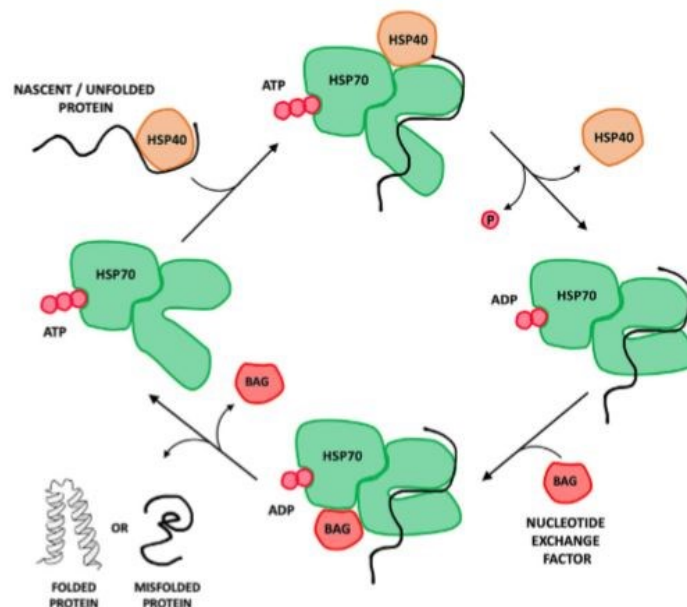


Figure 1. 6 Role of the BAG domain as NEF of HSP70/HSPA.

The unfolded or misfolded substrates interact with the ATP-bound HSP70/HSPA along with co-chaperones (e.g., HSP40). ATP to ADP hydrolysis causes the open to close conformational change of HSP70/HSPA substrate binding domain. BAGs, acting as NEFs, enhance the ADP-ATP exchange, thus the close to open conformational change of the substrate binding domain of HSP70/HSPA, permitting the substrate release (From Mariotto, Viola, Zanon, & Aveic, 2020).

BAG proteins contain other domains beyond the BAG domain (described below) (**Fig. 1.7**). BAG proteins homologues have been described in animals, plants, fungi, and yeasts, suggesting that this evolutionary conserved family of proteins plays fundamental basic functions in cells (Kabbage & Dickman, 2008; Kang et al., 2006; Takayama et al., 1999). It is likely that all BAG proteins derived from a common ancestor and that during evolution they acquired new domains, therefore new specialized functions.

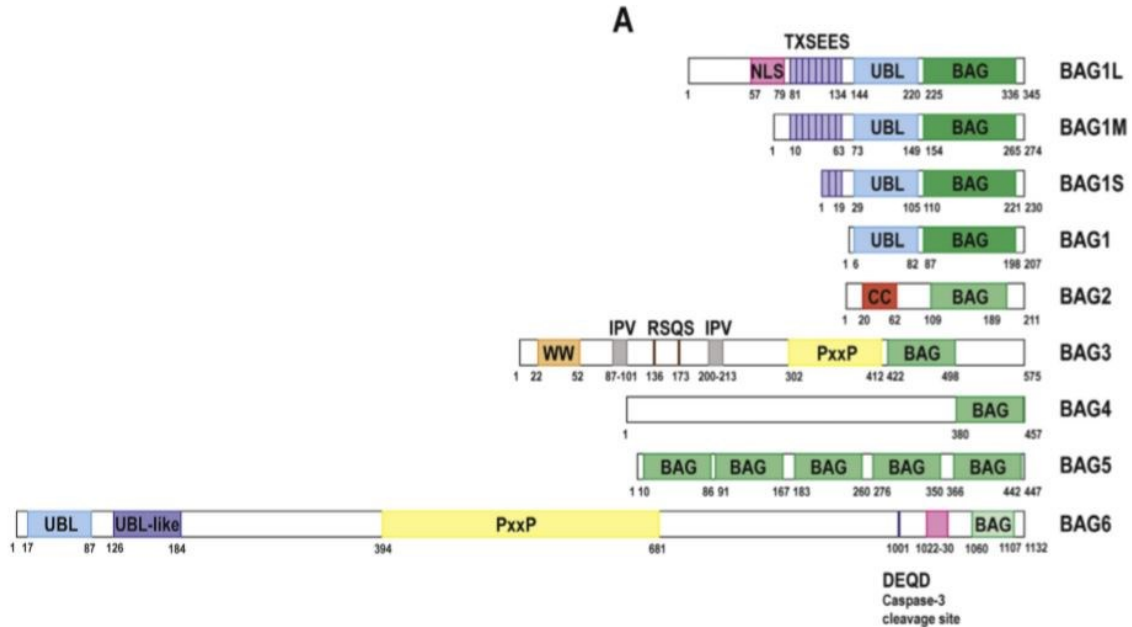


Figure 1. 7 The human BAG family (BAG1-6).

Representation of BAG family members and domains. Conserved BAG domains in green, ubiquitin-like domain (UBL) in blue is present in BAG1 (all isoforms) and BAG6. A nuclear localization signal (NLS; pink) is present in the isoform BAG1L, while TXSEES repeats (violet) are present in BAG1L/M/S isoforms. A proline-rich domain (PxxP; yellow) is present in BAG3 and BAG6, while a Tryptophan-Tryptophan (WW; orange) domain in BAG3 only. BAG3 shows two additional domains: the Ile-Pro-Leu (IPV) domains. (From Behl., 2016).

Among BAG family, **BAG3** (also known as Bis, CAIR-1) has the highest affinity to cytoplasmic HSP70/HSPA (Rauch & Gestwicki, 2014). BAG3 gene locates in the chromosome 10q.26.11 and encodes a 75 kDa protein and a shorter isoform (40 kDa) that has been described in synaptosomes (Bruno et al., 2008). BAG3 is ubiquitously expressed, with higher expression levels in heart and skeletal muscles and in cancer cells (Felzen et al., 2015; Gentilella & Khalili, 2011; Homma et al., 2006; Liao et al., 2001; Rosati et al., 2007). At a cellular level, BAG3 localizes predominantly in the cytosol and translocates to the perinuclear region after acute stress (Gamerding, Kaya, et al., 2011; Kyratsous & Silverstein, 2008). BAG3 expression is also enhanced by several stresses, such as oxidative stress, proteasome inhibition, heat shock (Basile et al., 2009; Du et al., 2009; Franceschelli et al., 2008; Pagliuca et al., 2003). Aging also positively modulates BAG3 expression (Gamerding et al., 2009). Well-known transcription factors that modulate directly or indirectly BAG3 expression are the Heat Shock transcription Factor1 (HSF1),

which binds to the two Heat Shock Responsive Elements (HREs) present in *bag3* gene promoter, Nuclear Factor-kappa-light-chain-enhancer of activated B cells (NF-κB) and Nuclear factor erythroid 2-related factor 2 (Nrf2) (Franceschelli et al., 2008; Tang et al., 2018; Wang et al., 2012; Wu et al., 2018). Beyond the BAG domain, BAG3 protein possesses several domains which makes BAG3 able to bind to multiple partners involved in several cellular pathways and to act as a scaffold protein. In particular, it possesses a Tryptophan-Tryptophan (WW) domain, a PxxP region and two Ile-Pro-Val (IPV) domains (**Fig. 1.8**). The **WW** domain is located at the N-terminus and is responsible for interactions with proline-rich regions. These include synaptopodin-2 (SYNPO2), located at the Z-disc of muscle cells. Here, SYNPO2 and BAG3, together with the vacuolar protein sorting (VPS) factors VPS16 and VPS18 and syntaxin-7, help the formation of the phagosome and the engulfment of damaged structural substrates of the CASA complex, such as filamin (Ulbricht et al., 2013). Other proline-rich proteins are LATS1, LATS2 and AMOTL1/2, which are inhibitors of the transcription factors YAP and TAZ; BAG3, by contacting LATS1/2 or AMOTL1/2, abrogates their inhibitory activity, letting YAP and TAZ entering the nuclei and activate transcription (Meriin et al., 2018; Ulbricht et al., 2013). Finally, the mTOR inhibitor tuberous sclerosis 1 (TSC1) is a target of the WW-domain of BAG3. TSC1 is part of the TSC complex and mediates indirectly the inhibition of mTORC1, one of the autophagy master regulators (Kathage et al., 2017). The two **IPV** domains, located at the N-terminus and in the middle of the protein, are responsible for the interaction with two sHSP/HSPBs: HSPB8 and HSPB6 (Fuchs et al., 2009; Hishiya et al., 2011). Small HSPs (described below) belong to the chaperone network and have an anti-aggregation and pro-degradative activity. BAG3 and HSPB8 complex has been intensely investigated: HSPB8 is the HSPBs with the highest affinity for BAG3 and interacts as a dimer, forming a 1:2 BAG3:HSPB8 stoichiometry complex (Carra, Seguin, & Landry, 2008; Morelli, Mediani, et al., 2017). Another feature of this unique liaison is also the observation of HSPB8 decreased stability after BAG3 depletion (Fang et al., 2017). BAG3, through the **PxxP** domain, which is upstream of the BAG domain, recognizes SH3-domain containing proteins, such as phospholipase C gamma (PLCγ), Src, and the dynein motor complex (Colvin et al., 2014; Doong et al., 2000; Gamerdinger, Kaya, et al., 2011). This latter interaction permits the routing of the CASA complex towards the Microtubule Organizing Center (MTOC), where aggresomes form, and depletion of this domain abolishes this function (Gamerdinger, Kaya, et al., 2011). BAG3 activity and function can be modulated also by PTMs. Phosphorylation sites have been reported at tyrosines Tyr451 or 457; phosphorylation at serines Ser187 by protein kinase C delta (PKCδ) has been reported in cancer studies (Doong et al., 2000; N. Li et al., 2013); phosphorylation of tyrosines by the focal adhesion kinase FAK was observed upon glucose

stimulation in pancreatic beta cells and seems to regulate insulin release (Iorio et al., 2015); in multiple myeloma cells, proteasome inhibition by bortezomib results in Ser377 phosphorylation (Ge et al., 2010). Another PTM is ubiquitination by the ubiquitin ligase CHIP, which has been described in myocytes (Arndt et al., 2010) and after caspase cleavage upon staurosporine stress (Virador et al., 2009). In addition, BAG3 caspase-mediated cleavage at aspartic acid Asp347 has been reported and linked to a loss of BAG3 anti-apoptotic function (Virador et al., 2009).

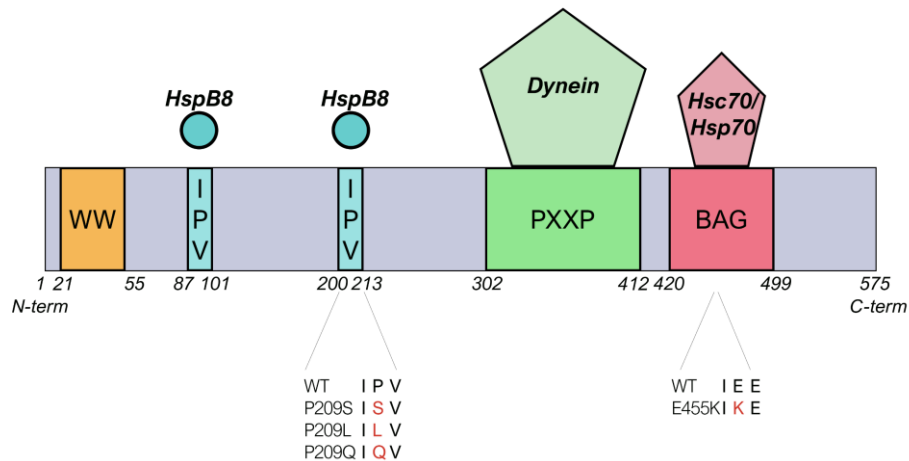


Figure 1. 8 Schematic representation of BAG3 domains and interacting partners.

BAG3 (575 amino acids length) has a WW domain (orange), two IPV domains (blue) for HSPBs interaction (e.g., HSPB8), a PxxP domain (green) for dynein motor complex interaction and a BAG domain (pink) for HSP70/HSPA interaction. Below, disease-causing mutations are reported: P209 substitutions with serine (S), leucine (L) or glutamine (Q) and the glutamic acid (E) substitution with a lysine (K) at position 455.

1.2.1 Insights into BAG3 mutations and related diseases

BAG3 mutations have been linked to diseases that affect skeletal and heart muscles and neurons. The first identified mutation is a heterozygous point mutation which causes a Proline to Leucine substitution at position 209 (**P209**) in the second IPV domain. This **P209L** mutation has been linked to myofibrillary myopathy (MFM) and cardiomyopathy (Lee et al., 2012; Selcen et al., 2009). Patients carrying the P209L mutation showed early onset (first or second decade) and rapid progression of disease (Selcen et al., 2009). Rare cases developed severe axonal neuropathy (Jaffer et al., 2012; Kostera-Pruszczyk et al., 2015). A Proline to Glutamine (**P209Q**) mutation has also been reported and linked to mild, late onset MFM and axonal neuropathy (Semmler et al., 2014). Recently, a Proline to Serine (**P209S**) substitution has been described in two families with peripheral neuropathy and one family with axonal Charcot-Marie-Tooth (CMT) disease, with no heart or skeletal muscle involvement (Shy et al., 2018). A Proline to Serine substitution at position 470 (P407S) in the BAG domain has been also found in two MFM cases (Meister-Broekema et al., 2018). BAG3 mutations have been related to dilated cardiomyopathy (DCM), such as the Glutamic

Acid to Lysine substitution at position 455 (**E455K**). At a molecular level, E455K mutation, which falls in the BAG domain, causes a decreased interaction between BAG3 and HSP70/HSPA (Villard et al., 2011).

BAG3 deficiency animal models have been developed and studied. Knock-down (KD) of BAG3 by morpholinos was associated to cardiac dysfunction and myofibrillar disintegration in Zebrafish (Norton et al., 2011; Ruparelia et al., 2014). DCM was observed in a Zebrafish model of BAG3 haploinsufficiency (Ding et al., 2019). BAG3 knock-out (KO) mice models are vital at birth, but develop a progressive myopathy at early stages of life which brings to death at day 25 (Homma et al., 2006). DCM mice models were developed with cardiac-targeted KO of BAG3 gene and recapitulated the disease observed in humans (Fang et al., 2017; Homma et al., 2006; Myers et al., 2018). Models of P209X mutations have also been studied. For instance, Zebrafish overexpressing a GFP-tagged human BAG3 carrying the P209L mutation leads to the observation of accumulation of mutant BAG3 protein (Ruparelia et al., 2014). Instead, the P215L mouse model, equivalent of the P209L mutation in humans, did not show any cardiac or muscular dysfunction (Fang, Bogomolovas, Zhou, et al., 2019). However, very recently, a KI(P215L)/KO mouse was generated and described as a first murine model recapitulating well the human myopathy phenotype (Robertson et al., 2020). Cell models and patients muscle biopsies gave more insights into P209 mutants dysfunction. Biopsies from patients affected by myopathy and peripheral neuropathy showed aggregated proteins accumulation (Selcen et al., 2009). Indeed, it has been observed that P209 mutants aggregate, sequestering CASA complex members and causing an alteration of SQSTM1/P62 phosphorylation (Guilbert et al., 2018; Meister-Broekema et al., 2018). It has been suggested that the aberrant behaviour of P209 mutants might affect the stress signalling axis KEAP1-Nrf2, as KEAP1 is sequestered in BAG3 P209 mutant aggregates (Guilbert et al., 2018). Interestingly, no loss of interaction with HSPB8 was observed, even if the mutation falls in the HSPB8-interacting IPV domain. Instead, it was recently demonstrated that P209 mutants affect the HSP70/HSPA activity and that the aggregating prone behaviour can be counteracted by impairing BAG3-HSP70/HSPA interaction, using drugs that inhibit HSP70 activity or by mutations that disrupt BAG domain interaction with HSP70/HSPA (Meister-Broekema et al., 2018).

1.2.2 A brief description of the other members of the BAG family

To give a complete overview of the BAG family, all the remaining members will be briefly described hereafter.

BAG1 gene is located on chromosome 9p13.3 and encodes four isoforms arising from different in-frame initiation translation sites of the same mRNA. The four isoforms, which differ only in the length of the N-terminal domain (NTD), are named BAG1L, BAG1M,

BAG1S and BAG1 p29, and have a molecular weight of 50, 46, 36 and 29 kDa, respectively (Packham et al., 1997; Yang et al., 1998). BAG1 mRNA translation into the different isoforms is dependent on a mechanism called “leaky scanning”, which describes the skipping of a weak initiation codon. This results in differential levels of BAG1 isoforms, depending on the strength of the sequence surrounding the initiation codon. A second mechanism rules the initiation of translation at the third start codon, which results in the production of the BAG1S isoform. In this case, translation is cap-independent since translation initiation factors recognize an internal ribosome entry site (IRES). Interestingly, this second mechanism of translation is described to be favoured upon stress, e.g. heat shock, when the cap-dependent translation is shut down (Coldwell et al., 2001). It has been recently shown that both translation mechanisms are regulated by the presence of G-quadruplex structures located in the 5'-untranslated region of BAG1 mRNA and their stabilization using small molecules affects BAG1 expression (Jodoin et al., 2019). Like BAG3, all four isoforms of BAG1 are expressed ubiquitously, but show a differential subcellular localization. For instance, BAG1L localizes predominantly in the nucleus, as it contains a nuclear localization signal (NLS) at the N-terminus, while BAG1M and BAG1S show a cytoplasmic localization. BAG1S and BAG1M are also found in the nucleus in response to stress (Takayama et al., 1998). BAG1 isoforms also possess a putative nucleolar localization sequence (Lee et al., 2007). 2 to 8 TXSEEX repeated sequences have been described and their function seems to be related to a regulatory activity of hormone receptors such as glucocorticoid or androgen receptor (Knee et al., 2001; Schneikert et al., 1999). In addition, BAG1 possesses a UBL domain, which permits the routing of polyubiquitinated substrates to the proteasome system. Indeed, as anticipated above, BAG1, together with HSP70/HSPA and the E3 ubiquitin ligase CHIP/STUB1, targets the polyubiquitinated substrates to the proteasome system. Therefore, while BAG3 mediates the autophagic disposal of substrates, BAG1 mediates their proteasomal degradation depending on the BAG1/BAG3 ratio (Minoia et al., 2014; Gamerdinger, Carra, et al., 2011). For instance, **BAG1/BAG3 switch (Fig. 1.9)** has been observed during aging or acute stress, with aged cells showing higher levels of BAG3 and lower levels of BAG1 in respect to young cells (Gamerdinger et al., 2009). Similarly, when BAG3-mediated autophagy is blocked, substrates are subjected to BAG1-mediated proteasomal degradation (Cristofani et al., 2017). Up to date, no mutations have been reported on BAG1 gene, but KO experiments revealed that its homozygous deletion is embryonically lethal in mice and is associated to abnormal apoptosis and defects in neuronal development (Götz et al., 2005). Oppositely, it has been demonstrated that BAG1 overexpression promotes neurite growth and axonal regeneration (Kermer et al., 2002; Planchamp et al., 2008). In addition, BAG1

exerted a neuroprotective activity in rodent stroke models through its anti-apoptotic function, and in cell models of Huntington Disease (HD), Amyotrophic Lateral Sclerosis (ALS) and Spinal and Bulbar Muscular Atrophy (SBMA), through its prodegradative activity against the toxic mutated Huntingtin (polyQ-Htt, carrying the expanded polyglutamine tract), the TAR DNA binding protein 43 (TDP-43) C-terminal fragments (CTFs) and the toxic mutated Androgen Receptor (polyQ-AR, carrying the expanded polyglutamine tract) (Cicardi et al., 2019; Cicardi et al., 2018; Jana & Nukina, 2005; Sroka et al., 2009).

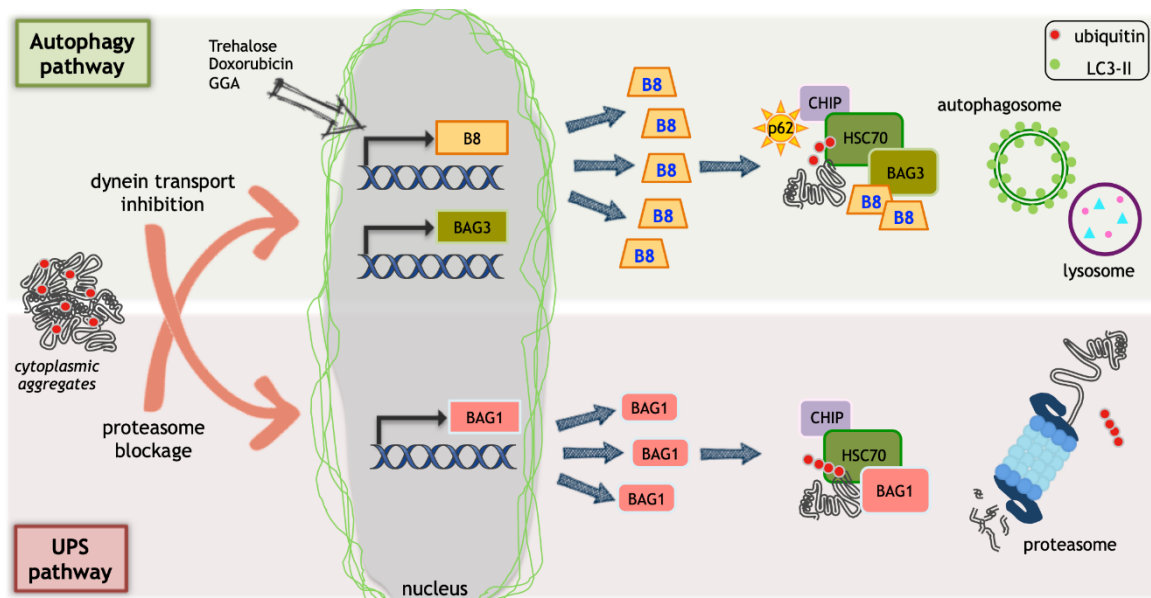


Figure 1. 9 BAG1/BAG3 switch.

When the proteasome is blocked or overwhelmed, BAG3 and HSPB8 are upregulated and promote CASA-mediated degradation of misfolded and aggregating substrates. Oppositely, when the CASA activity is blocked (e.g., by blocking dynein-mediated transport of the CASA complex), BAG1 is upregulated and, by interacting with HSP70/HSPA and CHIP, favours the proteasomal degradation of misfolded substrates. (From Cristofani et al., 2019).

BAG2 is a 23 kDa protein and, beyond the BAG domain, a predicted coiled-coil domain has been described at the NTD. BAG domain in BAG2 has been defined as a non-canonical BAG domain since it is characterized by a low homology in respect to the other members of the family. In addition, structural studies on the BAG2 isolated NTD and BAG domains revealed that they both homodimerize, suggesting that in cells the full-length BAG2 is found in tetramers and oligomers. Indeed, BAG2 is found in high molecular weight fractions in cells extracts. Even if BAG2 possesses a non-canonical dimeric BAG domain, it is still able to interact with HSP70/HSPA and to act as a NEF, although through a different binding mode (Xu et al., 2008). Differently from BAG1, BAG2 shows an inhibitory activity against CHIP-mediated ubiquitination, while it seems to promote client proteasomal degradation through a ubiquitin-independent pathway (Arndt et al., 2005; Dai et al., 2005). A role of BAG2 has been described in NDs. For instance, in Parkinson disease (PD) models, BAG2 was shown to interact with DJ-1, exerting neuroprotective functions and to inhibit CHIP

activity in the degradation of PINK1. Of note, both DJ-1 and PINK1 have been found mutated in PD patients (Carrettiero et al., 2009; Song et al., 2015).

Studies on **BAG4** are mainly focused on its debated role in apoptosis in cancer cells. Indeed, it is also named silencer of death domains (SODD), since it can bind to death domains of the tumour necrosis factor (TNF) receptors preventing trimerization and subsequent apoptotic pathway activation (Jiang et al., 1999).

BAG5 possesses four putative BAG domains but only one of these domains seems important for HSP70/HSPA interaction (Arakawa et al., 2010). Like BAG2, BAG5 was found to inhibit CHIP activity. It has been also demonstrated that BAG5 exerts a neuroprotective role in PD models by stabilizing PINK1, and in Alzheimer disease (AD), where its downregulation exacerbates β -amyloid-mediated toxicity and cell death (Guo et al., 2015; Kalia et al., 2011; Wang et al., 2014). However, studies also demonstrated a detrimental activity of BAG5 in PD models. For instance, BAG5 has been shown to enhance α -synuclein oligomerization and to promote dopaminergic neuron death in animal models of PD, through Parkin inhibition (Friesen et al., 2020; Kalia et al., 2004).

BAG6, also named BAT3/Scythe, is the last and largest member of BAG family. BAG domain in BAG6 shows a weak homology in respect to the other members of BAG family. Indeed, only a weak BAG6 activity on HSP70/HSPA was firstly described, but other studies demonstrated no interaction with HSP70/HSPA (Mock et al., 2015; Thress et al., 2001). BAG6, like BAG1, possesses a UBL domain (Tanaka et al., 2016). In addition, BAG6 possesses a C-terminal NLS and a central proline-rich region. Although it is still debated the belonging of BAG6 to the BAG family, it must be mentioned its role in PQC system. Indeed, BAG6 has been involved in tail-anchor PQC: by forming a complex with UBL4A and TRC35, BAG6 is able to interact with hydrophobic stretches of nascent polypeptides and to route them to proteasomal degradation when their insertion to their resident membranes, e.g. ER membrane, fails (Hayashishita et al., 2019; Kuwabara et al., 2015).

Interestingly, in contrast to BAG3, no mutations in any other member of BAG family have been described in literature, so far.

1.3 The small Heat Shock protein HSPB8 and the other HSPBs

HSPBs, or sHSPs, are a subset of chaperones characterized by a low molecular weight (15-30 kDa) and highly conserved in all kingdoms and in viruses (Caspers et al., 1995; Maaroufi & Tanguay, 2013). In mammals, HSPBs consist of ten members (HSPB1-HSPB10) and one related member (HSPB11) (Kappé et al., 2003). Some HSPBs, such as HSPB1, HSPB5 and HSPB8, are ubiquitously expressed, while others show a tissue specific expression. For instance, HSPB4 is expressed only in lens, HSPB2 and HSPB3 in

cardiac and muscle cells, HSPB9 and HSPB10 in testis (Kappé et al., 2003; Sugiyama et al., 2000; Treweek et al., 2015) (**Fig. 1.11**). Cardiac muscle, skeletal muscles and neurons show high expression and a wide variety of HSPBs, supporting a fundamental role in the maintenance of these cell types. The fundamental role of HSPBs activity in neuronal and muscle cells is further highlighted by the identification of HSPBs mutations associated to cardiomyopathies, myopathies, distal hereditary motor neuropathies (dHMNs) and CMT diseases (Datskevich et al., 2012; Garrido et al., 2012). On the other hand, HSPB4 and HSPB5, which are also known as α A-crystallin and α B-crystallin, have a crucial role in lenses maintenance and their mutations are associated to lens defects (Clark et al., 2012). HSPBs have been also related to cancer.

HSPBs share the common ATP-independent holdase activity, which is the ability to interact with misfolded substrates and avoid their aggregation without exerting ATPase activity (Leroux et al., 1997). However, HSPBs can indirectly interact with ATP-dependent chaperones with foldase activity, such as HSP70/HSPA, for the refolding of misfolded substrates (Franklin et al., 2005).

HSPBs are structurally defined by the presence of an α -crystallin domain (**ACD**) in the central region of their structure, which is a highly conserved 80-90 amino acids long domain consisting of 8 β -strands, which fold in a β -sandwich structure (Hayes et al., 2009). Outside the ACD, HSPBs share poor similarity of both the NTD and the C-terminal domain (CTD), except for the presence of a **SRLFDQxFG** motif in the NTD of sHSPs B1, B4, B5, B6, B8 and a **I/V-X-I/V** motif in the CTD of sHSPs B1, B2, B4 and B5 (Kriehuber et al., 2010) (**Fig. 1.12 and 1.13**).

A primary feature of HSPBs is their dynamic homo- or hetero- dimerization and oligomerization. HSPBs can form oligomers of 4-40 monomers, reaching molecular weight up to 900 kDa. All three ACD, NTD and CTD are fundamental for oligomerization and function (**Fig. 1.10**) In particular, the ACD is responsible for dimer formation, while the NTD and the CTD promote the stabilization of oligomeric and dimeric structures. For instance, it has been observed that truncation of the NTD causes the formation of smaller oligomers, while the absence of the I/V-X-I/V motif in the CTD of sHSPs B3, B6, B8 is thought to explain their low oligomerization tendency. In response to environmental stimuli, a dynamic change in subunit composition of oligomers can occur, changing the affinity for substrates binding, and so, the functional activity of oligomers (Basha et al., 2012; Van Montfort et al., 2001). It has been shown that PTMs, such as phosphorylation or oxidation, mediate the environmental stimuli to subunit exchanges in HSPBs oligomers. Transient phosphorylation can occur at Ser or Thr (Threonine) residues in response to heat shock, proinflammatory agents, oxidants but also to differentiating agents and mitogens. Phosphorylation may

change not only HSPBs oligomerization capability, but also their intracellular localization. For example, upon stress, phosphorylated HSPB1 or HSPB5 translocate into the nuclei. Other PTMs described include deamidation, glycation, oxidation, myristoylation and palmitoylation. For example, the oxidation of HSPB4 causes the formation of an intramolecular disulphide bond, which changes the subunit dynamics and its anti-aggregation activity (Garrido et al., 2012; Treweek et al., 2015).

As anticipated, HSPBs exert several activities in cells. First, HSPBs, acting as holdase chaperones, prevent the aggregation of misfolded substrates and help in the refolding activity mediated by chaperones with foldase activity. Second, when the substrate cannot be refolded, HSPBs favour its routing to the degradative pathways, which are autophagy and the UPS; for example, while HSPB1 and HSPB5 mediate proteasomal degradation, HSPB8 mediates the routing of substrates to autophagy, through the CASA pathway (Carra, Seguin, Lambert, et al., 2008; Parcellier et al., 2006; Zhang et al., 2010). Third, HSPBs interact with the cytoskeleton components. HSPB1, HSPB5, HSPB8 and HSPB6 interact with actin; in addition, HSPB5 can associate with intermediate filaments type III, regulating their assembly and preventing aggregation (Wettstein et al., 2012). Fourth, HSPBs are involved in the response to cellular stress and apoptosis, by regulating enzymes involved in oxidative-stress response, participating in redox metabolism, and blocking the activity of pro-apoptotic factors (Acunzo et al., 2012; Arrigo, 2007).

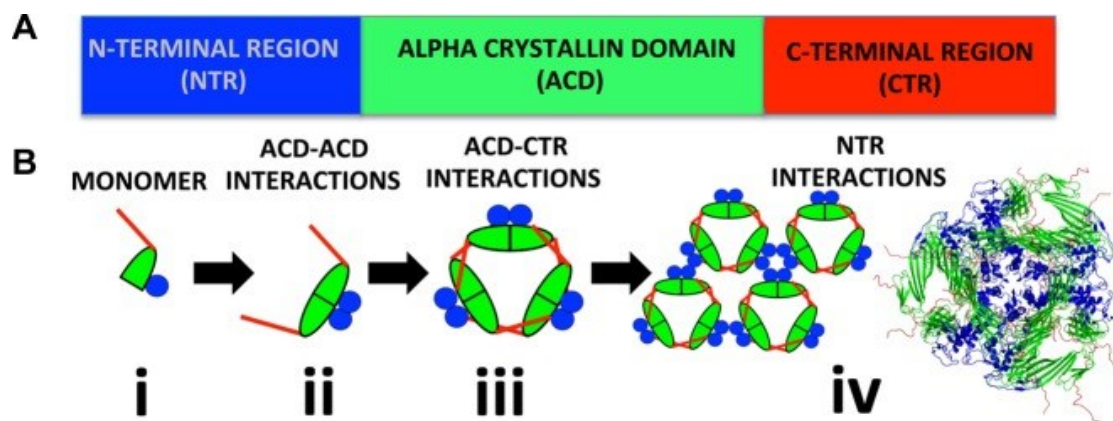


Figure 1.10 Schematic structure and oligomerization of HSPBs.

A. HSPBs share a common α -crystallin domain (ACD) and variable N- and C- terminal regions (NTR and CTR, corresponding to NTD and CTD in the text). **B.** HSPBs monomers (i) dimerize through the ACD domain. Dimers (ii), through their CTR and NTR, interact forming oligomeric assemblies (iii and iv). (From Delbecq, Rosenbaum, & Klevit, 2015).

Since my work in this thesis has been mainly focused on HSPB8 (HSP22 or H11), I will initially illustrate some of the specific features of this protein. **HSPB8** is a 22 kDa chaperone ubiquitously expressed, especially in cardiac and skeletal muscles. It is found mainly as a dimer and it oligomerizes only at high concentration. HSPB8 shows weak interaction with the other HSPBs, therefore it does not form hetero oligomers. Indeed, the obligate binding partner of HSPB8 is the co-chaperone BAG3, with whom forms a 2:1 stoichiometric complex

(Carra, Seguin, & Landry, 2008; Fuchs et al., 2009). HSPB8 interacts with the two IPV domains in BAG3 through the last two β -strands of the ACD domain (Fuchs et al., 2009). The dependency of HSPB8 on BAG3 is supported not only by the fact that HSPB8 stability depends on BAG3 interaction, but also because HSPB8 has the highest affinity to BAG3 in respect to other BAG3-binding HSPBs (Fang et al., 2017; Carra et al., 2008). In concert with BAG3, HSPB8 participates to the CASA complex (Arndt et al., 2010; Carra, Seguin, & Landry, 2008). HSPB8 is induced by different cell stresses, including mainly proteotoxic stress, but also in response to sodium-arsenite, oxidative and osmotic stress (Bartelt-Kirbach & Golenhofen, 2014; Wilhelmus et al., 2006) (Yew et al., 2005). In skeletal muscle cells, HSPB8 is involved in Z-disc maintenance, by facilitating the degradation of damaged structural proteins (Arndt et al., 2010). In neurons, HSPB8 exerts its chaperone and autophagy-promoting activity against a broad variety of misfolded substrates, such as ALS-related substrates TDP-43 and its CTFs, mutated superoxide dismutase 1 (SOD1), the *C9ORF72* gene-related Dipeptide Repeats (DPRs), but also α -synuclein and the elongated polyQ-AR and polyQ-Htt, which will be discussed below (Carra et al., 2005; Cristofani et al., 2019). Besides the pro-autophagic activity, HSPB8 promotes eIF2 α phosphorylation to shut down translation of unnecessary proteins in response to proteotoxic stress (Carra et al., 2009).

1.3.1 Insights into HSPB8 mutations and related diseases

HSPB8 mutations are causative of dHMNs, CMT2 and myopathies, characterized by high variability in onset and progression. The most often encountered mutation falls in a conserved residue of Lys at position 141, which has been found substituted with glutamic acid (K141E), asparagine (K141N), threonine (K141T) or methionine (K141M) (Echaniz-Laguna, Geuens, et al., 2017; Irobi et al., 2004; Nakhro et al., 2013). This conserved residue is fundamental for dimerization and correspond to R140 in HSPB1 or R120 in HSPB5, which, when mutated, are also causative of diseases (see below). Other dHMN-related mutations in HSPB8 are P90L and N138T (Echaniz-Laguna, Geuens, et al., 2017). Distal onset rimmed vacuolar myopathy, with neurogenic involvement, has been also linked to K141E mutation (Ghaoui et al., 2016). A similar phenotype of autosomal dominant rimmed vacuolar myopathy was described for HSPB8 pP173Sfs*43 mutation (Al-Tahan et al., 2019). Other two frameshift mutations, pQ170Gfs*45 and pT194Sfs*23 were linked to axial and distal myopathy and to proximal myopathy, respectively, without neurologic signs (Echaniz-Laguna, Lornage, et al., 2017; Nicolau et al., 2020). Histopathological features associated to the pQ170Gfs*45 mutation consist in signs of myofibrillar myopathy with protein aggregates formed by structural proteins such as desmin (DES), dystrophin, myotilin (MYOT) and members of the PQC, such as HSPB8 itself, BAG3, HSPB5, ubiquitin, but also

TDP-43, and rimmed vacuoles (Echaniz-Laguna, Lornage, et al., 2017). Similar histopathological signs were observed in pT194Sfs*23 mutation carriers, with myofibrillar aggregates and rimmed vacuoles and abnormalities in the stress granules (SGs)-associated protein TIA-1 (Nicolau et al., 2020).

HSPB8 K141E/N mutations have been extensively studied in patient biopsies, cells, and animal models. A first observation is that motoneurons (MNs) are the primary target of K141E/N mutations as only primary MNs and N2a cell models show important neurite degeneration, while primary sensory neurons are only mildly affected and primary cortical neurons and glia show no sign of neurodegeneration (Irobi et al., 2010). A second observation is that HSPB8 K141E/N mutants cytotoxicity is strictly linked to their aggregation prone behaviour as HSPB8 aggregates have been detected in cell models, patient fibroblasts and in animal models as well (Irobi et al., 2012). Animal models recapitulate quite well the human phenotype. For instance, homozygous KI mouse overexpressing HSPB8 K141N mutant shows MN pathology with progressive axonal degeneration and muscle atrophy, abnormal and degenerating organelles and accumulating mitochondria, which might suggest an impaired autophagic flux. Indeed, sciatic nerve of pre-symptomatic mice shows low autophagy potential while post-symptomatic mice show HSPB8 aggregation. Moreover, homozygous KI mouse shows MFM signs with Z-disc disorganization, likely independent from the neuronal pathology, and characterized by aggregating HSPB8, HSPB5, DES and presence of rimmed vacuoles. Instead, the heterozygous model shows no sign of MNs or muscle dysfunction, but accumulating abnormal mitochondria were observed in muscle (Bouhy et al., 2018). Drosophila models overexpressing the HSPB8 ortholog Hsp67Bc carrying the R126E or R126N mutations, which correspond to K141E or K141N mutants, show normal muscle performance, but have histopathological hallmarks of muscle dysfunction: the R126E mutant is associated to myofibrillar disorganization with mitochondrial abnormalities and alterations at the neuromuscular junctions, while the R126N mutant shows no mitochondrial abnormalities but protein aggregation which leads to a mild myofibrillar disorganization (Carra et al., 2010; Jabłońska et al., 2018). Interestingly, the presence of detectable HSPB8 aggregates correlates with a less severe phenotype, suggesting that HSPB8 mutant soluble oligomers are more toxic than HSPB8 aggregates (Jabłońska et al., 2018). Indeed, cell models without detectable aggregates, such as SH-SY5Y neuroblastoma cell line, show signs of HSPB8 mutant cytotoxicity and, when HSPB8 mutant oligomers are added to cell culture media, they exert a cytotoxic effect on cultured cells (Echaniz-Laguna, Geuens, et al., 2017; Sanbe et al., 2013). Mitochondria abnormalities observed in mice and Drosophila models, but also in patients fibroblast, suggest that these organelles are a target of HSPB8

mutant-mediated cytotoxicity (Irobi et al., 2010). In cardiomyocytes of mice models expressing HSPB8 K141N mutation, it has been observed that mutant HSPB8 shows increased mitochondrial localization (Sanbe et al., 2013). Aggregated mitochondria have been also observed in SH-SY5Y cell model expressing K141N mutation. Of note, a protective activity of HSPB8 in response to oxidative stress by inhibiting ROS formation and mitochondrial apoptotic pathway has been described (Jo et al., 2017; Yu et al., 2019). Indeed, higher ROS levels and reduced response to oxidative stress are observed in presence of HSPB8 K141N mutants (Yang et al., 2017). In addition, it has been reported a regulatory activity of HSPB8-BAG3 complex in the antioxidant axis of KEAP1-Nrf2. For instance, SH-SY5Y cells expressing HSPB8 K141N mutant show impaired Nrf2 nuclear translocation which can be reverted by antioxidants, and similar alterations have been observed in cells expressing the myopathy related P209L BAG3 mutant (Guilbert et al., 2018; Yang et al., 2017). HSPB8 has been also involved in RNA metabolism: HSPB8 can bind the RNA helicase DDX20, which is a component of Survival Motor Neuron (SMN) and small nuclear ribonucleoproteins (snRNP) complexes, and HSPB8 K141 mutants show alteration of DDX20 binding (Sun et al., 2010). Moreover, a deregulation in the RNA binding protein (RBPs) TDP-43 activity has been observed in dHMN and MFM patients carrying the K141E mutation: in particular, alteration of splicing of TDP-43 target genes and decreased mRNA levels of TDP-43 were observed in patients muscle (Cortese et al., 2018). In summary, mutations in HSPB8 K141 hotspot are characterized both by a loss of protective function, and by a likely gain of toxic function.

The effects of the novel HSPB8 frameshift mutations, which have been linked to dHMN and forms of myopathies, are less clear. All these three frameshift mutations fall in the C-terminus of HSPB8 and cause the production of HSPB8 proteins with extended C-terminal tails, with different aminoacidic sequences in the last 20-26 amino acids of the CTD of HSPB8 for pP173Sfs*43 and pQ170Gfs*45 mutations, while a minor change of only two amino acids for pT194Sfs*23 mutation (Al-Tahan et al., 2019; Echaniz-Laguna, Lornage, et al., 2017; Nicolau et al., 2020). It has been suggested that HSPB8 frameshift mutations cause an HSPB8 haploinsufficiency, since no expanded HSPB8 species have been detected and a halved decrease of HSPB8 protein was observed; this is likely related to a rapid degradation of mutant HSPB8, which has been reported in muscle and fibroblast cells (Echaniz-Laguna, Lornage, et al., 2017). However, HSPB8 KO in mice did not cause any myopathic phenotype, suggesting that a simple loss of function of HSPB8 frameshift mutants is not sufficient to induce muscle diseases. Indeed, it is likely that HSPB8 frameshift mutants cause an impairment in CASA pathway which determines an insufficient clearance of aggregates, as suggested by the accumulation of the autophagic markers LC3 and

SQSTM1/P62 in patient fibroblasts; alternatively, it is possible that HSPB8 mutants are prone to form aggregates themselves (Al-Tahan et al., 2019; Kwok et al., 2011). Moreover, an impairment of RNA metabolism and SGs formation are suggested as other pathomechanisms of HSPB8 frameshift mutations. Indeed, HSPB8 pT194Sfs*23 mutation was associated to abnormal punctate distribution of TIA-1, which is a RBPs that takes part in SGs formation (Nicolau et al., 2020).

1.3.2 A brief description of the other HSPBs

For the thoroughness of this work, all the remaining HSPBs will be described hereafter.

HSPB1 (HSP27) has been firstly found upregulated in HeLa cells in response to heat shock (Hickey & Weber, 1982). It is a 27 kDa protein constitutively expressed in all human tissues, especially in skeletal, smooth, and cardiac muscles (Sugiyama et al., 2000). Its constitutive and stress-induced expression assures an increased resistance to cellular stress. HSPB1 exerts its protective function through its chaperone activity, by preventing aggregation, cooperating indirectly in refolding, or promoting degradation of substrates. HSPB1 is mainly found in polydisperse oligomers of 400-600 kDa and its phosphorylation and oligomerization have been extensively studied and previously described (Arrigo, 2017). Dimerization is dependent on the formation of a disulphide bond between cysteine residues at position 137 and on the $\beta 7$ strand, which fall in the ACD, and is necessary for further oligomerization. HSPB1 phosphorylation can occur at Ser residue 15, 78, 82 and it influences the oligomerization state. (Diaz-Latoud et al., 2005; Mymrikov et al., 2010). Several functions under physiological and stressed conditions have been ascribed to HSPB1. For instance, HSPB1 interaction with cytoskeletal elements is well documented. It has been demonstrated that HSPB1, but also HSPB5, bind to intermediate filaments (e.g. keratins, GFAP) and their soluble subunits, suggesting a role in their correct assembly (Perng et al., 1999). HSPB1 binds and caps the plus end of actin filament preventing actin monomer addition and protects actin fibers after stress (Miron et al., 1991). HSPB1 binding to microtubules has been observed only after Taxol stabilization. Interestingly, CMT-related mutated HSPB1 (see below) shows a stronger binding affinity to microtubule components (Almeida-Souza et al., 2011). Another well studied function of HSPB1 concerns its multilevel anti-apoptotic activity. It has been demonstrated that HSPB1 is able to interfere with the activity of the pro-apoptotic proteins Bax and Bid, but also to sequester the cytochrome c released from mitochondria and hence to inhibit the caspase cascade activation (Bruey et al., 2000; Pandey et al., 2000; Paul et al., 2010). All HSPB1 activities reflect its role in protection against several cellular stressors, in particular thermal and oxidative stress. This protective activity is evident in cancer cells, where HSPB1 expression is associated to cell resistance against apoptosis and immune-system attacks and in favouring cancer cells

growth and dissemination (Ciocca et al., 2013). Up to 30 mutations in HSPB1 have been described along the whole structure of the protein and almost all show a dominant phenotype (Echaniz-Laguna, Geuens, et al., 2017; Houlden et al., 2008). HSPB1 mutations are the most frequent cause of hereditary neuropathies. In particular, HSPB1 mutations have been associated to adult-onset dHMNs and CMT2, sometimes characterized by myopathic features (Bugiardini et al., 2017; Houlden et al., 2008). HSPB1-related neuropathies are often benign even if some mutations are associated to a rapidly progressive phenotype that resembles ALS pathology (Capponi et al., 2016). Noteworthy, a heterozygous variant in the HSPB1 promoter was identified in an ALS patient (Dierick et al., 2007). HSPB1 mutations in the ACD affect homo- and hetero- dimerization, therefore oligomerization dynamics. It has been demonstrated that HSPB1 chaperone activity is enhanced when HSPB1 is in its monomeric state and this might explain the increased chaperone activity and response to heat shock observed in R127W and S135F mutants, which are characterized by reduced dimerization (Almeida-Souza et al., 2010). On the other hand, a C-terminal extension due to a frameshift mutation causes an impairment in dimer dissociation and has been associated to an ALS-like phenotype (Capponi et al., 2016). The mutation at the conserved residue R140 (R140G) also alters HSPB1 dynamics, determining an increase in oligomers size and aggregation propensity (Nefedova et al., 2013). HSPB1 aggregation has been observed in P182 mutants (Chalova et al., 2014). HSPB1 mutant pathogenic mechanisms have been related to its impairment in the chaperone activity. For instance, dysregulation in chaperone function toward cytoskeletal elements has been observed, such as alteration of neurofilaments assembly *in vivo* and *in vitro*, and microtubule hyperstabilization associated to impaired mitochondria transport (Ackerley et al., 2006; Almeida-Souza et al., 2011). Detrimental effects directly against mitochondria have been described as well, such as impaired mitochondrial respiration and increased oxidative stress (Kalmar et al., 2017). Another cellular pathway altered by HSPB1 mutants is autophagy: for instance, HSPB1 mutants associate with stronger affinity to SQSTM1/P62 causing an impairment in the autophagic flux (Haidar et al., 2019) In summary, similar to HSPB8, HSPB1 mutants studies evidence not only a loss of protective function, but suggest a likely toxic gain of function of the mutant proteins, corroborated by the evidence that HSPB1 deficient mice do not develop a disease-associated phenotype (Huang et al., 2007). Instead, mice models carrying mutations (e.g., S135F, P182L) recapitulate well neuropathic and myopathic features associated to mutated HSPB1 (Bouhy et al., 2016; d'Ydewalle et al., 2011).

HSPB2 (or MKBP) with its 20 kDa molecular weight is the HSPB with the lowest homology among HSPBs family. Interestingly, its gene is located near the HSPB5 gene, in the

opposite direction in the 5' flanking region, and this might be due to an ancestral gene duplication (Iwaki et al., 1997). HSPB2 is predominantly expressed in cardiac and skeletal muscle where it localizes in the cardiac intercalated discs, in Z-disc and in neuromuscular junctions (Shama et al., 1999; Sugiyama et al., 2000; Suzuki et al., 1998). In muscle cells, HSPB2 is found in mitochondria, exerting a protective activity during stress, as suggested by the evidence of mitochondrial alteration in mice models of HSPB2 deficiency after ischemia/reperfusion, while an enhanced protection against stress when HSPB2 is overexpressed.

HSPB2 activity is strictly related to **HSPB3** (HSP27L), which is the smallest HSPB with its 17 kDa molecular weight (Boelens et al., 1998; Grose et al., 2015; Ishiwata et al., 2012). Similarly, HSPB3 is expressed in cardiac and skeletal muscle, but also in smooth muscle and nervous system. HSPB2 and HSPB3 interact by forming a 3:1 ratio hetero tetramer, which subsequently oligomerizes (den Engelsman et al., 2009; Sugiyama et al., 2000). Interestingly, both HSPB2 and HSPB3 are not upregulated upon thermal stress. HSPB2 in concert with HSPB3 associates to several cytoskeletal elements in muscle cells, such as actin, myosin, titin and filamin, suggesting a role in contractile structures maintenance (Grose et al., 2015). Moreover, HSPB2 C-terminus drives its compartmentalization in membraneless organelles in a process named liquid-liquid phase separation (LLPS) (Morelli, Verbeek, et al., 2017). These HSPB2 containing droplet-like structures are found both in cytoplasm and nuclei and their formation seems to be negatively regulated by HSPB3. Indeed, increased levels of HSPB2 through its overexpression enhance the formation of these nuclear compartments causing an aberrant distribution of chromatin and lamin A and alteration of transcription (Morelli, Verbeek, et al., 2017). Outside muscle cells, HSPB2 and HSPB3 activities might be independent from hetero oligomerization. In neurons, HSPB3 localizes in the cytosol where it associates to actin, neurofilaments and mitochondria (La Padula et al., 2016). HSPB2 mutations have not been yet described. Instead, four HSPB3 dominant mutations have been found in neuropathies and myopathies. In particular, the N-terminus mutation R7S, which does not alter HSPB2-HSPB3 hetero dimerization, but impacts on oligomerization, has been related to dHMN (Kolb et al., 2010). Mutations R116P and Y118H are causative of axonal neuropathy and myopathy, and CMT2, respectively. These mutations fall in the dimerization surface in the ACD and determine the loss of interaction with HSPB2 partner (Nam et al., 2018). Moreover, the R116P mutation, which is topologically equivalent to R140G mutation in HSPB1, associates to HSPB3 aggregation and abnormal HSPB2 phase separation in nuclei (Morelli, Verbeek, et al., 2017). Finally, the HSPB3 frameshift pL34Ffs*50 mutation, which causes HSPB3

destabilization and its proteasomal degradation, was found in patients affected by myopathy.

HSPB4 (α A-crystallin, CRYAA) and **HSPB5** (α B-crystallin, CRYAB) are highly expressed in lenses. Lens fiber cells are post-mitotic cells, characterized by the absence of most of the light scattering intracellular organelles, such as nuclei and mitochondria, in order to guarantee the lens transparency (Bassnett, 2009). This means that most of the lens proteins are synthesized during early life and remain for the whole life. The most abundant proteins in lens are α -, β -, γ - crystallins and form the liquid-like structures of lenses. In order to maintain lens transparency, the α -crystallins HSPB4 and HSPB5, which represent one-third of total soluble proteins, exert an anti-aggregating activity against proteins that get damaged during aging (Kumar & Reddy, 2009). In lenses, HSPB4 and HSPB5 interact with cytoskeletal components, regulating the assembly and stability. For instance, they prevent intermediate filaments incorrect interaction, avoiding gel formation; they protect actin against stress and participate to actin dynamics in lamellipodia in lens epithelial cells; they stabilize the microtubules network (Andley, 2007). Another role ascribed to HSPB4 and HSPB5 consists in their pro-survival activity in response to stressors, such as thermal stress or UV-light. It has been demonstrated that HSPB4 and HSPB5 both abrogate UVA-induced apoptosis, by activating the AKT pathway and suppressing the RAF-MEK-ERK pathway, respectively. Moreover, both HSPB4 and HSPB5 interact with the pro-apoptotic proteins Bax, Bcl-Xs and caspase-3, inhibiting their activity (Andley, 2007). Interestingly, HSPB4 expression is confined in lenses and is synthesized later in respect to HSPB5 (Srinivas et al., 2008). Instead, HSPB5 is also expressed in skeletal and cardiac muscle cells and interacts with HSPB1, HSPB6 and HSPB8. In cardiac muscle, HSPB5 interacts with and maintains the correct folding of titin, a structural protein involved in muscle fibers integrity (Bullard et al., 2004). HSPB5 overexpression is associated to less cardiac tissue damage and better contractile function (Golenhofen et al., 1999). HSPB5 is also expressed in the central nervous system and its expression increases during life. HSPB5 is especially found in white matter, where it might exert a protective effect on myelin sheets (Quraisha et al., 2008). HSPB5 studies on neuroprotection against NDs show that HSPB5 possesses an antiaggregating activity against β -amyloid, α -synuclein and mutated SOD1, the misfolded proteins causative of AD, PD and ALS (Shammas et al., 2011; Waudby et al., 2010; Yerbury et al., 2013). Mutations in HSPB4 and HSPB5 have been reported and related to cataracts, myopathies, and cardiomyopathies, in line with their expression profile. HSPB4 mutations can be found along the whole structure of the protein: the N-terminus mutation W9X is associated to cataracts at early age, but heterozygous carriers do not develop the disease, suggesting that the wildtype allele is sufficient to compensate the loss of function of the

mutated allele (Pras et al., 2000); other mutations at conserved arginine residues at the N-terminus have been found associated to cataracts (Graw, 2009); mutations in conserved residues of the ACD have been also found: the G98R mutation, which might determine a misfolding or destabilization of the HSPB4, causes a dominant phenotype characterized by progressive cataracts at young age, while the R116C, which falls in a conserved residue fundamental for correct dimerization, is associated to congenital cataracts (Shroff et al., 2000). HSPB4 mutation phenotypes are in line with the double KO mouse model, which develops cataracts at early age (Brady et al., 1997). HSPB5 mutations at the N-terminus are associated to a dominant (R11H, P20S) or recessive (R56W) cataracts phenotype, likely due to a toxic gain of function of the mutated HSPB5, since the double KO mouse does not show any signs of lens defects. N-terminus mutations are not associated to muscle defects, suggesting that, N-terminal HSPB5 mutants are still functional. Instead, when the C-terminus is affected by mutations, a mild late onset cardiomyopathy (dominant mutants G154S or R157H) or congenital cataracts (A171T) are observed (Clark et al., 2012). HSPB5 ACD dominant mutations R120G (topologically equivalent to R116 in HSPB4) and D109H have been associated to myopathy, cardiomyopathy, and cataracts (Sacconi et al., 2012; Vicart et al., 1998). These two residues, together with the D140 residue, which is also found mutated and associated to dominant cataract (D140N), are fundamental for the structure of the ACD domain and its role in dimerization (Clark et al., 2011; Liu et al., 2006). Indeed, similar to what observed for the HSPB1 R140G mutant, the R120G mutation is associated to an increase in HSPB5 oligomers size and low dissociation of dimers. Studies in cells have demonstrated that the R120G mutation causes a loss of function in chaperone activity and coaggregation with the muscle structural protein DES in inclusion bodies. Frameshift or truncating mutations have been also found in HSPB5: homozygous frameshifts at the N-terminus or in the ACD have been associated to stiff baby syndrome with early death with no defects in lenses (Del Bigio et al., 2011; Forrest et al., 2011). Frameshift or truncating mutations at the C-terminus might cause defects in hetero oligomers assembly without affecting the ACD function and have been associated to a dominant myopathy; a frameshift mutation in the ACD, which results in HSPB5 misfolding and destabilization, has been associated to congenital cataract (Clark et al., 2012).

HSPB6 (HSP20), with a molecular weight of 17 kDa, is constitutively expressed in a wide variety of tissues but is predominant in smooth, cardiac and skeletal muscle cells, localizing in the cytoplasm (Brophy et al., 1999; Fan & Kranias, 2011; Kato et al., 1994). HSPB6 is found predominantly as a dimer in solution and forms hetero oligomers with the other HSPBs (HSPB1, HSPB5, HSPB2 and HSPB8) (Bukach et al., 2004; Kato et al., 1994). HSPB6 oligomerization and chaperone activity are likely regulated by its Ser-16

phosphorylation. In cardiomyocytes, HSPB6 colocalizes with HSPB5 in cytoskeletal structures and translocates in the nucleus during heat stress or in contractile structures after ischemic damage (Pipkin et al., 2003). Similarly, HSPB6 associates to actin fibers after proteasome inhibition in myoblasts (Verschuure et al., 2002). Of note, its expression seems not upregulated by heat shock, but by other stressors, such as LPS or exercise training (Boluyt et al., 2006; Wang et al., 2009). In the nervous system, HSPB6 shows an increased expression during development and, in hippocampus, upon oxidative or hyperosmotic stress (Bartelt-Kirbach & Golenhofen, 2014; Verschuure et al., 2003). When overexpressed, HSPB6 is neuroprotective. For instance, in neurons, HSPB6 exerts its chaperone activity by preventing β -amyloid and α -synuclein fibrils formations, similarly to what observed for HSPB5, and by counteracting cell damage upon ischemic injury both in brain and spinal cord (Bruinsma et al., 2011; Cameron et al., 2014; He et al., 2015; Lee et al., 2006; Zeng et al., 2010). In muscle tissues, HSPB6 regulates smooth muscle contraction and relaxation: it has been observed that during muscle contraction unphosphorylated HSPB6 stabilizes actin fibers by binding to F-actin and α -actinin, while its phosphorylation and unbinding to F-actin promote smooth muscle cells relaxation (Brophy et al., 1999). In cardiomyocytes, it has been reported that phosphorylated HSPB6 exerts an anti-apoptotic activity. Indeed, a phosphomimic of phosphorylated HSPB6 (S16D) increases the protection against apoptosis, while phospho-null S16A mutant does not exert any protective activities (Bukach et al., 2004; Fan & Kranias, 2011; Qian et al., 2009). Moreover, the naturally occurring DCM-related mutant P20L, which is associated to decreased HSPB6 phosphorylation, shows a loss of protective activity against apoptosis (Nicolaou et al., 2008). HSPB6 shows another cardiovascular protective activity: plasma HSPB6, which is secreted within exosomes by cardiomyocytes and artery walls, can inhibit thrombin-mediated platelet aggregation by blocking calcium influx (Kozawa et al., 2002; Matsuno et al., 1998).

HSPB7, also known as cardiovascular (cv)HSP, is highly expressed in myogenic tissues, mainly in heart. Like other HSPBs, it homo- and hetero- oligomerizes, and oligomerization is driven by dimerization through cysteine residues at position 125 (Yang et al., 2011). In cells, HSPB7 interacts with filamin A, actin binding proteins and monomeric actin, modulating F-actin polymerization and facilitating the turnover of damaged cytoskeletal elements (Wu et al., 2017). It has been also found in nuclei, in SC35 splicing speckles (Vos et al., 2009). As the other HSPBs, HSPB7 has a chaperone activity toward misfolded and aggregating prone proteins, such as polyQ-Htt and mutated parkin (Vos et al., 2010). However, its function seems not to be fundamental in NDs since its expression in the nervous system is low. Instead, as suggested by its alternative name, its activity is vital in cardiac muscle. HSPB7 KO in Zebrafish determines an abnormal cardiac morphogenesis, while in mice, both global

and cardiac-specific KO are embryonic lethal, with embryos characterized by small hearts, thinner ventricular walls, and abnormal actin bundles (Liao et al., 2017; Mercer et al., 2018; Rosenfeld et al., 2013). When KO is induced at later stages, mice develop cardiac arrhythmia and show filamin C aggregates in cardiomyocytes (Liao et al., 2017). Cardioprotective activity of HSPB7 is supported by the findings that HSPB7 variants have been associated to DCM and idiopathic heart failure (Cappola et al., 2010; Matkovich et al., 2010; Wang et al., 2016). HSPB7 exerts its anti-aggregating activity also in skeletal muscle and it is upregulated during aging (Doran et al., 2007). Skeletal muscle-specific KO mouse develops a progressive myopathy phenotype, likely related to autophagic dysfunction (Juo et al., 2016). HSPB7 link to autophagy needs further investigation, but it is likely independent to BAG3-mediated autophagy, since HSPB7, unlike HSPB8, HSPB5 and HSPB6, does not interact with BAG3 co-chaperone (Fang, Bogomolovas, Trexler, et al., 2019).

HSPB9 (CT51) and **HSPB10** (ODF1) are testis specific HSPBs and have a molecular weight of 17.5 kDa and 27 kDa, respectively. Their expression increases with age and is heat-shock inducible (Fontaine et al., 2003; Xun et al., 2015). As their expression is confined to testis and are not involved in muscle and neuronal diseases, such as the other HSPBs, studies on HSPB9 and HSPB10 are missing. The few studies performed revealed that HSPB9 is a cancer/testis antigen and might be a useful marker in cancer field (de Wit et al., 2004). Instead, studies on HSPB10 revealed that its KO results in infertility in mice, which is due to an impaired head to tail connection and unordered mitochondria in spermatozoa (Yang et al., 2012).

Name	Synonyms	Monomeric mass (kDa)	Oligomeric state of isolated protein (Mymrikov et al. 2017)	Main phosphorylation sites	Disease-associated missense mutations (Boncoraglio et al. 2012)
HSPB1	HSP27 HSP25 HSP28	22.8	Large oligomers, size depends on phosphorylation state	S15 S78 S82	G34R; P39L; E42K; G84R; L99M; R127W; S135F; R136W; R140G ; K141Q; T164A; T180I; P182L; P182S; R188W
HSPB2	MKBP	20.2	Small oligomers, tetramers with HSPB3		
HSPB3		17.0	Dimer/trimer tetramers with HSPB2		R7S; R116P
HSPB4	α A-Crystallin	19.9	Large oligomers	S45 S122	R49C; R54P; R116H ; R116C
HSPB5	α B-Crystallin	20.2	Large oligomers, size depends on phosphorylation	S19 S45 S59	P20S; R120G ; D140N; R157H; G157S
HSPB6	HSP20 p20	16.8	Dimer		
HSPB7	cvHSP	18.6	Dimer		
HSPB8	HSP22 H11 E2IG1	21.6	Monomer/dimer	S24 T87	K141E ; K141N ; K141T

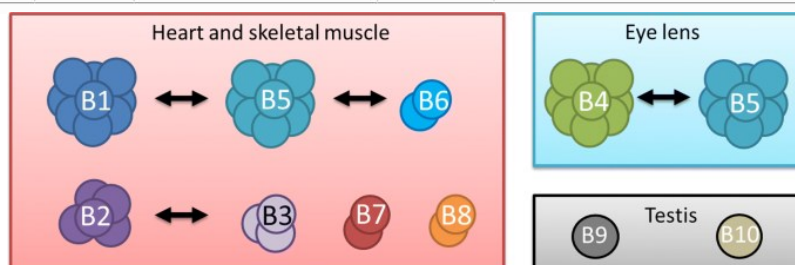


Figure 1. 11 List of HSPBs and schematic representation of oligomerization.

(Top) Alternative names, molecular weight, oligomeric state, phosphorylation sites and disease-associated mutations are reported. (Bottom) Representation of homo- and hetero- dimerization/oligomerization and interactions of HSPBs. Authors represented the number of subunits as an indicator of the size of HSPBs oligomers, explaining that the complex size of HSPB9 and HSPB10 oligomers is not known yet. Squared frames indicate the predominant tissue localization of the HSPBs. (From Boelens, 2020).

```

HSPB1 -----MTERRVFFSLLRGP---SWDPPFRDWYPHSRLFDQAFGLPRLP
HSPB2 -----MSGRSVPHAHATA---EYEFAN---FSRLGEQRFGGLLP
HSPB3 -----MAKTIIRHLIEIP---VRYQEEFEARGLEDCLRDLHALYA
HSPB4 -----MDVTIQHPWFKRT---LGPFFY---FSRLFDQDFGGLFE
HSPB5 -----MDIATHHPWIRRP---FFPFHS---FSRLFDQDFGGLLE
HSPB6 -----METIPVPVQPSWLRRA-SAPLPGLSAPGRLFDQDFGGLLE
HSPB7 -----MSHRTSSTFRAERSFHSSSSSSSSSSSSSASRALPAQDPPEKAL
HSPB8 -----MADGQMPFSCHY---PSRLRRDPPFRDPSLSRRLDDGFGMDPFP
HSPB9 -----MQRVGNFTFSNE-----SRVASRCPSVGLAE
HSPB10 MAALSCLLDSVRRDIKKVDRELRLQLRCIDFSTRCLCDLYMHPYCCCDLHPYPYGLCYSKRSRSCGLCD

```

```

HSPB1 EEWSQLWGGSSWPGYVRPLPPAAIESPAVAAPAYSRALSRQLSSGVSEIRHTADRWRVSLDVNHFAPDE
HSPB2 EEILT---PTLYHGYYVRPRAAPAGEG-----SRAGASELRRLSEGKFOAFLDVSHFTPDE
HSPB3 LPGPTIVDLRKTRAAQSPVDSAAE-----TPPREGKSHFOILLDVVQFIPED
HSPB4 YDLLPFLSSTISPYRQSLFRT-----VLDSGISEVRSRDRKVFIFLDVKHFSPE
HSPB5 SDLFP-TSTSLSPFYLRPPSFLRAPS-----WFDTLGSEMRLEKDRFSVNLVDVKHFSPEE
HSPB6 AELAALCPTTLAPYYLRAPSVALP-----VAQVPTDPGHFSVLLDVKHFSPEE
HSPB7 SMFSDDFGSFMRPHSEPLAFPARPG-----GAGNIKTLGDAYEFAVDVRFDFSPED
HSPB8 DDLTASWPDWALP-RLSSAWPGTLRSGMVRGPTATARFGVPAEGRTPPFPPEBWKVCVNVHSEKPEE
HSPB9 RNRVATMPVRLLRDSPAQQE-----DNDHARDGFQMKLDAHGFAPEE
HSPB10 LYPCCLCDYKLYCLRPSLRSLERKAIRAIIEDEKRELAKLRRTNRIASSCCSSNILGSVNVCGEFPDQ

```

```

HSPB1 LTVKTKDGVVEITGKHEERQDEHGY--ISRCFTIRKYT---LPPGVDPTQVSSLSPEGLTVEAPMPKL
HSPB2 VTVRTVDNILEVSARHPQRIDRHGF--VSREFCPTYV---LPADVDPWRVRAALSHDGIINLEAPRGGR
HSPB3 ILLIQTEGWLIIKACHGTRMDEHGF--ISRSFTIRQYK---LPDGVEIKDLSAVLCHDGIIVVEVKDPVG
HSPB4 LTVKVQDDFVEIHGKHNERQDDHGY--ISREFHRRYR---LPSNVDQSALSCLSADGMLTFCGPKIQ
HSPB5 LKVKVLGDVIEVHGKHEERQDEHGF--ISREFHRRYR---IPADVPLTITSLSSDGVLTVNGPRKQ-
HSPB6 IAVKVVGHEVEVHARHEERPDEHGF--VAREFHRRYR---LPPGVDPAAVTALSPEGVLSIQAPASA
HSPB7 IIVTTSNNHIEVRA---EKLAADGT--VMNTFAHKCQ---LPEDVDPTSVTSALREDGSLTIRARRHPH
HSPB8 LMVKTGKGYVEVSGKHEEKQDEGGI--VSKNFTKKIQ---LPAEVDVPTVFAVSLPEGLLIEAPQVPP
HSPB9 LVVQVDGQWLMVTGQQQLDVRDPER--VSYRMSQKVHRKMLPSNLSPTAMTCLTPSGQLWVRGQCVL
HSPB10 VKVRVKDGKVCVSAERENRYDCLGSKKYSYMNICKEFS--LPPCVDEKDVTSYGLGSCVKIIESECYPC

```

HSPB1	ATQSNEI--TIPVTFESRAQLGGPEAAKSDETAAK-----	205
HSPB2	HLDEVNEVYISLLPAPPDPEEEEEAAIVEP-----	182
HSPB3	TK-----	150
HSPB4	GLDATHAERATIPVSREEKPTSAPSS-----	173
HSPB5	---VSGPERTIPTREEKPAVTAAPKK-----	175
HSPB6	<u>QAPPPAAAK</u> -----	160
HSPB7	TEHVQQTFRTEIKI-----	170
HSPB8	YSTFGESSFNNELPQDSQEVCT-----	196
HSPB9	ALPEAQTGPSRPLGSLGSKASNLTR-----	159
HSPB10	TSPCSPCSPCPCNPCPCPNPCSPYDPCNPCYPCGRFSCRKML	250

Figure 1. 12 Alignment of the hHSPBs.

6-7 β -strands form the ACD. The red box indicates the conserved SRLFDQxFG motif in the NTD, while the I/V-X/I/V motif in both NTD and CTD, is highlighted in red. The underlined sequences at the CTD indicate flexible regions. The asterisk refers to the conserved arginine, which is associated to diseases when mutated. In black, residues conserved in 5 or more HSPBs. (From Boelens, 2020).

1.4 HSPB8-BAG3 functions

1.4.1 Chaperone-Assisted Selective Autophagy (CASA)

BAG3 and HSPB8 participate in a selective autophagic pathway for the removal of damaged and misfolded proteins, named CASA, through the formation of **CASA complex**. As mentioned above, the CASA complex is formed by the associated proteins HSPB8 and BAG3 bound to the chaperone HSP70/HSPA and CHIP (describe herein). The role of BAG3 and HSPB8 interaction in the removal of misfolded proteins through autophagy was firstly observed in cells overexpressing proteins with elongated polyQ tracts, such as polyQ-Htt (Carra, Seguin, Lambert, et al., 2008). However, the first description of CASA complex composition and activity was reported in skeletal muscle cells by Arndt and colleagues (Arndt et al., 2010), who demonstrated the importance of the CASA complex in Z-disc maintenance in *Drosophila*. In particular, the authors observed that BAG3, bound to HSPB8 and HSP70/HSPA, favours the disposal of CHIP-ubiquitinated damaged components of the Z-disc structures, such as filamin, through the autophagic receptor SQSTM1/P62. Moreover, CASA complex impairment, as in the case of BAG3 depletion or mutation, resulted in Z-disc disintegration and in a progressive muscle weakness and myopathy. It was later demonstrated that the removal of filamin relies on its tension-induced unfolding in muscle cells exposed to mechanical stress (Ulbricht et al., 2013).

As already mentioned, CASA activity has been also demonstrated to be very efficient against mutated proteins that are prone to misfold and are causative of NDs. For instance, CASA complex activity was found to reduce the accumulation of several mutant proteins carrying an elongated polyQ stretch, such as the polyQ-Htt related to HD, polyQ-ataxin-3 related to Spinocerebellar Ataxia (SCA) and the polyQ-AR related to SBMA disease (Carra et al., 2010; Carra, Seguin, Lambert, et al., 2008; Cicardi et al., 2019; Rusmini et al., 2013). Other misfolded substrates of CASA comprise the β -amyloid protein associated to AD and α -synuclein associated to PD (Bruinsma et al., 2011; Cao et al., 2017; Wilhelmus et al., 2006). Moreover, several mutant or aberrant proteins that are related to ALS are efficiently degraded through CASA and comprise the mutant SOD1 carrying the mutation G93A, the CTFs of TDP-43 (TDP-35 and TDP-25), which mislocalize and aggregate in ALS and Frontotemporal Dementia (FTD), and the DPRs that result from aberrant translation of the expanded G₄C₂ repeated sequence in the *C9ORF72* gene, which are also related to ALS and FTD (Cicardi et al., 2018; Crippa et al., 2016; Crippa et al., 2010; Cristofani et al., 2018).

1.4.2 The other members of CASA complex

HSP70/HSPA

HSP70/HSPAs are a group of 70kDa Heat Shock Proteins which act as a central hub in PQC system. HSP70/HSPAs can bind a wide array of proteins and promote their folding, refolding or degradation. Prokaryotes possess one single isoform of HSP70, named DnaK, while eukaryotes express different isoforms of HSP70/HSPA, such as HSP70-1 (HSPA1, inducible) or HSC70 (HSPA8, constitutive), which show differences in localization and expression profile. HSP70/HSPAs are ATPases that use ATP to promote substrates folding/refolding. The ATP molecule binds to the nucleotide binding domain (NBD) at the N-terminus of the HSP70/HSPA protein. The NBD is a V-shaped domain, and the ATP binding site is enclosed within the two lobes. Besides the NBD, HSP70/HSPAs possess a substrate binding domain (SBD) of 25 kDa, which is formed by two subdomains: a β -sheet structured SBD β domain, named Base, and a α -helical structured SBD α domain, named Lid. The SBD can assume an open or a closed conformation. Client proteins are characterized by the presence of hydrophobic sequences often flanked by positive residues (Rüdiger et al., 1997). In correctly folded proteins, hydrophobic sequences are usually buried in the core protein, while, in unfolded or misfolded proteins, these hydrophobic sequences are exposed and can be recognized by the SBD of HSP70/HSPA. The SBD and NBD are characterized by an allosteric interaction: when the NBD binds ATP, it induces the open conformation of the SBD by separating the Base and the Lid, and the client protein can be bound. Once the client protein binds to the open conformation, the SBD, in turn, induces a conformational change at the NBD interface and ATP hydrolysis. The SBD in its open conformation has a low affinity for the client proteins, but ATP hydrolysis induces the closed conformation. By getting closer, the Base and the Lid entrap the client protein with high affinity and promote its folding/refolding (Qi et al., 2013; Zhuravleva & Gierasch, 2015). HSP70/HSPAs activity is enhanced and regulated by co-chaperones, which are J-domain proteins (JDPs) and NEFs. JDPs, also known as DNAJ/HSP40s, target the client proteins to HSP70/HSPA and potentiate the closed conformation by stimulating HSP70/HSPA ATPase activity and efficient locking of the substrate (Kampinga & Craig, 2010). Instead, NEFs, such as the co-chaperones BAG3 and BAG1, potentiate the closed-to-open conformational change, by favouring ADP dissociation from the NBD for client protein release.

HSP70/HSPAs interacting proteins determine the fate of a client protein. In this manner, HSP70/HSPAs represent a platform for the client and its interacting partners drive its folding, refolding or degradation. For instance, by cooperating with HSP90, HSP70/HSPAs promote the folding of neo-synthesised proteins while, by cooperating with sHSPs and HSP100, HSP70/HSPAs favour the disaggregation of protein aggregates (Mogk et al.,

2018; Wegele et al., 2004). HSP70/HSPAs also help with the degradation of client proteins through the different degradative systems, UPS, chaperone-mediated autophagy (CMA) or CASA pathway. HSP70/HSPA drives proteasomal degradation of client proteins by forming a protein complex with CHIP and BAG1 (Lüders et al., 2000). Instead, by interacting with CHIP, BAG3 and HSPB8, HSP70/HSPA drives CASA-mediated degradation of substrates (Arndt et al., 2010; Rauch et al., 2017), while in CMA, HSP70/HSPA recognizes the KFERQ-motif in client substrates and drives lysosomal internalization of the substrate through the LAMP2A protein complex in the lysosomal membrane (Rout et al., 2014; Terlecky et al., 1992).

While HSP70/HSPAs mutations have not been described, mutations in their co-chaperones can occur. Indeed, beside the previously mentioned BAG3 mutations, also JDPs have been found mutated in diseases that affect muscle or neuronal cells. Noteworthy, the JDPs DNAJB6 and DNAJB2 mutations have been described in myopathies and neuropathies, respectively (Gess et al., 2014; Harms et al., 2012; Sarparanta et al., 2012). In addition, the DNAJB6 has been also found associated to the CASA complex, but its role in CASA has not been elucidated yet (Arndt et al., 2010; Sarparanta et al., 2012).

CHIP

The carboxy-terminus of HSC70 interacting protein (CHIP, STUB1) is a chaperone-associated E3 ligase, which targets HSP70/HSPA- and HSP90- protein clients to degradation (Ballinger et al., 1999). CHIP is a 34.5 kDa evolutionary conserved protein which localizes predominantly in the cytoplasm but is also found in the nucleus. It is highly expressed in tissues characterized by high metabolic activity and high protein turnover, such as skeletal and cardiac muscle and brain. CHIP structure consists in a U-box of approximately 90 amino acids at the C-terminus, the presence of a 34 amino acids domain carrying three pairs of tetratricopeptide repeats (TPRs) at the N-terminus, and a central coiled-coil region, which influences the dimerization and stability. The U-box domain of CHIP binds the E2 ubiquitin conjugating enzymes, while the TPR repeats are responsible for chaperone interaction (Ballinger et al., 1999; Murata et al., 2001; Nikolay et al., 2004). In this manner, CHIP represents a scaffold for chaperone-bound substrate ubiquitination. Up to date, 19 mutations in CHIP have been linked to autosomal recessive SCA (SCAR16) in some families, which is characterized by degeneration of the cerebellum and cognitive impairment (Cordoba et al., 2014; Heimdal et al., 2014; Shi et al., 2013). Mutations occur in the whole structure of CHIP protein, affecting differently the secondary structure, dimerization, oligomerization, or ubiquitination activity. For instance, in vitro experiments show that the N65S mutated CHIP is characterized by an increased dimerization and

impaired ubiquitination activity, while the T246M mutated CHIP is characterized by a complete loss of ubiquitination activity and an aggregation prone behaviour (Pakdaman et al., 2017). Overall, most of CHIP mutations are characterized by a decreased stability and activity in vitro and likely in vivo (Kanack et al., 2018). Indeed, loss of CHIP by genetic depletion determines a 20% of death at embryonic stages in mice, while 100% of mice fail to survive thermal stress (Dai et al., 2003). Moreover, it has been reported that CHIP genetic depletion determines an early aging phenotype in mice (Min et al., 2008). On the other hand, CHIP overexpression improves the clearance of aggregate prone proteins such as polyQ-AR, ataxin-1, α -synuclein and mutant SOD1 (Adachi et al., 2007; Al-Ramahi et al., 2006; Miller et al., 2005; Tetzlaff et al., 2008; Urushitani et al., 2004).

1.4.3 CASA complex dynamics

The working model of CASA dynamic establishes that the misfolded or unfolded substrate is recognized by the chaperones HSP70/HSPA and HSPB8. It is not yet clear how these chaperones can bind to different substrates, but it is widely accepted that chaperone binding to clients relies on the exposure of hydrophobic patches by the misfolded substrate. The chaperone binds to the misfolded protein, whereas BAG3 acts as a scaffold for the interaction with all other CASA members. The sorting of the substrate toward the autophagic pathway requires the ubiquitination activity of CHIP, interacting with HSP70/HSPA. Once the substrate is ubiquitinated by CHIP, the autophagic receptor SQSTM1/P62 interacts with the polyUb chain through its UBA domain (Arndt et al., 2010). The substrate is therefore targeted to the MTOC, by taking advantage of the interaction between the PxxP domain of BAG3 and the molecular motor dynein; at the MTOC, aggresomes are generated and most nascent autophagosomes are present (**Fig. 1.14**). Alternatively, it has been recently described another mechanism of CASA dynamic, which is based on HSPB8 direct recognition of SQSTM1/P62-regulated ubiquitinated microaggregates. In this model, HSPB8 acts in the early response to stress by concentrating misfolded and ubiquitinated substrates into microaggregates and assists SQSTM1/P62 oligomerization. In this pathway, HSPB8 favours the efficient coupling of BAG3 to SQSTM1/P62 for ubiquitinated microaggregates transport to the aggresome. Noteworthy, these two mechanisms that describe CASA early stages are not mutually exclusive. In fact, it has been proposed that HSP70/HSPA mediates CASA under basal conditions, while HSPB8 activity becomes fundamental under severe proteotoxic stress (Gamerding, Kaya, et al., 2011; Guilbert et al., 2018).

As mentioned above, routing to aggresome occurs through the dynein-mediated retrograde active transport of the CASA complex and the bound substrate along the microtubules network. Indeed, drugs that impair microtubules network, such as the microtubule-

depolymerizing drugs vinblastine or nocodazole, suppress aggresome formation (Gamerding, Kaya, et al., 2011; Guilbert et al., 2018). In addition, inhibition of retrograde transport blocks the BAG3-mediated routing of CASA cargo. This can be achieved by silencing dynein subunits, such as DYNC1H1, by overexpressing inhibitory p50/dynamitin subunit or by using drugs that inhibit the ATPase and motor activity of dynein, such as erythro-9-[3-2-(hydroxynonyl)] adenine (EHNA) or ciliobrevin D (Cristofani et al., 2017; García-Mata et al., 1999; Guilbert et al., 2018). The BAG3-dynein coupling occurs through the PxxP domain of BAG3, and the PxxP deletion abrogates dynein interaction and therefore aggresome formation (Gamerding, Kaya, et al., 2011). However, BAG3-dynein coupling might occur also indirectly through the 14-3-3 protein interaction, which is engaged by BAG3 through its two RSQS136 and RSQS173 motifs (Xu et al., 2013). Of note, BAG3 mediated aggresome formation requires its interaction with HSPB8 and HSP70/HSPA, as deletion of both IPV domains or BAG domain suppresses BAG3-mediated substrates targeting to aggresome (Gamerding, Kaya, et al., 2011; Guilbert et al., 2018).

Aggresomes, which are aggregates of aggregates, are the result of an active compartmentalization process of misfolded proteins. In fact, electron microscopy revealed that they are not a single large aggregate, but an accumulation of aggregated particles loosely associated with each other (García-Mata et al., 1999). The morphology and composition of aggresomes are dependent on the cell type and the aggregating substrate. For instance, some cells show a single round-shaped aggresome with a diameter between 1-3 μm while other cells show a ribbon-like or a crown-like structure surrounding the nucleus (García-Mata et al., 2002; Hu et al., 2020). Aggresome formation implicates the rearrangement of the cytoskeleton. In particular, intermediate filaments form a cage-like structure surrounding the aggresome and are also used as aggresome markers. The type of intermediate filaments depends on the cell type: epithelial cells show aggresomes surrounded by vimentin, glial cells by GFAP and neuronal cells by neurofilaments. Intermediate filaments rearrangement around the aggresomal structures is necessary for the recruitment of PQC system members, such as chaperones and proteasomes, and therefore for restoring proteostasis. Moreover, it has been reported that vimentin rearrangement during aggresome formation plays a fundamental role during neurogenesis, as it permits neural stem cells to exit quiescence and to undergo asymmetrical segregation of proteasomes during mitosis (Morrow et al., 2020). Other cytoskeletal components that can be found in aggresomes are γ -tubulin and pericentrin (Johnston et al., 1998). Although aggresomes were firstly described as cells junkyard, they are dynamic deposits of protein aggregates that recruit cytosolic PQC members to remove misfolded substrates. Indeed, it has been firstly demonstrated that the MTOC represents a specialized site for protein

degradation, also called degrasome, where misfolded proteins are routed for proteasomal degradation and this is supported by the constitutive presence of a fraction of proteasomes and chaperones at the MTOC (Wigley et al., 1999). Based on these observations, aggresomes are thought to be simply the visible result of an increase in misfolded protein load or an impairment in the proteostasis network. However, aggresomal deposits must be somehow removed. Since proteasomes cannot efficiently clear big protein aggregates, autophagic degradation permits the engulfment and disposal of aggregates in bulk. It remains an open question if aggresomes exert a cytotoxic effect, but a few pathogenic mechanisms have been hypothesized: first, misfolded proteins within the aggresome sequester PQC members which are no longer able to exert their basal physiological activity in proteostasis maintenance. Second, misfolded proteins can co-aggregate with their correctly folded counterpart or with proteins carrying the same structural determinants. For instance, it has been observed that the misfolded polyQ-Htt co-aggregated with its wildtype counterpart and with other proteins carrying polyQ stretches (Huang et al., 1998; Rajan et al., 2001). Third, since aggresome formation is driven by the activity of the dynein motor complex along microtubules, intracellular trafficking of essential components might be impaired by an overload on microtubules tracks. This is supported by the fact that the impairment in intracellular trafficking is a common pathogenic mechanism of several NDs.

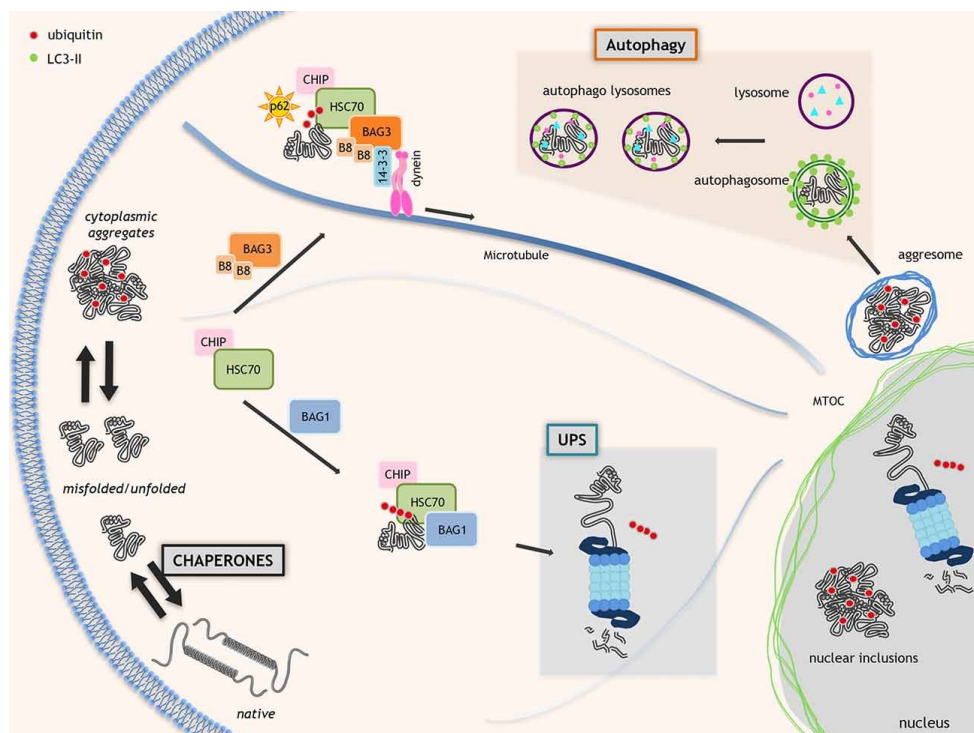


Figure 1. 14 HSPB8 and BAG3 functions in CASA.

CASA acts in the removal of misfolded and aggregating proteins. Substrates are recognized by chaperone HSPB8. CASA complex formation relies on the BAG3 protein, which acts as a scaffold protein, interacting with HSPB8, HSP70/HSPA and the dynein motor complex. Substrates undergo refolding by HSP70/HSPA action. If refolding fails, substrates are ubiquitinated by CHIP and routed to the MTOC, where aggresomes form, and degraded by lysosomes. (From Rusmini P et al., 2017).

1.4.4 Granulostasis

HSPB8-BAG3 complex roles in cellular homeostasis comprise also granulostasis, which is the process of SGs quality control in their composition and dynamics (**Fig. 1.15**). SGs are cytoplasmic membraneless organelles composed of stalled mRNA during translation process, translation initiation factors and several RBPs (Buchan & Parker, 2009). SGs assemble through a LLPS process, which consists in the demixing of two stably coexisting phases, one dense and one diluted, once a solution becomes over-saturated. The dense phase, composed of RBPs and RNAs, continuously exchanges materials with the dilute phase (P. Li et al., 2012). RBPs that promote LLPS are usually proteins carrying low complexity sequences, also known as prion-like domains, which are intrinsically disordered regions prone to aggregate (Molliex et al., 2015). Examples of such proteins are TIA-1, hnRNPA1 and Fused in Sarcoma (FUS). Unsurprisingly, mutations in FUS or hnRNPA1 are causative of ALS and FTD and accelerate the conversion of liquid-like SGs structures into an aggregate state, while SGs components, such as TIA-1, are found in ALS pathological inclusions (Monahan et al., 2016). SGs physiologically form in response to several stressors, such as oxidative stress, proteasome inhibition or heat shock, to shut down the translation of unnecessary mRNAs and promote the translation of genes involved in stress response, such as PQC factors. Shutting down translation requires the phosphorylation of the initiator factor eIF2 α for polyribosome disassembly. Released mRNAs and RBPs are then sequestered in SGs until the normal cell functions are restored. During polyribosome disassembly, newly synthesized polypeptides are also released. However, a relevant fraction of these polypeptides is characterized by co-translational misfolding, premature termination events, amino acids misincorporation or other defects. This fraction represents the so-called DRiPs, which are the main source of misfolded proteins in cells, but are generally promptly recognized by members of the PQC system, such as HSP70/HSPA or the Valosin-Containing Protein (VCP), and targeted to degradation through UPS or autophagy. When DRiPs sorting and degradation are impaired (e.g., VCP or HSP70/HSPA depletion), they accumulate into SGs, which become persistent and lose their dynamics. In this context, HSPB8-BAG3-HSP70 complex participates in granulostasis. Indeed, aberrant and persistent SGs, which might contain DRiPs or mutated RBPs, are recognized and disassembled by the HSPB8-BAG3-HSP70 complex. It has been proposed that HSPB8-BAG3-HSP70 complex acts in a two-step process: first, HSPB8 dissociates from BAG3-HSP70 and is recruited to SGs in response to stress, such as proteasome inhibition (MG-132 treatment) or oxidative stress (Arsenite treatment). Here, HSPB8 acts as a holdase, preventing the irreversible aggregation of misfolded substrates or DRiPs into SGs. Second, HSPB8 recruits BAG3-HSP70 machinery, which extracts misfolded substrates from SGs.

Hence, misfolded substrates are subjected to degradation or targeted to the aggresome for subsequent disposal (Ganassi et al., 2016; Mateju et al., 2017). In these manner, HSPB8-BAG3-HSP70 complex promotes granulostasis by separating DRiPs or other misfolded substrates from SGs rather than SGs degradation. Instead, SGs degradation occurs through the autophagic pathway when HSPB8-BAG3-HSP70 machinery is impaired.

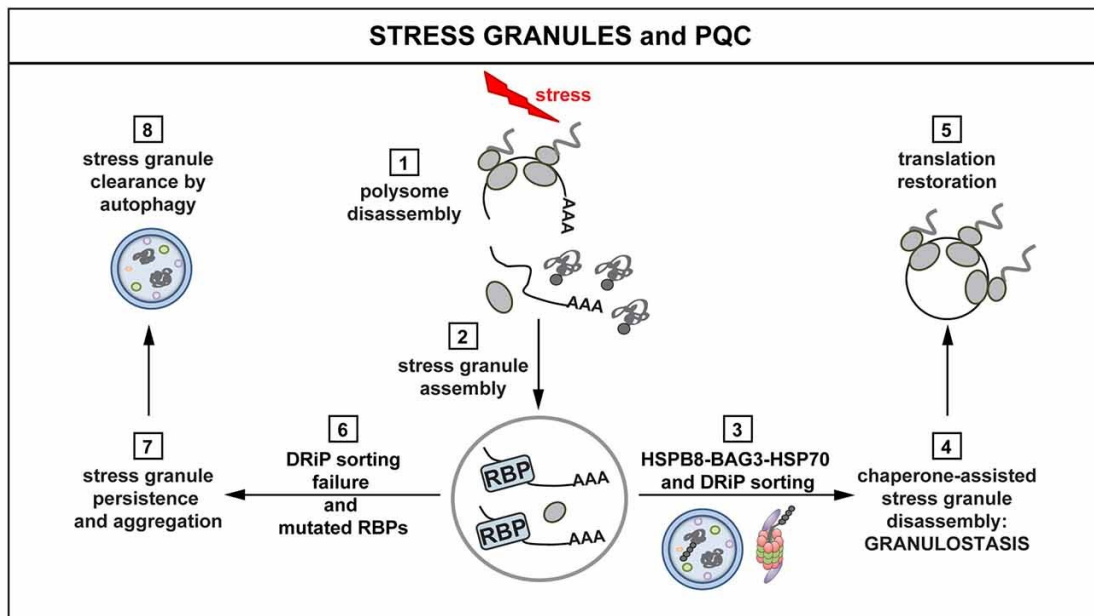


Figure 1. 15 Role of HSPB8-BAG3 and HSP70 in SGs.

Upon stress, polysome disassembles (1) and mRNAs are packaged into SGs (2). HSPB8-BAG3-HSP70 complex assures granulostasis by limiting misfolded proteins and DRiPs accumulation in SGs (3,4), therefore favouring the restoration of translation processes (5). If HSPB8-BAG3-HSP70 activity is impaired or when RBPs are mutated (e.g., disease-associated mutations) (6), DRiPs accumulate in SGs, leading to the presence of persistent and less dynamic SGs (7), which must be removed through autophagy. (From Alberti, Mateju, Mediani, & Carra, 2017).

1.4.5 Cell division

As previously said, CASA complex has been involved in cytoskeletal maintenance and dynamics. Beside the well described role of CASA complex in assuring the integrity of the actin-contraction structure of the sarcomere in muscle cell, it has been recently described a novel function of BAG3-HSPB8 in cell division. Cell division is characterized by a drastic rearrangement of cytoskeletal structures: at the onset of mitosis, actin remodelling into a stiff actin cortex determines cell retraction and rounding; thin actin fibers, called retraction fibers, attach to the substrate and guide spindle orientation parallel to the substrate. Correct orientation of mitotic spindle is necessary to mitotic progression and chromosome segregation. It has been demonstrated that BAG3 and HSPB8 contribute to the homeostasis of actin structures during mitosis. Indeed, BAG3, with HSPB8, localizes at the separating centrosomes or in the perinuclear material before nuclear envelope breakdown

and then at centrosomes at spindle poles during metaphase through anaphase transition. Of note, BAG3 is found hyperphosphorylated at the mitosis entry and is associated to HSPB8, SQSTM1/P62 and HDAC6. It has been reported that BAG3 depletion decreases the incidence of cell division, slows down mitotic process, and causes an increase in nuclear abnormalities such as micronucleation or multinucleation, which are hallmarks of improper mitosis and cytokinesis. In fact, aberrant positioning of mitotic spindle associated to a misalignment of chromosome was observed in BAG3 depleted cells. Interestingly, similar observation of defective mitotic spindle orientation and chromosome segregation arose in HSPB8 and SQSTM1/P62 depleted cells, as a result of actin cortex disorganization. Noteworthy, mitotic spindle dynamics of BAG3 are independent of HSP70/HSPA interaction. In fact, deletion of the IPVs, PxxP and BAG key domains in BAG3 protein resulted in a delayed mitosis, as observed for BAG3 complete depletion, but the use of the R480A BAG3 mutant, which specifically abolished HSP70/HSPA interaction, did not lead to an impairment of the mitotic process (Fuchs et al., 2015).

Besides mitotic spindle orientation and mitosis, BAG3 and HSPB8 act also in the latest phase of cell division, that is the cytokinesis. Cytokinesis consists in the abscission of daughter cells through the formation of an actomyosin ring. This actomyosin ring leads to the formation of an intracellular bridge that connects the two nascent daughter cells. To finalize cell division, this intracellular bridge must get thinner and thinner until complete cleavage and this event occurs with actin depolymerization. It has been demonstrated that BAG3 and HSPB8 depletion associates to a higher incidence and persistence of abnormally thick and long intracellular bridges, suggesting a role of HSPB8 and BAG3 in actin dynamics in cytokinetic structures. In particular, HSPB8 depletion was associated to an aberrant accumulation of F-actin at the intracellular bridges. This phenotype was reverted by limiting the pool of free G-actin or by inhibiting the Arp2/3 complex, which promotes actin polymerization. Noteworthy, Arp2/3 complex component ArpC2 has been found in BAG3 interactome studies. It has been suggested that HSPB8-BAG3 complex activity in cytokinesis consists in facilitating the autophagic clearance of actin-based structures. Indeed, autophagic activator drug rapamycin was able to prevent aberrant F-actin accumulation in HSPB8-depleted cells (Varlet et al., 2017).

1.5 A focused overview on diseases that affect motoneurons and muscle cells

Protein aggregation and PQC impairment are main features of diseases that affect MNs and muscle cells. Since MNs, as other neuronal cells, are post-mitotic cells and cannot be replaced, the nervous system is more vulnerable to damage and cell-loss than other tissues. In addition, MNs axons, that can reach 1 meter of length, make the delicate MNs architecture difficult to maintain. Similarly, skeletal muscle cells are post-mitotic and characterized by a low cellular turnover. The high metabolic activity and the damaging action of mechanical and other stressors against its structural proteome, must be efficiently counteracted by the PQC system. Mutations in PQC members, but also in components involved in cytoskeleton structures and intracellular trafficking are frequently causative of motor neurons diseases (MNDs) and muscle diseases. In the following sections, a brief overview of these diseases and the underlying genetics will be discussed, highlighting the overlap in genetic causes and pathomechanisms.

1.5.1 When motoneurons are affected by disease

MNDs represent a wide spectrum of diseases that affect upper (UMNs) and/or lower motoneurons (LMNs). UMNs locate in the motor cortex and project to the bulbar region or the spinal cord, giving rise to the corticobulbar and corticospinal tracts. Instead, LMNs locate in the brainstem and in the anterior horn of the spinal cord and directly innervate the skeletal muscle, through the neuromuscular junctions. One LMN and all the muscle fibers it innervates form a motor unit.

When diseases strike UMNs, clinical manifestations include spasticity, weakness, and hyperreflexia. In contrast, LMNs signs include muscle wasting, flaccidity, hyporeflexia and fasciculations. In addition, patients affected by the same MNDs might show a predominant bulbar involvement, with signs at bulbar muscles such as difficulties in eating, choking, swallowing and breathing, or a predominant spinal cord involvement, with clinical manifestations at the limbs (**Fig. 1.16**). Of note, MNDs can be pure or might show sensory involvement or signs of frontotemporal dysfunction. MNDs can be inherited or acquired (James & Talbot, 2006; Tiryaki & Horak, 2014). Because MNDs comprise a broad range of forms, here I will focus on a small group of diseases showing shared genetic bases (**Fig. 1.17 and 1.18**).

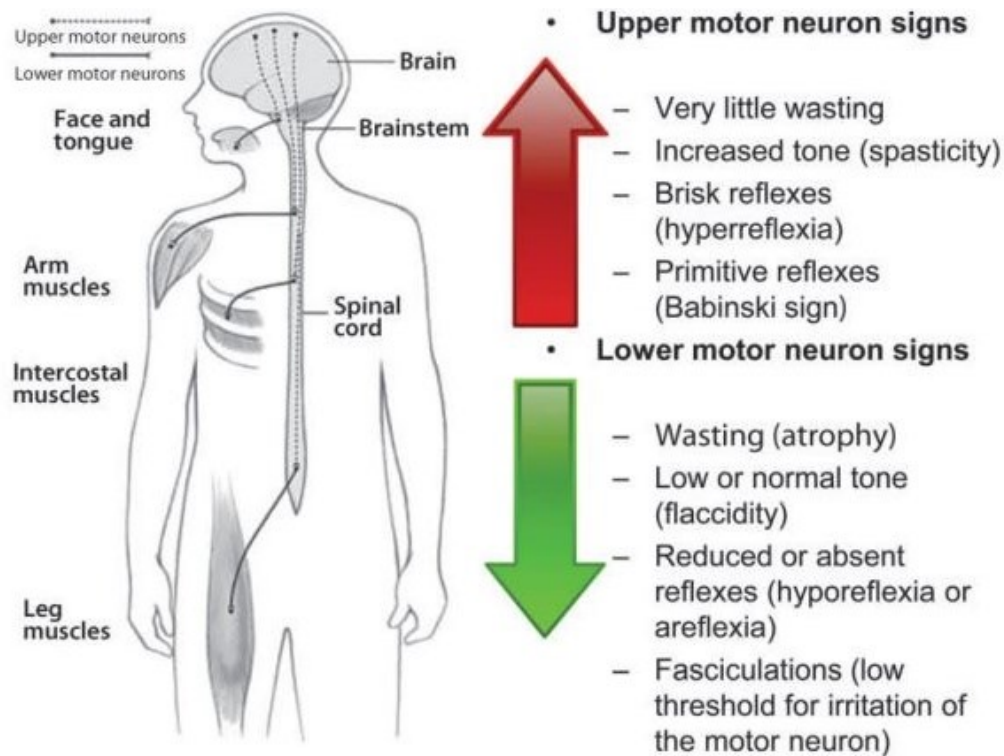


Figure 1. 16 Schematic representation of UMNs and LMNs localization and projection and list of typical UMNs and LMNs signs. (From Tiryaki & Horak, 2014).

When the disease strikes UMNs: Hereditary Spastic Paraplegia

Hereditary Spastic Paraplegias are a clinically and genetically heterogeneous group of inherited neurological disorders in which the main neurological symptoms are lower limb spasticity and weakness. Clinically, it can be classified in pure or complex forms. Pure forms are characterized by isolated pyramidal signs, like paraparesis, quadriparesis and spasticity that can be associated to deep sensory loss. In complex forms, beside the spastic paraplegia phenotypes, other neurological and non-neurological signs can occur, including cerebellar dysfunctions (ataxias and tremors), peripheral neuropathies, cognitive impairment, myopathic features, extrapyramidal signs (parkinsonism and chorea) and psychiatric disorders. Based on the onset, there is a type I form (or early onset) when spasticity occurs before 35 years of age, or type II form (or classical) when the onset occurs in patients older than 35 years. More than 70 genes have been associated to the disease, and the inheritance can be autosomal dominant, autosomal recessive, X-linked, but also dependent on mitochondrial transmission (de Souza et al., 2017). Albeit the several number of disease-causing genes, they can be grouped based on the involvement in a few intracellular pathways, mainly membrane trafficking, organelle shaping, axonal transport, mitochondrial dysfunction, lipid metabolism and myelination. For instance, mutations in the kinesin heavy chain KIF5A have been related to an early onset, pure form of Hereditary Spastic Paraplegia. KIF5A is part of the motor complex responsible for the anterograde

transport of cargos along the microtubules and, in vitro findings on mutated KIF5A, revealed a reduced cargo flux. Mutation in KIF1C and KIF1A have been also described. Over 150 mutations in spastin (SPAST), which is the most common cause of hereditary spastic paraplegia (up to 45% of all cases), have been found. SPAST is a AAA ATPase which catalyses internal breaks in microtubules and might also have a microtubule bundling activity. SPAST is also involved in endosomal trafficking. Indeed, SPAST interacts with CHMP1B, which acts in the endosomal sorting complex and with Atlastin-1, a transmembrane dynamin/guanylate-binding protein, which operates in vesicle trafficking through the ER and Golgi apparatus. Noteworthy, CHMP1B and Atlastin-1 have been also found mutated in patients. A role of the autophagic pathway has also been proposed: a failure in the autophagic lysosome reformation has been observed when spatascin or spastizin are mutated, as reported in some forms of the disease. The two proteins are fundamental in initiation of lysosomal tubulation. Mutations in proteins involved in mitochondria functions have been described. In particular, Paraplegin-1 is a member of the metalloprotease AAA complex, which acts in the PQC and ribosomal assembly regulation in mitochondria. Fibroblasts from patients showed an increase sensitivity to oxidative stress and reduced activity of the respiratory chain. HSPD1 gene, which encodes for the HSP60 and participates in mitochondrial PQC, has been also found mutated (Blackstone, 2018; Boutry et al., 2019; Salinas et al., 2008). Noteworthy, these intracellular pathways interconnect and are also related to other neurological disorders, such as ALS, SCA and CMT. For instance, mutations in KIF5A and spatascin have been reported also in CMT2 and ALS (Boutry et al., 2019; de Souza et al., 2017).

When the disease strikes both UMNs and LMNs: ALS

Amyotrophic Lateral Sclerosis is the most frequent adult onset MND and is characterized by degeneration of both UMNs and LMNs. ALS was described by the neurologist Jean-Martin Charcot in 1869 and is also known as Lou Gehrig's disease, from the name of a famous baseball player who was diagnosed with ALS in 1939. The age of onset is between 40 and late 60 years old. At the onset, ALS patients suffer from spasm and muscle weakness, but rapidly manifest a complete muscular paralysis. Within 2-5 years, most of patients die from respiratory failure. Since both UMNs and LMNs are affected, patients can experience both spasticity, fasciculations, flaccidity, muscle weakness and wasting, hypo and hyper-reflexia symptoms. A spinal onset of the disease is common in about two-third patients, while a bulbar onset involves the remnant one-third (Cleveland & Rothstein, 2001; Grad et al., 2017; Hughes, 1982; Mulder, 1982). ALS patients can suffer from cognitive impairment. Almost 50% of patients are affected by mild cognitive impairments, while 15%

of patients develop FTD. Overlaps in genetics and histopathological findings resulted in a definition of an ALS-FTD spectrum of disease (Abramzon et al., 2020; Bennion Callister & Pickering-Brown, 2014; Kwong et al., 2007). In other cases, patients manifesting PD-like symptoms have been documented. ALS divides into familial (fALS) or sporadic (sALS) form of disease, based on the inheritance. The first form represents less than 10% of cases, while the latter more than 90%. Genetic causes of fALS are ascribed to mutations in the gene encoding the SOD1, in the 20% of fALS cases, in the genes encoding the RBPs TDP-43 or FUS, in the 4% of cases each, and to a hexanucleotide expansion in the *C9ORF72* gene, in the 35% of cases. SOD1 was the first gene found associated to ALS (Rosen, 1993). More than 170 mutations in SOD1 have been described, but the most frequent are the substitutions A4V, G93A, H46R and D90A. Most of the mutations show an autosomal dominant inheritance (Orrell, 2000). The SOD1 gene, which is highly conserved, encodes a 15.9 kDa ubiquitous protein, which localizes both in the cytoplasm, nucleus and mitochondria and acts as a homodimer. SOD1 has an antioxidant activity, which consists in catalysing the conversion of superoxide anions into peroxide hydrogen and oxygen (Bunton-Stasyshyn et al., 2015). Mutated SOD1 is characterized by misfolding and accumulation in insoluble species, which cause cellular damage through oxidative stress and proteostasis impairment mechanisms (Kato et al., 2000; Parone et al., 2013). SOD1 mutations also impact on the enzymatic activity, which is impaired or decreased, and results in a deficiency in oxidative stress response. It has been also demonstrated that mutated SOD1 is associated to mitochondrial damage. Transgenic mice carrying mutated SOD1 show vacuolated mitochondria and cell models show mitochondria depolarization, calcium homeostasis impairment and alterations in mitochondria membrane permeability, which impact on the apoptotic pathway. Another effect on mitochondria is the alteration of ATP levels, which might affect intracellular activity, such as the axonal transport (Pasinelli & Brown, 2006). Other ALS-related mutations involve TDP-43 and FUS, which are RBPs and act in RNA splicing, transport, and stability, and in SGs formation (Y. R. Li et al., 2013; Ratti & Buratti, 2016). TDP-43 is a 43 kDa protein which shuttles from the nucleus to the cytoplasm but resides mainly in the nucleus. TDP-43 possesses two RNA binding motifs (RRM1 and RRM2), a NLS and a putative nuclear export signal (NES). The CTD is a glycine-rich domain, also called prion-like domain because it is a highly disorder unstructured region (Ratti & Buratti, 2016). TDP-43 involvement in ALS dates to 2006, when TDP-43 and its fragments were identified in cytoplasmic protein inclusions in ALS and FTD patients (Neumann et al., 2006). Later, more than 40 TDP-43 mutations have been identified in fALS and sALS patients (Sreedharan et al., 2008). Mutations in TDP-43 are often found in the CTD, causing the destabilisation of the prion-like domain, or in the NLS,

causing TDP-43 cytoplasmic retention. However, also wildtype TDP-43 is characterized by an aberrant behaviour in ALS specimens and models. Pathogenic features of aberrant TDP-43 include its fragmentation forming the CTFs TDP-35 and TDP-25, hyperphosphorylation, ubiquitination and cytoplasmic mislocalization (Buratti, 2018; Ederle & Dormann, 2017). Aberrant TDP-43 is also characterized by a loss of function in the regulation of RNA metabolism. Like TDP-43, FUS is a 53 kDa RBP involved in RNA splicing and transport from the nucleus to the cytoplasm and found mutated in ALS cases (Kwiatkowski et al., 2009; Ratti & Buratti, 2016; Vance et al., 2009). FUS has one RRM, two Arg-Gly-Gly (RRG) repeats, one zinc-finger domain, a NLS and a N-terminal prion-like domain. Most of FUS mutations, up to 46 documented, fall into the prion-like domain, the NLS or the RGG domain (Ratti & Buratti, 2016). FUS mutants are prone to mislocalize into the cytoplasm and form inclusions, which colocalize with TDP-43 (Ederle & Dormann, 2017). C9ORF72 mutation consists in a G₄C₂ hexanucleotide expansion repeat in an intronic region of the *C9ORF72* gene (DeJesus-Hernandez et al., 2011; Renton et al., 2011). The number of repeats in healthy subjects is usually within 5 to 10, while it reaches hundreds, or even thousands repeats in ALS patients. C9ORF72 mutation has been also found in FTD, AD and Lewy bodies dementia. Three main pathogenic mechanisms have been described: a loss of function of the encoded protein due to a decreased expression, a toxic function linked to the accumulation of RNA in RNA foci and a toxicity mediated to the accumulation of DPRs products (Gendron et al., 2013; Mizielinska et al., 2013). C9ORF72 gene product is thought to be physiologically involved in autophagy, endocytosis and in the regulation of the immune response in microglia and macrophages. It has been demonstrated that the decreased expression is not sufficient to neuronal death. Indeed, C9ORF72 KO mice are not characterized by motoneuronal defects nor neuronal degeneration (Koppers et al., 2015; Sudria-Lopez et al., 2016). Instead, RNA foci containing hexanucleotide expansions have been observed in the spinal cord and brain of ALS/FTD patients. In cell and animal models, RNA foci localize in the nuclei, cytoplasm, and neurites. These aberrant RNAs can sequester RBPs, altering RNA metabolism, splicing, and translation (DeJesus-Hernandez et al., 2017). Instead, the accumulation of DPRs is the result of the unconventional translation process called Repeat-associated non-ATG translation (RAN-translation), which is independent from the presence of the ATG initiation codon. RAN-translation permits the codification of the hexanucleotide repeat expansion, whose products consist in five DPRs (poly -GA, -GP, -GR, -PR and -PA), characterized by an unstructured conformation and prone to form nuclear and cytoplasmic inclusions (Davidson et al., 2014). Other proteins whose genes have been found mutated in less than 1% of ALS patients are SQSTM1/p62, ubiquilin-2 (UBQLN2), optineurin (OPTN), VCP. UBQLN2, p62 and OPTN bind

ubiquitinated proteins routing them to the protein degradative systems and can be found in TDP-43- or SOD1- positive inclusions. Instead, VCP is involved in the unfolded protein response (UPR) and in the endoplasmic reticulum-associated degradation (ERAD). Other mutations have been found in other RBPs and in structural or regulatory proteins of the cytoskeleton (Brown & Al-Chalabi, 2017; Taylor et al., 2016).

Altogether, ALS mutated proteins are involved or alter many intracellular processes, which are the PQC system, SGs dynamics, RNA metabolism, cytoskeletal dynamics, oxidative stress response and mitochondrial function. A hallmark of ALS, shared with many other NDs, is the presence of intracellular proteinaceous inclusions in dying MNs. Most ALS cases, up to 97%, show TDP-43 positive inclusions, even when TDP-43 is not mutated. Instead, SOD1 or FUS protein inclusions are observed in cases carrying mutations in the respective genes. Similarly, ALS cases related to the C9ORF72 hexanucleotide expansion show the presence of proteinaceous inclusions of DPRs and RNA foci (Hardiman et al., 2017; Taylor et al., 2016).

When the disease strikes LMNs: Spinal Muscular Atrophy, Spinal Bulbar Muscular Atrophy, and distal Hereditary Motor Neuropathies

Spinal Muscular Atrophy (SMA) refers to a group of genetic disorders characterized by degeneration of the anterior horn cells in the spinal cord and motor nuclei in the brainstem, resulting in weakness and atrophy of the proximal muscles of the limbs and trunk. SMA is classified in 4 types (I-IV), based on the age of onset and the clinical course. Type I and II affect infants, type III affects patients at or after one year of age and is characterized by a milder phenotype with signs of weakness, but the ability to walk unaided is retained; type IV affects adults, has an onset at the third or fourth decade of life and is slowly progressive with a normal life expectancy (D'Amico et al., 2011; Harding & Thomas, 1980). The inheritance is autosomal recessive in most of the cases and resides on a deletion of the exon 7 in the Survival Motor Neuron 1 (SMN1) gene on chromosome 5q13 (Lefebvre et al., 1995). Humans have two copies of SMN genes: SMN1 and SMN2, which differ in a single nucleotide that determines an alternative splicing of exon 7, resulting in a small amount of the full-length protein for SMN2. When SMN1 is mutated, SMA occurs, and the severity of the disease is determined by the copy number of SMN2, which supplies SMN protein (Singh & Singh, 2018). SMN is essential for cell survival since KO in mice is lethal at embryonic level (Schrank et al., 1997). SMN protein is ubiquitous in cells and tissues and, since it is a nucleic acid binding protein, acts in transcription, splicing and translation processes. Evidence supports that SMN plays a role in the biogenesis of snRNPs and in mRNA splicing of transcripts that are fundamental in MNs; other evidence supports that SMN has a MN specific function in mRNA transport along the axon and to neurites (Singh et al., 2017).

Notably, SMN protein aberrant expression or localization have been also associated to ALS (Rodriguez-Muela et al., 2017).

A small percentage of patients, 4-5%, show a clinically typical SMA with additional features but have no identifiable mutation in SMN1 gene: these SMA variants, or non-5q SMA, can be inherited in an autosomal dominant or X-linked manner. These SMA variants show a clinical and genetic overlap with hereditary spastic paraplegia, ALS, dHMN, CMT2 and diseases that affect muscle cells. Examples of mutated genes in SMA variants are the dynein heavy chain DYNC1H1 and the bicaudal D homologue 2 (BICD2), which are involved in microtubule-mediated transport; the vesicle-associated membrane protein VAPB, which has been also found mutated in ALS; GLE1, a nucleoporin that plays a role in the nuclear export of RNAs; the lamin A/C (LMNA), which is found mutated in laminopathies (Peeters et al., 2014).

Spinal and bulbar muscular atrophy (SBMA), or Kennedy's disease, is a slowly progressive degenerative disease of LMNs affecting only males (Kennedy et al., 1968). SBMA onset typically occurs in men between 30 and 50 years of age, who manifest proximal lower limb weakness and a progressive decline of muscle strength. Beside MNs degeneration, signs of cell-autonomous toxicity in muscle are observed (Cortes et al., 2014; Sorarù et al., 2008). Sensory neurons are also affected in SBMA causing symptoms such as neuropathic pain, vibratory sensation, and numbness (Antonini et al., 2000; Li et al., 1995). Non neuromuscular symptoms include androgen insensitivity, gynecomastia, infertility, and testicular atrophy, but also metabolic disorders, such as glucose homeostasis impairment, insulin resistance, cholesterol and triglyceride dysmetabolism (Dejager et al., 2002; Rosenbohm et al., 2018). SBMA is a X-linked inherited disease caused by a CAG trinucleotide repeat expansion in the AR gene (La Spada et al., 1991). Other triplet diseases that were later identified include HD, dentatorubropallidoluysian atrophy and SCA types 1, 2, 3, 6, 7 and 17. The AR belongs to the steroid hormone receptors family. As the other steroid hormone receptors, AR possesses a variable NTD, a highly conserved DNA binding domain, a hinge domain and a ligand binding domain at the C-terminus (Brinkmann et al., 1989). AR, in absence of its ligands, resides in the cytoplasm and is maintained in an inactive state by chaperones HSP70/HSPA and HSP90 (Pratt & Toft, 1997; Pratt & Welsh, 1994). Once androgens bind to the ligand binding domain, AR changes its conformational state, dissociates from chaperones and shuttles in the nucleus, where it modulates the transcription of genes that are under the regulation of androgen-responsive elements (Ni et al., 2013). CAG repeat expansion falls in the first exon of AR gene; healthy individuals have a number of CAGs repeats between 11 and 36, while SBMA patients between 38 and 62

(Atsuta et al., 2006; Rhodes et al., 2009). The expansion encodes an expanded polyQ tract which is prone to misfold and aggregate, as observed throughout the nervous system and in peripheral tissues of patients (Adachi et al., 2005; Li, Miwa, et al., 1998; Li, Nakagomi, et al., 1998). These aggregates, similar to what observed in other NDs, sequester other proteins that are fundamental for normal cell functions, such as chaperones, members of the degradative system and transcriptional activators (Stenoien et al., 1999). Interestingly, the toxicity of the polyQ-AR is androgen-dependent: in fact, male mice models do not develop symptoms upon castration, while female mice models show symptoms upon androgen treatment, suggesting that polyQ-AR misfolding is induced by the conformational change after ligand binding (Chevalier-Larsen et al., 2004; Katsuno et al., 2002). PolyQ-AR-mediated pathomechanisms include the impairment of the PQC system, the transcriptional activity, mitochondrial activity, and axonal transport (Katsuno et al., 2006; McCampbell et al., 2000; Ranganathan et al., 2009; Rusmini et al., 2016).

Distal Hereditary Motor Neuropathies (dHMNs) are a heterogeneous group of diseases sharing a slow length-dependent motor neuropathy. The onset is in the first two or in the third decades of life. Signs of distal wasting, weakness, reduced or absent reflexes and EMG changes are observed in patients and suggest a distal denervation. Bulbar involvement is rare. Instead, minor sensory involvement is quite common. Indeed, dHMNs share a clinical and genetic overlap with hereditary sensory neuropathies and axonal Charcot-Marie-Tooth type 2 (CMT2) (Rossor et al., 2012). Classification of dHMN is based on inheritance and phenotype. Seven types of dHMN have been described: types I, II, V and VII show an autosomal dominant inheritance, while III, IV and VI show an autosomal recessive inheritance. However, mutations have been identified only in 15-20% of patients (Rossor et al., 2012). The most frequent causes of autosomal dominant dHMN are related to mutations in genes encoding the HSPBs, such as HSPB1, HSPB8 and HSPB3 (Evgrafov et al., 2004; Irobi et al., 2004; Kolb et al., 2010). Pathogenic mechanisms related to HSPB1 mutation consist in its aggregation along with cytoskeletal defects, such as neurofilaments co-aggregation and impaired axonal transport (Ackerley et al., 2006; Zhai et al., 2007). HSPB8 mutations, similarly, are characterized by an aggregation prone behaviour and co-aggregation with HSPB1 (Carra et al., 2005; Irobi et al., 2004). Another dHMN-related mutation has been found in the glycyl-tRNA synthetase (GARS) gene, which is essential for translation through its activity in catalysing the attachment of amino acids on their respective tRNA. Several studies could not demonstrate a reduction in the enzymatic activity of mutated GARS, while mutants GARS impairment in neurites localization was reported, leading to the hypothesis that the most likely pathomechanism is related to defects in axonal

transport (Motley et al., 2010). Mutations in Berardinelli-Seip Congenital Lipodystrophy type 2 (BSCL2) have been found not only in dHMN but also in congenital generalised lipodystrophy type 2, Hereditary Spastic Paraplegia and Silver syndrome. BSCL2 encodes for Seipin, which localizes in the ER and, when mutated in dHMN, misfolds, leading to the activation of the UPR and thus, the apoptotic pathway (Ito & Suzuki, 2009). Mutations in members of the microtubule motor machinery have been found in dHMN, such as in the gene encoding the p150 subunit of dynactin 1 (DCTN1) and the DYNC1H1, stressing the involvement of the microtubule-mediated intracellular trafficking in the disease (Puls et al., 2003; Weedon et al., 2011). Other mutations related to dHMN are found in the copper-transporting ATPase ATP7A, involved in the metalation of copper enzymes, in senataxin (SETX), involved in transcription and splicing and found mutated also in ALS, and in the transient receptor vallanoid 4 (TRPV4), which encodes a calcium-selective channel (Rossor et al., 2012). In summary, pathogenic mechanisms related to dHMN and shared with the other diseases described above are related again to protein misfolding, impaired cytoskeletal dynamics and intracellular trafficking, and RNA dysmetabolism.

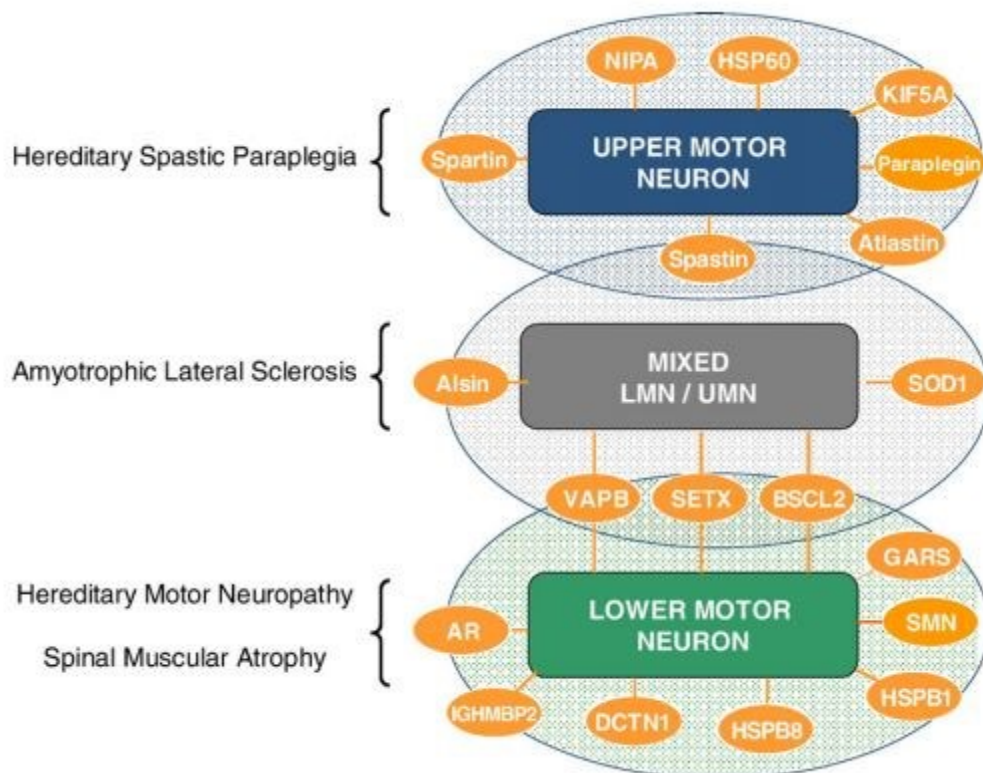


Figure 1. 17 Examples of genetic overlap in diseases that affect UMNs, LMNs or both (MIXED).
(From James & Talbot, 2006).

1.5.2 Neuropathies with sensory involvement

As mentioned above, MNDs can show sensory involvement. Besides motor neuropathies, there are forms of neuropathies that affect both MNs and sensory neurons. Of interest, there are **CMT** diseases, a group of heterogeneous motor and sensory neuropathies, which divide into demyelinating (CMT1) and axonal (CMT2) forms of disease. CMT, which is the most common neuropathy, is characterized by high heterogeneity in terms of pattern of inheritance (autosomal dominant or recessive or X-linked) and clinical signs (Mathis et al., 2015). More than 90 genetic variations have been related to CMT. The pathogenic mechanisms comprise RNA dysmetabolism, impairments in endosomal sorting, protein aggregation and proteostasis dysfunction, intracellular trafficking defects and cytoskeletal abnormalities, channelopathies and mitochondrial dysfunctions. It is not surprisingly, based on what has been reported above, that many of these genes have been also found related to dHMNs. In particular, the genetic overlap has been observed as both CMT, especially type 2, and dHMN can be caused by mutations in HSPBs, GARS, BCSL2, TRPV4, DYNC1H1.

1.5.3 When muscle cells are affected by disease

A broad range of conditions might affect skeletal muscle cells. Muscular diseases can be primary, when muscles are the target of the disease, or secondary to other conditions, as in MNDs. Muscle diseases that involve the PQC system and proteostasis impairment are of interest in this introduction. Indeed, in muscles, autophagy has a crucial role in the control of muscle mass and its impairment can occur in all stages of the autophagic pathway (Margeta, 2020). For instance, the autophagic flux is altered in **Autophagic Vacuolar Myopathies (AVM)**. AVMs are a group of lysosomal storage diseases of muscle cells, characterized by the engulfment of autophagosomes inside skeletal myofibers, and are due to mutations of proteins involved in lysosome function or fusion with autophagosomes. AVMs include Pompe disease and Danon disease. Pompe disease belongs to the glycogen storage diseases and is caused by the deficiency of the lysosomal enzyme acid α -glucosidase. Because of the absence of acid α -glucosidase, glycogen accumulates into lysosomes and cannot be hydrolysed to glucose. Pathological features of Pompe disease are the presence of glycogen-filled lysosomes and impairment in autophagosomal turnover (Kohler et al., 2018). Danon disease is another glycogen storage disease characterized by muscle weakness, cardiomyopathy, and mental retardation. It is caused by mutations in the gene encoding the lysosome-associated membrane protein 2 (LAMP2), which determine an impairment in lysosome biogenesis, maturation, and function. Indeed, skeletal muscles of affected patients show large vacuoles with sarcolemmal proteins surrounded by

lysosomes (Cenacchi et al., 2020). Proteostasis impairment is also a hallmark of other muscle disorders such as **myofibrillar myopathies (MFM)** and **Inclusion Body Myositis (IBM)**. MFMs, beside the genetic and clinical variability, share the common histopathological feature of myofibrillar disorganization and abnormal protein aggregation. Clinical manifestations are distal weakness, which might associate to proximal or generalized weakness, cardiomyopathy, usually dilated, and respiratory insufficiency. MFMs manifest usually in adulthood but can also occur at early stages of life. The inheritance is mainly autosomal dominant, but also autosomal recessive and X-linked patterns of inheritance are described. However, the genetic causes are unknown in the 50% of patients. Typical forms of MFMs are classified based on mutations of the following seven genes: DES, CRYAB, MYOT, filamin C, LDB3/ZASP, BAG3 and plectin. Other mutations described in MFMs involve genes coding for four-and-a-half LIM domain protein 1 (FHL1), titin, DNAJB6, α -actin, HSPB8, lamin A, and SQSTM1/P62 + TIA-1 (digenic inheritance). The identified MFMs causative genes encode structural proteins, mainly associated to the Z-disc structures, or PQC system members. Indeed, myofibrillar disorganization starts from the Z-disc with progressive disintegration of its structure, which can be associated to accumulating proteins, including DES, MYOT, CRYAB, filamin C, BAG3, other structural components and factors, such as ubiquitin or TDP-43. Rimmed or non-rimmed vacuoles and mitochondria abnormalities can be observed in muscle fibers from biopsies of patients (Fichna et al., 2018; Palmio & Udd, 2016). Sporadic IBM represents the most common form of myopathy at the age of 50. IBM develops with a progressive asymmetric weakness at quadriceps and finger flexors and histopathological features are rimmed vacuoles, protein aggregates, mitochondrial abnormalities. Protein aggregates can be positive for TDP-43, SQSTM1/P62, ubiquitin, phosphorylated tau or β -amyloid. In addition, muscle fibers are surrounded by inflammatory cells, suggesting an important role of inflammation in the development of the disease. Indeed, sIBM pathogenesis involves both the inflammatory and degenerative pathways. Genes variants found associated to sIBM are FYCO1, an autophagic adaptor protein, SQSTM1/P62 and VCP (Naddaf et al., 2018). IBM is also a clinical feature of the **Multiple System Proteinopathy (MSP)**, previously known as IBMPFD, along with Paget disease of bones and FTD. MSP is an adult-onset multisystemic disease characterized by proximal and distal muscle weakness, increased bone turnover and deformities and a progressive cognitive impairment. MSP is caused by mutations in VCP in the 50% of cases, but also HNRNPA1, HNRNPA2B1, SQSTM1/p62 and MATR3 can be found mutated in a subset of patients. MSP is characterized by similar histopathological findings of rimmed vacuoles and protein aggregates observed in sIBM, but the inflammatory component is less prominent (Adam et al., 1993).

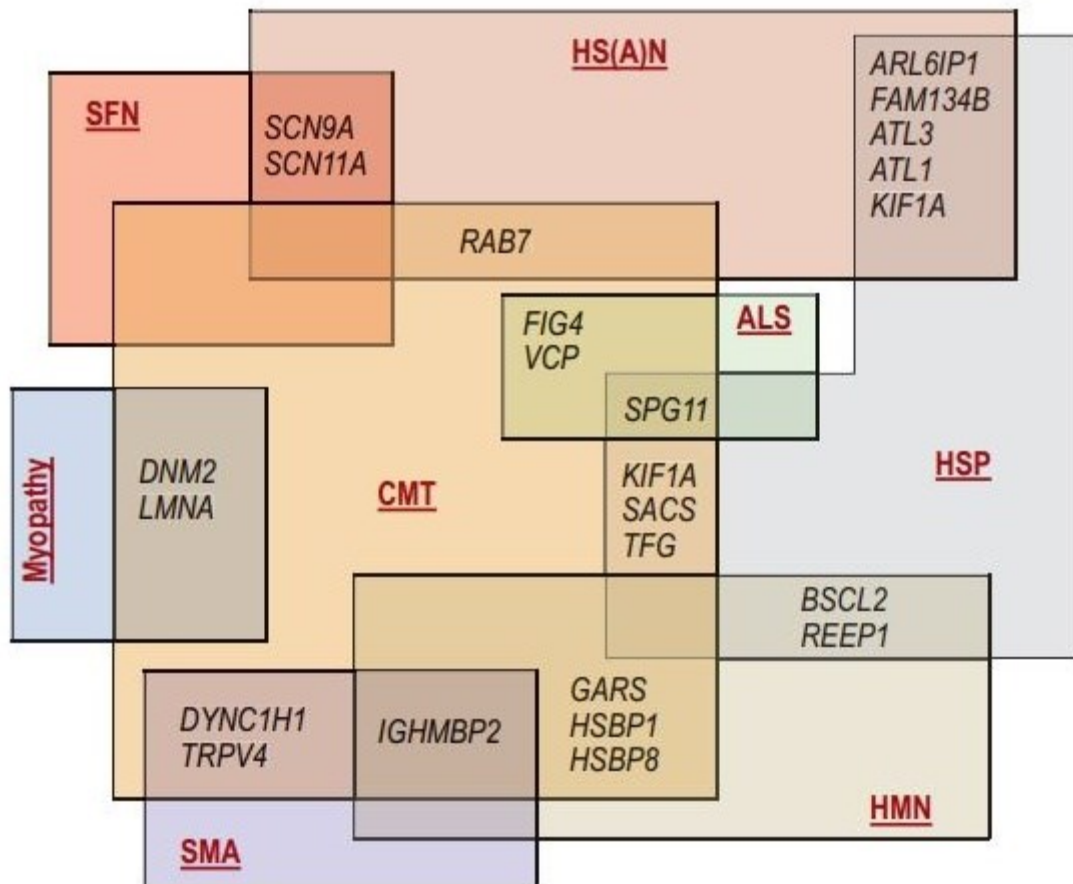


Figure 1. 18 Examples of genetic overlap among MNDs and myopathies. (From Eggermann et al., 2018).

Chapter II

2. Characterization and role of BAG3 mutants in neuromuscular diseases

2.1 BACKGROUND AND AIMS

BAG3 is a scaffold protein for CASA complex formation exerting its activity in the clearance of damaged and misfolded proteins. BAG3 interacts with chaperone HSP70/HSPA through its BAG domain and acts as a NEF by promoting ADP-ATP exchange. In this manner, BAG3 helps HSP70/HSPA activity in the refolding process of misfolded substrates. Misfolded substrates can be also recognized by chaperone HSPB8, a small HSP that acts as holdase. BAG3 and HSPB8 are obligate partners and form a 1:2 stoichiometric complex through two IPV domains in BAG3 structure. When misfolded substrates cannot be refolded and aggregate, CASA complex favours their ubiquitination by the HSP70/HSPA-interactor CHIP and routing to the aggresome, at the MTOC, for subsequent disposal through the autophagosome-lysosomal pathway. This is achieved by BAG3 interaction with the dynein motor complex through the PxxP domain. CASA activity has been well described in muscle cells, where it operates in the maintenance of Z-disc structures, and in neurons, where it favours the clearance of aggregating prone proteins related to NDs, such as ALS. Unsurprisingly, mutations in CASA complex members are found in diseases that affect these cell types. In particular, the hotspot mutations in the second IPV domain, which consist in the substitution of the Proline in position 209 (P209), have been related to early onset MFM and cardiomyopathy with severe axonal neuropathy (P209L), mild late onset MFM and axonal neuropathy (P209Q) or peripheral neuropathy and CMT (P209S). Instead, the substitution Glu455Lys (E455K), which falls in the BAG domain decreasing the interaction with HSP70/HSPA, has been related to DCM.

In collaboration with the Peripheral Neuropathy Research Group of the Institute Born Bunge (University of Antwerp, Antwerp, Belgium) and the Department of Biomedical, Metabolic and Neural Sciences of the University of Modena and Reggio Emilia, I investigated BAG3 mutants biochemical behaviour and activity in CASA pathway.

I evaluated BAG3 P209 mutant localization, levels, and aggregation prone behaviour in respect to the BAG3 WT and to the E455K. Since BAG3 P209 mutations are related to different phenotypes that affect or neurons or muscle cells, I confirmed BAG3 mutants behaviour both in a motoneuronal-like cell type, represented by NSC-34 cells, and in a muscle cell type, represented by C2C12 myoblasts. Since I observed an aggregating prone behaviour of BAG3 P209 mutants in the perinuclear region, I investigated whether these aggregates were actually aggresomes. In addition, BAG3 P209 mutant interaction with CASA partners was evaluated. As BAG3 mediates CASA pathway, I tested if P209 mutants were characterized by a detrimental function in the removal of already described substrates of CASA complex. Since BAG3 P209 mutants showed a similar biochemical behaviour, I focused on the P209L mutant to deepen BAG3 mutants preferential degradation pathways.

I confirmed that BAG3 P209L aggregating mutant is preferentially degraded through autophagy. This observation pushed me to test the therapeutic potential of the pro-autophagic compound trehalose in the clearance of BAG3 P209L aggregates. Trehalose is a natural compound that has been recently proven by our laboratory to stimulate autophagy and therefore to facilitate the clearance of aggregating prone proteins related to NDs. Most of these data have been published in (Adriaenssens et al., 2020).

2.2 Materials and Methods

Chemicals and reagents

The proteasome inhibitor MG-132 (Z-Leu-Leu-Leu-al) (Sigma Aldrich, Merck, Darmstadt, Germany) was used at 10 μ M overnight. The autophagic inhibitor 3-methyladenine (3-MA) (Sigma Aldrich, Merck, Darmstadt, Germany) was dissolved in medium and used at 10 mM for 36 hrs. The dynein ATPase inhibitor EHNA was used at 100 μ M for 24 hrs. D-(+)-trehalose dihydrate (trehalose) (Sigma-Aldrich, T9531) was dissolved in DMEM low glucose medium (Euroclone Pero, MI, Italy) at 100 mM for 48 hrs to stimulate autophagy.

Plasmids

The following plasmids were used:

- pEGFP-N1, purchased from Invitrogen (Carlsband, CA, USA), encodes for the GFP protein;
- pCDNA3, purchased from Invitrogen (Carlsband, CA, USA), is an empty vector used as a control;
- pBAG3-GFP wildtype (WT) and mutants P209S (PS), P209L (PL), P209Q (PQ) and E455K (EK) encode for GFP-tagged BAG3 WT or mutants and were kindly provided by Elias Adriaenssens (E.A.) and Professor Vincent Timmerman (V.T.) (Peripheral Neuropathy Research Group, Department of Biomedical Sciences, Institute Born Bunge, University of Antwerp, Antwerp, Belgium). Plasmids carrying the point mutations were obtained by in vitro mutagenesis as described in (Adriaenssens et al., 2020) using the pBAG3-GFP WT, a kind gift of Josée N. Lavoie (Fuchs et al., 2015);
- pSOD1-G93A encodes for the ALS-associated mutant SOD1-G93A and was previously described (Crippa et al., 2010);
- pFLAG-tagged poly-GA, which encodes the ALS-associated DPR polyGA (100 repeats) and kindly provided by Prof. Daisuke Ito, was previously described (Cristofani et al., 2017).

Cell cultures

HEK293T stably expressing the V5-tagged HSPB8 (HEK293T-HSPB8-V5) were kindly provided by E.A. and V.T. and obtained by lentiviral infection as described in (Adriaenssens et al., 2020). HEK293T-HSPB8-V5 and murine myoblasts C2C12 were grown in high glucose DMEM (Euroclone) completed with glutamine 1mM (Euroclone), penicillin G 100 U/mL (SERVA, Electrophoresis GmbH, Heidelberg, Germany), streptomycin 100 U/mL

(SERVA) and 10% fetal bovine serum (FBS) (GIBCO, Thermo Scientific Life Science Research, Waltham, MA, USA). Murine Neuroblastoma x Spinal Cord 34 (NSC-34) were grown in high glucose DMEM completed with glutamine 1mM (Euroclone), penicillin G 100U/mL (SERVA), streptomycin 100U/mL (SERVA) and 5% FBS (Sigma-Aldrich). Cells were maintained at 37°C, 5% CO₂.

Transfection

The day before transfection, cells were seeded at the following cellular densities:

- HEK293T-HSPB8-V5: 90 000 cells/mL in a 12-wells multiwell for western blot (WB) and Filter Retardation Assay (FRA), 75 000 cells/mL in a 24-wells multiwell for Flow cytometric analysis of Inclusions and Trafficking (FLoIT), 75 000 cells/ml in a 24-wells multiwell for fluorescence microscopy (FM) and immunofluorescence analyses (IF);
- C2C12: 65 000 cells/ml in a 12-wells multiwell for WB and FRA, 50 000 cells/ml in a 24-wells multiwell for FM.
- NSC-34: 90 000 cells/ml in a 12-wells multiwell for WB and FRA, 70 000 cells/ml in a 24-wells multiwell for FM or IF.

HEK293T-HSPB8-V5 and C2C12 cells were transfected using Lipofectamine3000/P3000 reagents following the manufacturers' instruction (Invitrogen, Thermo Scientific Life Science Research, Waltham, MA, USA). NSC-34 were transfected using Lipofectamine Transfection Reagent (Invitrogen, Thermo Scientific Life Science Research, Waltham, MA, USA). Plasmids pCDNA3 or pEGFP-N1, as mock, or BAG3-GFP constructs (wildtype or mutants) were transfected alone or co-transfected with plasmids encoding SOD1-G93A or poly-GA.

Protein extractions and quantification

48 hrs after transfection, cells were harvested and centrifuged 5 min at 100 g at 4°C. Cell pellets were then resuspended in Phosphate Buffer Saline (PBS) added with protease inhibitors cocktail (Sigma-Aldrich) and lysed using slight sonication. For Nonidet P-40 (NP-40) soluble and insoluble fractionation, cells pellets were resuspended in NP-40 lysis buffer (150 mM NaCl, 20 mM TrisBase, NP-40 0.5%, 1.5 mM MgCl₂, Glycerol 3%, pH 7.4) added with Complete Protease inhibitor (Roche Applied Science) and 1 mM DTT. The resuspended pellets were passed through a syringe 10 times for cell lysis and then centrifuged at 16100 g for 15 min at 4°C. Supernatants were collected and pellets resuspended in the same volume of NP-40 lysis buffer and sonicated. Protein content quantification was performed with bicinchoninic acid (BCA) assay (Euroclone).

Western Blot and Filter Retardation Assay

SDS-PAGE was performed loading same quantities of protein extracts, heated to 100°C for 5 min after adding sample buffer (0.6 g/100 mL Tris, 2 g/100 mL SDS, 10% glycerol, 5% β -mercaptoethanol, pH 6.8). 10 μ g of HEK293T-HSPB8-V5 protein lysates and 25 μ g of NSC-34 and C2C12 protein lysates were loaded. A trans-turbo system (Bio-Rad Laboratories, cat. 1704150) was used to electro-transfer proteins to 0.45- μ m nitrocellulose membranes (Bio-Rad Laboratories, Hercules, CA, USA). To detect insoluble species, FRA was performed. Briefly, 3 μ g (for BAG3-GFP) and 6 μ g (for SOD1-G93A) of total protein lysates were loaded onto a 20% MeOH-treated 0.2- μ m cellulose acetate membrane (Whatman 100404180) and filtered by gentle vacuum. Insoluble species that are larger than the pores are retained and fixed on the membrane through a final 20% MeOH treatment. WB and FRA membranes were incubated with a blocking solution of 5% of non-fat dried milk in TBS-Tween (20 mM Tris-HCl pH 7.5, 0.5 M NaCl, 0.05% Tween-20) for 1 h and then incubated with primary antibodies diluted in the same solution overnight at 4°C. Primary antibodies used were: mouse monoclonal anti-GFP antibody (ab1218, Abcam), mouse monoclonal anti- α -tubulin (T6199, Sigma-Aldrich), homemade rabbit polyclonal anti-BAG3 (Carra, Seguin, & Landry, 2008), homemade rabbit polyclonal anti-HSPB8 (#23) (Carra et al., 2005), mouse monoclonal anti-HSPB8 (ab66063, Abcam), rabbit polyclonal anti-HSPB8 (PA5-76780, ThermoFisher), rabbit polyclonal anti-Cu/Zn superoxide dismutase SOD1 (SOD-100, Enzo Life Sciences), rabbit polyclonal anti-LC3 (L8918, Sigma-Aldrich). Then, membranes were washed three times in TBS-Tween for 10 min and incubated with the peroxidase-conjugated secondary antibodies goat anti-rabbit and anti-mouse IgG-HRP (111-035-003, 115-035-003; Jackson ImmunoResearch Laboratories, Inc.). Immunodetection was achieved by pouring a solution of enhanced chemiluminescent (ECL) detection reagent (Clarity™ ECL western Blotting substrate, Bio-Rad Laboratories, cat. 1705060) and by acquiring images using a Chemidoc XRS System (Bio-Rad Laboratories). Optical densities were analysed using Image Lab Software (Bio-Rad Laboratories).

Fluorescence microscopy and immunofluorescence

For BAG3-GFP WT or mutants intracellular localization and distribution assessment, transfected cells were fixed with a solution 1:1 of 4% paraformaldehyde and 4% sucrose in 0.2 N PB (0.06 M KH_2PO_4 , 0.31 M Na_2HPO_4 ; pH 7.4) for 25 min at 37°C and then washed with PBS solution 3 times 5 min. Nuclei were stained with Hoechst33342 (in PBS; 33342, Sigma-Aldrich) or DAPI (in PBS) and coverslips mounted with MOWIOL onto slides.

For colocalization studies with the aggresomal marker Vimentin, HEK293T-HSPB8-V5 were transfected with BAG3-GFP constructs and left untreated or treated overnight with MG-132

prior fixation. For the evaluation of trehalose treatment on BAG3 WT or mutants clearance, NSC-34 cells were transfected with BAG3-GFP constructs and then treated with trehalose for 48 hrs. After fixation with a solution 1:1 of 4% paraformaldehyde and 4% sucrose in 0.2 N PB and washing with PBS, cells were permeabilized with a solution of 0.2% Triton X-100 in PBS. Cells were then incubated with blocking solution for 1 hr at RT and then with the primary antibody overnight at 4°C. The primary antibodies were rabbit polyclonal anti-vimentin antibody (dilution 1:500, Santa Cruz Biotechnology, sc-5565) and rabbit polyclonal anti-TFEB antibody (1:400, Bethyl Laboratories). The following day, cells were washed twice with PBS and incubated for 1 hr at RT with goat anti-rabbit 549 AlexaFluor (1:1000, Life Technologies, Thermo Fischer, A-11012). After three washes with PBS solution and nuclei staining with DAPI (1:10000 in PBS), coverslips were mounted with MOWIOL onto slides. An Axiovert 200 microscope (Zeiss, Oberkochen, Germany) with a photometric CoolSnap CCD camera (Robber Scientific, Trenton, NJ, USA) was used for images capture. Images were processed using Metamorph software (Universal Imaging, Downingtown, PA). Confocal microscopy experiments on BAG3 WT and mutants were conducted as follows: BAG3 and vimentin colocalization was performed after HEK293T-HSPB8-V5 transfection with BAG3-GFP constructs. Cells were fixed in ice-cold methanol (67-65-1, Sigma-Aldrich, Saint Louis, MI, USA) for 20 minutes. After blocking with 5% BSA (9048-46-8, Sigma-Aldrich, Saint Louis, MI, USA), cells were incubated with anti-GFP (Alexa Fluor 488 anti-GFP antibody; 338008, BioLegend, San Diego, CA, USA) and anti-vimentin (dilution 1:200; ab28028, Abcam, Cambridge, UK) antibodies for one hour at RT and then with the secondary antibodies. Nuclei were stained with Hoechst33342 (H3570, Life Technologies, Carlsbad, CA, USA) and cells were mounted with DAKO fluorescent mounting medium (S3023, DAKO). Images were captured with a Zeiss 2 4 2 4 LSM700 laser scanning confocal microscope using a 63×/1.4 NA objective and analysed in ImageJ/FIJI.

For colocalization studies between BAG3 and SQSTM1/P62 or FLAG-HDAC6, HEK293T-HSPB8-V5 cells were transfected with BAG3-GFP constructs alone or co-transfected with FLAG-HDAC6. Cells were fixed with 3.7% formaldehyde in PBS for 9 min at RT and permeabilized with cold acetone for 5 min at -20°C. After blocking for 1 h at RT with BSA 3% and 0.1% Triton X-100, cells were incubated with anti-SQSTM1/P62 (sc-28359, Santa Cruz Biotechnology, Inc., Santa Cruz, CA, USA) or anti-FLAG (F3165, Sigma-Aldrich, Saint Louis, MI, USA) overnight at 4°C. The following day, cells were washed and incubated for 1 hr at RT with a mouse secondary antibody (A21203, Life Technologies, Carlsbad, CA, USA) and nuclei were stained with DAPI. Images were obtained using a Leica SP8 AOB system (Leica Microsystems) and a 63x oil-immersion lens and analysed in ImageJ/FIJI.

Flow cytometry and intracellular trafficking (FLoIT) and Nuclei isolation

48 hrs after HEK293T-HSPB8-V5 transient transfection with pEGFP-N1 or BAG3-GFP constructs, medium was removed and cells were harvested in PBS with 10% FBS (Gibco, Thermo Fisher Scientific, Waltham, MA, USA) and centrifuged for 5 min at 100 *g* at 4°C. Cells were resuspended in PBS with 10% FBS (Gibco, Thermo Fisher Scientific, Waltham, MA, USA) and analysed by flow cytometry to determine the transfection efficiency in respect to untransfected control cells. Subsequently, a solution of PBS containing 1% (v/v) Triton X-100, a protease inhibitors cocktail (Sigma-Aldrich, Saint Louis, MI, USA) and DAPI (0.02 µg/µl) was added to a final concentration of 0.5% (v/v) Triton X-100 and DAPI 0.01 µg/µl. After two minutes incubation at RT, the cell lysates were analysed by flow cytometry. Three untransfected control samples without DAPI were analysed to set gates on nuclei population. For transfection efficiency analysis, excitation wavelengths and emission collection windows were FITC (488 nm, 530/50 nm), Pacific Blue (405 nm, 445/45 nm). Voltage of 418 (FSC), 199 (SSC), 373/482 (FITC for cell transfection or inclusion analysis respectively), 501 (Pacific Blue) were used. Nuclei were counted based on the Pacific Blue positive population. Inclusions were identified for fluorescence and FSC compared to cells transfected with eGFPN1 vector as control. Flow cytometry was performed using NovoCyte Flow Cytometer 3000 (ACEA Biosciences Inc., Agilent, Santa Clara, CA, USA) and results were analysed by NovoExpress software 1.2.5 (ACEA Biosciences Inc., Agilent, Santa Clara, CA, USA). Following the equation set by (Whiten et al., 2016), the number of inclusions was normalized to the number of counted nuclei and reported as inclusions/100 transfected cells. Nuclei population was analysed based on FITC fluorescence and a percentage of nuclei enriched with GFP-positive entities was determined. An aliquot of the intact nuclei suspensions was then mixed with MOWIOL and mounted between coverslips and slides for intact nuclei observation at the microscope (Axiovert 200 microscope).

Immunoprecipitation

48 after transfection, cells were lysed with lysis buffer [20 mM Tris-HCl pH 7.4, 2.5 mM MgCl₂, 100 mM KCl, 0.5% NP-40, Complete Protease inhibitor (Roche Applied Science, Indianapolis, IN, USA)] and incubated in ice for 30 min. Samples were centrifuged for 10 min at 20,000 *g* and equal amounts of supernatant (NP-40-soluble fraction only) was loaded on GFP-Trap beads (gta-20, Chromotek, Martinsried, Germany), for 1hr at 4°C. After three washing steps with wash buffer [20 mM Tris-HCl pH 7.4, 2.5 mM MgCl₂, 100 mM KCl, Complete Protease inhibitor (Roche Applied Science, Indianapolis, IN, USA)], proteins were eluted from the beads with Sarkosyl elution buffer (140 mM NaCl, 50 mM Tris-HCl pH 8, 1 mM EDTA, 0.3% Sarkosyl, 10% glycerol) and samples supplemented with NuPAGE LDS

sample buffer (Life Technologies, Carlsbad, CA, USA) and loaded on 4-12% NuPAGE gels (Life Technologies, Carlsbad, CA, USA). Proteins were transferred to nitrocellulose membranes (Hybond-P; GE Healthcare, Wauwatosa, WI, USA) and detected using antibodies anti-GFP (ab290, Abcam, Cambridge, UK), anti-V5 (R96025, Invitrogen, Carlsbad, CA, USA), anti-SQSTM1/P62 (5114, Cell Signaling, Danvers, MA, USA), anti-Hsp70/Hsc70 (ab5439, Abcam, Cambridge, UK), or anti-Tubulin (ab7291, Abcam, Cambridge, UK) and enhanced chemiluminescent ECL Plus solution (Pierce, Life Technologies, Carlsbad, CA, USA) and LAS4000 (GE Healthcare, Wauwatosa, WI, USA).

Protein solubility prediction

CamSol browser (<http://www.vendruscolo.ch.cam.ac.uk/camsolmethod.html>) was used to obtain the intrinsic solubility profile of BAG3 WT and mutants. The full-length protein sequence of BAG3 (NP_004272.2) or their mutants were used as inputs, following the procedure described in (Sormanni et al., 2015).

Statistic

Student T tests or One-Way ANOVA with Bonferroni's multiple comparisons tests were performed, as indicated in each figure, and using PRISM software (GraphPad Software, La Jolla, CA, USA).

2.3 RESULTS

2.3.1 P209 substitutions in the IPV domain cause BAG3 aggregation and decreased solubility

BAG3 mutations are related to neuromuscular diseases. For instance, P209 mutations have been related to early onset myopathy and cardiomyopathy (P209L), late onset myopathy (P209Q) and late-onset CMT neuropathy (P209S). Instead, E455K mutant has been linked to DCM. BAG3 P209 mutations related to neuropathies and myopathies fall in the second IPV domain, the region responsible for HSPB8 binding, while the E455K substitution involves the BAG domain which binds HSP70/HSPA (**Fig. 2.1 A**). To evaluate BAG3 WT and mutants localization, I transfected HEK293T previously engineered to stably express HSPB8-V5 (HEK293T-HSPB8-V5, herein), with plasmids encoding GFP-tagged BAG3 WT or mutants and then analysed cells by fluorescence microscopy (FM). I found that BAG3 WT localized predominantly in a diffuse form in the cytoplasm, as expected (**Fig. 2.1 B**). Instead, only few cells overexpressing mutants carrying the P209 point mutation (P209S/L/Q) showed a diffuse cytoplasmic distribution of the mutant BAG3, while most cells were characterized by multiple small aggregates or one large aggregate at the perinuclear region. On the opposite, cells overexpressing the BAG3 E455K mutant showed a diffuse localization of BAG3 protein and complete absence of aggregates. By counting cells (**Fig 2.1 B**), I calculated that small aggregates were present in 10.5% of cells transfected with the BAG3 WT, 8.4% of cells transfected with the P209S mutant, 13.7% of cells transfected with the P209L mutant, 9.1% of cells transfected with the P209Q mutant. Instead, large aggregates were present in 9.8% of cells transfected with BAG3 WT, 31.4% of cells transfected with P209S mutant, 36.5% of cells transfected with P209L, 34.4% of cells transfected with P209Q mutant. No aggregates were detected in cells overexpressing the BAG3 E455K mutant. Then, to evaluate the levels and the presence of high molecular weight (HMW) insoluble species of BAG3 WT or mutants, I performed WB and FRA on protein extracts obtained from HEK293T-HSPB8-V5 cell line transiently transfected with GFP-tagged BAG3 WT or mutants constructs. Proteins from the whole cell lysates extracted in PBS, a buffer with low detergent power, were analysed in WB (**Fig. 2.1 C**) and the results showed that BAG3 WT or mutants levels are very similar; thus, the mutants are not characterized by a decreased stability or by an increased degradation. Instead, the same samples processed using FRA to determine the overall amount of insoluble material present in the transfected cells clearly showed that BAG3 carrying the point mutation P209 are highly prone to form insoluble species and to accumulate in respect to the BAG3 WT. To confirm the low solubility of BAG3 P209 mutants in respect to the WT protein, I next

evaluated the partitioning of BAG3 proteins into soluble and insoluble fractions by protein extraction in a NP-40 buffer, which is characterized by higher detergent power in respect to PBS buffer. As expected, WB and FRA analyses of the NP-40 soluble and insoluble extracts confirmed a differential partitioning of BAG3 WT or mutants between the two fractions. Indeed, WB conducted in the NP-40 soluble fraction (**Fig. 2.1 D**) showed decreased levels of BAG3 P209 mutants; conversely, the levels of BAG3 E455K mutant were very similar to those found for the BAG3 WT. FRA results showed no significant differences of HMW species of BAG3 E455K mutant in respect to the BAG3 WT. Instead, WB and FRA of NP-40 insoluble extracts (**Fig. 2.1 D**) showed a significant parallel increase in P209 mutants levels in respect to BAG3 WT, confirming their low solubility, while no accumulation was observed for the E455K mutant. Interestingly, HSPB8 protein levels paralleled the partitioning of BAG3 WT and mutants.

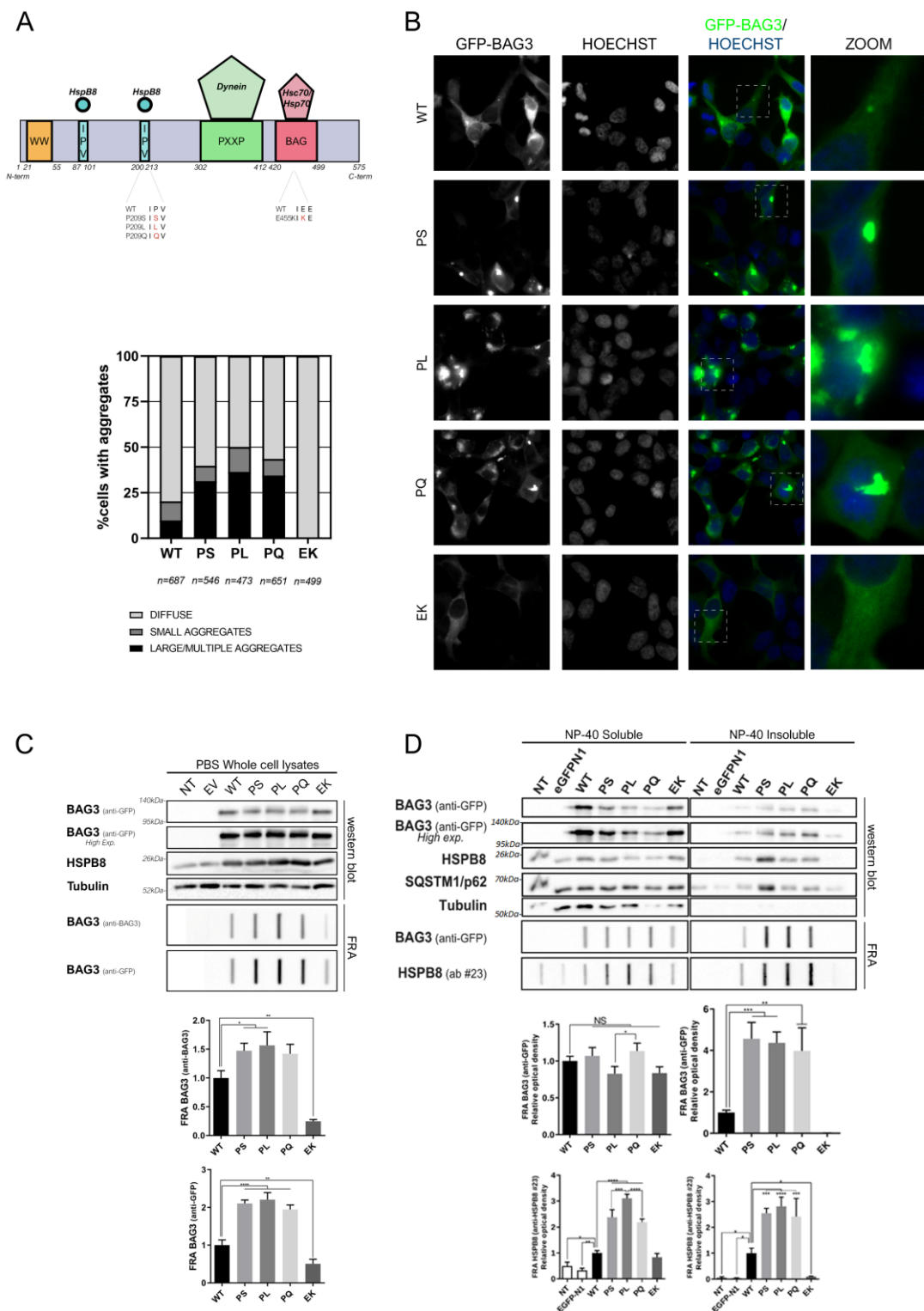


Figure 2. 1 P209 substitutions in the IPV domain cause BAG3 aggregation and decreased solubility.
A. Schematic representation of BAG3 WT structure and interacting partners; P209 and E455K mutations are reported **B.** Fluorescence microscopy on GFP-tagged BAG3 WT or mutants. Nuclei were stained with Hoechst (63x magnification). Graph bars show quantification of cells as means of BAG3-GFP transfected cells containing aggregates, expressed as percentage. Six random fields were selected for analysis. The mean number of cells counted per field was 95 and the number of cells per genotype is reported. **C.** WB and FRA analyses of PBS-whole cell lysates of HEK293T stably expressing HSPB8-V5 untransfected (NT) or transiently transfected with an empty vector (EV) or BAG3-GFP constructs. FRA relative optical densities are reported in the graphs as

means \pm SD of normalized values. One-way ANOVA with Bonferroni's test were performed: * $p < 0.05$, ** $p < 0.01$, **** $p < 0.0001$ ($n=3$) **D.** WB and FRA analyses after NP-40 soluble/insoluble extraction of HEK293T stably expressing HSPB8-V5, untransfected (NT) or transiently transfected with eGFPN1 or BAG3-GFP constructs. FRA relative optical densities are reported in the graphs as means \pm SD of normalized values. One-way ANOVA with Bonferroni's test were performed: * $p < 0.05$, ** $p < 0.01$, *** $p < 0.001$, **** $p < 0.0001$ ($n=3$). The constructs were abbreviated as follows: non-transfected (NT), empty vector (EV), wildtype (WT), P209S (PS), P209L (PL), P209Q (PQ), E455K (EK).

2.3.2 Aggregation propensity of BAG3 P209 mutants is confirmed in motoneuronal and muscle cells models

It is not yet clear how mutations at the same P209 hotspot residue are associated to different phenotypes. To get insights into the mutation-phenotype relationship, I evaluated if BAG3 mutants behave differently in a motoneuronal and muscle cell models. I used the murine Neuroblastoma x Spinal Cord 34 (NSC-34), which is a hybrid cell line that shows features of motoneurons, and the murine C2C12 cell line as muscle cells model. Both NSC-34 and C2C12 are routinely used in our laboratory to study MNDs and muscle cells involvement (Cicardi et al., 2019; Cicardi et al., 2018; Onesto et al., 2011). Localization and distribution analysis of BAG3 WT and mutants in both cell lines (**Fig 2.2 A**) confirmed that BAG3 WT and the E455K mutant mainly localize in the cytoplasm in a diffuse manner. Similar to the previous results obtained in HEK293T cells, all P209 mutants form a single big aggregate and/or several small aggregates in the cytoplasm; thus, BAG3 mutants aggregates formation is independent from the cell line considered. The aggregation prone behaviour of P209 mutants was confirmed in WB and FRA after NP-40 soluble-insoluble extraction (**Fig 2.2 B**). Indeed, BAG3 WT and E455K were present mainly in the NP-40 soluble fraction while BAG3 P209 mutants showed decreased protein levels in the NP-40 soluble fraction and a parallel increase in the NP-40 insoluble fractions in the cell lysates of both cell lines analysed by WB. FRA results confirmed the formation of HMW species of BAG3 P209 mutants in the NP-40 insoluble fraction. Therefore, all BAG3 P209 mutants form insoluble species and aggregates independently from the cell type, suggesting that the phenotype observed in patients carrying the P209 mutations might be related to other genetic or environmental factors.

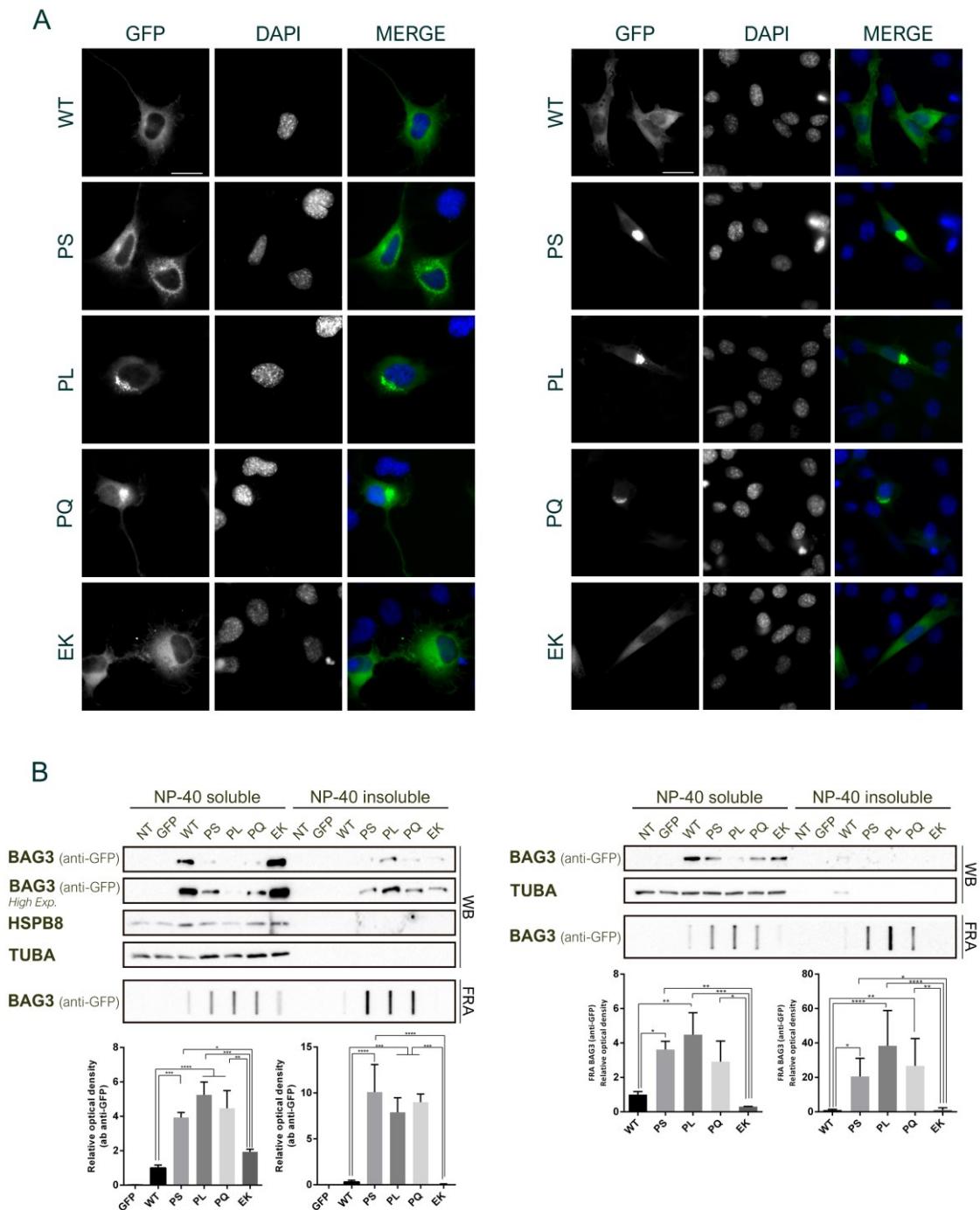


Figure 2. 2 Evaluation of mutation-phenotype relationship using models of neuronal and muscle cells.
A. FM results on motoneuronal-like NSC-34 cells and C2C12 myoblasts transiently transfected with BAG3-GFP constructs confirmed the aggregation of P209 BAG3 mutants. Nuclei were stained with DAPI. (Scale bar = 10 μ m; 63X magnification). **B.** WB and FRA on NP-40 soluble and insoluble protein fractions in NSC-34 and C2C12 untransfected (NT) or after transient transfection with eGFPN1, as mock, or BAG3-GFP constructs. Graphs show FRA relative optical densities as means \pm SD of normalized values. One-Way ANOVA with Bonferroni's multiple comparisons test were used for statistical analysis: * $p < 0.05$, ** $p < 0.01$, *** $p < 0.001$, **** $p < 0.0001$ ($n = 3$).

2.3.3 In silico analysis of BAG3 mutants by CamSol method reveals a decreased intrinsic solubility profile of P209 mutants

Previous analyses did not highlight any differences in the biochemical behaviour of BAG3 P209 mutants in both motoneuronal and muscle cells. However, among P209 mutants, the P209L mutant, which causes the most severe phenotype, always showed a higher tendency to aggregation in respect to the P209S and P209Q mutants. On these bases, I decide to apply an *in silico* approach to evaluate differences in the intrinsic solubility profile for each BAG3 mutant. Using the CamSol Method (Sormanni et al., 2015) on the BAG3 WT protein sequence, I determined that both IPV domains, which permit HSPB8 binding, are characterized by a low intrinsic solubility (**Fig. 2.3**). Usually, globular folded proteins are characterized by low solubility regions that form the hydrophobic core of the protein. I assumed that the two IPV domains could not be buried in the inner part of BAG3 protein, as they are fundamental for HSPBs interaction. Interestingly, by analysing the intrinsic solubility profile of P209 mutants, I determined that all these three substitutions in the IPV domain exacerbate the low intrinsic solubility profile, with a score of -2.10 (P209S), -2.17 (P209L) and -2.15 (P209Q) in respect to -1.62 for BAG3 WT. These decreases follow the trend of the aggregation propensity of the three P209 mutants observed in the localization and solubility experiments reported above, with a slight worse behaviour of the P209L mutant. Instead, E455K mutant showed a slight decrease in the intrinsic solubility profile that does not relate to the biochemical behaviour of the E455K mutant and suggests that the high solubility of this mutant in respect to BAG3 WT might be dependent on HSP70/HSPA loss of interaction.

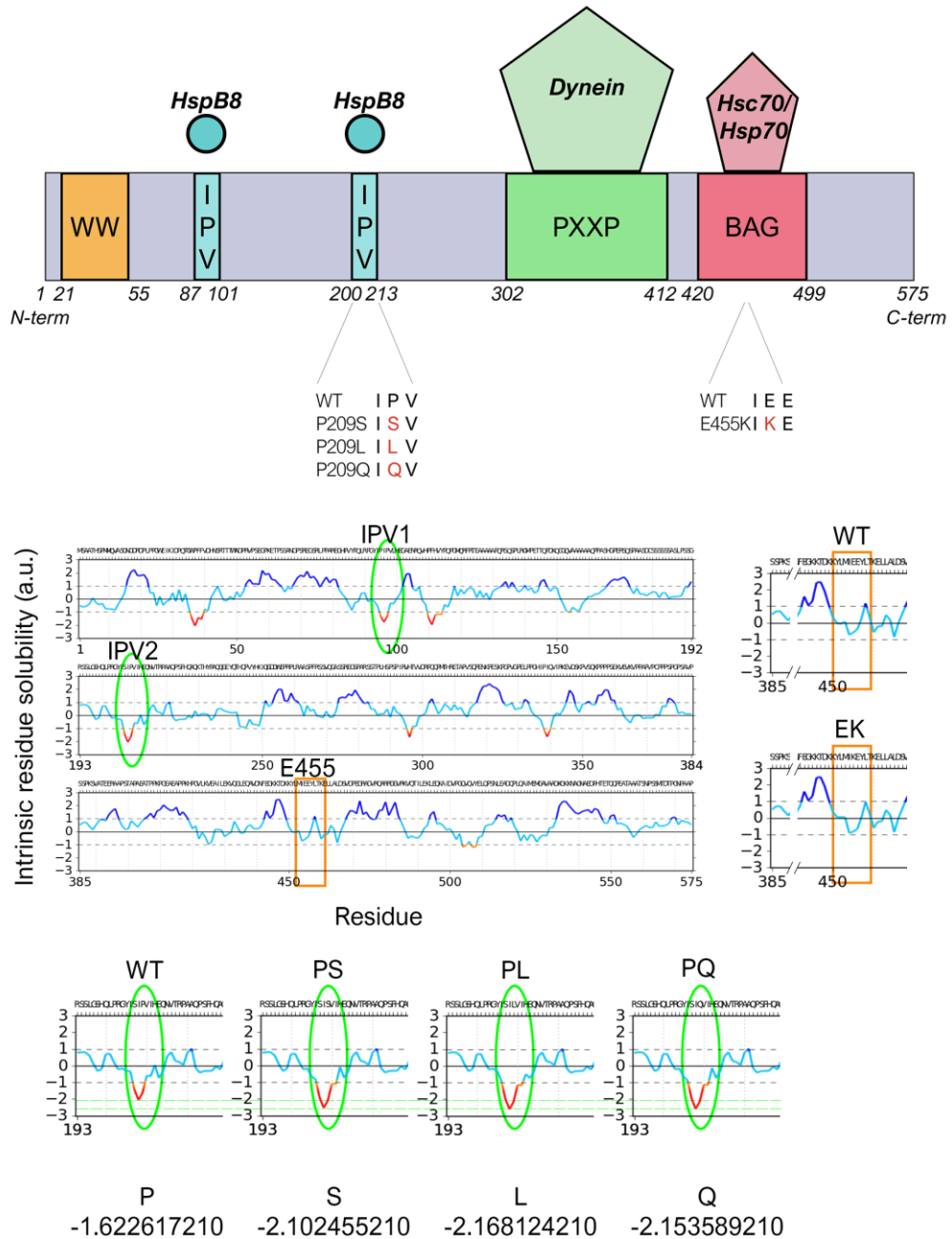


Figure 2. 3 *In silico* analysis of BAG3 mutants by CamSol method reveals a decreased intrinsic solubility profile of P209 mutants.

Bio-informatic analysis of the intrinsic solubility profile of the full-length BAG3 WT reveals a low solubility of both IPV domains. On the bottom, graphs of the intrinsic solubility profile of P209 mutations in the second IPV domain and the corresponding value are reported. On the right, the intrinsic solubility profile of E455K mutation is reported in comparison to the BAG3 WT.

2.3.4 BAG3 aggregates are in the cytoplasm and adhere to the nuclear envelope

Since the previous results failed to detect differences in the aggregation propensity among P209 mutants that could explain a relationship with their mild or severe phenotype, I used flow cytometric analysis of inclusions and trafficking (FLoIT) technique (Whiten et al., 2016), a new high-throughput assay which permits the analyses of a higher number of cells using flow cytometry. FLoIT is based on the detection of cytoplasmic aggregates or inclusions formed by proteins with a fluorescent tag, that can be stably or transiently expressed in cells. After plasma membranes lysis and nuclei staining, fluorescent aggregates or inclusions can be counted and normalized on cells number. A fraction of not lysed cells is also analysed, to obtain the transfection efficiency for data normalization. **Fig. 2.4 A** shows plots obtained by FLoIT analyses on HEK293T-HSPB8-V5 cells and transiently expressing BAG3-GFP WT or mutants. **Fig. 2.4 A a/b** show representative plots of lysed cells with intact Pacific Blue+ nuclei and GFP+ entities, which are aggregates or inclusions. **Fig. 2.4 A c** shows distribution of GFP+ inclusions based on dimension and complexity: as expected, BAG3 WT formed small amounts of insoluble species; instead, BAG3 P209 mutants formed higher amounts of insoluble species in respect to BAG3 WT, while BAG3 E455K was completely soluble. In **Fig. 2.4 A d** GFP and DAPI double positive entities are reported: these double positive entities might be interpreted as BAG3 aggregates or soluble protein inside the nuclei. As reported in the bar graph (**Fig. 2.4 B**), BAG3-GFP cytoplasmic inclusion quantification normalized on transfected cells, confirmed the aggregation prone behaviour of P209 mutants in respect to the BAG3 WT, while a complete solubility of BAG3 E455K. GFP protein formed 3.33 ± 3.13 cytoplasmic inclusions every 100 transfected cells, BAG3 WT 6.03 ± 1.41 , BAG P209S 34.44 ± 7.64 , BAG3 P209L 46.11 ± 8.47 , P209Q 39.30 ± 10.10 and E455K 1.27 ± 0.71 . GFP and DAPI double positive entities were calculated: 0.40 ± 0.57 for GFP protein alone, 10.61 ± 6.39 for BAG3 WT, 28.24 ± 10.62 for BAG P209S, 32.43 ± 11.57 for BAG3 P209L, 30.53 ± 11.18 for P209Q and 0.42 ± 0.39 for BAG3 E455K. Moreover, FLoIT analysis revealed a higher aggregation propensity of the P209L mutants, statistically significant in respect to the neuropathy-related P209S mutant, but not significantly different in respect to the myopathy/neuropathy-related P209Q mutant. To get an insight into GFP and DAPI positive entities, I collected and analysed the intact nuclei of FLoIT analyses to investigate the presence of BAG3 nuclear aggregates. As observed in **Fig. 2.4 C**, BAG3 WT was not completely excluded from nuclei. P209 mutants were not characterized by higher accumulation inside the nuclei or nuclear aggregates, but by cytoplasmic aggregates adhering tightly to the nuclear envelope. As expected, the BAG3 E455K mutant did not form structures associated to the nuclear membrane.

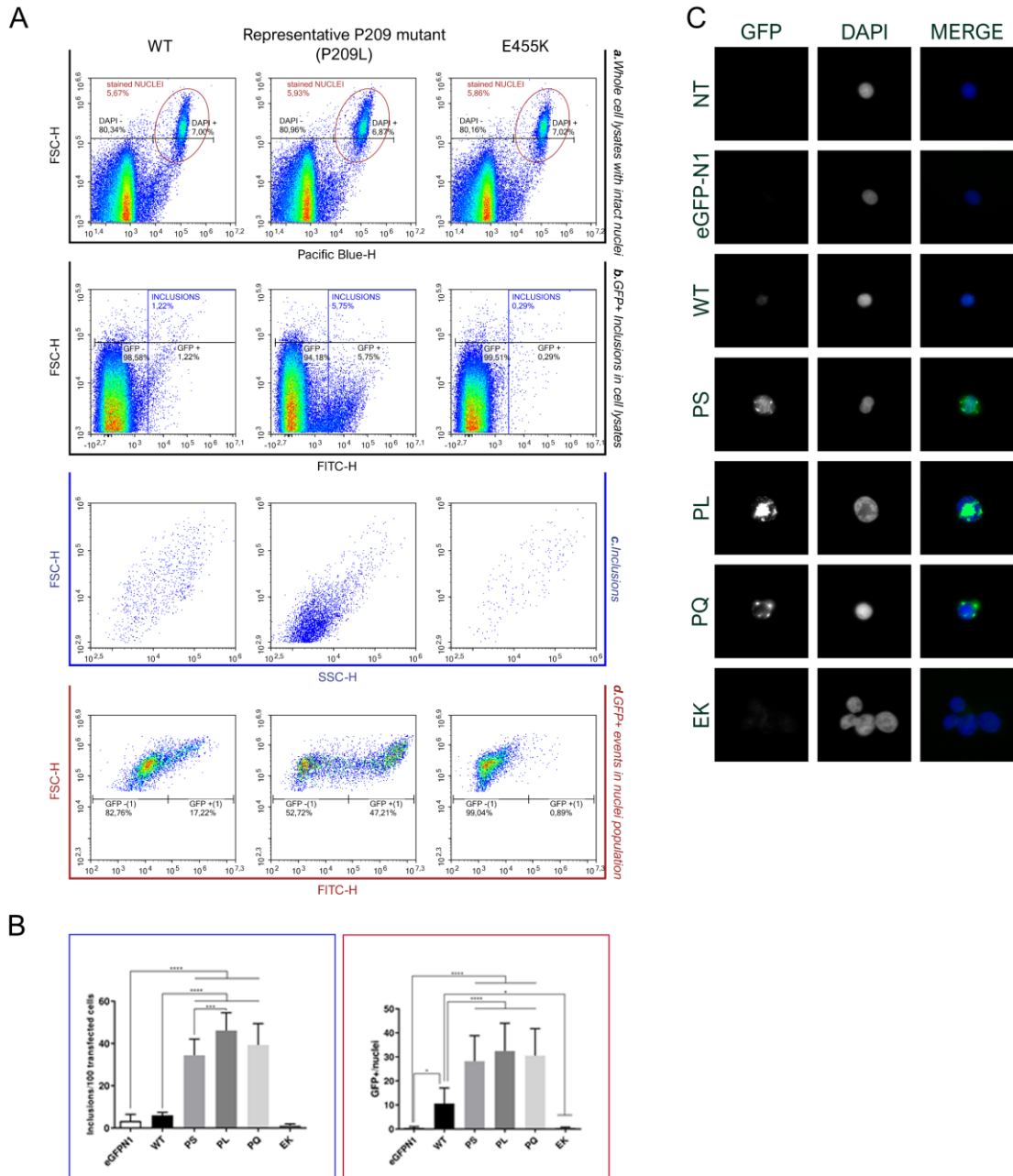


Figure 2. 4 BAG3 aggregates are in the cytoplasm and adhere to the nuclear envelope.

A. FLoIT analysis graphs. HEK293T-HSPB8-V5 cells untransfected or transiently transfected with BAG3-GFP WT or mutants were analysed by flow cytometry for transfection efficiency evaluation ($\gamma = \text{GFP}^+/\text{cells}$). (a) After plasma membrane lysis, cellular lysates were read: nuclei populations were defined as Pacific Blue + populations after adding DAPI and excluded from cytoplasmic inclusion analysis. (b) The remaining particles were defined as GFP+ inclusions in respect to cells transfected with pEGFP-N1. (c) Distribution of GFP+ inclusions based on dimension and complexity. (d) Stained nuclei were analysed based on FITC fluorescence and dimension. **B.** On the bottom, bar graphs report the means \pm SD of BAG3-GFP cytoplasmic inclusions (blue frame) and GFP-positive nuclei (red frame) per 100 transfected cells. One-Way ANOVA with Bonferroni's multiple comparisons test were used for statistical analysis; * $p < 0.05$, *** $p < 0.001$, **** $p < 0.0001$ ($n = 12$). **C.** Microscope analysis of FLoIT-derived intact nuclei of HEK293T stably expressing HSPB8-V5 and untransfected (NT) or transiently transfected with eGFPN1 or BAG3-GFP constructs. Nuclei were stained with DAPI during FLoIT analysis. (63X magnification).

2.3.5 Nuclear envelope-associated aggregates are aggresomes

BAG3, as part of the CASA complex, utilizes the active retrograde transport to route aggregates at the MTOC, where aggresomes are generated. The aggresome is a membraneless structure defined as “aggregate of aggregates”, which is then degraded through autophagy, a specific process that indicates the autophagic degradation of cell aggregates. Aggresomes are surrounded by a cage formed by intermediate filaments, such as vimentin or neurofilaments in epithelial cells and neurons, respectively. Other typical markers of the aggresomes are γ -tubulin, HDAC6, ubiquitin and proteasome subunits. To investigate if P209 mutants BAG3 perinuclear aggregates were aggresome, I performed an IF for vimentin. MG-132, which inhibits the proteasome and induces aggresome formation, was used as a positive control. As shown in **Fig. 2.5 A**, BAG3 WT did not colocalize with vimentin under basal condition, while treatment with MG-132 induced the formation of a vimentin and BAG3 -positive aggresome, located near the nucleus. Instead, BAG3 P209L, used as a representative P209 mutant, colocalized with vimentin, both on basal untreated condition and after MG-132 treatment. Interestingly, E455K mutant remained soluble and localized less with vimentin, even after aggresome formation induction. These results were then confirmed for all BAG3 P209 mutants by confocal microscopy. As observed in **Fig. 2.5 B**, BAG3 P209 mutants localize not only with vimentin, but also with HDAC6, another aggresome marker.

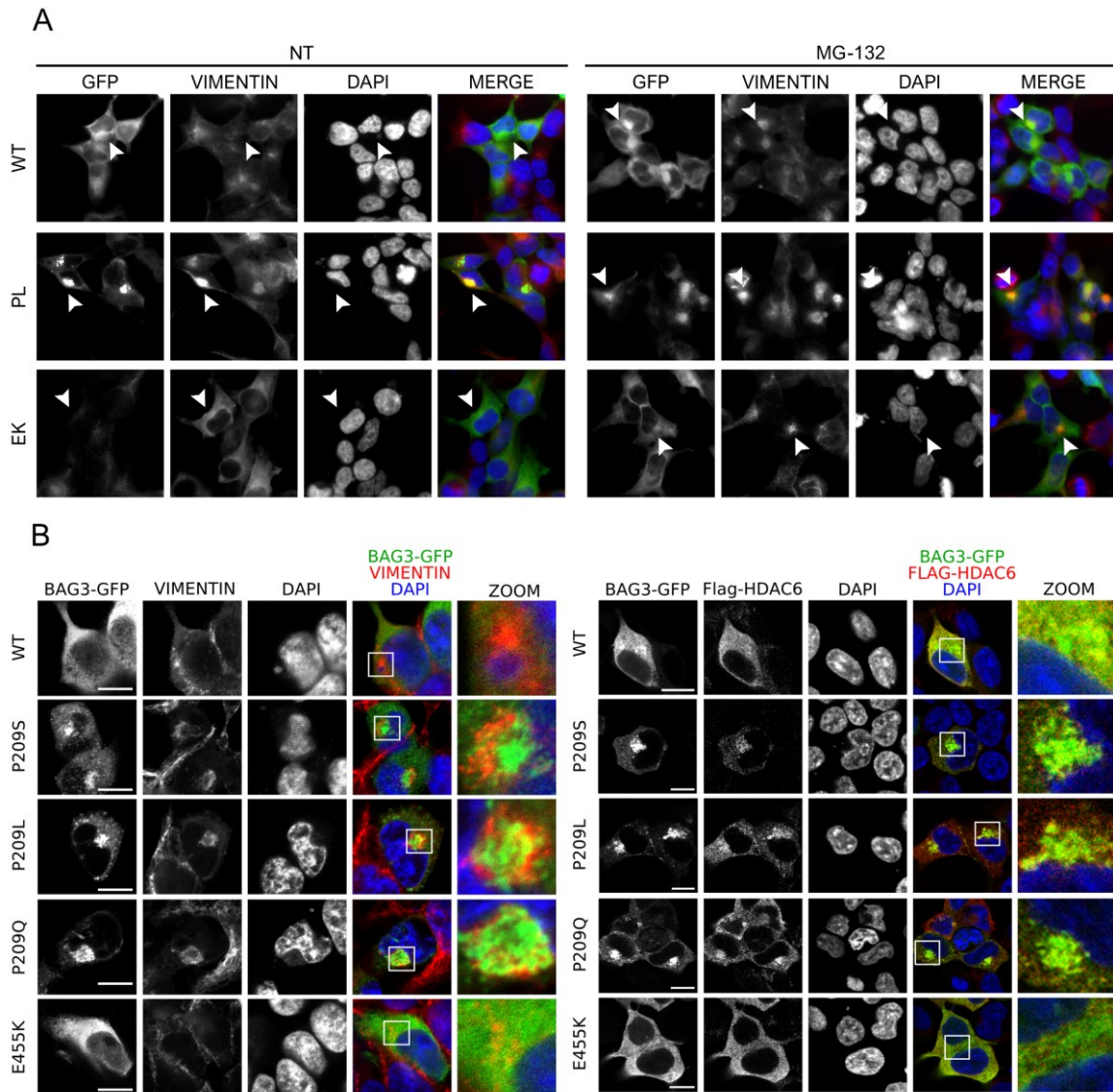


Figure 2. 5 Nuclear envelope-associated aggregates are aggresomes.

A. GFP-tagged BAG3 WT, P209L (representative of P209 mutants) or E455K mutants and vimentin colocalization. HEK293T cells stably expressing HSPB8-V5 transfected with GFP-tagged BAG3 were treated with MG-132 (10 μ M, overnight) or left untreated. IF was performed against Vimentin (red), and nuclei were stained with DAPI. (63X magnification) **B.** Confocal microscopy confirmed that all BAG3 P209 mutants accumulate at aggresomes. Colocalization was assessed between BAG3-GFP and aggresome-markers vimentin, and transiently transfected FLAG-HDAC6. Nuclei were stained with DAPI (blue). Scale bar = 10 μ m.

2.3.6 Interaction and colocalization of BAG3 mutants with CASA-complex members

After assessing the aggregation propensity of the BAG3 P209 mutants, I evaluated their ability to interact and sequester other members of the CASA complex. Indeed, P209 mutations fall in one of the two HSPB8-binding domains, suggesting that these mutations might impact on HSPB8 binding. Surprisingly, co-immunoprecipitation results (**Fig. 2.6 A**) did not reveal a loss of interaction between BAG3 P209 mutants and HSPB8. Similarly, the interaction of the BAG3 mutants with HSP70/HSPA was not affected, with the exception of the BAG3 carrying the BAG-domain E455K mutation, which has been already described with a diminished interaction with the HSP70/HSPA chaperone (Fang et al., 2017). Interestingly, an increased interaction with the autophagic adaptor SQSTM1/P62 was observed, in line with results already published by (Guilbert et al., 2018). These results were then corroborated by IF, using confocal microscopy. As shown in **Fig. 2.6 B**, BAG3 P209 mutants colocalized with HSPB8, HSP70/HSPA and SQSTM1/P62 at the aggresome. This effect in relocating CASA-members suggested a likely impairment of CASA pathway.

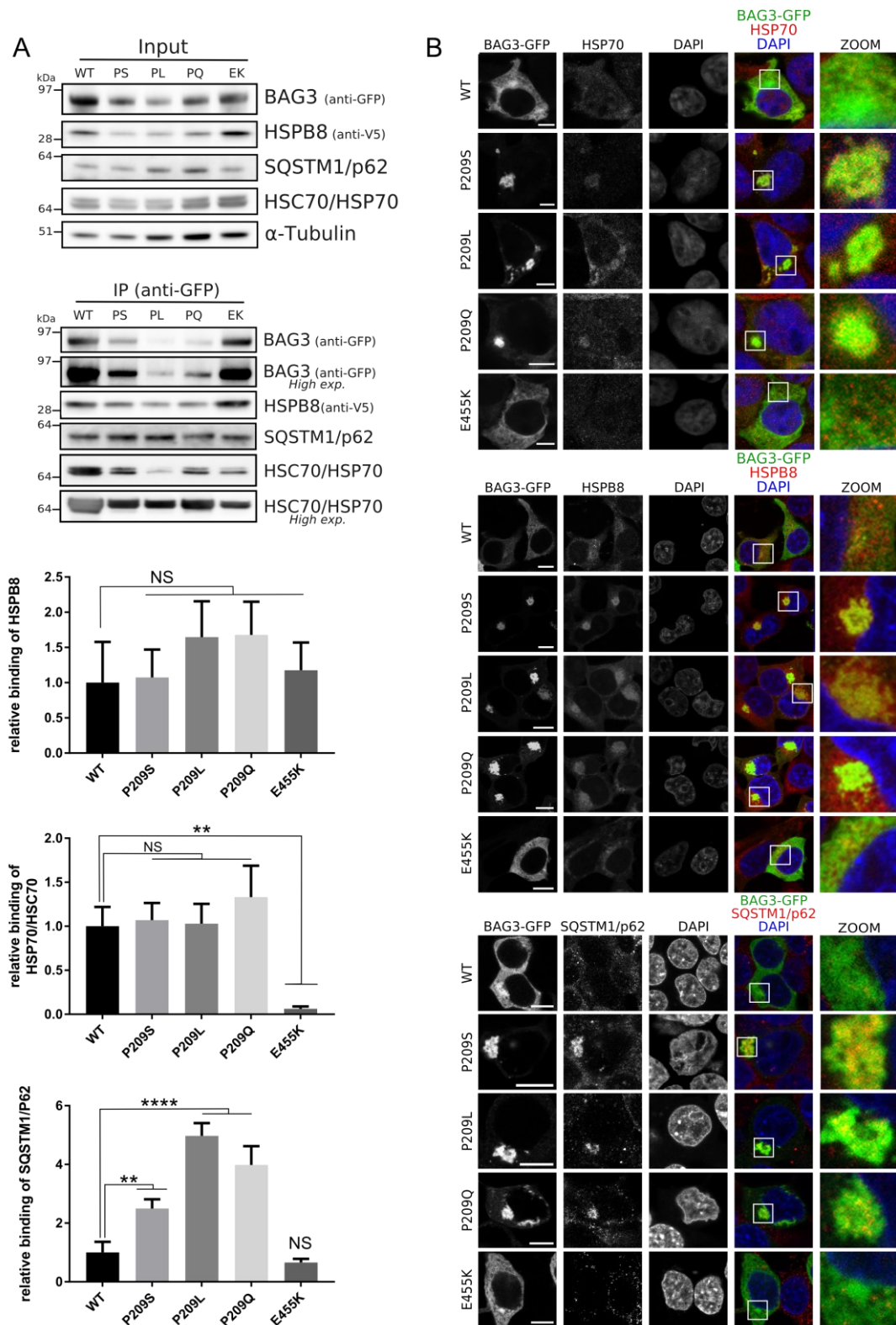


Figure 2. 6 Interaction and colocalization of BAG3 mutants with CASA-complex members.

A. Co-immunoprecipitation results on HEK293T cells stably overexpressing HSPB8-V5 and transiently transfected with BAG3-GFP constructs. Quantifications of the relative binding between BAG3 and CASA-members were performed correcting the levels of the bound protein for the amount of immunoprecipitated BAG3 as represented in the graph bar (means \pm SD). One-Way ANOVA with Bonferroni's multiple comparisons test were used for statistical analysis. NS = non-significant, ** $p < 0.01$, and **** $p < 0.0001$ ($n = 3$). **B.** IF results of HEK293T cells stably overexpressing HSPB8-V5 and transiently transfected with BAG3-GFP constructs to assess colocalization with CASA members HSP70 and HSPB8 (Scale bar = 5 μ m) and the autophagic adaptor SQSTM1/P62 (Scale bar = 10 μ m). Nuclei were stained with DAPI.

2.3.7 BAG3 P209 mutants cause the failure of CASA activity

Given the role of the CASA complex in the removal of damaged and misfolded prone proteins, I next evaluated if the pro-degradative activity of BAG3 mutants was impaired. Thus, I tested the effect of the BAG3 mutants on the clearance of well-known substrates of CASA complex in HEK293T cells. Among the various possibilities, I selected two different “reporter proteins”: i) the SOD1 carrying the ALS-causative mutations G93A and ii) a poly-GA dipeptide, which is one of the five C9ORF72-related DPRs, causative of some familial forms of ALS-FTD. Indeed, our laboratory previously demonstrated that both these misfolded and aggregating substrates are cleared when CASA activity is potentiated by HSPB8 overexpression (Crippa et al., 2010; Cristofani et al., 2018). As reported in **Fig. 2.7 A**, co-transfection of BAG3 P209 mutants with SOD1-G93A resulted in higher levels of HMW species of the misfolded SOD1-G93A in FRA, while no significant changes were detected on protein levels in WB in respect to the BAG3 WT or the E455K mutant. Accordingly, when BAG3 constructs were co-transfected with a flag-tagged poly-GA (**Fig. 2.7 B**), a similar trend was observed in the accumulation of HMW species in presence of the P209 BAG3 mutants, in respect to the BAG3 WT or E455K. These results suggest that CASA complex activity is impaired, and CASA-substrates are no more processed through the CASA when P209 mutants are present.

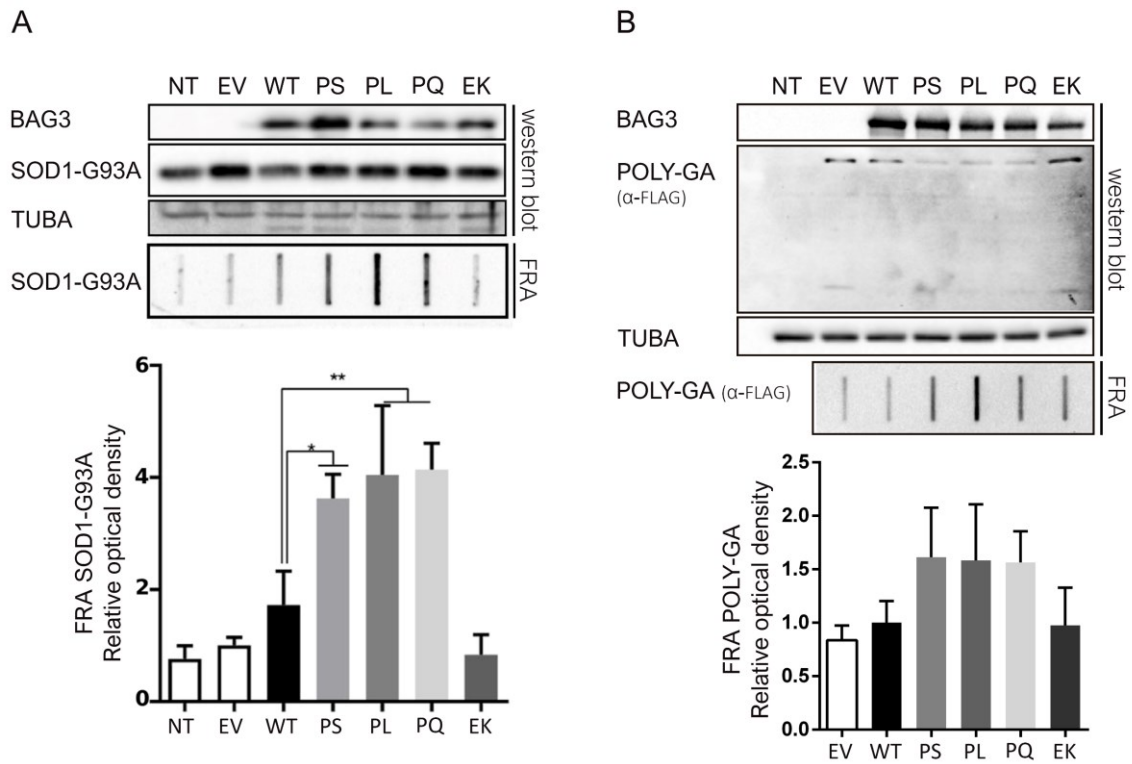


Figure 2. 7 BAG3 P209 mutants cause the failure of CASA activity.

A. WB and FRA results on HEK293T cells transiently co-transfected with an empty vector (EV) or BAG3-GFP constructs and mutant SOD1-G93A. Relative optical densities are reported in the graph as means ± SD of normalized values. One-Way ANOVA with Bonferroni's multiple comparisons test were used for statistical analysis. * $p < 0.05$, ** $p < 0.01$ ($n = 3$). **B.** WB and FRA results on HEK293T cells transiently co-transfected with an empty vector (EV) or BAG3-GFP constructs and FLAG-tagged polyGA, one of the five DPRs related to C9ORF72 hexanucleotide expansion. Relative optical densities are reported in the graph as means ± SD of normalized values ($n = 3$).

2.3.8 The degradation of the BAG3 mutants occurs mainly through autophagy

BAG3 degradation occurs mainly through the autophagic pathway in concert with all CASA complex (Arndt et al., 2010). To test whether BAG3 P209 aggregating prone mutants and the E455K mutant were degraded through autophagy as well, I evaluated protein levels and accumulation after autophagy or proteasome inhibition, using 3-MA and MG-132, respectively. BAG3 P209L mutant was used as representative of all P209 mutants. As shown in **Fig. 2.8 A**, autophagy inhibition resulted in an increase of all BAG3 WT and mutants total protein levels and insoluble species. Moreover, 3-MA treatment caused an increase in HSPB8 protein levels, in agreement to the fact that HSPB8 is also degraded through the autophagic pathway. I next evaluated the role of the proteasome on BAG3 degradation and accumulation, using MG-132 treatment alone or in combination with the dynein inhibitor EHNA, which has been proven to inhibit aggresome formation by blocking the ATP binding site of dynein (García-Mata et al., 1999). As shown in **Fig. 2.8 B**, upon proteasome inhibition there was an increase in all BAG3 WT and mutants protein levels, but less pronounced for BAG3 P209L. Instead, proteasome inhibition exerted a different impact in insoluble species accumulation among mutants, with a higher increase for BAG3 E455K mutant in respect to the BAG3 WT and no increase for BAG3 P209L. The interpretation of this differential increase in BAG3 WT or mutants after MG-132 treatment is not univocal: on one hand, this phenomenon supports the notion that the induction of aggresome formation has a slight impact on P209L aggregates, as these aggregates are already present in the aggresomal structures, in line with colocalization results of BAG3 P209L mutant with vimentin under untreated conditions. On the other hand, proteasome inhibition has a major effect on the clearance of the most soluble BAG3 mutant, which is the BAG3 E455K mutant. The latter hypothesis is in line with the observations that soluble proteins are preferentially routed to the proteasome system. Interestingly, EHNA treatment did not exert any effect on BAG3 protein levels and solubility, alone or in combination with MG-132. The lack of effect of EHNA against BAG3 P209L aggresome formation may be related to the fact that the compound cannot counteract the accumulation of preformed aggregates, as the treatment was performed after protein expression.

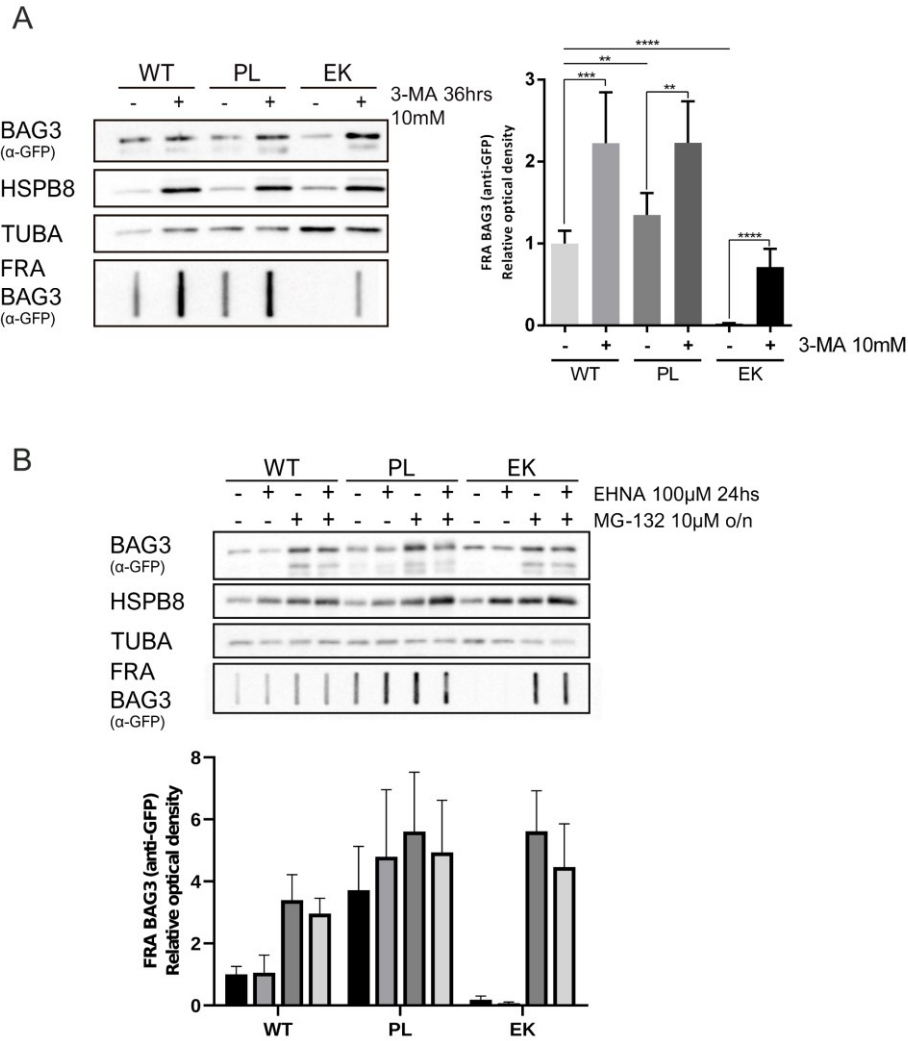


Figure 2. 8 BAG3 P209 mutant degradation occurs mainly through autophagy.

A. WB and FRA analyses of HEK293T stably expressing HSPB8-V5 transiently transfected with BAG3-GFP constructs, untreated or treated the autophagic inhibitor 3-MA, 10mM for 36hrs. Relative optical densities are reported in the bar graph as means \pm SD of normalized values. Student T tests were used for statistical analysis to compare the treated with untreated condition for each respective BAG3 variant; ** $p < 0.01$, *** $p < 0.001$, **** $p < 0.0001$ ($n=3$). **B.** WB and FRA analyses of HEK293T stably expressing HSPB8-V5 transiently transfected with BAG3-GFP constructs, untreated or treated with EHNA (24hs, 100 μ M) and/or MG-132 (overnight, 10 μ M). FRA relative optical densities are reported in the bar graphs as means \pm SD of normalized values. ($n=3$).

2.3.9 The autophagic stimulator trehalose favours the clearance of BAG3 P209L mutant aggregates

Therapeutic approaches to counteract BAG3 P209 mutants-related diseases are missing. Recently, it was demonstrated that the BAG3 P209L mutant exerts its toxic function by impeding HSP70/HSPA refolding cycle and that, by genetic or chemical inhibition of HSP70/HSPA-BAG3 interaction, BAG3 P209L aggregation can be reverted (Meister-Broekema et al., 2018). However, as authors warn, the drawbacks of a long-term use of non-specific inhibitors of HSP70/HSPA are not yet clear. Given these observations, I sought a different approach to favour the removal of BAG3 P209 mutants. Our laboratory has already demonstrated that misfolded substrates can be cleared by enhancing the autophagic machinery and flux by using the natural compound trehalose (Rusmini et al., 2019). Trehalose exerts its pro-autophagic activity by inducing a transient lysosomal permeabilization, which, in turn, activates the transcription factor EB (TFEB), also known as master regulator of autophagy. TFEB, when activated, is dephosphorylated and translocates into the nucleus, where it activates CLEAR element to promote the expression of autophagic genes. Therefore, trehalose, by causing a transient damage of lysosomes, induces lysophagy and, indirectly, the removal of aggregated proteins. Given that BAG3 P209 mutants aggregate and are removed through the autophagic pathway, I evaluated if trehalose also affects BAG3 P209 clearance. The data collected showed that the treatment with trehalose enhanced the autophagic flux, by enhancing the conversion of LC3-I to LC3-II as evaluated by WB (**Fig. 2.9 A**). Regarding BAG3 WT or mutants, trehalose had a slight impact in the clearance or stabilization of soluble BAG3 WT and E455K mutants, while decreased protein levels of the BAG3 P209L mutant. On the other hand, the analysis of the insoluble protein fraction by FRA showed that trehalose decreased the overall accumulation of insoluble BAG3 species both in the case of the WT and mutant proteins, but with a clear and significant impact only against the aberrant aggresome-forming BAG3 P209L mutant. Intracellular localization studies performed using IF (**Fig. 2.9 B**) confirmed a decrease in cells bearing aggregates, which resulted less bright or completely disappeared in cells positive for nuclear TFEB, suggesting a beneficial effect of trehalose on BAG3 aggregation.

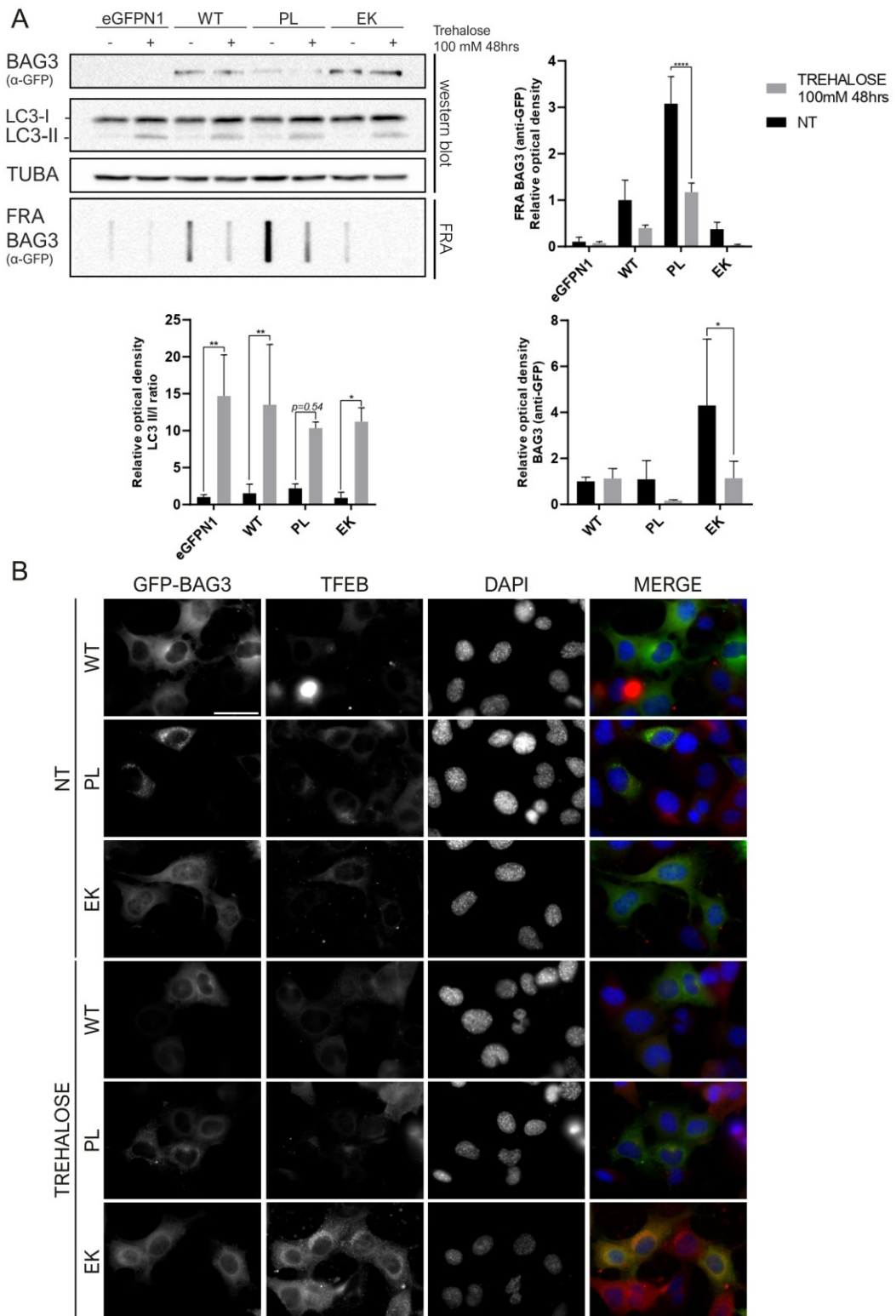


Figure 2. 9 The autophagic stimulator trehalose favours the clearance of BAG3 P209L mutant aggregates. **A.** WB and FRA analyses of NSC-34 transiently transfected with BAG3-GFP constructs, untreated or treated with the autophagic stimulator Trehalose, 100mM for 48 hrs. Relative optical densities are reported in the bar graph as means \pm SD of normalized values. Student T tests were used for statistical analysis to compare the treated with untreated condition for each respective BAG3 variant; * $p < 0.05$, ** $p < 0.01$, **** $p < 0.0001$ ($n = 3$). **B.** IF analyses of NSC-34 transiently transfected with BAG3-GFP constructs, untreated or treated with the autophagic stimulator Trehalose, 100mM for 48 hrs. IF was performed against TFEB (red), and nuclei were stained with DAPI. (63X magnification).

2.4 Discussion

BAG3 is an HSP70/HSPA co-chaperone and key member in the CASA pathway. BAG3 acts as a scaffold in CASA complex formation by interacting with HSPB8, HSP70/HSPA and the dynein motor complex. Through these multiple interactions, BAG3 permits the routing of misfolded substrates to the aggresome, located at the MTOC, and caged by vimentin or other cell specific intermediate filaments. Aggregates deposits are then addressed to degradation through the autophagy-lysosomal pathway. Aggresomes are the visible result of misfolded proteins overload and define one of the subcellular sites for protein degradation. Indeed, several members and structures of the PQC system, included CASA members, proteasomes, autophagic adaptors and vesicles, and ubiquitinated proteins can be found at the aggresome. However, in most cases aggresomes are not visible, since damaged and misfolded proteins, non-physiological oligomers and aggregates are efficiently removed by the PQC system in healthy cells. But when the proteostasis network is tampered by an increase of misfolded substrates, mutations in PQC system members or a blockade of the proteostasis pathways, substrates accumulation is inevitable. The accumulation of proteinaceous material is particularly observed in diseases affecting neurons and muscle cells, such as NDs, neuropathies and several form of muscle diseases. Indeed, neurons and muscle cells are characterized by low or absent cell renewal and a delicate structural architecture. Unsurprisingly, mutation in PQC members, included CASA members, are causative of neuromuscular diseases. Regarding BAG3, mutations have been found in CMT2 disease (P209S), severe and young-onset (P209L) or mild late-onset (P209Q) myopathies. Interestingly, all these mutants affect the same amino acid residue, which falls in the second IPV domains responsible for HSPB8 binding. Instead, a mutation in the BAG domain of BAG3 (E455K), that weakens the interaction with HSP70/HSPA, has been related to DCM. In this part of my studies, I found that disease-related P209 mutants are characterized by a decreased solubility, causing their aggregation, while the cardiomyopathy-related mutant solubility is unaffected or even increased. In addition, BAG3 P209 mutants are still able to interact with the other member of CASA complex, causing their segregation into BAG3 aggregates. I also observed that BAG3 P209 aggregates tend to locate at the perinuclear region and stick to the nuclear envelope, even after the lysis of the cell membranes and loss of cytoplasmic material. Indeed, I found that BAG3 P209 mutants aggregates locate at the aggresome, as supported by the aggresomal marker vimentin and HDAC6 colocalization. This BAG3 and CASA members relocation to aggresomes results in a failure of CASA in the removal of misfolded proteins, as demonstrated using the well-known CASA clients mutant SOD1-G93A and the polyGA DPR. The impairment in the clearance of misfolded substrates is not due to a defect in

autophagic flux (data not shown). Indeed, it was recently demonstrated by (Meister-Broekema et al., 2018) that this impairment is caused by the effect of BAG3 P209 mutants through the stalling of the HSP70/HSPA refolding cycle.

Another question of interest of my studies on BAG3 P209 mutants was related to a genotype-phenotype relationship. Indeed, the different P209 mutations have been related to phenotypes characterized by a different degree of severity. While the analyses of BAG3 mutants in motoneurons and muscle cells models did not reveal any significant differences in BAG3s P209 behaviour, which resulted aggregating in both cell lines, I obtained some information by analysing the contribute to solubility of the specific BAG3 substitutions. Indeed, an *in silico* approach revealed that the two IPV domains are characterized by a low intrinsic solubility. The substitution of the proline at position 209 with the diseases-related amino acids revealed an augmented decrease in the intrinsic solubility, more pronounced for the P209L mutant, which is linked to the worst phenotype. These results might explain the observation of a higher aggregation propensity of the BAG3 P209L mutant but fail to explain why the mutations in the same residue are related to diseases affecting different cell types, suggesting a role of the genetic or epigenetic background in the development of the diseases. Instead, E455K substitution did not have a strong impact on BAG3 solubility profile, suggesting that, while P209 mutated BAG3 is characterized by an intrinsic loss of solubility, E455K slightly higher solubility is dependent on its interaction to HSP70/HSPA. It has been recently demonstrated that inhibiting HSP70/HSPA activity counteracts the aggregation prone behaviour of BAG3 P209 mutant. However, a therapeutic strategy based on a non-selective inhibition of HSP70/HSPA members brings into questions:

- (i) which are the side effects of a general inhibition of the HSP70/HSPA, knowing that HSP70/HSPAs represent a central hub in proteostasis maintenance?;
- (ii) which are the long-term side effects related to the disruption of CASA complex, knowing its role in structural maintenance of muscle cells and neurons?

Thus, since CASA complex is physiologically degraded through autophagy, I reasoned that pushing its lysosomal degradation would have been a better therapeutic approach. In this manner, BAG3 misfolding and aggregating prone mutant and all the co-segregated co-factors and ubiquitinated proteins would be degraded, favouring the emptying and clearance of the aggresomes. In support to this notion, it was recently demonstrated that ubiquitin-positive accumulated proteins can be removed by autophagic induction in a Zebrafish model of BAG3 P209L-related DCM (Ding et al., 2019). After demonstrating that BAG3 P209 mutants are still dependent on the autophagic system for their degradation, similarly to the BAG3 WT (shown here and in (Arndt et al., 2010)), I tested the enhancement of the autophagic pathway by using trehalose. Trehalose is a natural compound that boosts

autophagy by causing a transient and mild permeabilization of lysosomes. By damaging lysosomes, trehalose activates a protective response in cells, which is the selective removal of lysosome, or lysophagy. The molecular mechanism underlying trehalose-mediated lysophagy activation was recently demonstrated in our laboratory (Rusmini et al., 2019) and is mediated by the activation of the autophagic master regulator TFEB. TFEB is a transcription factor that shuttles into the nucleus and enhances the expression of autophagy-related proteins. By enhancing autophagy, damaged lysosomes are removed, together with misfolded and aggregated proteins. Indeed, I observed that trehalose treatment in cells showed a beneficial effect by favouring the clearance of BAG3 P209L mutant insoluble species and defining a new therapeutic approach to investigate.

In conclusion, BAG3 P209 mutants are characterized by a similar biochemical behaviour in cells, suggesting that, independently from the phenotype, one therapeutic strategy to counteract its accumulation in cells could be effective in all BAG3 P209 mutant-related diseases.

Chapter III

3. Characterization and role of HSPB8 variants and mutants in neuromuscular diseases

3.1 BACKGROUND AND AIMS

HSPB8 belongs to the HSPB family, which shares a central ACD domain, and shows an antiaggregating and pro-degradative activity against a wide array of misfolded and aggregating prone proteins. These include the polyQ-AR, the polyQ-Htt, the ALS-mutated SOD1, the toxic CTFs of TDP-43 and the C9ORF72-related DPRs. HSPB8 prodegradative activity is exerted through the CASA complex. While several HSPBs are characterized by oligomerization, HSPB8 forms mainly dimers. In addition, the obligate partner of HSPB8 is BAG3, with whom interacts through a hydrophobic groove formed by its $\beta 4$ and $\beta 8$ sheets and form a 2:1 stoichiometric complex.

Similar to BAG3, HSPB8 mutations have been described in dHMNs, CMT2 and forms of myopathies. The most studied mutations all refer to substitutions of the Lys at position 141 (K141E/N/M) which have been found to affect HSPB8 dimerization. Little is known about the recently described frameshift mutations pP173Sfs*43, pQ170Gfs*45, and pT194Sfs*23, found in progressive distal neuropathy/myofibrillar pathology with rimmed vacuolar myopathy, adult-onset axial and distal myopathy and proximal limb-girdle rimmed vacuolar myopathy, respectively.

In addition, new variants of HSPB8 have been recently found in ALS patients by our collaborators Nicola Ticozzi, Vincenzo Silani and Antonia Ratti, (Department of Neurology and Laboratory of Neuroscience (IRCCS Istituto Auxologico Italiano, Milan) and Dipartimento di Fisiopatologia Medico-Chirurgica e dei Trapianti, Centro 'Dino Ferrari' (University of Milan) (*unpublished*). These variants include the substitution of the Ser at position 9 with a Pro (S9P), of the Pro at position 41 with a Ser (P41S) and of the Ser at position 181 with a Cysteine (S181C).

In this section, I will present results obtained on HSPB8 ALS-related variants and myopathy/neuropathy frameshift mutants.

I firstly focused on ALS-related variants by evaluating their proteins levels, localization, and aggregation in respect to HSPB8 WT. I next assessed the stability of the selected HSPB8 variants and the effect of HSPB8 ALS-variants on the HSPB8 WT. Moreover, I tested the dimerization ability of HSPB8 variants and the competition for BAG3 binding with HSPB8 WT.

Using a similar approach, I then performed a basal characterization of the novel frameshift mutants, evaluating their levels and aggregation prone behaviour. Next, I evaluated the effect of the frameshift mutants against the HSPB8 WT and the partner BAG3. Since I observed the formation of small cytoplasmic aggregates and since HSPB8 is involved in the formation of SQSTM1/P62-regulated ubiquitinated microaggregates, I then confirmed that HSPB8 frameshift mutants co-segregate with ubiquitinated proteins and SQSTM1/P62.

Finally, to gain more insights into the molecular mechanism underlying HSPB8 mutants, I tested whether the aggregation prone behaviour of HSPB8 frameshift mutants depends on the presence of the partner BAG3. Since HSPB8 frameshift mutants aggregate in a similar manner to BAG3 P209 mutants, I next evaluated the pro-autophagic compound trehalose in HSPB8 aggregates clearance. Indeed, I previously showed that trehalose assists in the removal of BAG3 aggregates representing a therapeutic strategy not only in NDs, but also in HSPB8 and BAG3 -related diseases.

3.2 Materials and Methods

Chemicals and reagents

Cycloheximide (Sigma-Aldrich, C4859) was used 10 μ M for 8 or 24 hrs. D-(+)-trehalose dihydrate (trehalose) (Sigma-Aldrich, T9531) was used at concentration and time previously mentioned.

Plasmids

The following plasmids were used:

- pCDNA3, purchased from Invitrogen (Carlsband, CA, USA), is an empty vector (EV) used as a control;
- pBAG3-GFP wildtype (WT) and mutants Δ IPV 1+2, Δ PxxP, Δ BAG, R480A encode for GFP-tagged BAG3 WT or functional mutants and were kindly provided by E.A. and V.T. (Peripheral Neuropathy Research Group, Department of Biomedical Sciences, Institute Born Bunge, University of Antwerp, Antwerp, Belgium). The pBAG3-GFP plasmids are a kind gift of Josée N. Lavoie and described in (Fuchs et al., 2015);
- pCi-HSPB8 wildtype and Lys141Glu (KE) encoding the WT or the neuropathy-associated mutant were previously described (Crippa et al., 2010);
- pCi-HSPB8 Ser9Pro (SP), Pro41Ser (PS), Ser181Cys (SC) carrying the ALS-associated point variants were obtained by pCi-HSPB8 wildtype mutagenesis (Eurofins genomics service);
- pCi-HSPB8 frameshift mutants Pro173Serfs*43, Thr194Serfs*23, Gln170Glyfs*45 were obtained by subcloning the predicted frameshifted sequence in pCi-HSPB8 wildtype vector, using Sall and Apal restriction enzymes and T4 ligase. All the enzymes were purchased from NEB (New England Biolabs, Ipswich, MA, England);
- pHSPB8-GFP-WT encodes for a GFP-tagged HSPB8 protein;
- pSQSTM1/P62-mCherry encodes for the mCherry-tagged SQSTM1/P62 autophagic adaptor protein.

Cell cultures

HEK293T-HSPB8-V5 and NSC-34 were grown as previously described.

Transfection

The day before transfection, cells were seeded at the cellular densities previously described.

Then, HEK293T-HSPB8-V5 and NSC-34 cells were transfected using Lipofectamine3000/P3000 reagent following the manufacturers' instruction (Invitrogen, Thermo Scientific Life Science Research, Waltham, MA, USA). Plasmids pCDNA3, as mock, or pCi-HSPB8 constructs (wildtype or mutants) were transfected alone or co-transfected with plasmid encoding BAG3-GFP WT or functional mutants, or SQSTM1/P62-mCherry, or HSPB8-GFP-WT.

Protein extractions and quantification

48 hrs after transfection, cells were harvested and centrifuged 5 min at 100 *g* at 4°C. Cell pellets were then resuspended in RIPA lysis buffer (0.15 M NaCl, 20 mM Na-deoxycholate, 100 μ M Na₃VO₄, 50 mM NaF, 5 mM Na-iodoacetate, 2.5 mM Tris-HCl pH 7.7, 10 mM EDTA pH 8.0, 0.08%w/v SDS, 0.8%v/v Triton X-100) added with protease inhibitors cocktail (Sigma-Aldrich) and lysed using slight sonication. For NP-40 soluble and insoluble fraction, cells pellets were treated as previously described. Protein content quantification was performed with bicinchoninic acid (BCA) assay (Cyanagen).

Western Blot and Filter Retardation Assay

SDS-PAGE was performed as previously described. 10 μ g of HEK293T-HSPB8-V5 protein lysates and 25 μ g of NSC-34 protein lysates were loaded and then electro-transferred onto 0.45- μ m nitrocellulose membranes (Bio-Rad Laboratories, Hercules, CA, USA). To detect insoluble species, FRA was performed by loading 3/6 μ g of total protein onto a 20% MeOH-treated 0.2- μ m cellulose acetate membrane (Whatman 100404180) and filtered. WB and FRA membranes were incubated with a blocking solution of 5% non-fat dried milk in TBS-Tween (20 mM Tris-HCl pH 7.5, 0.5 M NaCl, 0.05% Tween-20) for 1 h and then incubated with primary antibodies diluted in the same solution overnight. Primary antibodies used were: mouse monoclonal anti-GFP antibody (ab1218, Abcam or MAB-94345, Immunological Sciences), mouse monoclonal anti- α -tubulin (T6199, Sigma-Aldrich), homemade rabbit polyclonal anti-BAG3 (Carra, Seguin, & Landry, 2008), homemade rabbit polyclonal anti-HSPB8 (#23) (Carra et al., 2005), mouse monoclonal anti-HSPB8 (ab66063, Abcam), rabbit polyclonal anti-HSPB8 (ThermoFisher, PA5-76780), rabbit polyclonal anti-V5 (D3H8Q, #13202, Cell Signaling), rabbit polyclonal anti-LC3 (L8918, Sigma-Aldrich), rabbit polyclonal anti-p62/SQSTM1 antibody (ab91526, Abcam). Then, membranes were washed three times in TBS-Tween for 10 min and incubated with the peroxidase-conjugated

secondary antibodies goat anti-rabbit and anti-mouse IgG-HRP (111-035-003, 115-035-003; Jackson ImmunoResearch Laboratories, Inc.). Proteins were immunodetected as previously described.

Fluorescence microscopy and immunofluorescence

Cells were fixed with a solution 1:1 of 4% paraformaldehyde and 4% sucrose in 0.2 N PB (0.06 M KH₂PO₄, 0.31 M Na₂HPO₄; pH 7.4) for 25 min at 37 °C and then washed with PBS solution 3 times 5 min. Cells were permeabilized and nonspecific sites blocked using a solution of 0.1% Triton X-100, 1% BSA and 10% FBS in PBS for 40 minutes at RT. Then, the primary antibodies diluted in 0.1% BSA in PBS were incubated overnight at 4°C: rabbit polyclonal anti-HSPB8 (HPA015876, SIGMA LifeScience) and rabbit polyclonal anti-HSPB8 (PA5-76780, ThermoFisher). The following day, primary antibody was removed, and cells washed with 0.1% BSA in PBS. Then, secondary antibodies goat anti-rabbit 549 AlexaFluor (1:1000, Life Technologies, Thermo Fischer, A-11012) or goat anti-rabbit 488 AlexaFluor (1:1000, Life Technologies, Thermo Fischer, A-11008) diluted in 0.1% BSA in PBS were incubated for 1 hr at RT. Three washing steps with PBS, with the middle one containing DAPI (in PBS) to stain nuclei were made. Coverslips were then mounted with MOWIOL onto slides. An Axiovert 200 microscope (Zeiss, Oberkochen, Germany) with a photometric CoolSnap CCD camera (Robber Scientific, Trenton, NJ, USA) was used for images capture and images were processed using Metamorph software (Universal Imaging, Downingtown, PA), as previously described.

Immunoprecipitation

Cells were harvested and then centrifuged at 100 g for 5 min at 4°C. Pellets were resuspended in RIPA buffer with protease inhibitors cocktail and then centrifuged at maximum speed. For immunoprecipitation assay, SureBeads Protein A Magnetic Beads (BIO-RAD) were used, following the manufacturers' instructions. The home-made anti-BAG3 or the anti-V5 (D3H8Q, #13202, Cell Signalling) antibodies were used for immunoprecipitation. Samples were then run on SDS-PAGE and a WB was performed (see WB and FRA section).

Damaging missense mutations prediction

PolyPhen-2 browser (<http://genetics.bwh.harvard.edu/pph2/index.shtml>) (Adzhubei et al., 2010) and SIFT browser (<https://sift.bii.a-star.edu.sg/>) (Sim et al., 2012) were used to predict the impact of ALS-related amino acids substitution on HSPB8 structure and function.

Protein solubility prediction

CamSol browser (<http://www.vendruscolo.ch.cam.ac.uk/camsolmethod.html>) was used to obtain the intrinsic solubility profile of HSPB8 WT and mutants following the procedure described in (Sormanni et al., 2015). Tango browser (<http://tango.crg.es>) (Fernandez-Escamilla et al., 2004) was used to obtain the aggregation propensity of HSPB8 WT and mutants. In both cases the full-length protein sequence of HSPB8 (NP_055180.1) or their mutants were used as inputs.

For CamSol method, the reported graphs show the protein solubility profiles restricted to the HSPB8 CTD (amino acids 164-196 for HSPB8 WT, 164- predicted C-terminus for HSPB8 frameshift mutants).

For Tango, the graphs report the Beta-aggregation propensity obtained through the analyses restricted to the HSPB8 CTD (amino acids 160-196 for HSPB8 WT, 160- predicted C-terminus for HSPB8 frameshift mutants), using the following parameters: no protection at the N-terminus or C-terminus of the peptide sequence, pH 7, temperature 298.15 K, ionic strength 0.02 M, and concentration 1 M.

Statistic

Student T-tests or One-Way ANOVA with Bonferroni's multiple comparisons tests were performed, as indicated in each figure, and using PRISM software (GraphPad Software, La Jolla, CA, USA).

3.3 Results

3.3.1 ALS-related variants in HSPB8 do not affect protein levels, solubility and localization

The HSPB8 variants identified in ALS patients have never been described in literature, so far. Thus, I first evaluated if the amino acids residues affected in the variants are conserved in the HSPBs family. Based on the alignment proposed by Boelens et al. (2020), I observed that all the substitutions fall outside from the conserved residues of the HSPB family members, and do not affect functional motifs. However, all substitutions locate in the CTD and NTD of HSPB8, which are poorly conserved among HSPBs family and, thus, might mask potential specific functional properties of HSPB8. On these bases, I used PolyPhen-2 and SIFT as *in silico* tools for the prediction of a damaging effect of amino acids substitutions. PolyPhen-2 analyses showed that S9P and P41S are predicted to be benign on HSPB8 function, while the S181C substitution is possibly damaging. Similarly, the SIFT analyses revealed that, while S9P and P41S substitutions are predicted to be tolerated, the S181C substitution might affect protein function, even if with low confidence (**Fig. 3.1 A**). However, since the role of these substituted amino acids on HSPB8 structure and activities has not been assessed yet, prediction tools should be supported by experimental findings. Thus, independently from these predictions, I proceeded with the experimental analyses on HSPB8 variants in respect to the HSPB8 WT and to the known mutant K141E, as a positive control. I first analysed HSPB8 protein levels and aggregation, by transient overexpression of HSPB8s in NSC-34. Results showed that the ALS-related variants of HSPB8 are not characterized by variations of the overall protein levels if compared to the HSPB8 WT or the K141E mutant (**Fig. 3.1 B**). This observation suggested that the amino acids substitutions in these variants do not affect protein stability, excluding a potential haploinsufficiency mechanism related to the loss of HSPB8 and, thus, to an imbalance of the PQC system, as observed in NDs. In addition, I tested the HSPB8s accumulation in HMW insoluble species, to unveil a misfolding and aggregating prone behaviour of these ALS-related variants. Indeed, several mutated proteins causative of ALS are characterized by misfolding and aggregation, which determine a gain of proteotoxic function and a loss of function of the protein affected. However, the analyses of HMW insoluble species did not reveal differences between ALS-related HSPB8 variants and HSPB8 WT (**Fig. 3.1 B**). Even the K141E HSPB8 mutant did not accumulate in insoluble species, contrary to what is reported in literature (Irobi et al., 2004). In addition, I did not observe an effect of ALS-related variants on the levels of the binding partner BAG3 and on the autophagic adaptor SQSTM1/P62 (**Fig. 3.1 B**).

The absence of an aggregating prone behaviour of ALS-related HSPB8 variants was confirmed by analysing their intracellular distribution through IF (**Fig. 3.1 C**). Indeed, all HSPBs were characterized by a diffuse distribution, mainly cytoplasmatic, as previously reported for HSPB8 WT. Again, the K141E mutant was not characterized by formation of aggregates.

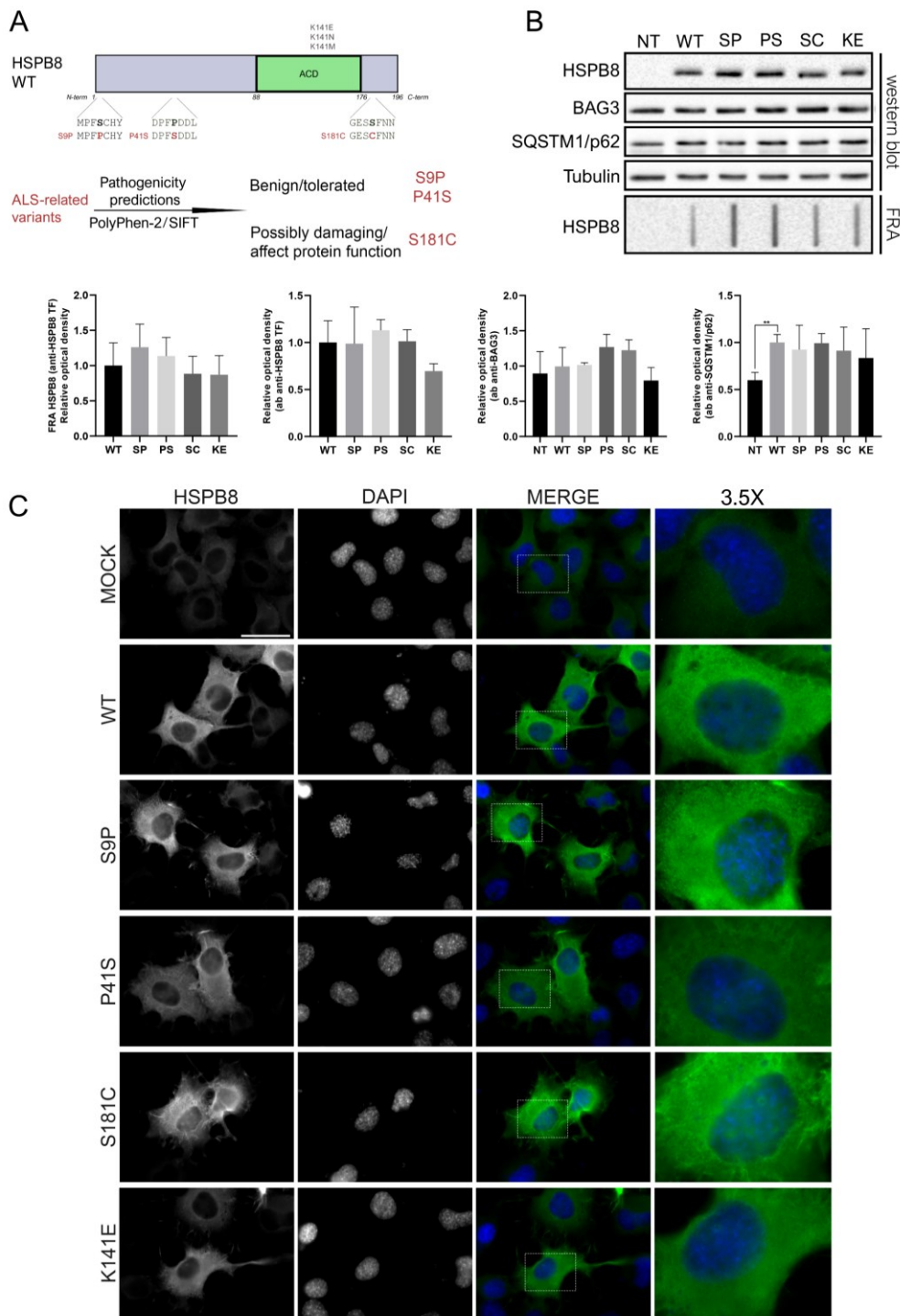


Figure 3. 1 ALS-related variants in HSPB8 do not affect protein levels, solubility, and localization.
A. Schematic representation of HSPB8 WT structure. ALS-related variants S9P, P41S, S181C, and the known mutant K141E are reported, and tools for pathogenicity predictions. **B.** WB and FRA analyses of whole cell lysates of NSC-34 untransfected (NT) or transiently transfected with HSPB8 constructs. WB/FRA relative optical densities are reported in the graphs as means \pm SD of normalized values. Student *t* tests were performed: ** $p < 0.01$ ($n = 3$). **C.** IF on NSC-34 transiently transfected with HSPB8 constructs or a mock. Nuclei were stained with DAPI (Scale bar = 10 μ m; 63X magnification). The constructs were abbreviated as follows: non-transfected (NT), empty vector (MOCK), wildtype (WT), S9P (SP), P41S (PS), S181C (SC), K141E (KE).

3.3.2 Analysis of the biochemical behaviour of ALS-related variants of HSPB8

Since our preliminary studies did not reveal differences in levels and aggregation prone behaviour of ALS-variant of HSPB8, I next evaluated the stability of HSPB8 variants through a cycloheximide (CHX) assay. Indeed, I hypothesized that differences in stability could have been masked using an overexpression system of HSPB8 constructs. Protein translation was blocked by CHX 8 or 24 hrs before collecting cells and HSPB8 WT and variants protein levels were evaluated (**Fig. 3.2 A**). I observed that the overexpressed HSPB8 WT protein levels were halved after 8 hrs treatment and almost completely absent after 24 hrs treatment. The ALS-related variants of HSPB8 were characterized by an almost identical rate of degradation, suggesting that they are not characterized by a different stability in respect to the HSPB8 WT. Again, no differences were observed between the HSPB8 WT and the known mutant HSPB8 K141E.

I next examined the biochemical behaviour of ALS-variants under native and non-reducing conditions, to test whether these mutants were characterized by unexpected quaternary or tertiary structures features. Indeed, even if I did not find substantial differences in the native structure between HSPB8 WT and ALS-variants, using native-PAGE (*data not shown*), I observed a unique feature of the S181C ALS-related variant of HSPB8 under non-reducing conditions. In particular, the S181C variant was characterized by a higher electrophoretic mobility in respect to the HSPB8 WT and the other HSPB8 variants and the mutant (**Fig. 3.2 B**). I speculated that this feature was likely related to the formation of a novel intramolecular disulphide bond, since HSPB8 protein possesses three other cysteines, at position 10, 99 and 195.

This observation prompted me to evaluate the ability of HSPB8 S181C to dimerize and interact with the CASA-partner BAG3. All the ALS-related variants and the K141E mutant were included in the analyses. First, I tested the effect of the ALS-related variants on the HSPB8 WT using the HEK293T cells that stably express the V5-tagged HSPB8, to discriminate the two HSPB8 forms. As shown in **Fig. 3.2 C**, the expression of HSPB8 WT, HSPB8 ALS-related variants and K141E mutant did not modify HSPB8-V5 protein levels, suggesting no impact on the WT counterpart stability and accumulation. Since HSPB8-V5 levels were unaffected by HSPB8 variants, I evaluated the dimerization by Co-IP, taking advantage of the V5 tag (**Fig. 3.2 D**). Results showed that both HSPB8 WT and variants were able to interact with the HSPB8-V5 WT, indicating no increased or decreased interaction. Instead, the HSPB8 K141E mutant showed a slight increased interaction with the HSPB8-V5, in line with data reported in literature (Fontaine et al., 2006). Thus, I evaluated the ability of ALS-related variant to compete with the HSPB8 WT for BAG3 binding (**Fig. 3.2 E**). I observed that all the transiently transfected HSPB8s were able to

interact with the partner BAG3 and to compete with the endogenous expressed HSPB8-V5. Indeed, Co-IP results showed that the endogenous HSPB8-V5 is able to interact with BAG3 in untransfected or mock-transfected samples, but, in presence of HSPB8 WT and variants, the amount of the co-immunoprecipitated HSPB8-V5 is reduced, indicating that all the exogenous HSPB8s compete with the endogenous protein for BAG3 binding.

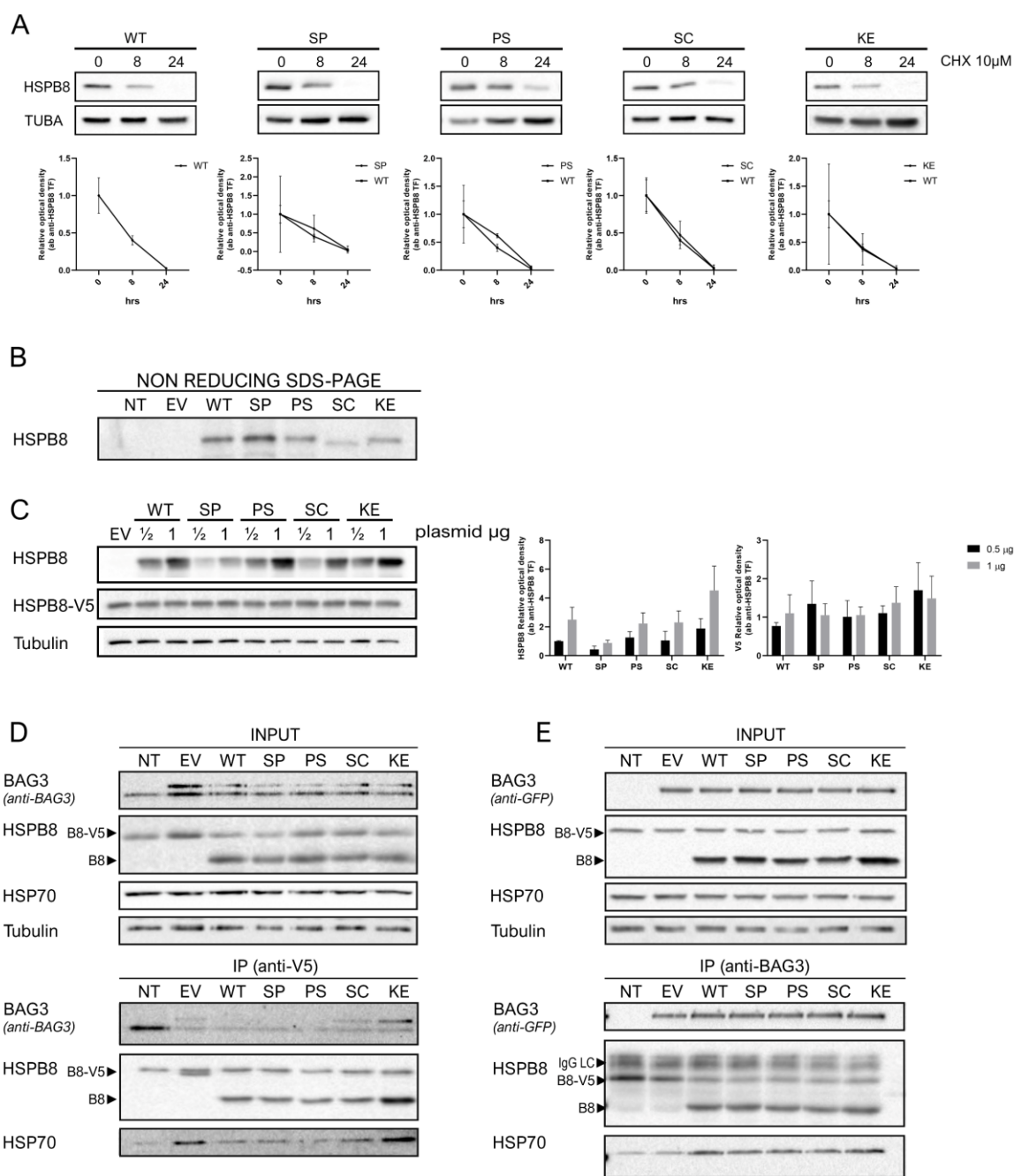


Figure 3. 2 Analysis of the biochemical behaviour of ALS-related variants of HSPB8.

A. WB analyses of whole cell lysates of NSC-34 untransfected (NT) or transiently transfected with HSPB8 constructs. To inhibit protein synthesis the cells were treated with 10 μ M cycloheximide (CHX) for 8 or 24 hrs. WB relative optical densities are reported in the graphs as means \pm SD of normalized values. (n=3) **B.** WB analyses of whole cell lysates of NSC-34 untransfected (NT) or transiently transfected with HSPB8 constructs or an empty vector, obtained after non-reducing SDS-PAGE **C.** WB of HEK293T stably expressing HSPB8-V5 and transiently transfected with HSPB8 constructs (0.5 or 1 μ g plasmid). Relative optical densities are reported in the bar graphs as means \pm SD of normalized values. (n=3). **D.** Co-immunoprecipitation results and relative whole cell lysates WB on HEK293T cells stably overexpressing HSPB8-V5 and transiently transfected with HSPB8 constructs, empty vector or untransfected (NT). HSPB8 dimers formation was evaluated by using an anti-V5 tag antibody. **E.** Co-immunoprecipitation results and relative whole cell lysates WB on HEK293T cells stably overexpressing HSPB8-V5 and transiently transfected with HSPB8 constructs. HSPB8 binding to BAG3 and competition with HSPB8-V5 was evaluated by using an anti-BAG3 antibody.

3.3.3 Focus on frameshift mutants of HSPB8: sequences analyses reveal a common elongated C-terminal tail with decreased solubility profile

HSPB8 frameshift mutants observed so far in myopathy or neuropathy cases are (i) the pPro173Serfs*43 caused by a duplication of the cytosine 515 (c.dup515C), (ii) the pGln170Glyfs*45 caused by a deletion of the cytosine and adenine 508-509 (c.del508_509CA) and (iii) the pThr194Serfs*23 caused by the duplication of the tract GTCA at position 577-580 (c.dup577_580GTCA). All these frameshift mutants are predicted to cause an elongation of the C-terminal tract of HSPB8 and, in the case of the first two mutations, a different sequence of the HSPB8 CTD. To clarify the nature of the sequence caused by the frameshift mutations, I compared potential homologies in the predicted protein sequences (**Fig. 3.3 A**). Surprisingly, I observed that all the mutations determined the same reading frameshift on the predicted translated sequences, resulting in the same modification of the CTD of HSPB8 for the Pro173Serfs*43 and Gln170Glyfs*45 mutants, and the addition of an identical elongated C-terminal tail for all the HSPB8 mutants. In fact, all frameshifts ended at the same alternative stop codon downstream to that utilized by the normal Open Reading Frame. By comparing the HSPB8 frameshift protein sequences in respect to the conserved residues and motifs among HSPBs, described in (Boelens, 2020), I observed that these mutations did not affect fundamental hot-spots of HSPB8 and did not fall in the ACD. However, the analyses of the intrinsic solubility profile and the aggregation propensity through CamSol and TANGO methods, respectively, gave more insight into the features of the mutated CTDs (**Fig. 3.3 B**). In particular, the last 18 amino acids of the elongated C-terminal tract are characterized by a low intrinsic solubility, as predicted by CamSol method. An increased aggregation propensity was observed in the same region, in particular the PILVLSP tract, and in the modified CTDs of HSPB8 Pro173Serfs*43 and Gln170Glyfs*45, corresponding to the PSELLNIWR tract, using Tango software. These interesting observations encouraged me to evaluate the behaviour of the frameshift mutants in cells.

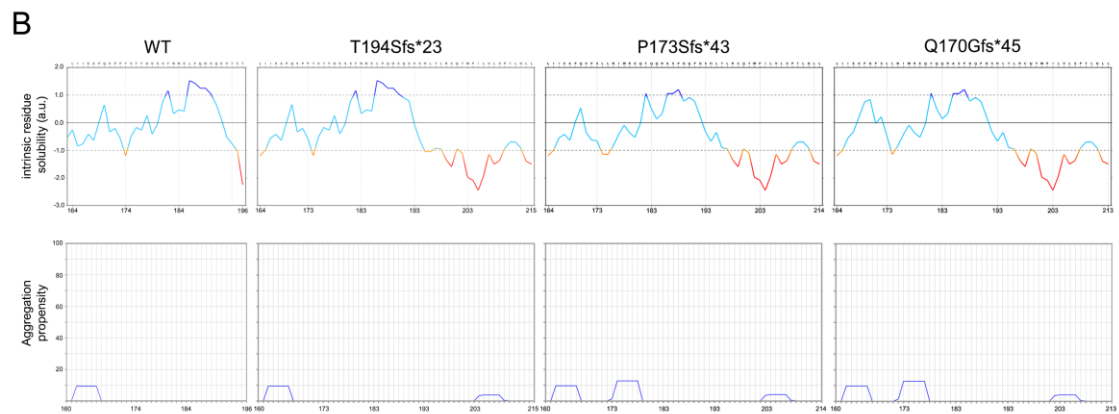
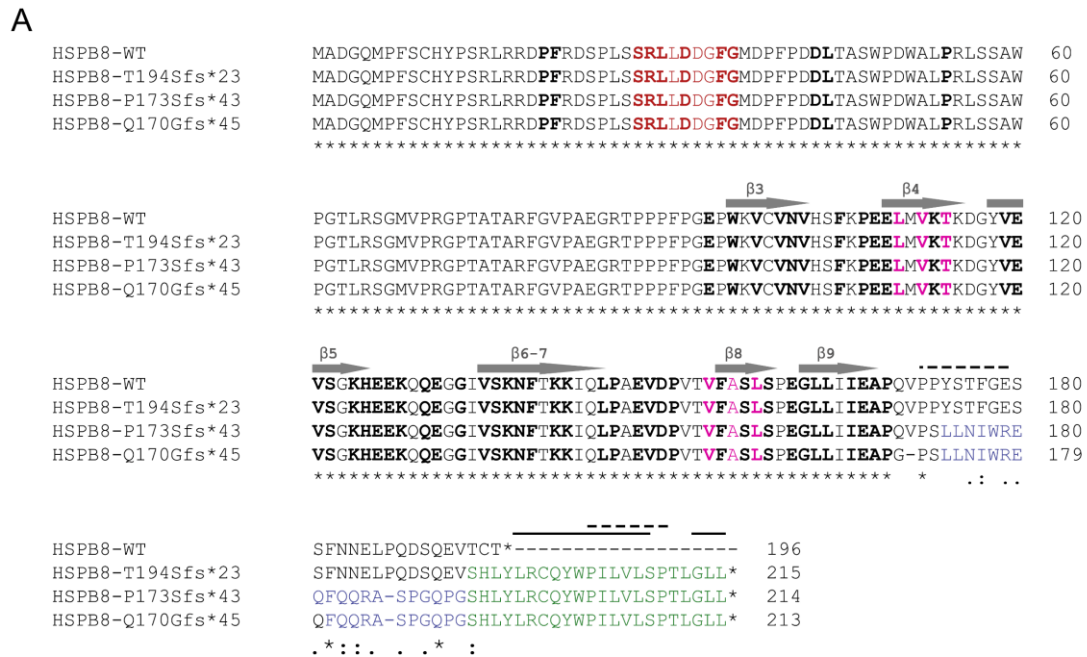


Figure 3. 3 Focus on frameshift mutants of HSPB8: sequences analyses reveal a common elongated C-terminal tail with decreased solubility profile.

A. Alignments of HSPB8 WT and frameshift mutant protein sequences (predicted) revealed a common modified CTD (blue) for P173Sfs*43 and Q170Gfs*45 mutants and a common C-terminal tail (green) for all HSPB8 frameshift mutants. Letters in uppercase and the down arrows indicate the conserved amino acids among HSPBs and the β -sheets, respectively, based on the alignment of Boelens et al., 2020. The SRLFDQxFG motif is indicated in red, the motifs responsible for BAG3 binding are indicated in pink. **B.** Bio-informatic analysis of the intrinsic solubility profile (Top, Camsol method) and the aggregation propensity (Bottom, Tango) of the CTD of HSPB8 WT and HSPB8 frameshift mutants reveal regions of low intrinsic solubility and high aggregation propensity of the elongated C-terminal tracts of the frameshift mutants.

3.3.4 Frameshift mutants of HSPB8 form insoluble species and cytoplasmic aggregates

Little is known about HSPB8 frameshift mutants and the feature I found in the common C-terminal tail has never been reported (**Fig. 3.4 A**). In literature, HSPB8 frameshift mutant proteins have never been observed by protein analyses techniques (e.g., WB), arising the hypothesis that these mutants are affected by mRNA decay or protein degradation. Thus, I first tested HSPB8 frameshift mutant protein levels and their propensity to form HMW insoluble species, by transient transfection of plasmids encoding HSPB8 WT and mutants. I observed that HSPB8 frameshift mutants were expressed and characterized by a proportional higher M.W., reflecting the predicted elongated protein sequences, as shown in WB (**Fig. 3.4 B**). In addition, HSPB8 frameshift mutants were characterized by a significant higher protein levels in respect to the HSPB8 WT and an aggregation prone behaviour, as reported in WB and FRA results (**Fig. 3.4 B**). Higher protein levels of the autophagic marker SQSTM1/P62 were detected in samples expressing the HSPB8 frameshift mutants in respect to those expressing the HSPB8 WT, while no significant differences in the BAG3 protein levels were observed. Interestingly, the Thr194Serfs*23 mutant, which shares the same CTD of HSPB8 WT, was characterized by lower protein levels in respect to the other frameshift mutants. In parallel, I used IF to evaluate the localization of HSPB8 mutants (**Fig. 3.4 C**) and found that, while HSPB8 WT is diffused mainly in the cytoplasm, as expected, the HSPB8 frameshift mutants formed several small cytoplasmic aggregates, mainly concentrated in the perinuclear region, paralleled by a decreased diffuse signal in respect to HSPB8 WT. In summary, these data support the previous observation of increased aggregation propensity of HSPB8 frameshift mutants which translates in the formation of small aggregates of the mutated proteins.

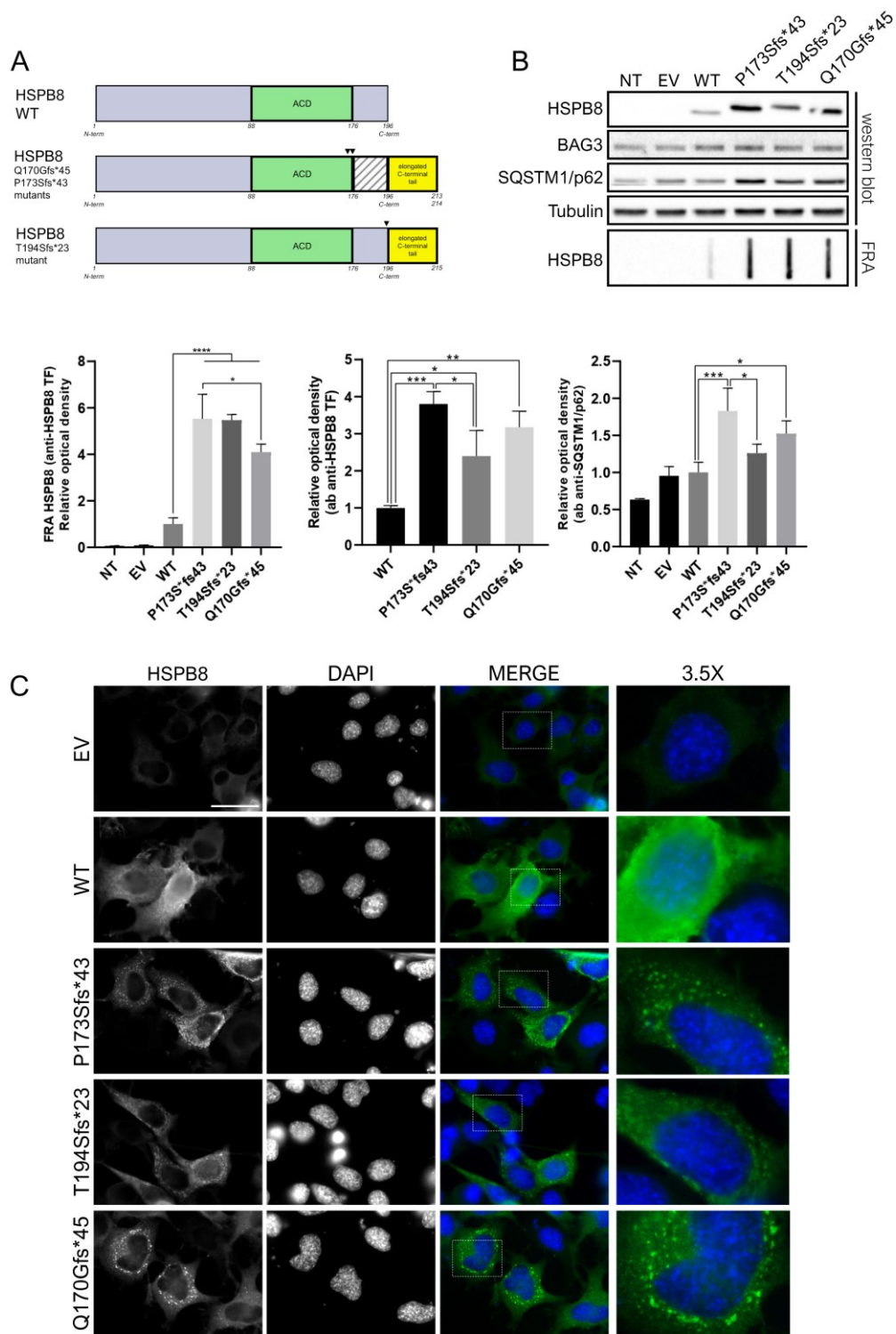


Figure 3. 4 Frameshift mutants of HSPB8 form insoluble species and cytoplasmic aggregates.

A. Schematic representation of HSPB8 WT and frameshift mutants structures **B.** WB and FRA analyses of whole cell lysates of NSC-34 untransfected (NT) or transiently transfected with HSPB8 constructs. WB/FRA relative optical densities are reported in the graphs as means \pm SD of normalized values. One-way ANOVA with Bonferroni's test was performed: * $p < 0.05$, ** $p < 0.01$, *** $p < 0.001$, **** $p < 0.0001$ ($n = 3$). **C.** IF on NSC-34 transiently transfected with HSPB8 constructs or an empty vector. Nuclei were stained with DAPI (Scale bar = $10 \mu\text{m}$; 63X magnification). The constructs were abbreviated as follows: non-transfected (NT), empty vector (EV), wildtype (WT).

3.3.5 Frameshift mutants of HSPB8 co-segregate with wildtype HSPB8, BAG3 and SQSTM1/P62 along with ubiquitinated proteins

Since HSPB8 frameshift mutants have been described in heterozygosis, I considered a fundamental step to evaluate the effect of the mutated forms of HSPB8 on its WT counterpart. Indeed, HSPB8 forms mainly homodimers, suggesting that these mutants can act in a dominant negative manner on the WT protein affecting its activity and solubility. To evaluate the effect of HSPB8 frameshift mutants on the HSPB8 WT, I took advantage of the previously described HEK293T cells that stably express a V5-tagged HSPB8. After transfecting HSPB8 frameshift variants, I tested the protein levels and accumulation of the V5-tagged HSPB8 WT protein, by specific immunodetection of the fused V5-tag. In addition, I tested HSPB8 frameshift mutants co-aggregation with the HSPB8 WT, by co-transfecting the constructs with a GFP-tagged HSPB8 WT, to directly observe the presence of GFP-positive aggregates. Interestingly, I found that HSPB8 frameshift mutants caused an increase in the protein levels and aggregation propensity of HSPB8 WT, suggesting their capability to sequester and co-segregate with the WT protein (**Fig. 3.5 A**).

To better define whether HSPB8 frameshift mutants also affect the main factors involved in the CASA complex, I tested their co-segregation along with HSPB8, by performing an NP-40 soluble/insoluble protein extraction. As shown in **Fig. 3.5 B**, the HSPB8 WT partitioned in the soluble fraction, while HSPB8 frameshift mutants were observed only in the insoluble extract, forming detergent resistant HMW insoluble species. In addition, I found that the partner BAG3 and the autophagic adaptor SQSTM1/P62, together with ubiquitinated proteins, were enriched in the insoluble fraction of HSPB8 frameshift mutants. The co-segregation of HSPB8 frameshift mutants with BAG3 and SQSTM1/P62 was confirmed by IF, observing the presence of HSPB8 and GFP-BAG3 WT or SQSTM1/P62-mCherry double positive aggregates (**Fig. 3.5 C**).

Collectively, these results suggest that HSPB8 frameshift mutants aggregation impacts on the HSPB WT and on the key factors of the CASA through a dominant negative effect, which might impair the entire selective pathway of damaged and misfolded protein degradation.

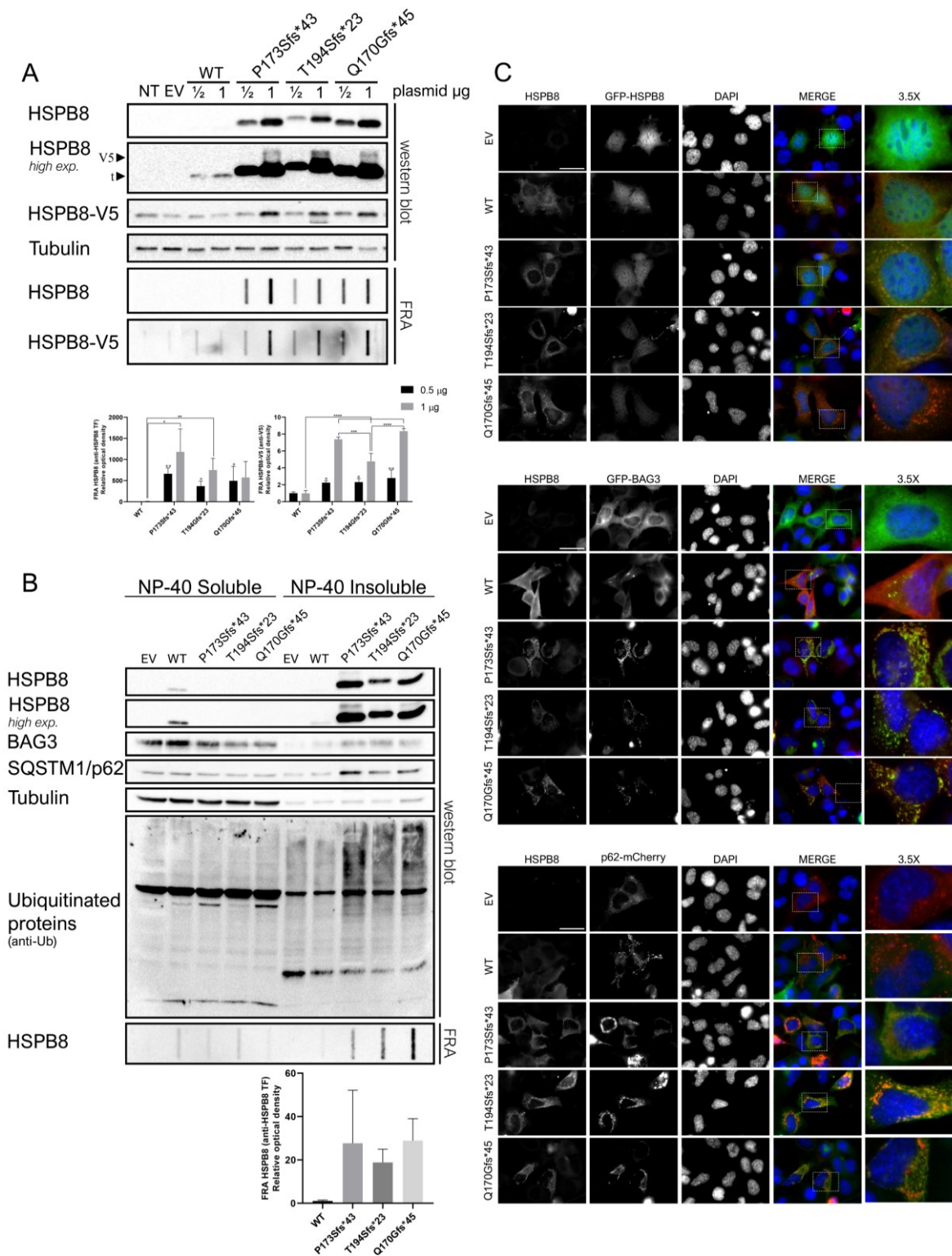


Figure 3. 5 Frameshift mutants of HSPB8 co-segregates with wildtype HSPB8, BAG3 and SQSTM1/P62 along with ubiquitinated proteins.

A. WB and FRA of HEK293T stably expressing HSPB8-V5 and transiently transfected with HSPB8 constructs (0.5 or 1 μ g plasmid) or an empty vector. FRA relative optical densities are reported in the bar graphs as means \pm SD of normalized values. ($n=3$). **B.** WB and FRA analyses after NP-40 soluble/insoluble extraction of NSC-34 transiently transfected with an empty vector or HSPB8 constructs. FRA relative optical densities are reported in the graph as means \pm SD of normalized values. ($n=3$). **C.** IF analyses of NSC-34 transiently co-transfected with an empty vector or HSPB8 constructs and GFP-HSPB8-WT (Top) or BAG3-GFP-WT (Middle) or SQSTM1/p62-mCherry (Bottom). IF was performed against HSPB8 (red in the two upper panels or green in the bottom panel), and nuclei were stained with DAPI. (Scale bar = 10 μ m; 63X magnification). The constructs were abbreviated as follows: untransfected (NT), empty vector (EV), wildtype (WT).

3.3.6 BAG3 co-aggregation with the frameshift mutants is mediated through its IPV motifs

HSPB8 interaction with BAG3 is mediated by the interaction of the grooves formed by $\beta 4$ and $\beta 8$ sheets of HSPB8 and the two IPV domains in BAG3. To evaluate if the co-aggregation of BAG3 with HSPB8 frameshift mutants was mediated through the canonical interaction of HSPB8 and BAG3 and if the aggregation prone behaviour of HSPB8 frameshift mutants was counteracted by the absence of BAG3-HSPB8 interaction, I used a GFP-tagged BAG3 deleted of the two IPV domains (Δ IPV 1+2). In addition, I tested the effect of GFP-tagged BAG3s unable to bind to the dynein motor complex (Δ PxxP domain) or the HSP70 (Δ BAG domain or R480A mutant). By performing a protein soluble/insoluble extraction (**Fig. 3.6 A**), I observed that HSPB8 WT is almost completely partitioned in the soluble fraction and a little fraction of HSPB8 was detected in the insoluble fraction when BAG3-GFP WT or BAG3-GFP Δ PxxP were present. Instead, HSPB8 frameshift mutant Pro173Serfs*43, used as a representative mutant, was always present in the insoluble fraction. To note, a faint band of HSPB8 frameshift mutant appeared in the soluble fraction in samples expressing the BAG3-GFP Δ BAG mutant. The partitioning of BAG3-GFP WT or mutants paralleled the expected HSPB8 WT or frameshift mutant behaviour in all cases, except for the BAG3-GFP Δ IPV 1+2. Indeed, upon HSPB8 WT expression, all GFP-tagged BAG3s partitioned in the soluble fraction and a little fraction of BAG3-GFP WT and BAG3-GFP Δ PxxP were detected in the insoluble fraction, together with HSPB8 WT. On the other hand, upon HSPB8 frameshift mutant Pro173Serfs*43 expression, all GFP-tagged BAG3s partitioned in the insoluble fraction, except for the GFP-tagged BAG3 Δ IPV 1+2. These results indicate that when the interaction between BAG3 and HSPB8 is abrogated, HSPB8 frameshift mutant is still aggregating, but is not able to sequester BAG3 into aggregates, as expected by the fact that the lack of the IPV domains does not allow the interaction between the two obligate partners. Noteworthy, BAG3-GFP Δ BAG was also detected in the soluble fraction upon HSPB8 frameshift mutant expression, suggesting a potential indirect role of HSP70/HSPA interaction with BAG3 on BAG3-HSPB8 aggregation. These results were confirmed using IF by analysing the co-aggregating HSPB8 frameshift mutant with GFP-tagged BAG3s (**Fig. 3.6 B**). Indeed, all the GFP-tagged BAG3s were characterized by a mainly diffuse cytoplasmic localization when HSPB8 WT was present. Instead, coaggregation with the HSPB8 frameshift mutants was observed for GFP-tagged BAG3 WT, Δ PxxP, Δ BAG and for the R480A mutants, while the BAG3 Δ IPV 1+2 was completely diffused in the cytoplasm.

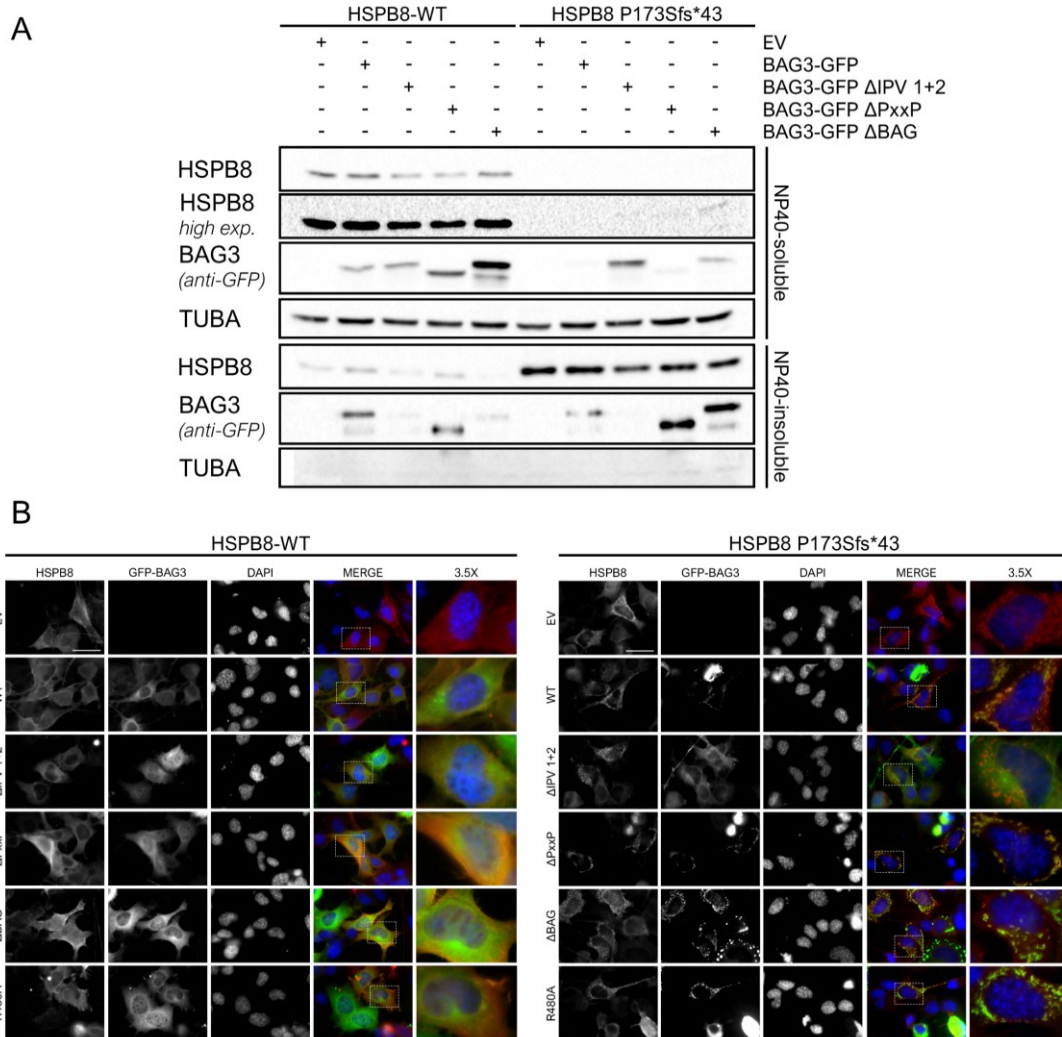


Figure 3. 6 BAG3 co-aggregation with the frameshift mutants is mediated through its IPV motifs.

A. WB analyses after NP-40 soluble/insoluble extraction of NSC-34 transiently co-transfected with an empty vector (EV) or BAG-GFP constructs (WT or mutated as indicated in paragraph 3.3.7) and with HSPB8 WT or Pro173Serfs*43 mutant constructs. **B.** IF analyses of NSC-34 transiently co-transfected with an empty vector (EV) or BAG-GFP constructs (WT or mutated as indicated in paragraph 3.3.7) and with HSPB8 WT or Pro173Serfs*43 mutant constructs. IF was performed against HSPB8 (red), BAG3-GFP is in green and nuclei were stained with DAPI. (Scale bar = 10 μ m; 63X magnification).

3.3.7 HSPB8 frameshift mutant aggregation is only partially diminished upon BAG3 depletion

Since I did not observe a reduced aggregation of HSPB8 Pro173Serfs*43 frameshift mutant in presence of the BAG3 depleted of the two IPV motifs, I reasoned that this effect could have been masked by endogenous BAG3 expression. Thus, I evaluated the formation of HMW insoluble species of HSPB8 Pro173Serfs*43 frameshift mutant after silencing of endogenous BAG3. As observed in **Fig. 3.7**, the silencing of BAG3 was partially efficient in respect to the untransfected (NT) cells and to cells transfected with a non-targeting siRNA (scramble), used as controls. HSPB8 WT protein levels were reduced after BAG3 silencing in respect to control. This is in line with data previously published (Carra, Seguin, Lambert, et al., 2008), which demonstrated that HSPB8 stability is negatively affected by depletion of BAG3. Similarly, the HSPB8 Pro173Serfs*43 frameshift mutant levels were slightly reduced after BAG3 silencing, suggesting that the binding of BAG3 affects HSPB8 stability independently from the frameshift mutation. HSPB8 Pro173Serfs*43 frameshift mutant HMW insoluble species were also slightly reduced but no statistically significant difference was observed. Even if the silencing of BAG3 was not completely efficient, these results suggested that the stability of the HSPB8 frameshift mutants is still affected by BAG3 binding but that HSPB8 aggregation prone behaviour might be independent from BAG3-HSPB8 interaction.

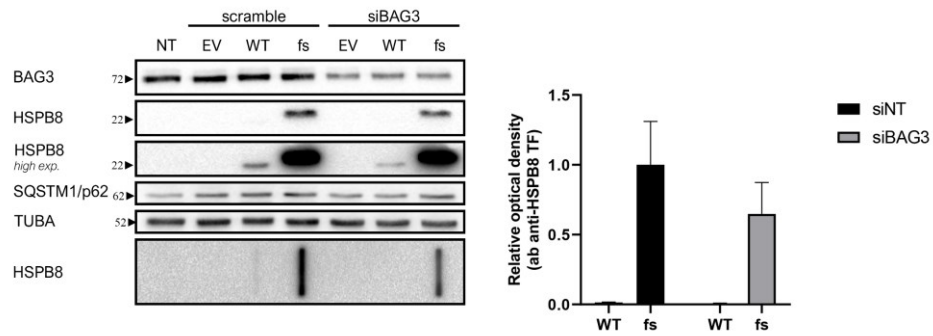


Figure 3. 7 HSPB8 frameshift mutant aggregation is only partially diminished upon BAG3 depletion. WB and FRA analyses of NSC-34 transiently transfected with a non-targeting (scramble) or a siRNA against endogenous BAG3 (siBAG3) for 72 hrs and with an empty vector (EV) or HSPB8 constructs (WT or Pro173Serfs*43 (fs)) for 48 hrs. FRA Relative optical densities are reported in the bar graph as means \pm SD of normalized values. Student T tests were used for statistical analysis to compare the conditions (scramble or silenced BAG3) for each respective HSPB8. (n=3).

3.3.8 Trehalose as a therapeutic strategy to remove HSPB8 frameshift mutant aggregates

As reported in literature, autophagy is responsible for the entire CASA complex degradation together with the bound substrates. In addition, I previously showed that BAG3 P209 mutants aggregates are efficiently removed by trehalose-mediated enhancement of the autophagic flux. Since HSPB8 frameshift mutants share a similar aggregating prone behaviour observed for BAG3 P209 mutants and both the mutated proteins caused the sequestration of their partner, I speculated that autophagic enhancement could favour the removal of HSPB8 frameshift aggregates, as well. Thus, I tested trehalose on cells overexpressing the HSPB8 WT and frameshift mutants and evaluated its effect on the aggregating HSPB8. As expected, trehalose treatment caused autophagic induction, supported by LC3-I to II conversion and SQSTM1/P62 increased levels (**Fig. 3.8 A**). Trehalose-mediated autophagic induction was accompanied to a reduction of HMW insoluble species of HSPB8 frameshift mutant, while had no effect on HSPB8 WT accumulation. Interestingly, trehalose treatment had a slight or absent impact on the soluble level of HSPB8, suggesting that only HSPB8 aggregates are targeted to lysosomal degradation. These results were then confirmed by IF (**Fig. 3.8 B**). Indeed, I observed a reduction in cells bearing cytoplasmic HSPB8 aggregates, accompanied by a relocalization, even if partial, of the autophagic regulator TFEB. In summary, trehalose treatment favoured the removal of the aggregating frameshift mutant of HSPB8, similar to what previously observed for BAG3 P209 mutant. Collectively, these results suggest that, similar to other NDs aggregating substrates and BAG3, also HSPB8 aggregates can be removed through autophagic enhancement.

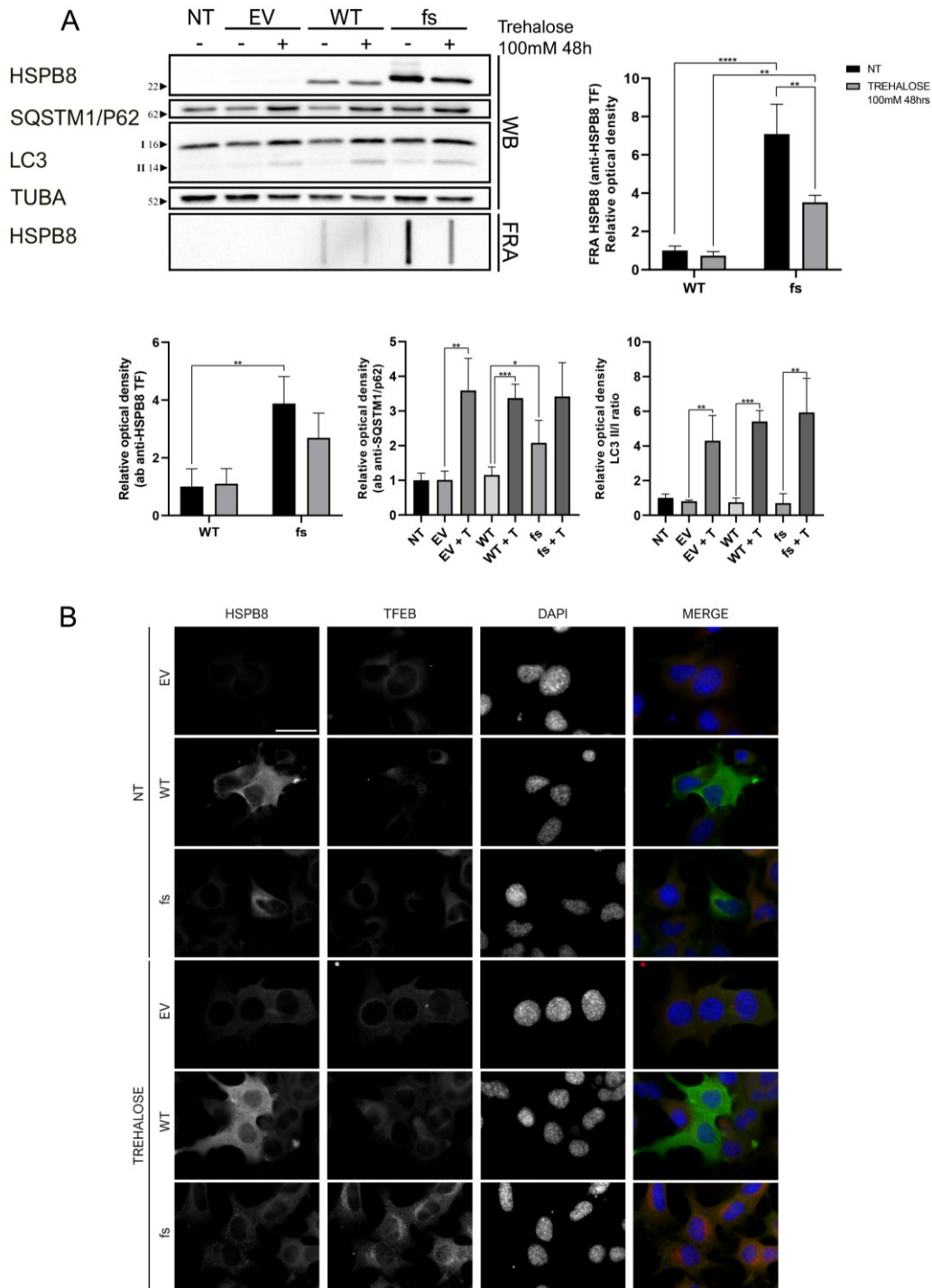


Figure 3. 8 Trehalose as a therapeutic strategy to remove HSPB8 frameshift mutants aggregates.

A. WB and FRA analyses of NSC-34 transiently transfected with an empty vector (EV) or HSPB8 constructs (WT or Pro173Serfs*43 (fs)), untreated or treated with the autophagic stimulator Trehalose, 100mM for 48 hrs. Relative optical densities are reported in the bar graph as means \pm SD of normalized values. Student T tests were used for statistical analysis to compare the treated with untreated condition for each respective HSPB8 or significant differences between HSPB8 WT and frameshift; * $p < 0.05$, ** $p < 0.01$, *** $p < 0.001$, **** $p < 0.0001$ ($n = 3$).

B. IF analyses of NSC-34 transiently transfected with empty vector (EV) or HSPB8 constructs (WT or Pro173Serfs*43 (fs)), untreated or treated with the autophagic stimulator Trehalose, 100mM for 48 hrs. IF was performed against TFEB (red), and nuclei were stained with DAPI. (Scale bar = 10 μ m, 63X magnification).

3.4 Discussion

HSPB8, which belongs to the HSPBs family, takes part in CASA complex. HSPB8 exerts a protective role in NDs and muscle maintenance by recognizing a wide subset of misfolded and damaged clients for subsequent degradation. Nevertheless, similarly to BAG3, mutations in HSPB8 have been found in myopathies and neuropathies. Besides HSPB8, other members of the HSPBs subfamily have been related to diseases affecting neurons and muscle cells.

Previous works in our laboratory demonstrated the pro-degradative activity of HSPB8 on several aggregating proteins causative of ALS, including the mutated SOD1, the CTFs of TDP-43, and the *C9ORF72*-related DPRs and on a related MN disease, the SBMA in the case of the polyQ-AR. Since HSPB8 counteracts proteotoxic stresses, but is causative of neuromuscular diseases when mutated, studies on newly identified variants of HSPB8 in ALS patients should not be underrated. Moreover, HSPB1 mutations, causing an ALS-like phenotype, have been already described, supporting that mutations in HSPBs particularly enriched in neurons might account for a fraction of ALS cases with an undefined aetiology. Thus, part of my studies consisted in the analysis of HSPB8 variants recently identified in ALS cases by our collaborators Nicola Ticozzi, Vincenzo Silani and Antonia Ratti, from the Department of Neurology and Laboratory of Neuroscience (IRCCS Istituto Auxologico Italiano, Milan) and Dipartimento di Fisiopatologia Medico-Chirurgica e dei Trapianti, Centro 'Dino Ferrari' (University of Milan). These variants include the substitution of the Ser at position 9 with a Pro (S9P), of the Pro at position 41 with a Ser (P41S) and of the Ser at position 181 with a Cysteine (S181C). Here, I demonstrated that the identified HSPB8 variants are not characterized by a misfolding and aggregating prone behaviour, which is a hallmark of ALS, excluding a gain of proteotoxic function. In addition, I observed no variation in the stability of the HSPB8 variants, whose levels and rate of degradation are comparable to the HSPB8 WT, excluding a potential disease-related mechanism of haploinsufficiency. I also proved that HSPB8 variants are able to dimerize with the WT counterpart and interact with the other members of the CASA complex, showing no competition for BAG3 binding. A mechanism of loss of function was excluded as well, since all HSPB8 variants retained the prodegradative activity against HSPB8 client proteins (*data not shown*). However, a serendipitous observation concerned the S181C variant, which is its ability to form an intramolecular disulphide bond. HSPB8 in its WT form contains three cysteine residues, which have been reported to be involved in the formation of intra- and inter- subunits disulphide bonds in vitro (Mymrikov et al., 2010). However, besides the cited study performed on cysteine mutants of HSPB8, which does not seem to affect HSPB8 function in vitro, no additional studies deeply investigated the role of these cysteine residues in

HSPB8 activity and interactions with other partners than BAG3, such as HSPBs or RNA binding proteins. Unfortunately, any additional information on the effect of S181C mutation on HSPB8 structure cannot be obtained, since the CTD, and the NTD as well, correspond to highly intrinsically disordered regions.

Although I did not observe a loss of function for the HSPB8 variants through a well-established aggregation assay of defined misfolded substrates of CASA complex (*data not shown*), I cannot rule out that the identified HSPB8 variants do not possess any detrimental or beneficial activity in ALS. Indeed, a limitation of these studies regards the use of transient transfection methods combined with assays (e.g., FRA) characterized by low sensitivity to detect small changes between HSPB8 WT or variants activity. In support to this hypothesis, I observed that the already demonstrated aggregation prone behaviour of the HSPB8 known mutant K141E was absent in our cell model and experimental conditions and that the partial loss of activity of this mutant sometimes could not reach a statistical significance. Moreover, HSPB8 activities are not strictly circumscribed to CASA. Indeed, the role of HSPB8 variants in granulostasis, cell cycle, cytoskeletal maintenance, and protective response to other stressors (e.g., oxidative stress) has not been investigated in this study, giving rise to the possibility that HSPB8 variants could impact in ALS through other molecular mechanisms.

In conclusion to this part of my studies, I believe that, even if no gain of toxic function or loss of protective function were clearly identified, further efforts should be made to define well the role of these HSPB8 variants in ALS disease.

The second part of my studies dedicated to HSPB8 concerned the investigation of the biochemical behaviour of the very recently identified HSPB8 frameshift mutants. Specifically, the mutations pPro173Serfs*43, pGln170Glyfs*45 and pThr194Serfs*23 have been described in patients suffering from progressive distal neuropathy/myofibrillar pathology with rimmed vacuolar myopathy, adult-onset axial and distal myopathy and proximal limb-girdle rimmed vacuolar myopathy, respectively. Actually, this study started with a focused analysis on pPro173Serfs*43 mutant, but a very strikingly observation encouraged the inclusion of the other two frameshift mutants in the characterization. Indeed, by analysing the predicted protein sequences caused by the frameshift mutations, I observed that all these mutants share a common elongated C-terminal tail. In addition, the mutations pPro173Serfs*43 and pGln170Glyfs*45, which fall very near to each other in the HSPB8 sequence, determined almost identical sequence modification of the CTD of HSPB8. My experimental findings demonstrated that all these mutants encode the predicted elongated form of HSPB8 and that are prone to form cytoplasmic aggregates. These

observations are partially in contrast with the literature. Indeed, HSPB8 frameshift mutant proteins have never been detected in protein extracts from patients-derived biopsies or fibroblasts and a decreased of 50-60% of total HSPB8 protein levels were observed. To explain these observations, mechanisms of mRNA decay or protein instability were hypothesized but not demonstrated. In addition, these results disagreed with the histopathological results in muscle biopsies, showing cytoplasmic protein aggregation of HSPB8 itself together with TDP-43, ubiquitin, HSPB5, other CASA members and structural proteins. One can argue that the overexpression of HSPB8 mutants in cell by transient transfection might determine artifacts. However, the fact that aggregation of the HSPB8 frameshift mutants was not observed in patients-derived fibroblast can be explained by the fact that fibroblast express very low levels of HSPB8, as reported in the Human Protein Atlas portal. In addition, the myopathy-related P209L mutant of BAG3, which is also expressed at low levels in fibroblast, did not form spontaneous detectable aggregates in patients-derived fibroblast in the recently published paper from (Meister-Broekema et al., 2018). BAG3 P209L mutant aggregation in patients-derived fibroblasts was observed after induction of BAG3 upregulation through proteasome inhibition; similarly, heat shock, which is potent HSPB8 inducer, permitted the observation of long-lasting HSPB8 aggregates in pPro173Serfs*43 fibroblasts (Al-Tahan et al., 2019).

Indeed, in line with patient biopsies observations, I proved that HSPB8 frameshift mutant aggregation determines, not only the co-aggregation of its WT counterpart, but also the co-segregation of CASA complex factors, such as BAG3, through its two IPV domains, and the autophagic adaptor SQSTM1/P62. These results suggest a dominant negative effect of these frameshift mutants against all CASA complex and affecting its activity. Indeed, along with the observation of decreased solubility of HSPB8 frameshift mutants and interactors, I observed an increase of insoluble ubiquitinated proteins, suggesting a failure of CASA activity. Since all these results are strikingly close to the previous observation on BAG3 P209 mutant, I tested if the boosting of the autophagic pathway could favour HSPB8 aggregates removal. Again, trehalose resulted effective in the removal of aggregates of HSPB8 frameshift mutants, suggesting that the enhancement of the autophagic pathway could be a promising therapeutic approach for myopathy and neuropathy diseases characterized by HSPB8 and BAG3 aggregation.

It must be said that the studies on the HSPB8 frameshift mutants are still ongoing. One fundamental topic that need investigation concern the role of HSP70/HSPA in HSPB8 aggregation. Since it has been described that the abrogation of HSP70/HSPA-BAG3 interaction counteracts the aggregation of BAG3 P209 mutants, I will investigate if this observation applies also to HSPB8 frameshift mutants or if HSPB8 aggregation takes place

independently from CASA complex. Nevertheless, BAG3-independent functions of HSPB8 have been described. For instance, it was recently demonstrated the role of HSPB8 in the early response to proteotoxic stress, upstream to BAG3 intervention. In this mechanistic model, HSPB8 concentrates misfolded proteins into ubiquitin-positive microaggregates, regulates the SQSTM1/P62 oligomerization and coupling to BAG3-HSP70/HSPA complex. In addition, HSPB8 acts independently from BAG3 in the early phases of granulostasis and, since co-aggregation of HSPB8 frameshift mutants with SGs marker TIA-1 has been observed in patient biopsies, the role of these new mutations in SGs dynamics or dysfunction must be addressed.

In addition, further investigations are needed to assess the activity of HSPB8 in the removal of known clients, such as mutant SOD1 or the elongated polyQ tract. Alternatively, if the misfolded clients can be routed to degradation through alternative pathways. Finally, since co-aggregation of HSPB8 frameshift mutants with TDP-43 has been described, the effect on HSPB8 on TDP-43 pathology (*ongoing studies*), which comprises severe muscle and neuronal phenotypes, will add important pieces in the puzzle of HSPB8-related neuromuscular diseases.

Finally, structural information of these HSPB8 frameshift mutants is missing. It will be of interest the evaluation of the amino acidic substitution observed in the modified CTD and in the elongated C-terminal tail. Do these new sequences contain motifs that determines aberrant protein-protein interaction? How do these sequences fold or misfold determining the formation of oligomers, fibrils, or amorphous aggregates? Which are the relative contributions of the modified CTD and the elongated C-terminal tail?

Collectively, these current studies are laying the foundations for the investigation of the molecular mechanisms underlying HSPB8-related pathology. These and future results might permit the grouping of the identified, and not already identified, frameshift mutants in a class with defined and shared disease-causing mechanisms.

Chapter IV

4. Differentiation of induced Pluripotent Stem Cells to Motoneurons to generate a model to study TDP-43 pathology

4.1 BACKGROUND

Protein misfolding and aggregation are hallmarks of several NDs. NDs comprise MNDs, characterized by MNs death and muscle waste and atrophy. Besides NDs, proteostasis impairment is observed in diseases affecting muscle cells. Among MNDs, ALS is the most common, with an annual incidence of 1-2 cases per 100 000 habitants (Wijesekera et al., 2009). The aetiology of ALS is unknown in most of the cases, but it is thought that ALS is a result of a multistep process involving environmental and genetic factors (Al-Chalabi et al., 2012). ALS can be divided into familial (fALS) or sporadic (sALS) forms, which account for the 5% and 95% of cases, respectively. In both fALS and sALS, a long list of genes has been found to be involved in the disease. Noteworthy, several of these mutated genes and of the impaired cellular pathways associated to ALS are also involved in other diseases affecting MNs and the skeletal muscle. Although the efforts of the scientific community are now deciphering the molecular mechanisms causative of MNs death, most sporadic cases have unknown causes, and no cure is effective in slowing down or block the onset and progression of these diseases. The generation of new models closer to human MNs and muscle cells are necessary to gain new insights into ALS and other neuromuscular diseases. In this context, the development of protocols that permit the obtainment of induced Pluripotent Stem Cells (iPSCs), their genetic manipulation through gene editing technology and their differentiation to specialized cell types, e.g., MNs and myocytes, represent valuable tools for the study of diseases affecting the neuromuscular system.

4.1.1 *TAR DNA binding protein - 43*

TDP-43 is an RNA binding protein encoded by the *TARDBP* gene. Its functions comprise mRNA transport, splicing, translation and SGs formation (Gao et al., 2018). TDP-43 is a 414 amino acids protein, containing an N-terminal domain, two RNA recognition motifs (RRM1 and RRM2) and a C-terminal glycine-rich unstructured domain, also known as prion like domain. TDP-43 contains both a nuclear localization signal (NLS) and a putative nuclear export signal (NES), which permit its nucleocytoplasmic shuttling (Blokhuys et al., 2013). Mutations in *TARDBP* gene accounts for only 4% of fALS cases. Although mutated TDP-43 has been found in a very few cases of ALS/FTD, TDP-43 inclusions are present in 97% of ALS cases and 45% of FTD cases (Ling et al., 2013). Besides ALS-FTD, TDP-43 has been also involved in SMA in association to its splicing activity on SMN2 transcript (Bose et al., 2008). However, TDP-43 pathology is not only restricted to neuronal cell types. Indeed, TDP-43 inclusions or co-aggregation have been also observed in muscle cells of patients suffering from ALS, IBM and muscle dystrophy, dHMN and MFM (Bengoechea et al., 2015; Cortese et al., 2018; Sorarú et al., 2010; Wehl et al., 2008).

TDP-43 proteinopathy has been attributed to an aberrant behaviour of TDP-43, characterized by mislocalization and PTMs, which cause its aggregation and dysfunction, and this may be related to the generation of proteolytic fragments of 25 and 35 KDa. Indeed, the role of TDP-43 and its toxic fragments in MNs-like and muscle cell models was previously investigated in our laboratory. We demonstrated that TDP-43 fragments accumulate in both cell types and that the expression of the TDP-25 toxic fragment was able to impair autophagy. On the other hand, by boosting the autophagic or proteasome systems, TDP-43 fragments aggregates can be cleared from cells (Cicardi et al., 2018). Not only proteolysis inducing selective TDP-43 cleavage in aggregating CTFs, but also other specific PTMs are involved in the pathogenic mechanism of TDP-43, like TDP-43 Ser-409/410 phosphorylation, TDP-43 ubiquitination and acetylation. These PTMs are associated with TDP-43 nuclear depletion and accumulation in cytoplasmic detergent-resistant inclusions. TDP-43 inclusions are related to a gain of proteotoxic function and its sequestration into physically compartmentalized aggregates results in a decreased TDP-43 bioavailability and nuclear distribution, associated to its loss of function in RNA metabolism.

4.2 AIM

The inaccessibility to the brain tissue in living human being has been a limiting factor in the study of MNDs. But, the recent set up of protocols that permit to reprogram somatic cells into induced Pluripotent Stem Cells (iPSCs) and their subsequent differentiation into different cell types, including specific subset of neurons, has overcome this issue (Takahashi et al., 2007, Takahashi and Yamanaka, 2006). iPSCs can be obtained by reprogramming skin fibroblasts or blood cells from patients or healthy donors by using a cocktail of four transcription factors (OCT4, SOX2, KLF4, and c-MYC). Then, iPSCs can be differentiated and used as human cell models to investigate molecular mechanisms related to a disease and for drug discovery. Another issue that rises in the study of complex diseases is the genetic variability among cell models derived from different patients and healthy donors. By genome editing techniques (e.g., CRISPR/Cas9 system), isogenic iPSC lines can be generated, and the disease-not-related genetic background noise can be limited. While often using the CRISPR/Cas9 technique, a genetic mutation can be repaired in iPSCs derived from ALS patients generating isogenic control cell line sharing the same genetic background of the given patients, it is also possible to introduce a novel mutation into a desired normal gene (e.g., TARDBP) in normal iPSCs to produce isogenic mutated cell lines mimicking a specific human disorder (Cong et al., 2013). Once iPSCs are obtained, protocols for their differentiation can be used to obtain the desired cell type generally affected in the disease object of the study.

Here, I applied a new protocol for the obtainment of iPSCs-derived MNs on previously generated isogenic TDP-43-DENDRA2 reporter cell lines (**Fig 4.1 A**). These iPSCs clones were obtained by gene editing on a healthy donor-derived cell line of iPSCs with CRISPR/Cas9 technology, to express (i) wildtype (WT) or (ii) A315T mutated TDP-43 tagged at the C-terminus with DENDRA2. The DENDRA2 tag is a 23 kDa modified protein derived from octocoral *Dendronephthya sp.* and undergoes an irreversible photoconversion from green to red fluorescence, when activated with UV-violet (405 nm) or blue (488 nm) lights.

By using a small molecule-based differentiation protocol, I aimed to differentiate iPSCs to MNs and perform a basal characterization of the selected isogenic reporter cell lines.

Most of these data were obtained during a short-term fellowship at the iPS cells and neurodegenerative disease group lead by PhD Jared Sternecker (DFG-Center for Regenerative Therapies Dresden, Center for Molecular and Cellular Bioengineering (CMCB), Technische Universität Dresden) and in collaboration with PhD Lara Marrone. The gene edited iPSC lines were generated by PhD Maria Elena Cicardi in our laboratory during her PhD course with the assistance of Dr. Valeria Crippa, researcher in our laboratory.

4.3 Materials and methods

Chemicals and reagents

The following reagents were used: mTeSR1 (85850, Voden Medical Instruments), N2 Supplement (17502-048, GIBCO), B27 Supplement W/O VitA (12587-010, GIBCO), Neurobasal medium SFM (21103-049, GIBCO), Knock Out D-MEM (10829-018, GIBCO), Serum Replacement (10828-028, GIBCO), Collagenase (C6885-25MG, Sigma-Aldrich), ROCK Inhibitor (Y-27632, Selleckchem), Ascorbic Acid (A2218, Sigma-Aldrich), Retinoic Acid (R2625, Sigma-Aldrich), CHIR (SML 1046, Sigma-Aldrich), dbCAMP (D0627, Sigma-Aldrich), VPA (P4543, Sigma-Aldrich), Dorsomorphin (s7306, Selleckchem), SB-431542 (Cayman), PMA (10009634, Selleckchem), SAG (11914, Cayman), DAPT (131997, Cayman), DMH-14126/10 (Tocris), FGF basic (100-18B, peprotech), BDNF (450-02, peprotech), GDNF (450-10, peprotech), TGFb3 (100-36E, peprotech), Activin A (34-8993-85, Affymetrix e-bioscience), MG-132 (Z-Leu-Leu-Leu-al) (Sigma Aldrich), 3-MA (Sigma Aldrich).

Cell cultures

IPSCs were previously gene edited and characterized by PhD Maria Elena Cicardi, from our laboratory. IPSCs were expanded in mTeSR (Stem cell Technologies) at 37°C, 5% CO₂ on Matrigel (Corning)-coated multiwells. Medium was changed every day, and cells splitting was performed by enzymatic detachment using Accutase (Sigma) supplemented with 10 µM ROCK inhibitor (Y-27632, Selleckchem). MNPs and MNs were grown at the conditions described in the following section and maintained at 37°C, 5% CO₂ on Matrigel (Corning)-coated multiwells.

Cells were seeded at the following cellular densities:

- iPSCs: 400 000 cells/well in a 6-wells multiwell for maintenance, 500 000 cells/well in a 6-wells multiwell for Motoneuron Progenitors (MNPs) derivation;
- MNPs: 400 000 cells/well in a 6-wells multiwell for maintenance, 400 000 cells/well in a 12-wells multiwell for Motoneurons (MNs) differentiation, 30 000 cells/well in a 96-wells multiwell for IF;
- MNs: 1 800 000 cells/ml in a 12-wells multiwell for WB and FRA, 40 000 cells/well in a 96-wells multiwell for IF.

Differentiation of iPSCs to MNs

MNs derivation was obtained by applying the protocols set by (Reinhardt et al., 2013) and (Du et al., 2015) and adapted by Dr. Sternecker laboratory (Center for Molecular and

Cellular Bioengineering (CMCB) - DFG-Center for Regenerative Therapies (Technische Universität Dresden, Dresden, Germany)) (**Fig. 4.1 B**). This protocol permits the derivation of MNP cells from iPSCs-formed Embryo Bodies (EBs). Next, MNPs can be expanded and differentiated to MNs. The MNs derivation is based on the use of small molecules that interfere by activating or inhibiting pathways responsible for cell differentiation, mimicking the differentiation process that takes place during embryogenesis. The first passage of the protocol consists in the neural induction by exposing detached iPSCs clumps to hES medium supplemented with 200 μ M ascorbic acid, and with 0.5 μ M dorsomorphin and 10 μ M SB-431542, which inhibit BMP and TGF β signalling, respectively, and to 3 μ M CHIR99021, a GSK3b inhibitor that stimulates the canonical WNT signal (Induction Medium [IM]). After four days, cells are exposed to N2B27 medium (DMEM-F12/Neurobasal medium 1:1, 0.5 % N2 supplement, 1 % B27 supplement without vitamin A, 1 % Penicillin/Streptomycin/Glutamine) supplemented with 0.5 μ M purmorphamine, a stimulator of the SHH pathway, and 0.10 μ M retinoic acid (RA), which specifies the spinal cord fate (Neuron Precursor Cells Medium [NPCM]). Because of the neurogenic effect of RA, the use of Valproic Acid (VPA, 0.5 μ M), a histone deacetylase inhibitor that indirectly activates Notch signalling, permits to expand MNPs for at least five times (Motor Neuron Precursor Medium [MNPM]).

Once the MNPs are obtained, they can be induced to differentiate into MNs, by exposing MNPs to Patterning medium. Patterning medium consists of N2B27 medium supplemented with 200 μ M ascorbic acid, 1 μ M retinoic acid (Sigma), 0.5 μ M SAG, 10 ng/ml BDNF (Peprotech), 10 ng/ml GDNF (Peprotech). After six days, MNs are cultured in Maturation medium, consisting of N2B27 supplemented with 5 ng/ml Activin A (for the first 2 days), 200 μ M ascorbic acid, 20 ng/ml BDNF, 20 ng/ml GDNF, 1 ng/ml TGF β 3, 100 μ M dbcAMP (Sigma). After at least 14 days, MNs are mature and used for subsequent analyses.

Protein Extraction and quantification

After 15-20 days MNs maturation, derived MNs were harvested and centrifuged 5 min at 100 g at 4 °C. Cell pellets were then resuspended in RIPA lysis buffer (0.15 M NaCl, 20 mM Na-deoxycholate, 100 μ M Na₃VO₄, 50 mM NaF, 5 mM Na-iodoacetate, 2.5 mM Tris-HCl pH 7.7, 10 mM EDTA pH 8, 0.08%w/v SDS, 0.8%v/v Triton X-100) added with protease inhibitors cocktail (Sigma-Aldrich) and lysed using slight sonication. For RIPA soluble/insoluble protein extraction, cells were lysed in RIPA buffer and centrifuged at 16100 g for 15 min. Supernatants were collected and pellets resuspended in sample buffer. Protein content quantification was performed with bicinchoninic acid (BCA) assay (Cyanagen).

Western Blot and Filter Retardation Assay

SDS-PAGE was performed as previously described. 25 µg of MNs protein lysates were loaded onto gels and then electro-transferred to 0.45-µm nitrocellulose membranes (Bio-Rad Laboratories, Hercules, CA, USA). To detect insoluble species, FRA was performed by loading 10 µg of total protein onto a 20% MeOH-treated 0.2-µm cellulose acetate membrane (Whatman 100404180) and filtered. WB and FRA membranes were incubated with a blocking solution of 5% of non-fat dried milk in TBS-Tween (20 mM Tris-HCl pH 7.5, 0.5 M NaCl, 0.05% Tween-20) for 1 h and then incubated with primary antibodies diluted in the same solution overnight. Primary antibodies used were: mouse monoclonal anti-DENDRA2 antibody (clone OT11G6, TA180094, TrueMAB), rabbit polyclonal anti-TDP-43 C-terminus (12892-1-AP, Proteintech), rat monoclonal anti-phospho TDP-43 (Ser409/Ser410) (clone 1D3, MABN14, Sigma-Aldrich), mouse monoclonal anti-α-tubulin (T6199, Sigma-Aldrich), rabbit polyclonal anti-LC3 (L8918, Sigma-Aldrich). Then, membranes were washed three times in TBS-Tween for 10 min and incubated with the peroxidase-conjugated secondary antibodies IgG-HRP goat anti-rabbit and anti-mouse (111-035-003, 115-035-003; Jackson ImmunoResearch Laboratories, Inc.) and anti-rat (sc-2065, Santa Cruz Biotechnology). After 4 times washing, proteins were immunodetected as previously described.

Fluorescence microscopy and immunofluorescence

Cells were fixed in a solution of 4% paraformaldehyde for 25 min at RT and then washed with PBS solution 3 times 5 min. Cells were permeabilized and nonspecific sites blocked using a solution of 0.1% Triton X-100, 1% BSA and 10% FBS in PBS for 40 minutes at RT. Then, the primary antibodies diluted in 0.1% BSA in PBS were incubated overnight: mouse monoclonal anti-Nestin antibody (MAB1259, R&D systems), rabbit polyclonal anti-HB9 (PA5-40456, Invitrogen), mouse monoclonal anti-Smi32 antibody (NE1023, Sigma Aldrich), rabbit polyclonal anti-TDP-43 (10782-2-AP, Proteintech), mouse monoclonal anti-α-tubulin (T6199, Sigma-Aldrich), rabbit polyclonal anti-CC3 (D175, #9541, Cell Signaling). The following day, primary antibodies were removed, and cells washed with 0.1% BSA in PBS. Then, secondary antibodies were added: goat anti-mouse AlexaFluor 647 (A-21241, Thermo) or donkey anti-rabbit AlexaFluor 647 (A-31573, Thermo), diluted in 0.1% BSA in PBS, were incubated for 1 hr at RT. Three washing steps with PBS, with the middle one containing Hoechst (in PBS) to stain nuclei were made. Cells were imaged on a Confocal Laser Scanning Microscope 700 (Zeiss).

4.4 Results

4.4.1 iPSCs differentiation to MNPs

Isogenic iPSCs lines expressing the DENDRA2-tagged WT or A315T mutated TDP-43 have been previously generated in our laboratory. After characterization of the selected iPSCs clones, I applied a small molecules-based protocol for differentiating iPSCs to MNPs and then, to MNs (**Fig. 4.1 A and B**). By analysing cell morphology and distribution using light microscopy, I observed that undifferentiated iPSCs, both from WT and mutated TDP-43 tagged with DENDRA2, correctly showed a typical colony forming behaviour (**Fig. 4.1 B**). The derivation of MNPs requires the passage of EBs formation. For EBs formation, cells were grown until complete confluence with MEF-derived conditioned medium supplemented with FGF2. During the phase of induction, colonies were scraped and cut into smaller pieces and exposed to the induction medium [IM]. EBs were grown in a low binding petri dish as floating rounded or tubular cell aggregates (**Fig. 4.1 B**). Then, cells were exposed to Neural Progenitor cells medium [NPCM]. After 2 days, EBs were collected and disaggregated on a Matrigel-coated 12-multiwell to obtain MNPs.

Because of the presence of contaminant flat cells, colonies of cells grown in NPC medium were manually selected or underwent sequential enzymatic-based detachment. Then, cells were split and plated in MNP medium. MNP medium has the same formulation of NPC medium, with small molecules that help in the differentiation to MNPs, but it contains VPA, that represses neurogenesis, permitting the expansion of MNPs for at least five passages. MNPs obtained from all four iPS cell lines (W80 and W54 expressing the DENDRA2-tagged TDP-43 WT; A5 and A19 expressing the DENDRA2-tagged TDP-43 A315T) grew in clusters, with cells that emit propagations outside the colonies (**Fig. 4.1 C**). IF showed that MNPs were positive for Nestin, which is expressed in precursors of neural lineage (**Fig. 4.2**). Under basal conditions, I did not observe any appreciable differences in TDP-43 WT (W80) or A315T mutant (A5) localization and distribution: in both MNPs cell lines, DENDRA2-tagged TDP-43 localized in the nuclei.

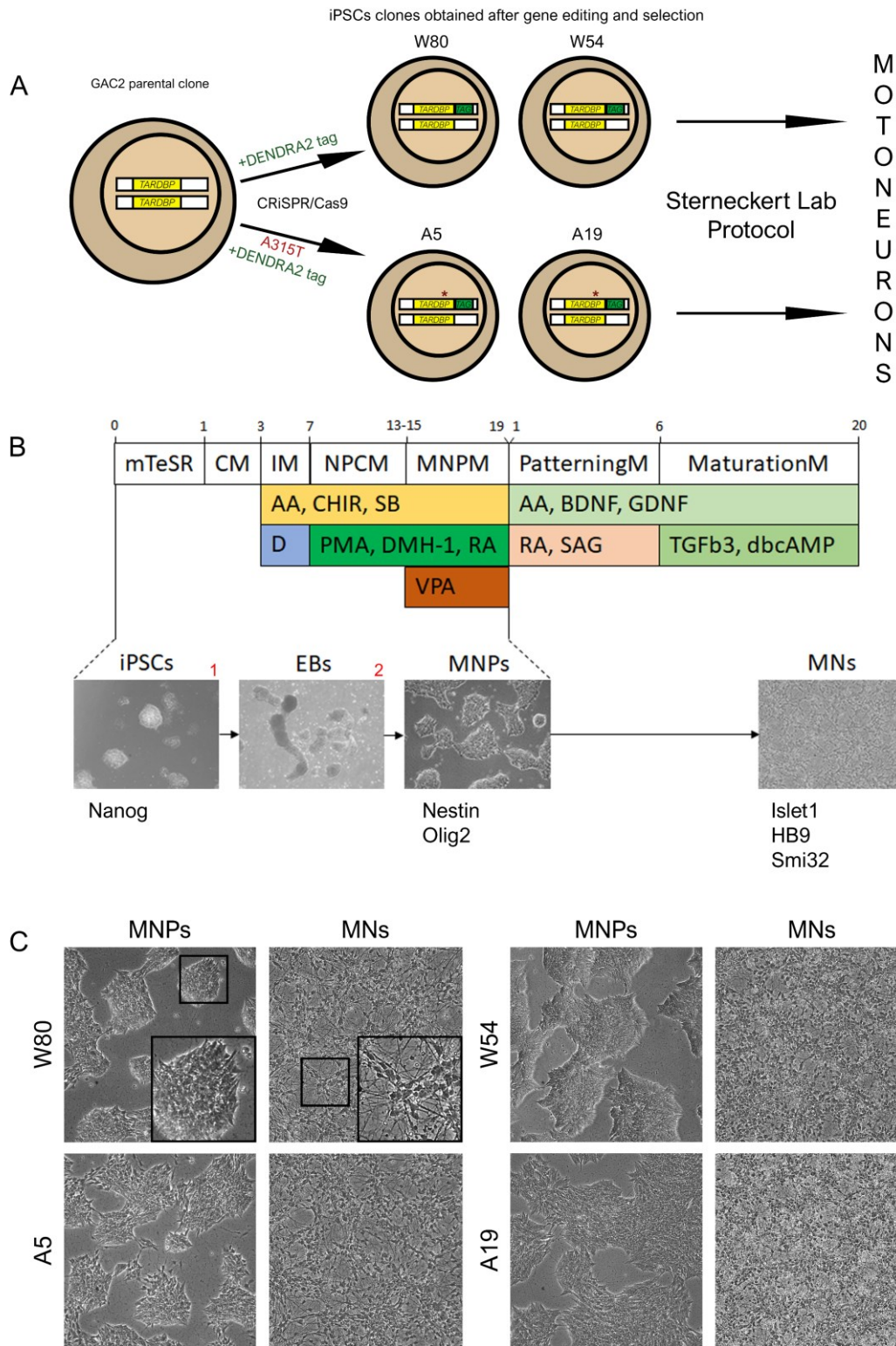


Figure 4. 1 Differentiation of iPSCs to MNs.

A. Schematic representation of isogenic reporter iPSC clones obtained by CRISPR/Cas9 gene editing and their differentiation to MNs. W80 and W54 are the selected clones after previous gene editing to express a DENDRA2-tagged TDP-43 WT (in heterozygosis); A5 and A19 are the selected clones after previous gene editing to express a DENDRA2-tagged TDP-43 carrying the A315T ALS-related mutation (in heterozygosis). **B.** Timeline and passages of the differentiation protocol with representative images of cell organization and morphology at the main steps. **C.** Microscope images of obtained MNPs and MNs of all four cell lines.

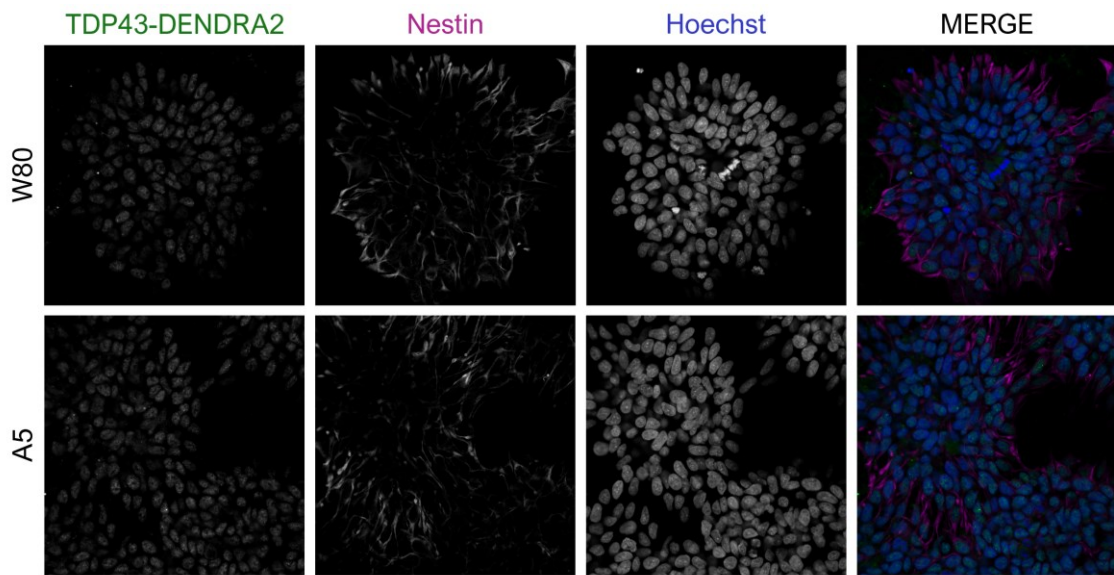


Figure 4. 2 MNPs derived from W80 and A5 iPSC lines.
DENDRA2-TDP-43 emits green fluorescence. Nestin, a pan-neuronal precursor cell marker was stained in purple, while nuclei were stained with Hoechst. (40X magnification).

4.4.2 Differentiated TDP-43 DENDRA2 cell lines are positive for neuronal markers

IPSCs-derived MNs were obtained by exposing cells to patterning medium, and then to maturation medium. As shown in **Fig. 4.1 C**, MNs grew in small clusters, emitting long propagations which resemble axons. These cells are characterized by a large cell body, a feature of MNs. At day 20, MNs were mature for subsequent analyses.

MNs obtained from MNPs differentiation were stained for MNs markers. As shown in **Fig. 4.3 (Top)**, motoneuronal-specific marker HB9 localized correctly in nuclei. Quantification of positive cells to HB9 showed that 8.4% of W80 cell line, 12.5% of A5 cell line, 9.1% of W54 cell line, 11.2% of A19 cell line are MNs. Notably, **Fig. 4.3 (bottom)** showed that all cell lines express the pan neural marker Smi-32, which stains for the non-phosphorylated Neurofilament H. TDP-43 DENDRA2 localizes in the nuclei in all cell lines and no appreciable differences in fluorescent signal were observed (**Fig. 4.3**).

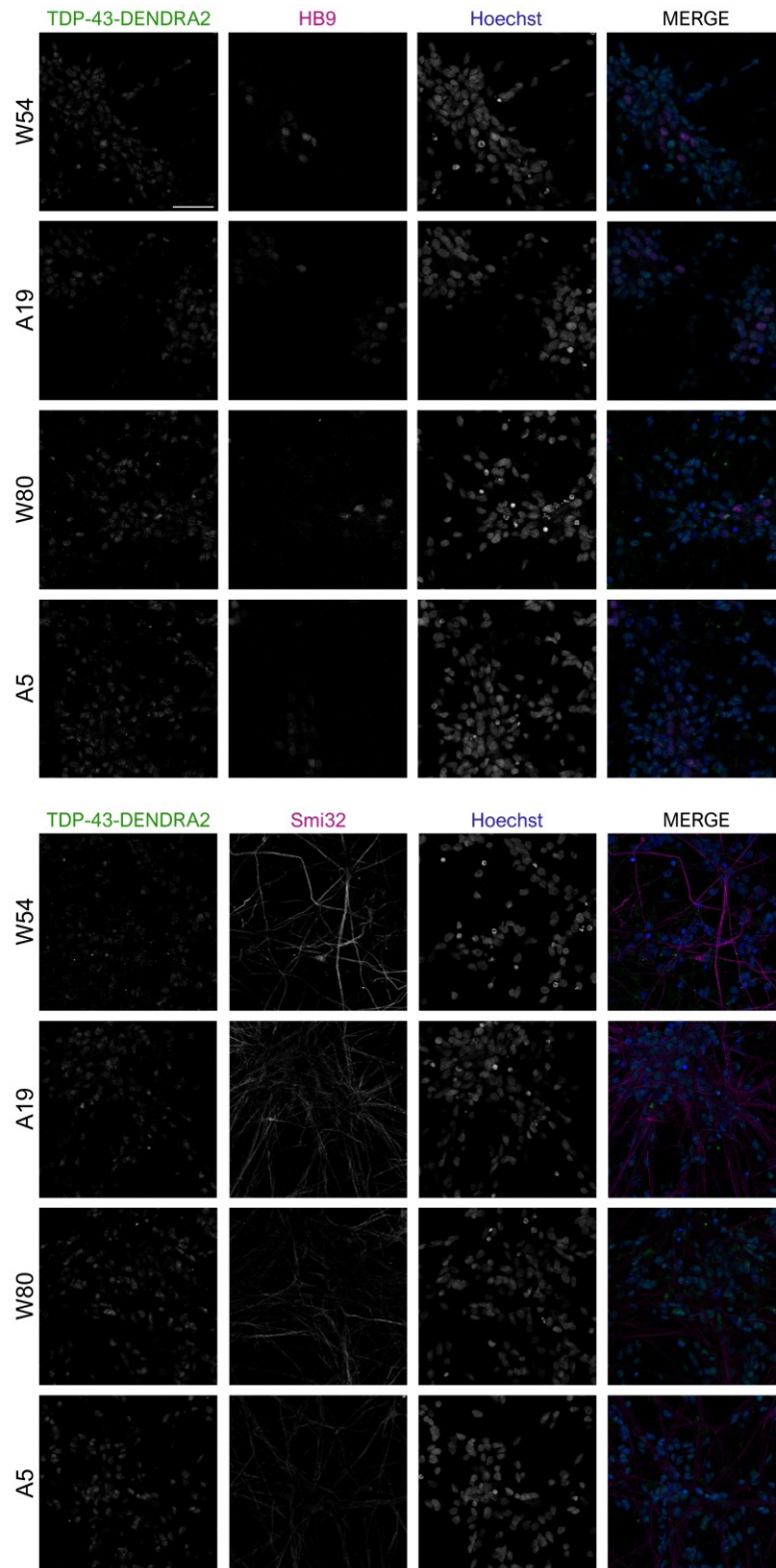


Figure 4. 3 Differentiated TDP-43 DENDRA2 cell lines are positive for neuronal markers

(Top) MNs derived from all four cell lines were stained with HB9 (purple), a motoneuronal specific marker and positive cells were counted. Nuclei were stained with Hoechst (Scale bar = 50 μ m; 20X magnification). **(Bottom)** IF for pan-neuronal cell marker Smi32 (purple). Nuclei were stained with Hoechst. (20X magnification).

4.4.3 TDP-43 DENDRA2 MNs characterization

To obtain insights into DENDRA2-tagged or untagged TDP-43 protein levels and aggregation prone behaviour, I performed a WB, FRA and IF on both the WT (W54 and W80) and the A315T mutated (A19 and A5) cell lines -derived mature MNs. TDP-43 behaviour was investigated under untreated conditions and upon proteasome and/or autophagic inhibition. I used MG-132 as a proteasome inhibitor, which is known to cause proteotoxic stress resulting in an exacerbation of TDP-43 cleavage and mislocalization (Berning et al., 2019). Instead, 3-MA was used for autophagy inhibition. As observed in **Fig. 4.4 A**, all WT and A315T mutated cell lines correctly expressed both the tagged and untagged TDP-43. Interestingly, all cell lines showed higher level of untagged-TDP-43 in respect to the DENDRA2-tagged TDP-43. This difference may be due to a loss of stability of TDP-43 protein when tagged, even if an interference of the tag with antibody recognition affecting the efficiency of detection is also possible. Interestingly, in cells undergoing proteotoxic stress induced by MG-132, I found that this type of stress did not induce an increase in endogenous TDP-43 levels, while it increased the overall levels of signals related to proteins that might recapitulate the TDP-43 CTFs (TDP-35 and TDP-25). Proteasome inhibition correlated with an increase in TDP-43 HMW insoluble species in all cell lines, as observed in FRA results. Instead, no differences in TDP-43 fragmentation or accumulation were observed in all cell lines upon autophagic blockade, using 3-MA. In addition, 3-MA did not exacerbate the effect of proteasome inhibition. Interestingly, proteasome, but not autophagic inhibition permitted the detection of a phosphorylated TDP-43 form, likely corresponding to the DENDRA2-tagged TDP-25 and 35 CTFs. To better understand the relative contribution of TDP-43 CTFs in the accumulation of HMW insoluble species, RIPA soluble/insoluble protein extracts were analysed. As reported in **Fig. 4.4 B**, both the tagged and the untagged TDP-43 were present in both soluble and insoluble fractions, but an increase in the insoluble fraction was observed in cells treated with the proteasome inhibitor. The presumed tagged TDP-35 and 25 fragments were also observed in the insoluble fractions of cells treated with the proteasome inhibitor. Again, 3-MA did not modify TDP-43 behaviour. These results suggest that proteasome inhibition correlates with an increase of TDP-43 fragmentation into insoluble species and are in line with the data previously published by us using immortalized motoneuronal models of ALS expressing TDP-43 and the two CTFs (Cicardi et al., 2018).

Analysis of the intracellular distribution of the TDP-43 protein with IF (**Fig. 4.5**) confirmed that under basal condition, both endogenous TDP-43 and DENDRA2-tagged TDP-43 resided in the nucleus of all iPSCs-derived MNs cell lines. Instead, after proteotoxic stress induction, performed using the proteasome inhibitor MG-132, the untagged TDP-43 seems

to mislocalize in the cytoplasm near the nucleus, while the DENDRA2-tagged TDP-43 was not clearly detectable outside the nucleus. Again, no effect of 3-MA on TDP-43 signal or localization was observed. Unfortunately, the magnification of the captured images was too low to appreciate the untagged and tagged TDP-43 localization and further IF experiments will be performed to validate these data. I finally evaluated the percentage of cells positive for active cleaved caspase-3 (CC3), when untreated or upon proteasome and/or autophagic inhibition (**Fig. 4.6**). Indeed, CC3 is a marker of MNs death and, in addition, its activity has been involved in TDP-43 fragmentation into CTFs. It has been shown that TDP-43 possesses three caspase-3 cleavage consensus sites, and that caspase-3 activity is induced by proteasome inhibition with MG-132 (Nonaka et al., 2009; Zhang et al., 2007). This results in an increase of TDP-43 fragmentation, due to caspase-3 activity, and TDP-43 accumulation in the cytoplasm, related to UPS blockage (Kleinberger et al., 2010; Nonaka et al., 2009). Under untreated conditions, no significant differences in the percentage of CC3-positive cells were observed among cell lines (W54 = 3.895 ± 1.615 ; A19 = 4.947 ± 2.941 ; W80 = 4.305 ± 0.870 ; A5 = 4.328 ± 1.181). Autophagy inhibition with 3-MA determined a slight but not significant increase in CC3-positive cells percentage (W54 = 6.160 ± 1.432 ; A19 = 5.693 ± 0.583 ; W80 = 8.402 ± 2.072 ; A5 = 4.294 ± 1.038), while proteasome inhibition with MG-132 caused a significant increase in CC3-positive cells in all cell lines (W54 = 10.787 ± 1.846 ; A19 = 12.683 ± 2.761 ; W80 = 16.576 ± 2.429 ; A5 = 10.461 ± 0.992). The combined treatment with autophagy and proteasome inhibitors caused an increase in the CC3 positivity, too, comparable to MG-132 treatment alone (W54 = 10.206 ± 2.363 ; A19 = 13.125 ± 2.377 ; W80 = 16.130 ± 2.027 ; A5 = 10.554 ± 1.041). This latter result suggested an absence of a synergic effect of the two treatments or a likely lack of effect of the autophagic inhibitor in the experiment. In conclusion, I finally confirmed that MG-132 treatment was associated to the presence of active CC3, indicating MNs death. Altogether, these results permitted to set up the experimental conditions of proteasome impairment to use as a paradigm model of TDP-43 misbehaviour in future experiments involving these iPSCs-derived MNs.

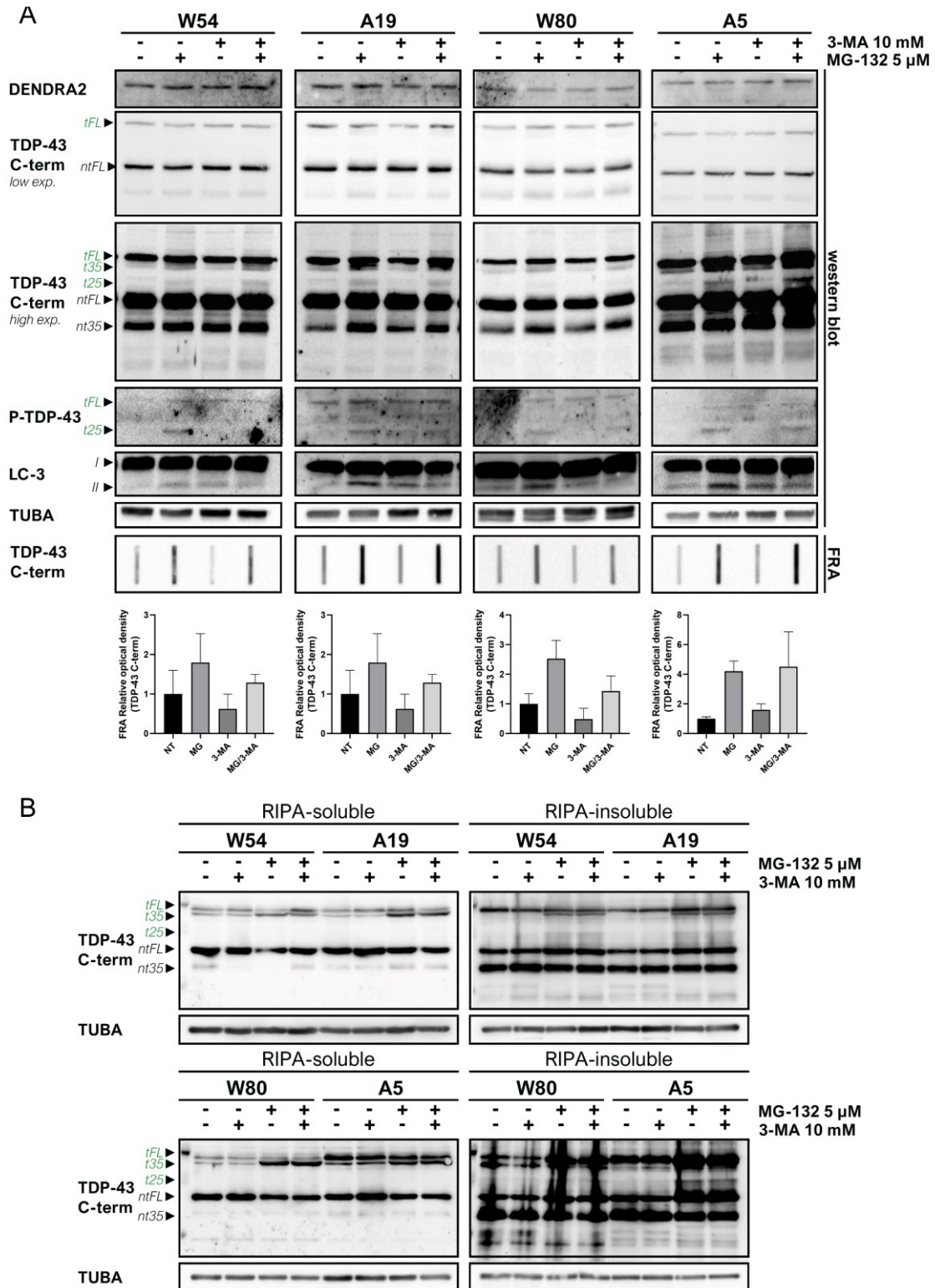


Figure 4. 4 TDP-43 fragmentation and solubility upon proteasome and/or autophagic inhibition.
A. WB and FRA results on protein extracts of MNs derived from TDP-43-DENDRA2 WT (W54 and W80) and A315T mutated (A19 and A5) iPSC lines, with or without MG-132 treatment (5 μ M, 24 hours) and/or 3-MA treatment (10 mM, 24 hours). Bar graphs report the relative optical densities of FRA.
B. WB results on RIPA-soluble and insoluble protein extracts of MNs derived from TDP-43-DENDRA2 WT (W54 and W80) and A315T mutated (A19 and A5) iPSC lines, with or without MG-132 treatment (5 μ M, 24 hours) and/or 3-MA treatment (10 mM, 24 hours).

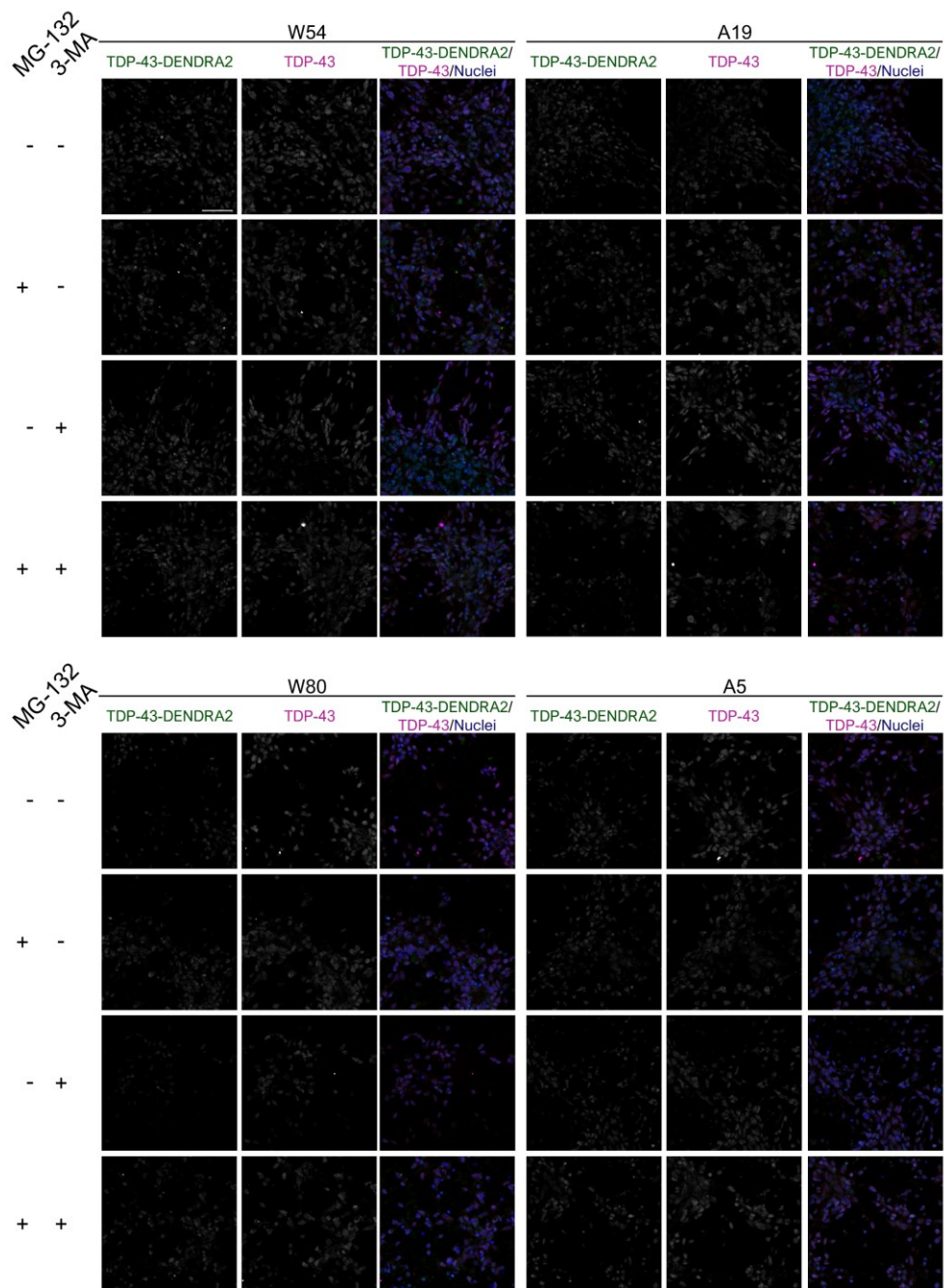


Figure 4. 5 Proteasome and/or autophagic inhibition effect on TDP-43 localization. IF on MNs derived from TDP-43-DENDRA2 WT (W54 and W80) and A315T mutated (A19 and A5) iPSC lines, with or without MG-132 treatment (5 μ M, 24 hours) and/or 3-MA treatment (10 mM, 24 hours). DENDRA2-TDP-43 emits green fluorescence. TDP-43 (both the untagged and the DENDRA2-tagged) was stained in purple, while nuclei were stained with Hoechst. (Scale bar = 50 μ m; 20X magnification).

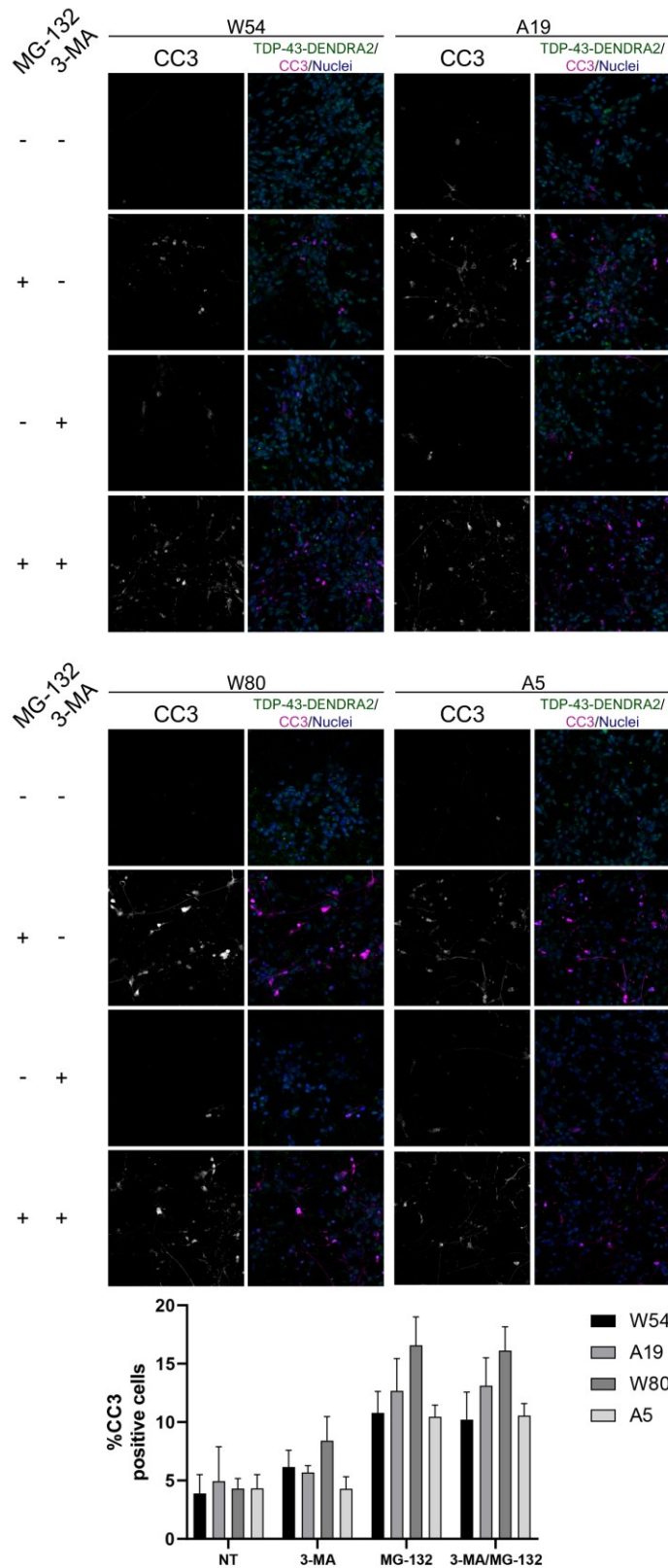


Figure 4.6 Proteasome but not autophagic inhibition correlates to CC3 activation. IF on MNs derived from TDP-43-DENDRA2 WT (W54 and W80) and A315T mutated (A19 and A5) iPSC lines, with or without MG-132 treatment (5 μ M, 24 hours) and/or 3-MA treatment (10 mM, 24 hours). DENDRA2-TDP-43 emits green fluorescence. Active cleaved caspase-3 (CC3) was stained in purple, while nuclei were stained with Hoechst. (Scale bar = 50 μ m; 20X magnification). On the bottom the graph relative to the percentages of CC3 positive cells, for each cell line and condition.

4.5 Discussion

TDP-43 is one of the proteins found mutated in ALS cases. Interestingly, mutations on TDP-43 account only for 5% of ALS cases, but 97% of cases show pathogenic inclusions of this protein in its full length or cleaved forms. Moreover, TDP-43 inclusions are present also in 45% of patients affected by FTD. TDP-43 is an mRNA binding protein involved in mRNA transport and processing and resides in the nucleus. Disease-related TDP-43 pathogenic mechanisms include its mislocalization in the cytoplasm, cleavage, phosphorylation, and aggregation. Many efforts have been done to deepen and identify new mechanisms or therapeutic approaches in TDP-43-related ALS, but a growing need to translate findings in patients has pushed investigators to validate results using cell models that are closer to human neurons and MNs. Protocols to differentiate iPSCs derived from healthy donors or patients have been developed and the use of gene editing techniques (CRISPR/Cas9) to obtain isogenic cell lines are routinely set.

Here, I show the application of a protocol to differentiate isogenic reporter cell lines expressing TDP-43 WT (W54 and W80 clones) or carrying the A315T disease-associated mutation (A19 and A5 clones).

With this protocol, I observed that the resulting clones generated a mixed population of neurons, comprising a small population of HB9-positive MNs. Even if I did not obtain a pure MN population, these cell lines will be helpful to study pathogenic TDP-43, as it causes both ALS and FTD, which affect, not only MNs, but also other different neuronal populations. In addition, it must be underlined that HB9 is considered a good marker for developing MNs, therefore a deeper evaluation of MNs markers characterizing also mature MNs is needed (e.g., ISL1, ChAT, VACHT). Preliminary data on the neuronal population derived from these iPSCs show that, under basal conditions both WT and A315T-mutated cell lines are not characterized by TDP-43 accumulation in intracellular inclusions, cytoplasmic mislocalization nor differences in TDP-43 protein levels. Instead, after proteasome inhibition, all cell lines show TDP-43 cleavage and aggregation, associated to activated cleaved caspase-3. These results are in line with several reports that demonstrated proteasome inhibition to correlate with TDP-43 misbehaviour. Instead, as expected from our previous publication (Cicardi et al., 2018) we did not observed effects or impairments on TDP-43 by inhibiting the autophagic pathway. However, since the autophagic marker LC3-I/II did not confirm an effective autophagic inhibition, further studies will be performed to evaluate the contribute of autophagy to TDP-43 behaviour and degradation in these cell models.

In conclusion, these results here presented demonstrated that the DENDRA2-tagged TDP-43 iPSCs can be used as a valuable cell model for study TDP-43 pathology, related to ALS and FTD.

Chapter V

5. Conclusions

Proteostasis dysfunction characterizes several diseases in which neuronal or muscular cell types are affected. Common molecular mechanisms at the basis of proteinopathies are protein misfolding and aggregation, and failure of the PQC system to restore proteostasis. Among the genetic causes of proteinopathies, several mutations occurring in specific factors involved in PQC network have been described. These encompass the members of the CASA complex, which is formed by chaperones HSPB8 and HSP70/HSPA, co-chaperone BAG3 and the ubiquitin-ligase CHIP, and acts in a form of selective autophagic degradation of damaged and misfolded substrates. Since the role of CASA is fundamental in proteostasis maintenance in neuronal and muscle cells, it is not surprising that mutations of some of its members are related to neuropathies and myopathies and the number of identified mutations is still growing. Indeed, how cellular functions are affected has not been investigated for all the mutants identified so far.

For these reasons, during my PhD course, I focused my studies on the characterization of mutants and variants of BAG3 and HSPB8, which are two key components of the CASA complex.

I studied some variants (S9P, P41S, S181C) of HSPB8 found in ALS patients. However, I could not appreciate significant differences in respect to the HSPB8 WT, that might relate to the ALS phenotype, except for the HSPB8 S181C. Indeed, this latter is characterized by intramolecular disulphide bond formation, whose effects are still under investigation.

On the other hand, I observed that all the myopathy and neuropathy causing BAG3 P209 and HSPB8 frameshift mutants share a common aggregation prone behaviour, which determines the co-segregation of BAG3 or HSPB8 with the other CASA members and with the autophagic adaptor SQSTM1/P62; the presence of these aggregates also associates to an increase of insoluble ubiquitinated proteins. These similarities suggest that the analysed BAG3 and HSPB8 mutants share a common disease-causative mechanism. However, several questions need a deeper investigation.

First, both BAG3 and HSPB8 mutated proteins form cytoplasmic aggregates that converge to the perinuclear region. Indeed, BAG3 mutants are found at the aggresome and this observation is likely applicable for HSPB8 mutants (*under investigation*). However, it is not yet clear how pre-aggresomal particles are formed and routed to the MTOC. Indeed, how HSPB8 or BAG3 mutants assemble in insoluble species has not been well investigated.

In addition, BAG3 mutants exert their toxicity by stalling HSP70/HSPA folding activity, and, by abrogating their interaction, BAG3 aggregation can be counteracted. With regard to this observation, evaluation on HSPB8-HSP70/HSPA relationship in HSPB8 aggregation and HSP70/HSPA dysfunction is needed.

Another difference between HSPB8 and BAG3 resides in their functions in CASA: BAG3 is the scaffold protein of CASA by interacting with HSPB8 and HSP70/HSPA. Although HSPB8 has the highest affinity in BAG3 binding, other HSPBs can bind to BAG3. This might suggest two scenarios that are of a certain interest:

- (i) HSPB8 might cause the segregation of other HSPBs together with BAG3;
- (ii) by favouring the binding of other HSPBs to BAG3, HSPB8 effect on BAG3 segregation might be bypassed.

On the other hand, HSPB8 and BAG3 independent functions have been described. It has been observed that HSPB8 acts independently from BAG3 in early response to proteotoxic stress by concentrating proteins into microaggregates and by mediating SQSTM1/P62 oligomerization. HSPB8 is the first line intervention which has been described also in granulostasis process, where it acts in response to stressors by preventing the irreversible aggregation of misfolded substrates or DRiPs into SGs. Thus, the BAG3-independent HSPB8 activities on CASA and SGs dynamics suggest that HSPB8 mutant dysfunctions might be upstream to the entire pathways.

Thus, although HSPB8 and BAG3 mutants share similar features, their relative contribution on CASA and SGs dysfunction will be investigated in future work.

The last part of this work focused on TDP-43, which is found in inclusions in most ALS cases. This strikingly observation determined an indisputable interest on TDP-43 in ALS research, with a particular focus to those many sporadic ALS cases. TDP-43 misbehaviour has been extensively investigated in our laboratory in MN-like and muscle cell models. In particular, the aggregation of TDP-43 and its toxic CTFs and the boosting of HSPB8-BAG3- and BAG1- mediated degradation for their clearance. However, the scientific research is asking for cell models recapitulating the features of the human cell types affected by disease.

Thus, here I showed results obtained in the differentiation of iPSC isogenic reporter cell lines to MNs, using a small molecules-based protocol. These cell lines have been previously generated using CRISPR/Cas9 technique to study TDP-43-related ALS. However, TDP-43 pathology is also present in FTD. Since FTD and ALS genetic and clinical features overlap in many patients, TDP-43 ALS-FTD is defined as a spectrum of disease. Thus, the neuronal-derived cell lines I obtained could be used to investigate ALS-FTD disease. Indeed, results

obtained by cell model validation, using drug-induced proteotoxic stress, were in line with the current literature from different investigators, including us. In conclusion, these data define TDP-43-DENDRA2 cell lines as a valuable tool to study TDP-43, with a particular interest on stress conditions that alter its behaviour.

References

- Abramzon, Y. A., Fratta, P., Traynor, B. J., & Chia, R. (2020). The Overlapping Genetics of Amyotrophic Lateral Sclerosis and Frontotemporal Dementia. *Front Neurosci*, *14*, 42. <https://doi.org/10.3389/fnins.2020.00042>
- Ackerley, S., James, P. A., Kalli, A., French, S., Davies, K. E., & Talbot, K. (2006). A mutation in the small heat-shock protein HSPB1 leading to distal hereditary motor neuronopathy disrupts neurofilament assembly and the axonal transport of specific cellular cargoes. *Hum Mol Genet*, *15*(2), 347-354. <https://doi.org/10.1093/hmg/ddi452>
- Acunzo, J., Katsogiannou, M., & Rocchi, P. (2012). Small heat shock proteins HSP27 (HspB1), α -crystallin (HspB5) and HSP22 (HspB8) as regulators of cell death. *Int J Biochem Cell Biol*, *44*(10), 1622-1631. <https://doi.org/10.1016/j.biocel.2012.04.002>
- Adachi, H., Katsuno, M., Minamiyama, M., Waza, M., Sang, C., Nakagomi, Y., Kobayashi, Y., Tanaka, F., Doyu, M., Inukai, A., Yoshida, M., Hashizume, Y., & Sobue, G. (2005). Widespread nuclear and cytoplasmic accumulation of mutant androgen receptor in SBMA patients. *Brain*, *128*(Pt 3), 659-670. <https://doi.org/10.1093/brain/awh381>
- Adachi, H., Waza, M., Tokui, K., Katsuno, M., Minamiyama, M., Tanaka, F., Doyu, M., & Sobue, G. (2007). CHIP overexpression reduces mutant androgen receptor protein and ameliorates phenotypes of the spinal and bulbar muscular atrophy transgenic mouse model. *J Neurosci*, *27*(19), 5115-5126. <https://doi.org/10.1523/JNEUROSCI.1242-07.2007>
- Adam, M. P., Ardinger, H. H., Pagon, R. A., Wallace, S. E., Bean, L. J. H., Stephens, K., & Amemiya, A. (1993). GeneReviews. In. <https://doi.org/NBK1476>
- Adriaenssens, E., Tedesco, B., Mediani, L., Asselbergh, B., Crippa, V., Antoniani, F., Carra, S., Poletti, A., & Timmerman, V. (2020). BAG3 Pro209 mutants associated with myopathy and neuropathy relocate chaperones of the CASA-complex to aggresomes. *Sci Rep*, *10*(1), 8755. <https://doi.org/10.1038/s41598-020-65664-z>
- Adzhubei, I. A., Schmidt, S., Peshkin, L., Ramensky, V. E., Gerasimova, A., Bork, P., Kondrashov, A. S., & Sunyaev, S. R. (2010). A method and server for predicting damaging missense mutations. *Nat Methods*, *7*(4), 248-249. <https://doi.org/10.1038/nmeth0410-248>
- Al-Ramahi, I., Lam, Y. C., Chen, H. K., de Gouyon, B., Zhang, M., Pérez, A. M., Branco, J., de Haro, M., Patterson, C., Zoghbi, H. Y., & Botas, J. (2006). CHIP protects from the neurotoxicity of expanded and wild-type ataxin-1 and promotes their ubiquitination and degradation. *J Biol Chem*, *281*(36), 26714-26724. <https://doi.org/10.1074/jbc.M601603200>
- Al-Tahan, S., Weiss, L., Yu, H., Tang, S., Saporta, M., Vihola, A., Mozaffar, T., Udd, B., & Kimonis, V. (2019). New family with. *Neurol Genet*, *5*(4), e349. <https://doi.org/10.1212/NXG.0000000000000349>
- Alberti, S., Mateju, D., Mediani, L., & Carra, S. (2017). Granulostasis: Protein Quality Control of RNP Granules. *Front Mol Neurosci*, *10*, 84. <https://doi.org/10.3389/fnmol.2017.00084>
- Almeida-Souza, L., Asselbergh, B., d'Ydewalle, C., Moonens, K., Goethals, S., de Winter, V., Azmi, A., Irobi, J., Timmermans, J. P., Gevaert, K., Remaut, H., Van Den Bosch, L., Timmerman, V., & Janssens, S. (2011). Small heat-shock protein HSPB1 mutants stabilize microtubules in Charcot-Marie-Tooth neuropathy. *J Neurosci*, *31*(43), 15320-15328. <https://doi.org/10.1523/JNEUROSCI.3266-11.2011>
- Almeida-Souza, L., Goethals, S., de Winter, V., Dierick, I., Gallardo, R., Van Durme, J., Irobi, J., Gettemans, J., Rousseau, F., Schymkowitz, J., Timmerman, V., & Janssens, S. (2010). Increased monomerization of mutant HSPB1 leads to protein hyperactivity in Charcot-Marie-Tooth neuropathy. *J Biol Chem*, *285*(17), 12778-12786. <https://doi.org/10.1074/jbc.M109.082644>
- Anding, A. L., & Baehrecke, E. H. (2017). Cleaning House: Selective Autophagy of Organelles. *Dev Cell*, *41*(1), 10-22. <https://doi.org/10.1016/j.devcel.2017.02.016>

- Andley, U. P. (2007). Crystallins in the eye: Function and pathology. *Prog Retin Eye Res*, 26(1), 78-98. <https://doi.org/10.1016/j.preteyeres.2006.10.003>
- Antonini, G., Gragnani, F., Romaniello, A., Pennisi, E. M., Morino, S., Ceschin, V., Santoro, L., & Cruccu, G. (2000). Sensory involvement in spinal-bulbar muscular atrophy (Kennedy's disease). *Muscle Nerve*, 23(2), 252-258. [https://doi.org/10.1002/\(sici\)1097-4598\(200002\)23:2<252::aid-mus17>3.0.co;2-p](https://doi.org/10.1002/(sici)1097-4598(200002)23:2<252::aid-mus17>3.0.co;2-p)
- Arakawa, A., Handa, N., Ohsawa, N., Shida, M., Kigawa, T., Hayashi, F., Shirouzu, M., & Yokoyama, S. (2010). The C-terminal BAG domain of BAG5 induces conformational changes of the Hsp70 nucleotide-binding domain for ADP-ATP exchange. *Structure*, 18(3), 309-319. <https://doi.org/10.1016/j.str.2010.01.004>
- Arndt, V., Daniel, C., Nastainczyk, W., Alberti, S., & Höhfeld, J. (2005). BAG-2 acts as an inhibitor of the chaperone-associated ubiquitin ligase CHIP. *Mol Biol Cell*, 16(12), 5891-5900. <https://doi.org/10.1091/mbc.e05-07-0660>
- Arndt, V., Dick, N., Tawo, R., Dreiseidler, M., Wenzel, D., Hesse, M., Fürst, D. O., Saftig, P., Saint, R., Fleischmann, B. K., Hoch, M., & Höhfeld, J. (2010). Chaperone-assisted selective autophagy is essential for muscle maintenance. *Curr Biol*, 20(2), 143-148. <https://doi.org/10.1016/j.cub.2009.11.022>
- Arrigo, A. P. (2007). The cellular "networking" of mammalian Hsp27 and its functions in the control of protein folding, redox state and apoptosis. *Adv Exp Med Biol*, 594, 14-26. https://doi.org/10.1007/978-0-387-39975-1_2
- Arrigo, A. P. (2017). Mammalian HspB1 (Hsp27) is a molecular sensor linked to the physiology and environment of the cell. *Cell Stress Chaperones*, 22(4), 517-529. <https://doi.org/10.1007/s12192-017-0765-1>
- Atsuta, N., Watanabe, H., Ito, M., Banno, H., Suzuki, K., Katsuno, M., Tanaka, F., Tamakoshi, A., & Sobue, G. (2006). Natural history of spinal and bulbar muscular atrophy (SBMA): a study of 223 Japanese patients. *Brain*, 129(Pt 6), 1446-1455. <https://doi.org/10.1093/brain/awl096>
- Balchin, D., Hayer-Hartl, M., & Hartl, F. U. (2016). In vivo aspects of protein folding and quality control. *Science*, 353(6294), aac4354. <https://doi.org/10.1126/science.aac4354>
- Ballinger, C. A., Connell, P., Wu, Y., Hu, Z., Thompson, L. J., Yin, L. Y., & Patterson, C. (1999). Identification of CHIP, a novel tetratricopeptide repeat-containing protein that interacts with heat shock proteins and negatively regulates chaperone functions. *Mol Cell Biol*, 19(6), 4535-4545. <https://doi.org/10.1128/mcb.19.6.4535>
- Bartelt-Kirbach, B., & Golenhofen, N. (2014). Reaction of small heat-shock proteins to different kinds of cellular stress in cultured rat hippocampal neurons. *Cell Stress Chaperones*, 19(1), 145-153. <https://doi.org/10.1007/s12192-013-0452-9>
- Basha, E., O'Neill, H., & Vierling, E. (2012). Small heat shock proteins and α -crystallins: dynamic proteins with flexible functions. *Trends Biochem Sci*, 37(3), 106-117. <https://doi.org/10.1016/j.tibs.2011.11.005>
- Basile, A., Darbinian, N., Kaminski, R., White, M. K., Gentilella, A., Turco, M. C., & Khalili, K. (2009). Evidence for modulation of BAG3 by polyomavirus JC early protein. *J Gen Virol*, 90(Pt 7), 1629-1640. <https://doi.org/10.1099/vir.0.008722-0>
- Bassnett, S. (2009). On the mechanism of organelle degradation in the vertebrate lens. *Exp Eye Res*, 88(2), 133-139. <https://doi.org/10.1016/j.exer.2008.08.017>
- Behl, C. (2016). Breaking BAG: The Co-Chaperone BAG3 in Health and Disease. *Trends Pharmacol Sci*, 37(8), 672-688. <https://doi.org/10.1016/j.tips.2016.04.007>
- Bengoechea, R., Pittman, S. K., Tuck, E. P., True, H. L., & Weihl, C. C. (2015). Myofibrillar disruption and RNA-binding protein aggregation in a mouse model of limb-girdle muscular dystrophy 1D. *Hum Mol Genet*, 24(23), 6588-6602. <https://doi.org/10.1093/hmg/ddv363>
- Bennion Callister, J., & Pickering-Brown, S. M. (2014). Pathogenesis/genetics of frontotemporal dementia and how it relates to ALS. *Exp Neurol*, 262 Pt B, 84-90. <https://doi.org/10.1016/j.expneurol.2014.06.001>

- Blackstone, C. (2018). Converging cellular themes for the hereditary spastic paraplegias. *Curr Opin Neurobiol*, 51, 139-146. <https://doi.org/10.1016/j.conb.2018.04.025>
- Blokhuis, A. M., Groen, E. J., Koppers, M., van den Berg, L. H., & Pasterkamp, R. J. (2013). Protein aggregation in amyotrophic lateral sclerosis. *Acta Neuropathol*, 125(6), 777-794. <https://doi.org/10.1007/s00401-013-1125-6>
- Boelens, W. C. (2020). Structural aspects of the human small heat shock proteins related to their functional activities. *Cell Stress Chaperones*, 25(4), 581-591. <https://doi.org/10.1007/s12192-020-01093-1>
- Boelens, W. C., Van Boekel, M. A., & De Jong, W. W. (1998). HspB3, the most deviating of the six known human small heat shock proteins. *Biochim Biophys Acta*, 1388(2), 513-516. [https://doi.org/10.1016/s0167-4838\(98\)00215-5](https://doi.org/10.1016/s0167-4838(98)00215-5)
- Boluyt, M. O., Brevick, J. L., Rogers, D. S., Randall, M. J., Scalia, A. F., & Li, Z. B. (2006). Changes in the rat heart proteome induced by exercise training: Increased abundance of heat shock protein hsp20. *Proteomics*, 6(10), 3154-3169. <https://doi.org/10.1002/pmic.200401356>
- Bose, J. K., Wang, I. F., Hung, L., Tarn, W. Y., & Shen, C. K. (2008). TDP-43 overexpression enhances exon 7 inclusion during the survival of motor neuron pre-mRNA splicing. *J Biol Chem*, 283(43), 28852-28859. <https://doi.org/10.1074/jbc.M805376200>
- Bouhy, D., Geuens, T., De Winter, V., Almeida-Souza, L., Katona, I., Weis, J., Hochepped, T., Goossens, S., Haigh, J. J., Janssens, S., & Timmerman, V. (2016). Characterization of New Transgenic Mouse Models for Two Charcot-Marie-Tooth-Causing HspB1 Mutations using the Rosa26 Locus. *J Neuromuscul Dis*, 3(2), 183-200. <https://doi.org/10.3233/JND-150144>
- Bouhy, D., Juneja, M., Katona, I., Holmgren, A., Asselbergh, B., De Winter, V., Hochepped, T., Goossens, S., Haigh, J. J., Libert, C., Ceuterick-de Groote, C., Irobi, J., Weis, J., & Timmerman, V. (2018). A knock-in/knock-out mouse model of HSPB8-associated distal hereditary motor neuropathy and myopathy reveals toxic gain-of-function of mutant Hspb8. *Acta Neuropathol*, 135(1), 131-148. <https://doi.org/10.1007/s00401-017-1756-0>
- Boutry, M., Morais, S., & Stevanin, G. (2019). Update on the Genetics of Spastic Paraplegias. *Curr Neurol Neurosci Rep*, 19(4), 18. <https://doi.org/10.1007/s11910-019-0930-2>
- Brady, J. P., Garland, D., Duglas-Tabor, Y., Robison, W. G., Groome, A., & Wawrousek, E. F. (1997). Targeted disruption of the mouse alpha A-crystallin gene induces cataract and cytoplasmic inclusion bodies containing the small heat shock protein alpha B-crystallin. *Proc Natl Acad Sci U S A*, 94(3), 884-889. <https://doi.org/10.1073/pnas.94.3.884>
- Briknarová, K., Takayama, S., Brive, L., Havert, M. L., Knee, D. A., Velasco, J., Homma, S., Cabezas, E., Stuart, J., Hoyt, D. W., Satterthwait, A. C., Llinás, M., Reed, J. C., & Ely, K. R. (2001). Structural analysis of BAG1 cochaperone and its interactions with Hsc70 heat shock protein. *Nat Struct Biol*, 8(4), 349-352. <https://doi.org/10.1038/86236>
- Brinkmann, A. O., Faber, P. W., van Rooij, H. C., Kuiper, G. G., Ris, C., Klaassen, P., van der Korput, J. A., Voorhorst, M. M., van Laar, J. H., & Mulder, E. (1989). The human androgen receptor: domain structure, genomic organization and regulation of expression. *J Steroid Biochem*, 34(1-6), 307-310. [https://doi.org/10.1016/0022-4731\(89\)90098-8](https://doi.org/10.1016/0022-4731(89)90098-8)
- Brive, L., Takayama, S., Briknarová, K., Homma, S., Ishida, S. K., Reed, J. C., & Ely, K. R. (2001). The carboxyl-terminal lobe of Hsc70 ATPase domain is sufficient for binding to BAG1. *Biochem Biophys Res Commun*, 289(5), 1099-1105. <https://doi.org/10.1006/bbrc.2001.6087>
- Brophy, C. M., Dickinson, M., & Woodrum, D. (1999). Phosphorylation of the small heat shock-related protein, HSP20, in vascular smooth muscles is associated with changes in the macromolecular associations of HSP20. *J Biol Chem*, 274(10), 6324-6329. <https://doi.org/10.1074/jbc.274.10.6324>
- Brown, R. H., & Al-Chalabi, A. (2017). Amyotrophic Lateral Sclerosis. *N Engl J Med*, 377(16), 1602. <https://doi.org/10.1056/NEJMc1710379>
- Bruey, J. M., Ducasse, C., Bonniaud, P., Ravagnan, L., Susin, S. A., Diaz-Latoud, C., Gurbuxani, S., Arrigo, A. P., Kroemer, G., Solary, E., & Garrido, C. (2000). Hsp27 negatively regulates cell

- death by interacting with cytochrome c. *Nat Cell Biol*, 2(9), 645-652. <https://doi.org/10.1038/35023595>
- Bruinsma, I. B., Bruggink, K. A., Kinast, K., Versleijen, A. A., Segers-Nolten, I. M., Subramaniam, V., Kuiperij, H. B., Boelens, W., de Waal, R. M., & Verbeek, M. M. (2011). Inhibition of α -synuclein aggregation by small heat shock proteins. *Proteins*, 79(10), 2956-2967. <https://doi.org/10.1002/prot.23152>
- Bruno, A. P., Festa, M., Dal Piaz, F., Rosati, A., Turco, M. C., Giuditta, A., & Marzullo, L. (2008). Identification of a synaptosome-associated form of BAG3 protein. *Cell Cycle*, 7(19), 3104-3105. <https://doi.org/10.4161/cc.7.19.6774>
- Buchan, J. R., & Parker, R. (2009). Eukaryotic stress granules: the ins and outs of translation. *Mol Cell*, 36(6), 932-941. <https://doi.org/10.1016/j.molcel.2009.11.020>
- Budenholzer, L., Cheng, C. L., Li, Y., & Hochstrasser, M. (2017). Proteasome Structure and Assembly. *J Mol Biol*, 429(22), 3500-3524. <https://doi.org/10.1016/j.jmb.2017.05.027>
- Bugiardini, E., Rossor, A. M., Lynch, D. S., Swash, M., Pittman, A. M., Blake, J. C., Hanna, M. G., Houlden, H., Holton, J. L., Reilly, M. M., & Matthews, E. (2017). Homozygous mutation in. *Neurol Genet*, 3(4), e168. <https://doi.org/10.1212/NXG.0000000000000168>
- Bukach, O. V., Seit-Nebi, A. S., Marston, S. B., & Gusev, N. B. (2004). Some properties of human small heat shock protein Hsp20 (HspB6). *Eur J Biochem*, 271(2), 291-302. <https://doi.org/10.1046/j.1432-1033.2003.03928.x>
- Bullard, B., Ferguson, C., Minajeva, A., Leake, M. C., Gautel, M., Labeit, D., Ding, L., Labeit, S., Horwitz, J., Leonard, K. R., & Linke, W. A. (2004). Association of the chaperone alphaB-crystallin with titin in heart muscle. *J Biol Chem*, 279(9), 7917-7924. <https://doi.org/10.1074/jbc.M307473200>
- Bunton-Stasyshyn, R. K., Saccon, R. A., Fratta, P., & Fisher, E. M. (2015). SOD1 Function and Its Implications for Amyotrophic Lateral Sclerosis Pathology: New and Renascent Themes. *Neuroscientist*, 21(5), 519-529. <https://doi.org/10.1177/1073858414561795>
- Buratti, E. (2018). TDP-43 post-translational modifications in health and disease. *Expert Opin Ther Targets*, 22(3), 279-293. <https://doi.org/10.1080/14728222.2018.1439923>
- Cameron, R. T., Quinn, S. D., Cairns, L. S., MacLeod, R., Samuel, I. D., Smith, B. O., Carlos Penedo, J., & Baillie, G. S. (2014). The phosphorylation of Hsp20 enhances its association with amyloid- β to increase protection against neuronal cell death. *Mol Cell Neurosci*, 61, 46-55. <https://doi.org/10.1016/j.mcn.2014.05.002>
- Cao, Y. L., Yang, Y. P., Mao, C. J., Zhang, X. Q., Wang, C. T., Yang, J., Lv, D. J., Wang, F., Hu, L. F., & Liu, C. F. (2017). A role of BAG3 in regulating SNCA/ α -synuclein clearance via selective macroautophagy. *Neurobiol Aging*, 60, 104-115. <https://doi.org/10.1016/j.neurobiolaging.2017.08.023>
- Cappola, T. P., Li, M., He, J., Ky, B., Gilmore, J., Qu, L., Keating, B., Reilly, M., Kim, C. E., Glessner, J., Frackelton, E., Hakonarson, H., Syed, F., Hindes, A., Matkovich, S. J., Cresci, S., & Dorn, G. W. (2010). Common variants in HSPB7 and FRMD4B associated with advanced heart failure. *Circ Cardiovasc Genet*, 3(2), 147-154. <https://doi.org/10.1161/CIRCGENETICS.109.898395>
- Capponi, S., Geuens, T., Geroldi, A., Origone, P., Verdiani, S., Cichero, E., Adriaenssens, E., De Winter, V., Bandettini di Poggio, M., Barberis, M., Chiò, A., Fossa, P., Mandich, P., Bellone, E., & Timmerman, V. (2016). Molecular Chaperones in the Pathogenesis of Amyotrophic Lateral Sclerosis: The Role of HSPB1. *Hum Mutat*, 37(11), 1202-1208. <https://doi.org/10.1002/humu.23062>
- Carra, S., Boncoraglio, A., Kanon, B., Brunsting, J. F., Minoia, M., Rana, A., Vos, M. J., Seidel, K., Sibon, O. C., & Kampinga, H. H. (2010). Identification of the Drosophila ortholog of HSPB8: implication of HSPB8 loss of function in protein folding diseases. *J Biol Chem*, 285(48), 37811-37822. <https://doi.org/10.1074/jbc.M110.127498>
- Carra, S., Brunsting, J. F., Lambert, H., Landry, J., & Kampinga, H. H. (2009). HspB8 participates in protein quality control by a non-chaperone-like mechanism that requires eIF2{alpha}

- phosphorylation. *J Biol Chem*, 284(9), 5523-5532. <https://doi.org/10.1074/jbc.M807440200>
- Carra, S., Seguin, S. J., Lambert, H., & Landry, J. (2008). HspB8 chaperone activity toward poly(Q)-containing proteins depends on its association with Bag3, a stimulator of macroautophagy. *J Biol Chem*, 283(3), 1437-1444. <https://doi.org/10.1074/jbc.M706304200>
- Carra, S., Seguin, S. J., & Landry, J. (2008). HspB8 and Bag3: a new chaperone complex targeting misfolded proteins to macroautophagy. *Autophagy*, 4(2), 237-239. <https://doi.org/10.4161/auto.5407>
- Carra, S., Sivilotti, M., Chávez Zobel, A. T., Lambert, H., & Landry, J. (2005). HspB8, a small heat shock protein mutated in human neuromuscular disorders, has in vivo chaperone activity in cultured cells. *Hum Mol Genet*, 14(12), 1659-1669. <https://doi.org/10.1093/hmg/ddi174>
- Carrettiero, D. C., Hernandez, I., Neveu, P., Papagiannakopoulos, T., & Kosik, K. S. (2009). The cochaperone BAG2 sweeps paired helical filament-insoluble tau from the microtubule. *J Neurosci*, 29(7), 2151-2161. <https://doi.org/10.1523/JNEUROSCI.4660-08.2009>
- Caspers, G. J., Leunissen, J. A., & de Jong, W. W. (1995). The expanding small heat-shock protein family, and structure predictions of the conserved "alpha-crystallin domain". *J Mol Evol*, 40(3), 238-248. <https://doi.org/10.1007/bf00163229>
- Cenacchi, G., Papa, V., Pegoraro, V., Marozzo, R., Fanin, M., & Angelini, C. (2020). Review: Danon disease: Review of natural history and recent advances. *Neuropathol Appl Neurobiol*, 46(4), 303-322. <https://doi.org/10.1111/nan.12587>
- Chalova, A. S., Sudnitsyna, M. V., Strelkov, S. V., & Gusev, N. B. (2014). Characterization of human small heat shock protein HspB1 that carries C-terminal domain mutations associated with hereditary motor neuron diseases. *Biochim Biophys Acta*, 1844(12), 2116-2126. <https://doi.org/10.1016/j.bbapap.2014.09.005>
- Chevalier-Larsen, E. S., O'Brien, C. J., Wang, H., Jenkins, S. C., Holder, L., Lieberman, A. P., & Merry, D. E. (2004). Castration restores function and neurofilament alterations of aged symptomatic males in a transgenic mouse model of spinal and bulbar muscular atrophy. *J Neurosci*, 24(20), 4778-4786. <https://doi.org/10.1523/JNEUROSCI.0808-04.2004>
- Chiti, F., & Dobson, C. M. (2017). Protein Misfolding, Amyloid Formation, and Human Disease: A Summary of Progress Over the Last Decade. *Annu Rev Biochem*, 86, 27-68. <https://doi.org/10.1146/annurev-biochem-061516-045115>
- Cicardi, M. E., Cristofani, R., Crippa, V., Ferrari, V., Tedesco, B., Casarotto, E., Chierichetti, M., Galbiati, M., Piccolella, M., Messi, E., Carra, S., Pennuto, M., Rusmini, P., & Poletti, A. (2019). Autophagic and Proteasomal Mediated Removal of Mutant Androgen Receptor in Muscle Models of Spinal and Bulbar Muscular Atrophy. *Front Endocrinol (Lausanne)*, 10, 569. <https://doi.org/10.3389/fendo.2019.00569>
- Cicardi, M. E., Cristofani, R., Rusmini, P., Meroni, M., Ferrari, V., Vezzoli, G., Tedesco, B., Piccolella, M., Messi, E., Galbiati, M., Boncoraglio, A., Carra, S., Crippa, V., & Poletti, A. (2018). Tdp-25 Routing to Autophagy and Proteasome Ameliorates its Aggregation in Amyotrophic Lateral Sclerosis Target Cells. *Sci Rep*, 8(1), 12390. <https://doi.org/10.1038/s41598-018-29658-2>
- Ciechanover, A. (1994). The ubiquitin-proteasome proteolytic pathway. *Cell*, 79(1), 13-21. [https://doi.org/10.1016/0092-8674\(94\)90396-4](https://doi.org/10.1016/0092-8674(94)90396-4)
- Ciocca, D. R., Arrigo, A. P., & Calderwood, S. K. (2013). Heat shock proteins and heat shock factor 1 in carcinogenesis and tumor development: an update. *Arch Toxicol*, 87(1), 19-48. <https://doi.org/10.1007/s00204-012-0918-z>
- Clark, A. R., Lubsen, N. H., & Slingsby, C. (2012). sHSP in the eye lens: crystallin mutations, cataract and proteostasis. *Int J Biochem Cell Biol*, 44(10), 1687-1697. <https://doi.org/10.1016/j.biocel.2012.02.015>
- Clark, A. R., Naylor, C. E., Bagn eris, C., Keep, N. H., & Slingsby, C. (2011). Crystal structure of R120G disease mutant of human α B-crystallin domain dimer shows closure of a groove. *J Mol Biol*, 408(1), 118-134. <https://doi.org/10.1016/j.jmb.2011.02.020>

- Cleveland, D. W., & Rothstein, J. D. (2001). From Charcot to Lou Gehrig: deciphering selective motor neuron death in ALS. *Nat Rev Neurosci*, 2(11), 806-819. <https://doi.org/10.1038/35097565>
- Coldwell, M. J., deSchoolmeester, M. L., Fraser, G. A., Pickering, B. M., Packham, G., & Willis, A. E. (2001). The p36 isoform of BAG-1 is translated by internal ribosome entry following heat shock. *Oncogene*, 20(30), 4095-4100. <https://doi.org/10.1038/sj.onc.1204547>
- Colvin, T. A., Gabai, V. L., Gong, J., Calderwood, S. K., Li, H., Gummuluru, S., Matchuk, O. N., Smirnova, S. G., Orlova, N. V., Zamulaeva, I. A., Garcia-Marcos, M., Li, X., Young, Z. T., Rauch, J. N., Gestwicki, J. E., Takayama, S., & Sherman, M. Y. (2014). Hsp70-Bag3 interactions regulate cancer-related signaling networks. *Cancer Res*, 74(17), 4731-4740. <https://doi.org/10.1158/0008-5472.CAN-14-0747>
- Cordoba, M., Rodriguez-Quiroga, S., Gatto, E. M., Alurralde, A., & Kauffman, M. A. (2014). Ataxia plus myoclonus in a 23-year-old patient due to STUB1 mutations. *Neurology*, 83(3), 287-288. <https://doi.org/10.1212/WNL.0000000000000600>
- Cortes, C. J., Ling, S. C., Guo, L. T., Hung, G., Tsunemi, T., Ly, L., Tokunaga, S., Lopez, E., Sopher, B. L., Bennett, C. F., Shelton, G. D., Cleveland, D. W., & La Spada, A. R. (2014). Muscle expression of mutant androgen receptor accounts for systemic and motor neuron disease phenotypes in spinal and bulbar muscular atrophy. *Neuron*, 82(2), 295-307. <https://doi.org/10.1016/j.neuron.2014.03.001>
- Cortese, A., Laurà, M., Casali, C., Nishino, I., Hayashi, Y. K., Magri, S., Taroni, F., Stuani, C., Saveri, P., Moggio, M., Ripolone, M., Prella, A., Pisciotta, C., Sagnelli, A., Pichiecchio, A., Reilly, M. M., Buratti, E., & Pareyson, D. (2018). Altered TDP-43-dependent splicing in HSPB8-related distal hereditary motor neuropathy and myofibrillar myopathy. *Eur J Neurol*, 25(1), 154-163. <https://doi.org/10.1111/ene.13478>
- Crippa, V., D'Agostino, V. G., Cristofani, R., Rusmini, P., Cicardi, M. E., Messi, E., Loffredo, R., Pancher, M., Piccolella, M., Galbiati, M., Meroni, M., Cereda, C., Carra, S., Provenzani, A., & Poletti, A. (2016). Transcriptional induction of the heat shock protein B8 mediates the clearance of misfolded proteins responsible for motor neuron diseases. *Sci Rep*, 6, 22827. <https://doi.org/10.1038/srep22827>
- Crippa, V., Sau, D., Rusmini, P., Boncoraglio, A., Onesto, E., Bolzoni, E., Galbiati, M., Fontana, E., Marino, M., Carra, S., Bendotti, C., De Biasi, S., & Poletti, A. (2010). The small heat shock protein B8 (HspB8) promotes autophagic removal of misfolded proteins involved in amyotrophic lateral sclerosis (ALS). *Hum Mol Genet*, 19(17), 3440-3456. <https://doi.org/10.1093/hmg/ddq257>
- Cristofani, R., Crippa, V., Cicardi, M. E., Tedesco, B., Ferrari, V., Chierichetti, M., Casarotto, E., Piccolella, M., Messi, E., Galbiati, M., Rusmini, P., & Poletti, A. (2020). A Crucial Role for the Protein Quality Control System in Motor Neuron Diseases. *Front Aging Neurosci*, 12, 191. <https://doi.org/10.3389/fnagi.2020.00191>
- Cristofani, R., Crippa, V., Rusmini, P., Cicardi, M. E., Meroni, M., Licata, N. V., Sala, G., Giorgetti, E., Grunseich, C., Galbiati, M., Piccolella, M., Messi, E., Ferrarese, C., Carra, S., & Poletti, A. (2017). Inhibition of retrograde transport modulates misfolded protein accumulation and clearance in motoneuron diseases. *Autophagy*, 13(8), 1280-1303. <https://doi.org/10.1080/15548627.2017.1308985>
- Cristofani, R., Crippa, V., Vezzoli, G., Rusmini, P., Galbiati, M., Cicardi, M. E., Meroni, M., Ferrari, V., Tedesco, B., Piccolella, M., Messi, E., Carra, S., & Poletti, A. (2018). The small heat shock protein B8 (HSPB8) efficiently removes aggregating species of dipeptides produced in C9ORF72-related neurodegenerative diseases. *Cell Stress Chaperones*, 23(1), 1-12. <https://doi.org/10.1007/s12192-017-0806-9>
- Cristofani, R., Rusmini, P., Galbiati, M., Cicardi, M. E., Ferrari, V., Tedesco, B., Casarotto, E., Chierichetti, M., Messi, E., Piccolella, M., Carra, S., Crippa, V., & Poletti, A. (2019). The Regulation of the Small Heat Shock Protein B8 in Misfolding Protein Diseases Causing

- Motoneuronal and Muscle Cell Death. *Front Neurosci*, 13, 796. <https://doi.org/10.3389/fnins.2019.00796>
- D'Amico, A., Mercuri, E., Tiziano, F. D., & Bertini, E. (2011). Spinal muscular atrophy. *Orphanet J Rare Dis*, 6, 71. <https://doi.org/10.1186/1750-1172-6-71>
- d'Ydewalle, C., Krishnan, J., Chiheb, D. M., Van Damme, P., Irobi, J., Kozikowski, A. P., Vanden Berghe, P., Timmerman, V., Robberecht, W., & Van Den Bosch, L. (2011). HDAC6 inhibitors reverse axonal loss in a mouse model of mutant HSPB1-induced Charcot-Marie-Tooth disease. *Nat Med*, 17(8), 968-974. <https://doi.org/10.1038/nm.2396>
- Dai, Q., Qian, S. B., Li, H. H., McDonough, H., Borchers, C., Huang, D., Takayama, S., Younger, J. M., Ren, H. Y., Cyr, D. M., & Patterson, C. (2005). Regulation of the cytoplasmic quality control protein degradation pathway by BAG2. *J Biol Chem*, 280(46), 38673-38681. <https://doi.org/10.1074/jbc.M507986200>
- Dai, Q., Zhang, C., Wu, Y., McDonough, H., Whaley, R. A., Godfrey, V., Li, H. H., Madamanchi, N., Xu, W., Neckers, L., Cyr, D., & Patterson, C. (2003). CHIP activates HSF1 and confers protection against apoptosis and cellular stress. *EMBO J*, 22(20), 5446-5458. <https://doi.org/10.1093/emboj/cdg529>
- Datskevich, P. N., Nefedova, V. V., Sudnitsyna, M. V., & Gusev, N. B. (2012). Mutations of small heat shock proteins and human congenital diseases. *Biochemistry (Mosc)*, 77(13), 1500-1514. <https://doi.org/10.1134/S0006297912130081>
- Davidson, Y. S., Barker, H., Robinson, A. C., Thompson, J. C., Harris, J., Troakes, C., Smith, B., Al-Saraj, S., Shaw, C., Rollinson, S., Masuda-Suzukake, M., Hasegawa, M., Pickering-Brown, S., Snowden, J. S., & Mann, D. M. (2014). Brain distribution of dipeptide repeat proteins in frontotemporal lobar degeneration and motor neurone disease associated with expansions in C9ORF72. *Acta Neuropathol Commun*, 2, 70. <https://doi.org/10.1186/2051-5960-2-70>
- de Souza, P. V. S., de Rezende Pinto, W. B. V., de Rezende Batistella, G. N., Bortholin, T., & Oliveira, A. S. B. (2017). Hereditary Spastic Paraplegia: Clinical and Genetic Hallmarks. *Cerebellum*, 16(2), 525-551. <https://doi.org/10.1007/s12311-016-0803-z>
- de Wit, N. J., Verschuure, P., Kappé, G., King, S. M., de Jong, W. W., van Muijen, G. N., & Boelens, W. C. (2004). Testis-specific human small heat shock protein HSPB9 is a cancer/testis antigen, and potentially interacts with the dynein subunit TCTEL1. *Eur J Cell Biol*, 83(7), 337-345. <https://doi.org/10.1078/0171-9335-00396>
- Dejager, S., Bry-Gauillard, H., Bruckert, E., Eymard, B., Salachas, F., LeGuern, E., Tardieu, S., Chadarevian, R., Giral, P., & Turpin, G. (2002). A comprehensive endocrine description of Kennedy's disease revealing androgen insensitivity linked to CAG repeat length. *J Clin Endocrinol Metab*, 87(8), 3893-3901. <https://doi.org/10.1210/jcem.87.8.8780>
- DeJesus-Hernandez, M., Finch, N. A., Wang, X., Gendron, T. F., Bieniek, K. F., Heckman, M. G., Vasilevich, A., Murray, M. E., Rousseau, L., Weesner, R., Lucido, A., Parsons, M., Chew, J., Josephs, K. A., Parisi, J. E., Knopman, D. S., Petersen, R. C., Boeve, B. F., Graff-Radford, N. R., de Boer, J., Asmann, Y. W., Petrucelli, L., Boylan, K. B., Dickson, D. W., van Blitterswijk, M., & Rademakers, R. (2017). In-depth clinico-pathological examination of RNA foci in a large cohort of C9ORF72 expansion carriers. *Acta Neuropathol*, 134(2), 255-269. <https://doi.org/10.1007/s00401-017-1725-7>
- DeJesus-Hernandez, M., Mackenzie, I. R., Boeve, B. F., Boxer, A. L., Baker, M., Rutherford, N. J., Nicholson, A. M., Finch, N. A., Flynn, H., Adamson, J., Kouri, N., Wojtas, A., Sengdy, P., Hsiung, G. Y., Karydas, A., Seeley, W. W., Josephs, K. A., Coppola, G., Geschwind, D. H., Wszolek, Z. K., Feldman, H., Knopman, D. S., Petersen, R. C., Miller, B. L., Dickson, D. W., Boylan, K. B., Graff-Radford, N. R., & Rademakers, R. (2011). Expanded GGGGCC hexanucleotide repeat in noncoding region of C9ORF72 causes chromosome 9p-linked FTD and ALS. *Neuron*, 72(2), 245-256. <https://doi.org/10.1016/j.neuron.2011.09.011>

- Del Bigio, M. R., Chudley, A. E., Sarnat, H. B., Campbell, C., Goobie, S., Chodirker, B. N., & Selcen, D. (2011). Infantile muscular dystrophy in Canadian aboriginals is an α B-crystallinopathy. *Ann Neurol*, *69*(5), 866-871. <https://doi.org/10.1002/ana.22331>
- Delbecq, S. P., Rosenbaum, J. C., & Klevit, R. E. (2015). A Mechanism of Subunit Recruitment in Human Small Heat Shock Protein Oligomers. *Biochemistry*, *54*(28), 4276-4284. <https://doi.org/10.1021/acs.biochem.5b00490>
- den Engelsman, J., Boros, S., Dankers, P. Y., Kamps, B., Vree Egberts, W. T., Böde, C. S., Lane, L. A., Aquilina, J. A., Benesch, J. L., Robinson, C. V., de Jong, W. W., & Boelens, W. C. (2009). The small heat-shock proteins HSPB2 and HSPB3 form well-defined heterooligomers in a unique 3 to 1 subunit ratio. *J Mol Biol*, *393*(5), 1022-1032. <https://doi.org/10.1016/j.jmb.2009.08.052>
- Diaz-Latoud, C., Buache, E., Javouhey, E., & Arrigo, A. P. (2005). Substitution of the unique cysteine residue of murine Hsp25 interferes with the protective activity of this stress protein through inhibition of dimer formation. *Antioxid Redox Signal*, *7*(3-4), 436-445. <https://doi.org/10.1089/ars.2005.7.436>
- Dierick, I., Irobi, J., Janssens, S., Theuns, J., Lemmens, R., Jacobs, A., Corsmit, E., Hersmus, N., Van Den Bosch, L., Robberecht, W., De Jonghe, P., Van Broeckhoven, C., & Timmerman, V. (2007). Genetic variant in the HSPB1 promoter region impairs the HSP27 stress response. *Hum Mutat*, *28*(8), 830. <https://doi.org/10.1002/humu.9503>
- Ding, Y., Dvornikov, A. V., Ma, X., Zhang, H., Wang, Y., Lowerison, M., Packard, R. R., Wang, L., Chen, J., Zhang, Y., Hsiai, T., Lin, X., & Xu, X. (2019). Haploinsufficiency of mechanistic target of rapamycin ameliorates. *Dis Model Mech*, *12*(10). <https://doi.org/10.1242/dmm.040154>
- Doong, H., Price, J., Kim, Y. S., Gasbarre, C., Probst, J., Liotta, L. A., Blanchette, J., Rizzo, K., & Kohn, E. (2000). CAIR-1/BAG-3 forms an EGF-regulated ternary complex with phospholipase C-gamma and Hsp70/Hsc70. *Oncogene*, *19*(38), 4385-4395. <https://doi.org/10.1038/sj.onc.1203797>
- Doong, H., Vrailas, A., & Kohn, E. C. (2002). What's in the 'BAG'?--A functional domain analysis of the BAG-family proteins. *Cancer Lett*, *188*(1-2), 25-32. [https://doi.org/10.1016/s0304-3835\(02\)00456-1](https://doi.org/10.1016/s0304-3835(02)00456-1)
- Doran, P., Gannon, J., O'Connell, K., & Ohlendieck, K. (2007). Aging skeletal muscle shows a drastic increase in the small heat shock proteins alphaB-crystallin/HspB5 and cvHsp/HspB7. *Eur J Cell Biol*, *86*(10), 629-640. <https://doi.org/10.1016/j.ejcb.2007.07.003>
- Du, Z. W., Chen, H., Liu, H., Lu, J., Qian, K., Huang, C. L., Zhong, X., Fan, F., & Zhang, S. C. (2015). Generation and expansion of highly pure motor neuron progenitors from human pluripotent stem cells. *Nat Commun*, *6*, 6626. <https://doi.org/10.1038/ncomms7626>
- Du, Z. X., Zhang, H. Y., Meng, X., Gao, Y. Y., Zou, R. L., Liu, B. Q., Guan, Y., & Wang, H. Q. (2009). Proteasome inhibitor MG132 induces BAG3 expression through activation of heat shock factor 1. *J Cell Physiol*, *218*(3), 631-637. <https://doi.org/10.1002/jcp.21634>
- Echaniz-Laguna, A., Geuens, T., Petiot, P., Péréon, Y., Adriaenssens, E., Haidar, M., Capponi, S., Maisonobe, T., Fournier, E., Dubourg, O., Degos, B., Salachas, F., Lenglet, T., Eymard, B., Delmont, E., Pouget, J., Juntas Morales, R., Goizet, C., Latour, P., Timmerman, V., & Stojkovic, T. (2017). Axonal Neuropathies due to Mutations in Small Heat Shock Proteins: Clinical, Genetic, and Functional Insights into Novel Mutations. *Hum Mutat*, *38*(5), 556-568. <https://doi.org/10.1002/humu.23189>
- Echaniz-Laguna, A., Lornage, X., Lannes, B., Schneider, R., Bierry, G., Dondaine, N., Boland, A., Deleuze, J. F., Böhm, J., Thompson, J., Laporte, J., & Biancalana, V. (2017). HSPB8 haploinsufficiency causes dominant adult-onset axial and distal myopathy. *Acta Neuropathol*, *134*(1), 163-165. <https://doi.org/10.1007/s00401-017-1724-8>
- Ederle, H., & Dormann, D. (2017). TDP-43 and FUS en route from the nucleus to the cytoplasm. *FEBS Lett*, *591*(11), 1489-1507. <https://doi.org/10.1002/1873-3468.12646>

- Eggermann, K., Gess, B., Häusler, M., Weis, J., Hahn, A., & Kurth, I. (2018). Hereditary Neuropathies. *Dtsch Arztebl Int*, 115(6), 91-97. <https://doi.org/10.3238/arztebl.2018.0091>
- Evgrafov, O. V., Mersiyanova, I., Irobi, J., Van Den Bosch, L., Dierick, I., Leung, C. L., Schagina, O., Verpoorten, N., Van Impe, K., Fedotov, V., Dadali, E., Auer-Grumbach, M., Windpassinger, C., Wagner, K., Mitrovic, Z., Hilton-Jones, D., Talbot, K., Martin, J. J., Vasserman, N., Tverskaya, S., Polyakov, A., Liem, R. K., Gettemans, J., Robberecht, W., De Jonghe, P., & Timmerman, V. (2004). Mutant small heat-shock protein 27 causes axonal Charcot-Marie-Tooth disease and distal hereditary motor neuropathy. *Nat Genet*, 36(6), 602-606. <https://doi.org/10.1038/ng1354>
- Fan, G. C., & Kranias, E. G. (2011). Small heat shock protein 20 (HspB6) in cardiac hypertrophy and failure. *J Mol Cell Cardiol*, 51(4), 574-577. <https://doi.org/10.1016/j.yjmcc.2010.09.013>
- Fang, X., Bogomolovas, J., Trexler, C., & Chen, J. (2019). The BAG3-dependent and -independent roles of cardiac small heat shock proteins. *JCI Insight*, 4(4). <https://doi.org/10.1172/jci.insight.126464>
- Fang, X., Bogomolovas, J., Wu, T., Zhang, W., Liu, C., Veevers, J., Stroud, M. J., Zhang, Z., Ma, X., Mu, Y., Lao, D. H., Dalton, N. D., Gu, Y., Wang, C., Wang, M., Liang, Y., Lange, S., Ouyang, K., Peterson, K. L., Evans, S. M., & Chen, J. (2017). Loss-of-function mutations in co-chaperone BAG3 destabilize small HSPs and cause cardiomyopathy. *J Clin Invest*, 127(8), 3189-3200. <https://doi.org/10.1172/JCI94310>
- Fang, X., Bogomolovas, J., Zhou, P. S., Mu, Y., Ma, X., Chen, Z., Zhang, L., Zhu, M., Veevers, J., Ouyang, K., & Chen, J. (2019). P209L mutation in Bag3 does not cause cardiomyopathy in mice. *Am J Physiol Heart Circ Physiol*, 316(2), H392-H399. <https://doi.org/10.1152/ajpheart.00714.2018>
- Felzen, V., Hiebel, C., Koziollek-Drechsler, I., Reißig, S., Wolfrum, U., Kögel, D., Brandts, C., Behl, C., & Morawe, T. (2015). Estrogen receptor α regulates non-canonical autophagy that provides stress resistance to neuroblastoma and breast cancer cells and involves BAG3 function. *Cell Death Dis*, 6, e1812. <https://doi.org/10.1038/cddis.2015.181>
- Fernandez-Escamilla, A. M., Rousseau, F., Schymkowitz, J., & Serrano, L. (2004). Prediction of sequence-dependent and mutational effects on the aggregation of peptides and proteins. *Nat Biotechnol*, 22(10), 1302-1306. <https://doi.org/10.1038/nbt1012>
- Fichna, J. P., Maruszak, A., & Żekanowski, C. (2018). Myofibrillar myopathy in the genomic context. *J Appl Genet*, 59(4), 431-439. <https://doi.org/10.1007/s13353-018-0463-4>
- Fontaine, J. M., Rest, J. S., Welsh, M. J., & Benndorf, R. (2003). The sperm outer dense fiber protein is the 10th member of the superfamily of mammalian small stress proteins. *Cell Stress Chaperones*, 8(1), 62-69. [https://doi.org/10.1379/1466-1268\(2003\)82.0.co;2](https://doi.org/10.1379/1466-1268(2003)82.0.co;2)
- Fontaine, J. M., Sun, X., Hoppe, A. D., Simon, S., Vicart, P., Welsh, M. J., & Benndorf, R. (2006). Abnormal small heat shock protein interactions involving neuropathy-associated HSP22 (HSPB8) mutants. *FASEB J*, 20(12), 2168-2170. <https://doi.org/10.1096/fj.06-5911fje>
- Forrest, K. M., Al-Sarraj, S., Sewry, C., Buk, S., Tan, S. V., Pitt, M., Durward, A., McDougall, M., Irving, M., Hanna, M. G., Matthews, E., Sarkozy, A., Hudson, J., Barresi, R., Bushby, K., Jungbluth, H., & Wraige, E. (2011). Infantile onset myofibrillar myopathy due to recessive CRYAB mutations. *Neuromuscul Disord*, 21(1), 37-40. <https://doi.org/10.1016/j.nmd.2010.11.003>
- Franceschelli, S., Rosati, A., Lerose, R., De Nicola, S., Turco, M. C., & Pascale, M. (2008). Bag3 gene expression is regulated by heat shock factor 1. *J Cell Physiol*, 215(3), 575-577. <https://doi.org/10.1002/jcp.21397>
- Franklin, T. B., Krueger-Naug, A. M., Clarke, D. B., Arrigo, A. P., & Currie, R. W. (2005). The role of heat shock proteins Hsp70 and Hsp27 in cellular protection of the central nervous system. *Int J Hyperthermia*, 21(5), 379-392. <https://doi.org/10.1080/02656730500069955>
- Friesen, E. L., Zhang, Y. T., Earnshaw, R., De Snoo, M. L., O'Hara, D. M., Agapova, V., Chau, H., Ngana, S., Chen, K. S., Kalia, L. V., & Kalia, S. K. (2020). BAG5 Promotes Alpha-Synuclein Oligomer

- Formation and Functionally Interacts With the Autophagy Adaptor Protein p62. *Front Cell Dev Biol*, 8, 716. <https://doi.org/10.3389/fcell.2020.00716>
- Fuchs, M., Luthold, C., Guilbert, S. M., Varlet, A. A., Lambert, H., Jetté, A., Elowe, S., Landry, J., & Lavoie, J. N. (2015). A Role for the Chaperone Complex BAG3-HSPB8 in Actin Dynamics, Spindle Orientation and Proper Chromosome Segregation during Mitosis. *PLoS Genet*, 11(10), e1005582. <https://doi.org/10.1371/journal.pgen.1005582>
- Fuchs, M., Poirier, D. J., Seguin, S. J., Lambert, H., Carra, S., Charette, S. J., & Landry, J. (2009). Identification of the key structural motifs involved in HspB8/HspB6-Bag3 interaction. *Biochem J*, 425(1), 245-255. <https://doi.org/10.1042/BJ20090907>
- Gamerding, M., Carra, S., & Behl, C. (2011). Emerging roles of molecular chaperones and co-chaperones in selective autophagy: focus on BAG proteins. *J Mol Med (Berl)*, 89(12), 1175-1182. <https://doi.org/10.1007/s00109-011-0795-6>
- Gamerding, M., Hajieva, P., Kaya, A. M., Wolfrum, U., Hartl, F. U., & Behl, C. (2009). Protein quality control during aging involves recruitment of the macroautophagy pathway by BAG3. *EMBO J*, 28(7), 889-901. <https://doi.org/10.1038/emboj.2009.29>
- Gamerding, M., Kaya, A. M., Wolfrum, U., Clement, A. M., & Behl, C. (2011). BAG3 mediates chaperone-based aggresome-targeting and selective autophagy of misfolded proteins. *EMBO Rep*, 12(2), 149-156. <https://doi.org/10.1038/embor.2010.203>
- Ganassi, M., Mateju, D., Bigi, I., Mediani, L., Poser, I., Lee, H. O., Seguin, S. J., Morelli, F. F., Vinet, J., Leo, G., Pansarasa, O., Cereda, C., Poletti, A., Alberti, S., & Carra, S. (2016). A Surveillance Function of the HSPB8-BAG3-HSP70 Chaperone Complex Ensures Stress Granule Integrity and Dynamism. *Mol Cell*, 63(5), 796-810. <https://doi.org/10.1016/j.molcel.2016.07.021>
- Gao, J., Wang, L., Huntley, M. L., Perry, G., & Wang, X. (2018). Pathomechanisms of TDP-43 in neurodegeneration. *J Neurochem*. <https://doi.org/10.1111/jnc.14327>
- García-Mata, R., Gao, Y. S., & Sztul, E. (2002). Hassles with taking out the garbage: aggravating aggresomes. *Traffic*, 3(6), 388-396. <https://doi.org/10.1034/j.1600-0854.2002.30602.x>
- García-Mata, R., Bebök, Z., Sorscher, E. J., & Sztul, E. S. (1999). Characterization and dynamics of aggresome formation by a cytosolic GFP-chimera. *J Cell Biol*, 146(6), 1239-1254. <https://doi.org/10.1083/jcb.146.6.1239>
- Garrido, C., Paul, C., Seigneuric, R., & Kampinga, H. H. (2012). The small heat shock proteins family: the long forgotten chaperones. *Int J Biochem Cell Biol*, 44(10), 1588-1592. <https://doi.org/10.1016/j.biocel.2012.02.022>
- Ge, F., Xiao, C. L., Bi, L. J., Tao, S. C., Xiong, S., Yin, X. F., Li, L. P., Lu, C. H., Jia, H. T., & He, Q. Y. (2010). Quantitative phosphoproteomics of proteasome inhibition in multiple myeloma cells. *PLoS One*, 5(9). <https://doi.org/10.1371/journal.pone.0013095>
- Gendron, T. F., Bieniek, K. F., Zhang, Y. J., Jansen-West, K., Ash, P. E., Caulfield, T., Daugherty, L., Dunmore, J. H., Castanedes-Casey, M., Chew, J., Cosio, D. M., van Blitterswijk, M., Lee, W. C., Rademakers, R., Boylan, K. B., Dickson, D. W., & Petrucelli, L. (2013). Antisense transcripts of the expanded C9ORF72 hexanucleotide repeat form nuclear RNA foci and undergo repeat-associated non-ATG translation in c9FTD/ALS. *Acta Neuropathol*, 126(6), 829-844. <https://doi.org/10.1007/s00401-013-1192-8>
- Gentilella, A., & Khalili, K. (2011). BAG3 expression in glioblastoma cells promotes accumulation of ubiquitinated clients in an Hsp70-dependent manner. *J Biol Chem*, 286(11), 9205-9215. <https://doi.org/10.1074/jbc.M110.175836>
- Gess, B., Auer-Grumbach, M., Schirmacher, A., Strom, T., Zitzelsberger, M., Rudnik-Schöneborn, S., Röhr, D., Halfter, H., Young, P., & Senderek, J. (2014). HSP70-related hereditary neuropathies: novel mutations and extended clinical spectrum. *Neurology*, 83(19), 1726-1732. <https://doi.org/10.1212/WNL.0000000000000966>
- Ghaoui, R., Palmio, J., Brewer, J., Lek, M., Needham, M., Evilä, A., Hackman, P., Jonson, P. H., Penttilä, S., Vihola, A., Huovinen, S., Lindfors, M., Davis, R. L., Waddell, L., Kaur, S., Yiannikas, C., North, K., Clarke, N., MacArthur, D. G., Sue, C. M., & Udd, B. (2016). Mutations in HSPB8

- causing a new phenotype of distal myopathy and motor neuropathy. *Neurology*, 86(4), 391-398. <https://doi.org/10.1212/WNL.0000000000002324>
- Golenhofen, N., Htun, P., Ness, W., Koob, R., Schaper, W., & Drenckhahn, D. (1999). Binding of the stress protein alpha B-crystallin to cardiac myofibrils correlates with the degree of myocardial damage during ischemia/reperfusion in vivo. *J Mol Cell Cardiol*, 31(3), 569-580. <https://doi.org/10.1006/jmcc.1998.0892>
- Grad, L. I., Rouleau, G. A., Ravits, J., & Cashman, N. R. (2017). Clinical Spectrum of Amyotrophic Lateral Sclerosis (ALS). *Cold Spring Harb Perspect Med*, 7(8). <https://doi.org/10.1101/cshperspect.a024117>
- Graw, J. (2009). Genetics of crystallins: cataract and beyond. *Exp Eye Res*, 88(2), 173-189. <https://doi.org/10.1016/j.exer.2008.10.011>
- Grose, J. H., Langston, K., Wang, X., Squires, S., Mustafi, S. B., Hayes, W., Neubert, J., Fischer, S. K., Fasano, M., Saunders, G. M., Dai, Q., Christians, E., Lewandowski, E. D., Ping, P., & Benjamin, I. J. (2015). Characterization of the Cardiac Overexpression of HSPB2 Reveals Mitochondrial and Myogenic Roles Supported by a Cardiac HspB2 Interactome. *PLoS One*, 10(10), e0133994. <https://doi.org/10.1371/journal.pone.0133994>
- Guilbert, S. M., Lambert, H., Rodrigue, M. A., Fuchs, M., Landry, J., & Lavoie, J. N. (2018). HSPB8 and BAG3 cooperate to promote spatial sequestration of ubiquitinated proteins and coordinate the cellular adaptive response to proteasome insufficiency. *FASEB J*, 32(7), 3518-3535. <https://doi.org/10.1096/fj.201700558RR>
- Guo, K., Li, L., Yin, G., Zi, X., & Liu, L. (2015). Bag5 protects neuronal cells from amyloid β -induced cell death. *J Mol Neurosci*, 55(4), 815-820. <https://doi.org/10.1007/s12031-014-0433-1>
- Götz, R., Wiese, S., Takayama, S., Camarero, G. C., Rossoll, W., Schweizer, U., Troppmair, J., Jablonka, S., Holtmann, B., Reed, J. C., Rapp, U. R., & Sendtner, M. (2005). Bag1 is essential for differentiation and survival of hematopoietic and neuronal cells. *Nat Neurosci*, 8(9), 1169-1178. <https://doi.org/10.1038/nn1524>
- Haidar, M., Asselbergh, B., Adriaenssens, E., De Winter, V., Timmermans, J. P., Auer-Grumbach, M., Juneja, M., & Timmerman, V. (2019). Neuropathy-causing mutations in HSPB1 impair autophagy by disturbing the formation of SQSTM1/p62 bodies. *Autophagy*, 15(6), 1051-1068. <https://doi.org/10.1080/15548627.2019.1569930>
- Hardiman, O., Al-Chalabi, A., Chio, A., Corr, E. M., Logroscino, G., Robberecht, W., Shaw, P. J., Simmons, Z., & van den Berg, L. H. (2017). Amyotrophic lateral sclerosis. *Nat Rev Dis Primers*, 3, 17085. <https://doi.org/10.1038/nrdp.2017.85>
- Harding, A. E., & Thomas, P. K. (1980). Hereditary distal spinal muscular atrophy. A report on 34 cases and a review of the literature. *J Neurol Sci*, 45(2-3), 337-348. [https://doi.org/10.1016/0022-510x\(80\)90177-x](https://doi.org/10.1016/0022-510x(80)90177-x)
- Harms, M. B., Sommerville, R. B., Allred, P., Bell, S., Ma, D., Cooper, P., Lopate, G., Pestronk, A., Weihl, C. C., & Baloh, R. H. (2012). Exome sequencing reveals DNAJB6 mutations in dominantly-inherited myopathy. *Ann Neurol*, 71(3), 407-416. <https://doi.org/10.1002/ana.22683>
- Hartl, F. U. (1996). Molecular chaperones in cellular protein folding. *Nature*, 381(6583), 571-579. <https://doi.org/10.1038/381571a0>
- Hartl, F. U., Bracher, A., & Hayer-Hartl, M. (2011). Molecular chaperones in protein folding and proteostasis. *Nature*, 475(7356), 324-332. <https://doi.org/10.1038/nature10317>
- Hayashishita, M., Kawahara, H., & Yokota, N. (2019). BAG6 deficiency induces mis-distribution of mitochondrial clusters under depolarization. *FEBS Open Bio*, 9(7), 1281-1291. <https://doi.org/10.1002/2211-5463.12677>
- Hayes, D., Napoli, V., Mazurkie, A., Stafford, W. F., & Graceffa, P. (2009). Phosphorylation dependence of hsp27 multimeric size and molecular chaperone function. *J Biol Chem*, 284(28), 18801-18807. <https://doi.org/10.1074/jbc.M109.011353>

- He, F., Shi, E., Yan, L., Li, J., & Jiang, X. (2015). Inhibition of micro-ribonucleic acid-320 attenuates neurologic injuries after spinal cord ischemia. *J Thorac Cardiovasc Surg*, *150*(2), 398-406. <https://doi.org/10.1016/j.jtcvs.2015.03.066>
- Heimdal, K., Sanchez-Guixé, M., Aukrust, I., Bollerslev, J., Bruland, O., Jablonski, G. E., Erichsen, A. K., Gude, E., Koht, J. A., Erdal, S., Fiskerstrand, T., Haukanes, B. I., Boman, H., Bjørkhaug, L., Tallaksen, C. M., Knappskog, P. M., & Johansson, S. (2014). STUB1 mutations in autosomal recessive ataxias - evidence for mutation-specific clinical heterogeneity. *Orphanet J Rare Dis*, *9*, 146. <https://doi.org/10.1186/s13023-014-0146-0>
- Hickey, E. D., & Weber, L. A. (1982). Modulation of heat-shock polypeptide synthesis in HeLa cells during hyperthermia and recovery. *Biochemistry*, *21*(7), 1513-1521. <https://doi.org/10.1021/bi00536a008>
- Hishiya, A., Salman, M. N., Carra, S., Kampinga, H. H., & Takayama, S. (2011). BAG3 directly interacts with mutated alphaB-crystallin to suppress its aggregation and toxicity. *PLoS One*, *6*(3), e16828. <https://doi.org/10.1371/journal.pone.0016828>
- Homma, S., Iwasaki, M., Shelton, G. D., Engvall, E., Reed, J. C., & Takayama, S. (2006). BAG3 deficiency results in fulminant myopathy and early lethality. *Am J Pathol*, *169*(3), 761-773. <https://doi.org/10.2353/ajpath.2006.060250>
- Houlden, H., Laura, M., Wavrant-De Vrièze, F., Blake, J., Wood, N., & Reilly, M. M. (2008). Mutations in the HSP27 (HSPB1) gene cause dominant, recessive, and sporadic distal HMN/CMT type 2. *Neurology*, *71*(21), 1660-1668. <https://doi.org/10.1212/01.wnl.0000319696.14225.67>
- Hu, L. D., Wang, J., Chen, X. J., & Yan, Y. B. (2020). Lanosterol modulates proteostasis via dissolving cytosolic sequestosomes/aggresome-like induced structures. *Biochim Biophys Acta Mol Cell Res*, *1867*(2), 118617. <https://doi.org/10.1016/j.bbamcr.2019.118617>
- Huang, C. C., Faber, P. W., Persichetti, F., Mittal, V., Vonsattel, J. P., MacDonald, M. E., & Gusella, J. F. (1998). Amyloid formation by mutant huntingtin: threshold, progressivity and recruitment of normal polyglutamine proteins. *Somat Cell Mol Genet*, *24*(4), 217-233. <https://doi.org/10.1023/b:scam.0000007124.19463.e5>
- Huang, L., Min, J. N., Masters, S., Mivechi, N. F., & Moskophidis, D. (2007). Insights into function and regulation of small heat shock protein 25 (HSPB1) in a mouse model with targeted gene disruption. *Genesis*, *45*(8), 487-501. <https://doi.org/10.1002/dvg.20319>
- Hughes, J. T. (1982). Pathology of amyotrophic lateral sclerosis. *Adv Neurol*, *36*, 61-74.
- Iorio, V., Festa, M., Rosati, A., Hahne, M., Tiberti, C., Capunzo, M., De Laurenzi, V., & Turco, M. C. (2015). BAG3 regulates formation of the SNARE complex and insulin secretion. *Cell Death Dis*, *6*, e1684. <https://doi.org/10.1038/cddis.2015.53>
- Irobi, J., Almeida-Souza, L., Asselbergh, B., De Winter, V., Goethals, S., Dierick, I., Krishnan, J., Timmermans, J. P., Robberecht, W., De Jonghe, P., Van Den Bosch, L., Janssens, S., & Timmerman, V. (2010). Mutant HSPB8 causes motor neuron-specific neurite degeneration. *Hum Mol Genet*, *19*(16), 3254-3265. <https://doi.org/10.1093/hmg/ddq234>
- Irobi, J., Holmgren, A., De Winter, V., Asselbergh, B., Gettemans, J., Adriaensen, D., Ceuterick-de Groote, C., Van Coster, R., De Jonghe, P., & Timmerman, V. (2012). Mutant HSPB8 causes protein aggregates and a reduced mitochondrial membrane potential in dermal fibroblasts from distal hereditary motor neuropathy patients. *Neuromuscul Disord*, *22*(8), 699-711. <https://doi.org/10.1016/j.nmd.2012.04.005>
- Irobi, J., Van Impe, K., Seeman, P., Jordanova, A., Dierick, I., Verpoorten, N., Michalik, A., De Vriendt, E., Jacobs, A., Van Gerwen, V., Vennekens, K., Mazanec, R., Tournev, I., Hilton-Jones, D., Talbot, K., Kremensky, I., Van Den Bosch, L., Robberecht, W., Van Vandekerckhove, J., Van Broeckhoven, C., Gettemans, J., De Jonghe, P., & Timmerman, V. (2004). Hot-spot residue in small heat-shock protein 22 causes distal motor neuropathy. *Nat Genet*, *36*(6), 597-601. <https://doi.org/10.1038/ng1328>
- Ishiwata, T., Orosz, A., Wang, X., Mustafi, S. B., Pratt, G. W., Christians, E. S., Boudina, S., Abel, E. D., & Benjamin, I. J. (2012). HSPB2 is dispensable for the cardiac hypertrophic response but

- reduces mitochondrial energetics following pressure overload in mice. *PLoS One*, 7(8), e42118. <https://doi.org/10.1371/journal.pone.0042118>
- Ito, D., & Suzuki, N. (2009). Seipinopathy: a novel endoplasmic reticulum stress-associated disease. *Brain*, 132(Pt 1), 8-15. <https://doi.org/10.1093/brain/awn216>
- Iwaki, A., Nagano, T., Nakagawa, M., Iwaki, T., & Fukumaki, Y. (1997). Identification and characterization of the gene encoding a new member of the alpha-crystallin/small hsp family, closely linked to the alphaB-crystallin gene in a head-to-head manner. *Genomics*, 45(2), 386-394. <https://doi.org/10.1006/geno.1997.4956>
- Jabłońska, J., Dubińska-Magiera, M., Jagla, T., Jagla, K., & Daczewska, M. (2018). Drosophila Hsp67Bc hot-spot variants alter muscle structure and function. *Cell Mol Life Sci*, 75(23), 4341-4356. <https://doi.org/10.1007/s00018-018-2875-z>
- Jaffer, F., Murphy, S. M., Scoto, M., Healy, E., Rossor, A. M., Brandner, S., Phadke, R., Selcen, D., Jungbluth, H., Muntoni, F., & Reilly, M. M. (2012). BAG3 mutations: another cause of giant axonal neuropathy. *J Peripher Nerv Syst*, 17(2), 210-216. <https://doi.org/10.1111/j.1529-8027.2012.00409.x>
- James, P. A., & Talbot, K. (2006). The molecular genetics of non-ALS motor neuron diseases. *Biochim Biophys Acta*, 1762(11-12), 986-1000. <https://doi.org/10.1016/j.bbadis.2006.04.003>
- Jana, N. R., & Nukina, N. (2005). BAG-1 associates with the polyglutamine-expanded huntingtin aggregates. *Neurosci Lett*, 378(3), 171-175. <https://doi.org/10.1016/j.neulet.2004.12.031>
- Ji, C. H., & Kwon, Y. T. (2017). Crosstalk and Interplay between the Ubiquitin-Proteasome System and Autophagy. *Mol Cells*, 40(7), 441-449. <https://doi.org/10.14348/molcells.2017.0115>
- Jiang, Y., Woronicz, J. D., Liu, W., & Goeddel, D. V. (1999). Prevention of constitutive TNF receptor 1 signaling by silencer of death domains. *Science*, 283(5401), 543-546. <https://doi.org/10.1126/science.283.5401.543>
- Jo, H. S., Kim, D. W., Shin, M. J., Cho, S. B., Park, J. H., Lee, C. H., Yeo, E. J., Choi, Y. J., Yeo, H. J., Sohn, E. J., Son, O., Cho, S. W., Kim, D. S., Yu, Y. H., Lee, K. W., Park, J., Eum, W. S., & Choi, S. Y. (2017). Tat-HSP22 inhibits oxidative stress-induced hippocampal neuronal cell death by regulation of the mitochondrial pathway. *Mol Brain*, 10(1), 1. <https://doi.org/10.1186/s13041-016-0281-8>
- Jodoin, R., Carrier, J. C., Rivard, N., Bisailon, M., & Perreault, J. P. (2019). G-quadruplex located in the 5'UTR of the BAG-1 mRNA affects both its cap-dependent and cap-independent translation through global secondary structure maintenance. *Nucleic Acids Res*, 47(19), 10247-10266. <https://doi.org/10.1093/nar/gkz777>
- Johnston, J. A., Ward, C. L., & Kopito, R. R. (1998). Aggresomes: a cellular response to misfolded proteins. *J Cell Biol*, 143(7), 1883-1898. <https://doi.org/10.1083/jcb.143.7.1883>
- Juo, L. Y., Liao, W. C., Shih, Y. L., Yang, B. Y., Liu, A. B., & Yan, Y. T. (2016). HSPB7 interacts with dimerized FLNC and its absence results in progressive myopathy in skeletal muscles. *J Cell Sci*, 129(8), 1661-1670. <https://doi.org/10.1242/jcs.179887>
- Kabbage, M., & Dickman, M. B. (2008). The BAG proteins: a ubiquitous family of chaperone regulators. *Cell Mol Life Sci*, 65(9), 1390-1402. <https://doi.org/10.1007/s00018-008-7535-2>
- Kalia, L. V., Kalia, S. K., Chau, H., Lozano, A. M., Hyman, B. T., & McLean, P. J. (2011). Ubiquitylation of α -synuclein by carboxyl terminus Hsp70-interacting protein (CHIP) is regulated by Bcl-2-associated athanogene 5 (BAG5). *PLoS One*, 6(2), e14695. <https://doi.org/10.1371/journal.pone.0014695>
- Kalia, S. K., Lee, S., Smith, P. D., Liu, L., Crocker, S. J., Thorarinsdottir, T. E., Glover, J. R., Fon, E. A., Park, D. S., & Lozano, A. M. (2004). BAG5 inhibits parkin and enhances dopaminergic neuron degeneration. *Neuron*, 44(6), 931-945. <https://doi.org/10.1016/j.neuron.2004.11.026>
- Kalmar, B., Innes, A., Wanisch, K., Kolaszynska, A. K., Pandraud, A., Kelly, G., Abramov, A. Y., Reilly, M. M., Schiavo, G., & Greensmith, L. (2017). Mitochondrial deficits and abnormal mitochondrial retrograde axonal transport play a role in the pathogenesis of mutant Hsp27-

- induced Charcot Marie Tooth Disease. *Hum Mol Genet*, 26(17), 3313-3326. <https://doi.org/10.1093/hmg/ddx216>
- Kampinga, H. H., & Craig, E. A. (2010). The HSP70 chaperone machinery: J proteins as drivers of functional specificity. *Nat Rev Mol Cell Biol*, 11(8), 579-592. <https://doi.org/10.1038/nrm2941>
- Kampinga, H. H., Hageman, J., Vos, M. J., Kubota, H., Tanguay, R. M., Bruford, E. A., Cheetham, M. E., Chen, B., & Hightower, L. E. (2009). Guidelines for the nomenclature of the human heat shock proteins. *Cell Stress Chaperones*, 14(1), 105-111. <https://doi.org/10.1007/s12192-008-0068-7>
- Kanack, A. J., Newsom, O. J., & Scaglione, K. M. (2018). Most mutations that cause spinocerebellar ataxia autosomal recessive type 16 (SCAR16) destabilize the protein quality-control E3 ligase CHIP. *J Biol Chem*, 293(8), 2735-2743. <https://doi.org/10.1074/jbc.RA117.000477>
- Kang, C. H., Jung, W. Y., Kang, Y. H., Kim, J. Y., Kim, D. G., Jeong, J. C., Baek, D. W., Jin, J. B., Lee, J. Y., Kim, M. O., Chung, W. S., Mengiste, T., Koiwa, H., Kwak, S. S., Bahk, J. D., Lee, S. Y., Nam, J. S., Yun, D. J., & Cho, M. J. (2006). AtBAG6, a novel calmodulin-binding protein, induces programmed cell death in yeast and plants. *Cell Death Differ*, 13(1), 84-95. <https://doi.org/10.1038/sj.cdd.4401712>
- Kappé, G., Franck, E., Verschuure, P., Boelens, W. C., Leunissen, J. A., & de Jong, W. W. (2003). The human genome encodes 10 alpha-crystallin-related small heat shock proteins: HspB1-10. *Cell Stress Chaperones*, 8(1), 53-61. [https://doi.org/10.1379/1466-1268\(2003\)82.0.co;2](https://doi.org/10.1379/1466-1268(2003)82.0.co;2)
- Kathage, B., Gehlert, S., Ulbricht, A., Lüdecke, L., Tapia, V. E., Orfanos, Z., Wenzel, D., Bloch, W., Volkmer, R., Fleischmann, B. K., Fürst, D. O., & Höhfeld, J. (2017). The cochaperone BAG3 coordinates protein synthesis and autophagy under mechanical strain through spatial regulation of mTORC1. *Biochim Biophys Acta Mol Cell Res*, 1864(1), 62-75. <https://doi.org/10.1016/j.bbamcr.2016.10.007>
- Kato, K., Goto, S., Inaguma, Y., Hasegawa, K., Morishita, R., & Asano, T. (1994). Purification and characterization of a 20-kDa protein that is highly homologous to alpha B crystallin. *J Biol Chem*, 269(21), 15302-15309.
- Kato, S., Takikawa, M., Nakashima, K., Hirano, A., Cleveland, D. W., Kusaka, H., Shibata, N., Kato, M., Nakano, I., & Ohama, E. (2000). New consensus research on neuropathological aspects of familial amyotrophic lateral sclerosis with superoxide dismutase 1 (SOD1) gene mutations: inclusions containing SOD1 in neurons and astrocytes. *Amyotroph Lateral Scler Other Motor Neuron Disord*, 1(3), 163-184. <https://doi.org/10.1080/14660820050515160>
- Katsuno, M., Adachi, H., Kume, A., Li, M., Nakagomi, Y., Niwa, H., Sang, C., Kobayashi, Y., Doyu, M., & Sobue, G. (2002). Testosterone reduction prevents phenotypic expression in a transgenic mouse model of spinal and bulbar muscular atrophy. *Neuron*, 35(5), 843-854. [https://doi.org/10.1016/s0896-6273\(02\)00834-6](https://doi.org/10.1016/s0896-6273(02)00834-6)
- Katsuno, M., Adachi, H., Minamiyama, M., Waza, M., Tokui, K., Banno, H., Suzuki, K., Onoda, Y., Tanaka, F., Doyu, M., & Sobue, G. (2006). Reversible disruption of dynactin 1-mediated retrograde axonal transport in polyglutamine-induced motor neuron degeneration. *J Neurosci*, 26(47), 12106-12117. <https://doi.org/10.1523/JNEUROSCI.3032-06.2006>
- Kaushik, S., & Cuervo, A. M. (2012). Chaperone-mediated autophagy: a unique way to enter the lysosome world. *Trends Cell Biol*, 22(8), 407-417. <https://doi.org/10.1016/j.tcb.2012.05.006>
- Kaushik, S., & Cuervo, A. M. (2018). The coming of age of chaperone-mediated autophagy. *Nat Rev Mol Cell Biol*, 19(6), 365-381. <https://doi.org/10.1038/s41580-018-0001-6>
- Kennedy, W. R., Alter, M., & Sung, J. H. (1968). Progressive proximal spinal and bulbar muscular atrophy of late onset. A sex-linked recessive trait. *Neurology*, 18(7), 671-680. <https://doi.org/10.1212/wnl.18.7.671>

- Kermer, P., Krajewska, M., Zapata, J. M., Takayama, S., Mai, J., Krajewski, S., & Reed, J. C. (2002). Bag1 is a regulator and marker of neuronal differentiation. *Cell Death Differ*, 9(4), 405-413. <https://doi.org/10.1038/sj.cdd.4400972>
- Klaips, C. L., Jayaraj, G. G., & Hartl, F. U. (2018). Pathways of cellular proteostasis in aging and disease. *J Cell Biol*, 217(1), 51-63. <https://doi.org/10.1083/jcb.201709072>
- Kleinberger, G., Wils, H., Ponsaerts, P., Joris, G., Timmermans, J. P., Van Broeckhoven, C., & Kumar-Singh, S. (2010). Increased caspase activation and decreased TDP-43 solubility in progranulin knockout cortical cultures. *J Neurochem*, 115(3), 735-747. <https://doi.org/10.1111/j.1471-4159.2010.06961.x>
- Knee, D. A., Froesch, B. A., Nuber, U., Takayama, S., & Reed, J. C. (2001). Structure-function analysis of Bag1 proteins. Effects on androgen receptor transcriptional activity. *J Biol Chem*, 276(16), 12718-12724. <https://doi.org/10.1074/jbc.M010841200>
- Kohler, L., Puertollano, R., & Raben, N. (2018). Pompe Disease: From Basic Science to Therapy. *Neurotherapeutics*, 15(4), 928-942. <https://doi.org/10.1007/s13311-018-0655-y>
- Kolb, S. J., Snyder, P. J., Poi, E. J., Renard, E. A., Bartlett, A., Gu, S., Sutton, S., Arnold, W. D., Freimer, M. L., Lawson, V. H., Kissel, J. T., & Prior, T. W. (2010). Mutant small heat shock protein B3 causes motor neuropathy: utility of a candidate gene approach. *Neurology*, 74(6), 502-506. <https://doi.org/10.1212/WNL.0b013e3181cef84a>
- Kopito, R. R. (2000). Aggresomes, inclusion bodies and protein aggregation. *Trends Cell Biol*, 10(12), 524-530. [https://doi.org/10.1016/s0962-8924\(00\)01852-3](https://doi.org/10.1016/s0962-8924(00)01852-3)
- Koppers, M., Blokhuis, A. M., Westeneng, H. J., Terpstra, M. L., Zundel, C. A., Vieira de Sá, R., Schellevis, R. D., Waite, A. J., Blake, D. J., Veldink, J. H., van den Berg, L. H., & Pasterkamp, R. J. (2015). C9orf72 ablation in mice does not cause motor neuron degeneration or motor deficits. *Ann Neurol*, 78(3), 426-438. <https://doi.org/10.1002/ana.24453>
- Kostera-Pruszczyk, A., Suszek, M., Płoski, R., Franaszczuk, M., Potulska-Chromik, A., Pruszczyk, P., Sadurska, E., Karolczak, J., Kamińska, A. M., & Rędownicz, M. J. (2015). BAG3-related myopathy, polyneuropathy and cardiomyopathy with long QT syndrome. *J Muscle Res Cell Motil*, 36(6), 423-432. <https://doi.org/10.1007/s10974-015-9431-3>
- Kozawa, O., Matsuno, H., Niwa, M., Hatakeyama, D., Oiso, Y., Kato, K., & Uematsu, T. (2002). HSP20, low-molecular-weight heat shock-related protein, acts extracellularly as a regulator of platelet functions: a novel defense mechanism. *Life Sci*, 72(2), 113-124. [https://doi.org/10.1016/s0024-3205\(02\)02144-6](https://doi.org/10.1016/s0024-3205(02)02144-6)
- Kriehuber, T., Rattei, T., Weinmaier, T., Bepperling, A., Haslbeck, M., & Buchner, J. (2010). Independent evolution of the core domain and its flanking sequences in small heat shock proteins. *FASEB J*, 24(10), 3633-3642. <https://doi.org/10.1096/fj.10-156992>
- Kumar, C. M., Mande, S. C., & Mahajan, G. (2015). Multiple chaperonins in bacteria--novel functions and non-canonical behaviors. *Cell Stress Chaperones*, 20(4), 555-574. <https://doi.org/10.1007/s12192-015-0598-8>
- Kumar, P. A., & Reddy, G. B. (2009). Modulation of alpha-crystallin chaperone activity: a target to prevent or delay cataract? *IUBMB Life*, 61(5), 485-495. <https://doi.org/10.1002/iub.176>
- Kuwabara, N., Minami, R., Yokota, N., Matsumoto, H., Senda, T., Kawahara, H., & Kato, R. (2015). Structure of a BAG6 (Bcl-2-associated athanogene 6)-Ubl4a (ubiquitin-like protein 4a) complex reveals a novel binding interface that functions in tail-anchored protein biogenesis. *J Biol Chem*, 290(15), 9387-9398. <https://doi.org/10.1074/jbc.M114.631804>
- Kwiatkowski, T. J., Bosco, D. A., Leclerc, A. L., Tamrazian, E., Vanderburg, C. R., Russ, C., Davis, A., Gilchrist, J., Kasarskis, E. J., Munsat, T., Valdmanis, P., Rouleau, G. A., Hosler, B. A., Cortelli, P., de Jong, P. J., Yoshinaga, Y., Haines, J. L., Pericak-Vance, M. A., Yan, J., Ticozzi, N., Siddique, T., McKenna-Yasek, D., Sapp, P. C., Horvitz, H. R., Landers, J. E., & Brown, R. H. (2009). Mutations in the FUS/TLS gene on chromosome 16 cause familial amyotrophic lateral sclerosis. *Science*, 323(5918), 1205-1208. <https://doi.org/10.1126/science.1166066>

- Kwok, A. S., Phadwal, K., Turner, B. J., Oliver, P. L., Raw, A., Simon, A. K., Talbot, K., & Agashe, V. R. (2011). HspB8 mutation causing hereditary distal motor neuropathy impairs lysosomal delivery of autophagosomes. *J Neurochem*, *119*(6), 1155-1161. <https://doi.org/10.1111/j.1471-4159.2011.07521.x>
- Kwong, L. K., Neumann, M., Sampathu, D. M., Lee, V. M., & Trojanowski, J. Q. (2007). TDP-43 proteinopathy: the neuropathology underlying major forms of sporadic and familial frontotemporal lobar degeneration and motor neuron disease. *Acta Neuropathol*, *114*(1), 63-70. <https://doi.org/10.1007/s00401-007-0226-5>
- Kyratsous, C. A., & Silverstein, S. J. (2008). The co-chaperone BAG3 regulates Herpes Simplex Virus replication. *Proc Natl Acad Sci U S A*, *105*(52), 20912-20917. <https://doi.org/10.1073/pnas.0810656105>
- La Padula, V., Staszewski, O., Nestel, S., Busch, H., Boerries, M., Roussa, E., Prinz, M., & Kriegstein, K. (2016). HSPB3 protein is expressed in motoneurons and induces their survival after lesion-induced degeneration. *Exp Neurol*, *286*, 40-49. <https://doi.org/10.1016/j.expneurol.2016.08.014>
- La Spada, A. R., Wilson, E. M., Lubahn, D. B., Harding, A. E., & Fischbeck, K. H. (1991). Androgen receptor gene mutations in X-linked spinal and bulbar muscular atrophy. *Nature*, *352*(6330), 77-79. <https://doi.org/10.1038/352077a0>
- Lamark, T., Svenning, S., & Johansen, T. (2017). Regulation of selective autophagy: the p62/SQSTM1 paradigm. *Essays Biochem*, *61*(6), 609-624. <https://doi.org/10.1042/EBC20170035>
- Lamb, C. A., Yoshimori, T., & Tooze, S. A. (2013). The autophagosome: origins unknown, biogenesis complex. *Nat Rev Mol Cell Biol*, *14*(12), 759-774. <https://doi.org/10.1038/nrm3696>
- Latonen, L. (2019). Phase-to-Phase With Nucleoli - Stress Responses, Protein Aggregation and Novel Roles of RNA. *Front Cell Neurosci*, *13*, 151. <https://doi.org/10.3389/fncel.2019.00151>
- Lee, H. C., Cherk, S. W., Chan, S. K., Wong, S., Tong, T. W., Ho, W. S., Chan, A. Y., Lee, K. C., & Mak, C. M. (2012). BAG3-related myofibrillar myopathy in a Chinese family. *Clin Genet*, *81*(4), 394-398. <https://doi.org/10.1111/j.1399-0004.2011.01659.x>
- Lee, S., Carson, K., Rice-Ficht, A., & Good, T. (2006). Small heat shock proteins differentially affect Abeta aggregation and toxicity. *Biochem Biophys Res Commun*, *347*(2), 527-533. <https://doi.org/10.1016/j.bbrc.2006.06.128>
- Lee, S. S., Crabb, S. J., Janghra, N., Carlberg, C., Williams, A. C., Cutress, R. I., Packham, G., & Hague, A. (2007). Subcellular localisation of BAG-1 and its regulation of vitamin D receptor-mediated transactivation and involucrin expression in oral keratinocytes: implications for oral carcinogenesis. *Exp Cell Res*, *313*(15), 3222-3238. <https://doi.org/10.1016/j.yexcr.2007.06.010>
- Lefebvre, S., Bürglen, L., Reboullet, S., Clermont, O., Burlet, P., Viollet, L., Benichou, B., Cruaud, C., Millasseau, P., & Zeviani, M. (1995). Identification and characterization of a spinal muscular atrophy-determining gene. *Cell*, *80*(1), 155-165. [https://doi.org/10.1016/0092-8674\(95\)90460-3](https://doi.org/10.1016/0092-8674(95)90460-3)
- Leroux, M. R., Melki, R., Gordon, B., Batelier, G., & Candido, E. P. (1997). Structure-function studies on small heat shock protein oligomeric assembly and interaction with unfolded polypeptides. *J Biol Chem*, *272*(39), 24646-24656. <https://doi.org/10.1074/jbc.272.39.24646>
- Li, M., Miwa, S., Kobayashi, Y., Merry, D. E., Yamamoto, M., Tanaka, F., Doyu, M., Hashizume, Y., Fischbeck, K. H., & Sobue, G. (1998). Nuclear inclusions of the androgen receptor protein in spinal and bulbar muscular atrophy. *Ann Neurol*, *44*(2), 249-254. <https://doi.org/10.1002/ana.410440216>
- Li, M., Nakagomi, Y., Kobayashi, Y., Merry, D. E., Tanaka, F., Doyu, M., Mitsuma, T., Hashizume, Y., Fischbeck, K. H., & Sobue, G. (1998). Nonneural nuclear inclusions of androgen receptor protein in spinal and bulbar muscular atrophy. *Am J Pathol*, *153*(3), 695-701. [https://doi.org/10.1016/S0002-9440\(10\)65612-X](https://doi.org/10.1016/S0002-9440(10)65612-X)

- Li, M., Sobue, G., Doyu, M., Mukai, E., Hashizume, Y., & Mitsuma, T. (1995). Primary sensory neurons in X-linked recessive bulbospinal neuropathy: histopathology and androgen receptor gene expression. *Muscle Nerve*, *18*(3), 301-308. <https://doi.org/10.1002/mus.880180306>
- Li, N., Du, Z. X., Zong, Z. H., Liu, B. Q., Li, C., Zhang, Q., & Wang, H. Q. (2013). PKC δ -mediated phosphorylation of BAG3 at Ser187 site induces epithelial-mesenchymal transition and enhances invasiveness in thyroid cancer FRO cells. *Oncogene*, *32*(38), 4539-4548. <https://doi.org/10.1038/onc.2012.466>
- Li, P., Banjade, S., Cheng, H. C., Kim, S., Chen, B., Guo, L., Llaguno, M., Hollingsworth, J. V., King, D. S., Banani, S. F., Russo, P. S., Jiang, Q. X., Nixon, B. T., & Rosen, M. K. (2012). Phase transitions in the assembly of multivalent signalling proteins. *Nature*, *483*(7389), 336-340. <https://doi.org/10.1038/nature10879>
- Li, W. W., Li, J., & Bao, J. K. (2012). Microautophagy: lesser-known self-eating. *Cell Mol Life Sci*, *69*(7), 1125-1136. <https://doi.org/10.1007/s00018-011-0865-5>
- Li, Y. R., King, O. D., Shorter, J., & Gitler, A. D. (2013). Stress granules as crucibles of ALS pathogenesis. *J Cell Biol*, *201*(3), 361-372. <https://doi.org/10.1083/jcb.201302044>
- Liao, Q., Ozawa, F., Friess, H., Zimmermann, A., Takayama, S., Reed, J. C., Kleeff, J., & Büchler, M. W. (2001). The anti-apoptotic protein BAG-3 is overexpressed in pancreatic cancer and induced by heat stress in pancreatic cancer cell lines. *FEBS Lett*, *503*(2-3), 151-157. [https://doi.org/10.1016/s0014-5793\(01\)02728-4](https://doi.org/10.1016/s0014-5793(01)02728-4)
- Liao, W. C., Juo, L. Y., Shih, Y. L., Chen, Y. H., & Yan, Y. T. (2017). HSPB7 prevents cardiac conduction system defect through maintaining intercalated disc integrity. *PLoS Genet*, *13*(8), e1006984. <https://doi.org/10.1371/journal.pgen.1006984>
- Ling, S. C., Polymenidou, M., & Cleveland, D. W. (2013). Converging mechanisms in ALS and FTD: disrupted RNA and protein homeostasis. *Neuron*, *79*(3), 416-438. <https://doi.org/10.1016/j.neuron.2013.07.033>
- Liu, Y., Zhang, X., Luo, L., Wu, M., Zeng, R., Cheng, G., Hu, B., Liu, B., Liang, J. J., & Shang, F. (2006). A novel alphaB-crystallin mutation associated with autosomal dominant congenital lamellar cataract. *Invest Ophthalmol Vis Sci*, *47*(3), 1069-1075. <https://doi.org/10.1167/iovs.05-1004>
- Lüders, J., Demand, J., & Höhfeld, J. (2000). The ubiquitin-related BAG-1 provides a link between the molecular chaperones Hsc70/Hsp70 and the proteasome. *J Biol Chem*, *275*(7), 4613-4617. <https://doi.org/10.1074/jbc.275.7.4613>
- Maaroufi, H., & Tanguay, R. M. (2013). Analysis and phylogeny of small heat shock proteins from marine viruses and their cyanobacteria host. *PLoS One*, *8*(11), e81207. <https://doi.org/10.1371/journal.pone.0081207>
- Margeta, M. (2020). Autophagy Defects in Skeletal Myopathies. *Annu Rev Pathol*, *15*, 261-285. <https://doi.org/10.1146/annurev-pathmechdis-012419-032618>
- Mariotto, E., Viola, G., Zanon, C., & Aveic, S. (2020). A BAG's life: Every connection matters in cancer. *Pharmacol Ther*, *209*, 107498. <https://doi.org/10.1016/j.pharmthera.2020.107498>
- Mateju, D., Franzmann, T. M., Patel, A., Kopach, A., Boczek, E. E., Maharana, S., Lee, H. O., Carra, S., Hyman, A. A., & Alberti, S. (2017). An aberrant phase transition of stress granules triggered by misfolded protein and prevented by chaperone function. *EMBO J*, *36*(12), 1669-1687. <https://doi.org/10.15252/embj.201695957>
- Mathis, S., Goizet, C., Tazir, M., Magdelaine, C., Lia, A. S., Magy, L., & Vallat, J. M. (2015). Charcot-Marie-Tooth diseases: an update and some new proposals for the classification. *J Med Genet*, *52*(10), 681-690. <https://doi.org/10.1136/jmedgenet-2015-103272>
- Matkovich, S. J., Van Booven, D. J., Hindes, A., Kang, M. Y., Druley, T. E., Vallania, F. L., Mitra, R. D., Reilly, M. P., Cappola, T. P., & Dorn, G. W. (2010). Cardiac signaling genes exhibit unexpected sequence diversity in sporadic cardiomyopathy, revealing HSPB7 polymorphisms associated with disease. *J Clin Invest*, *120*(1), 280-289. <https://doi.org/10.1172/JCI39085>

- Matsuno, H., Kozawa, O., Niwa, M., Usui, A., Ito, H., Uematsu, T., & Kato, K. (1998). A heat shock-related protein, p20, plays an inhibitory role in platelet activation. *FEBS Lett*, *429*(3), 327-329. [https://doi.org/10.1016/s0014-5793\(98\)00626-7](https://doi.org/10.1016/s0014-5793(98)00626-7)
- McCampbell, A., Taylor, J. P., Taye, A. A., Robitschek, J., Li, M., Walcott, J., Merry, D., Chai, Y., Paulson, H., Sobue, G., & Fischbeck, K. H. (2000). CREB-binding protein sequestration by expanded polyglutamine. *Hum Mol Genet*, *9*(14), 2197-2202. <https://doi.org/10.1093/hmg/9.14.2197>
- Meister-Broekema, M., Freilich, R., Jagadeesan, C., Rauch, J. N., Bengoechea, R., Motley, W. W., Kuiper, E. F. E., Minoia, M., Furtado, G. V., van Waarde, M. A. W. H., Bird, S. J., Rebelo, A., Zuchner, S., Pytel, P., Scherer, S. S., Morelli, F. F., Carra, S., Weihl, C. C., Bergink, S., Gestwicki, J. E., & Kampinga, H. H. (2018). Myopathy associated BAG3 mutations lead to protein aggregation by stalling Hsp70 networks. *Nat Commun*, *9*(1), 5342. <https://doi.org/10.1038/s41467-018-07718-5>
- Mercer, E. J., Lin, Y. F., Cohen-Gould, L., & Evans, T. (2018). Hspb7 is a cardioprotective chaperone facilitating sarcomeric proteostasis. *Dev Biol*, *435*(1), 41-55. <https://doi.org/10.1016/j.ydbio.2018.01.005>
- Meriin, A. B., Narayanan, A., Meng, L., Alexandrov, I., Varelas, X., Cissé, I. I., & Sherman, M. Y. (2018). Hsp70-Bag3 complex is a hub for proteotoxicity-induced signaling that controls protein aggregation. *Proc Natl Acad Sci U S A*, *115*(30), E7043-E7052. <https://doi.org/10.1073/pnas.1803130115>
- Miller, V. M., Nelson, R. F., Gouvion, C. M., Williams, A., Rodriguez-Lebron, E., Harper, S. Q., Davidson, B. L., Rebagliati, M. R., & Paulson, H. L. (2005). CHIP suppresses polyglutamine aggregation and toxicity in vitro and in vivo. *J Neurosci*, *25*(40), 9152-9161. <https://doi.org/10.1523/JNEUROSCI.3001-05.2005>
- Min, J. N., Whaley, R. A., Sharpless, N. E., Lockyer, P., Portbury, A. L., & Patterson, C. (2008). CHIP deficiency decreases longevity, with accelerated aging phenotypes accompanied by altered protein quality control. *Mol Cell Biol*, *28*(12), 4018-4025. <https://doi.org/10.1128/MCB.00296-08>
- Minoia, M., Boncoraglio, A., Vinet, J., Morelli, F. F., Brunsting, J. F., Poletti, A., Krom, S., Reits, E., Kampinga, H. H., & Carra, S. (2014). BAG3 induces the sequestration of proteasomal clients into cytoplasmic puncta: implications for a proteasome-to-autophagy switch. *Autophagy*, *10*(9), 1603-1621. <https://doi.org/10.4161/auto.29409>
- Miron, T., Vancompernelle, K., Vandekerckhove, J., Wilchek, M., & Geiger, B. (1991). A 25-kD inhibitor of actin polymerization is a low molecular mass heat shock protein. *J Cell Biol*, *114*(2), 255-261. <https://doi.org/10.1083/jcb.114.2.255>
- Mizielinska, S., Lashley, T., Norona, F. E., Clayton, E. L., Ridler, C. E., Fratta, P., & Isaacs, A. M. (2013). C9orf72 frontotemporal lobar degeneration is characterised by frequent neuronal sense and antisense RNA foci. *Acta Neuropathol*, *126*(6), 845-857. <https://doi.org/10.1007/s00401-013-1200-z>
- Mock, J. Y., Chartron, J. W., Zaslaver, M., Xu, Y., Ye, Y., & Clemons, W. M. (2015). Bag6 complex contains a minimal tail-anchor-targeting module and a mock BAG domain. *Proc Natl Acad Sci U S A*, *112*(1), 106-111. <https://doi.org/10.1073/pnas.1402745112>
- Mogk, A., Bukau, B., & Kampinga, H. H. (2018). Cellular Handling of Protein Aggregates by Disaggregation Machines. *Mol Cell*, *69*(2), 214-226. <https://doi.org/10.1016/j.molcel.2018.01.004>
- Molliex, A., Temirov, J., Lee, J., Coughlin, M., Kanagaraj, A. P., Kim, H. J., Mittag, T., & Taylor, J. P. (2015). Phase separation by low complexity domains promotes stress granule assembly and drives pathological fibrillization. *Cell*, *163*(1), 123-133. <https://doi.org/10.1016/j.cell.2015.09.015>

- Monahan, Z., Shewmaker, F., & Pandey, U. B. (2016). Stress granules at the intersection of autophagy and ALS. *Brain Res*, 1649(Pt B), 189-200. <https://doi.org/10.1016/j.brainres.2016.05.022>
- Morelli, F. F., Mediani, L., Heldens, L., Bertacchini, J., Bigi, I., Carrà, A. D., Vinet, J., & Carra, S. (2017). An interaction study in mammalian cells demonstrates weak binding of HSPB2 to BAG3, which is regulated by HSPB3 and abrogated by HSPB8. *Cell Stress Chaperones*, 22(4), 531-540. <https://doi.org/10.1007/s12192-017-0769-x>
- Morelli, F. F., Verbeek, D. S., Bertacchini, J., Vinet, J., Mediani, L., Marmiroli, S., Cenacchi, G., Nasi, M., De Biasi, S., Brunsting, J. F., Lammerding, J., Pegoraro, E., Angelini, C., Tupler, R., Alberti, S., & Carra, S. (2017). Aberrant Compartment Formation by HSPB2 Mislocalizes Lamin A and Compromises Nuclear Integrity and Function. *Cell Rep*, 20(9), 2100-2115. <https://doi.org/10.1016/j.celrep.2017.08.018>
- Morrow, C. S., Porter, T. J., Xu, N., Arndt, Z. P., Ako-Asare, K., Heo, H. J., Thompson, E. A. N., & Moore, D. L. (2020). Vimentin Coordinates Protein Turnover at the Aggresome during Neural Stem Cell Quiescence Exit. *Cell Stem Cell*, 26(4), 558-568.e559. <https://doi.org/10.1016/j.stem.2020.01.018>
- Motley, W. W., Talbot, K., & Fischbeck, K. H. (2010). GARS axonopathy: not every neuron's cup of tRNA. *Trends Neurosci*, 33(2), 59-66. <https://doi.org/10.1016/j.tins.2009.11.001>
- Mulder, D. W. (1982). Clinical limits of amyotrophic lateral sclerosis. *Adv Neurol*, 36, 15-22.
- Murata, S., Minami, Y., Minami, M., Chiba, T., & Tanaka, K. (2001). CHIP is a chaperone-dependent E3 ligase that ubiquitylates unfolded protein. *EMBO Rep*, 2(12), 1133-1138. <https://doi.org/10.1093/embo-reports/kve246>
- Myers, V. D., Tomar, D., Madesh, M., Wang, J., Song, J., Zhang, X. Q., Gupta, M. K., Tahrir, F. G., Gordon, J., McClung, J. M., Kontos, C. D., Khalili, K., Cheung, J. Y., & Feldman, A. M. (2018). Haplo-insufficiency of Bcl2-associated athanogene 3 in mice results in progressive left ventricular dysfunction, β -adrenergic insensitivity, and increased apoptosis. *J Cell Physiol*, 233(9), 6319-6326. <https://doi.org/10.1002/jcp.26482>
- Mymrikov, E. V., Bukach, O. V., Seit-Nebi, A. S., & Gusev, N. B. (2010). The pivotal role of the beta 7 strand in the intersubunit contacts of different human small heat shock proteins. *Cell Stress Chaperones*, 15(4), 365-377. <https://doi.org/10.1007/s12192-009-0151-8>
- Naddaf, E., Barohn, R. J., & Dimachkie, M. M. (2018). Inclusion Body Myositis: Update on Pathogenesis and Treatment. *Neurotherapeutics*, 15(4), 995-1005. <https://doi.org/10.1007/s13311-018-0658-8>
- Nakhro, K., Park, J. M., Kim, Y. J., Yoon, B. R., Yoo, J. H., Koo, H., Choi, B. O., & Chung, K. W. (2013). A novel Lys141Thr mutation in small heat shock protein 22 (HSPB8) gene in Charcot-Marie-Tooth disease type 2L. *Neuromuscul Disord*, 23(8), 656-663. <https://doi.org/10.1016/j.nmd.2013.05.009>
- Nam, D. E., Nam, S. H., Lee, A. J., Hong, Y. B., Choi, B. O., & Chung, K. W. (2018). Small heat shock protein B3 (HSPB3) mutation in an axonal Charcot-Marie-Tooth disease family. *J Peripher Nerv Syst*, 23(1), 60-66. <https://doi.org/10.1111/jns.12249>
- Nefedova, V. V., Datskevich, P. N., Sudnitsyna, M. V., Strelkov, S. V., & Gusev, N. B. (2013). Physico-chemical properties of R140G and K141Q mutants of human small heat shock protein HspB1 associated with hereditary peripheral neuropathies. *Biochimie*, 95(8), 1582-1592. <https://doi.org/10.1016/j.biochi.2013.04.014>
- Neumann, M., Sampathu, D. M., Kwong, L. K., Truax, A. C., Micsenyi, M. C., Chou, T. T., Bruce, J., Schuck, T., Grossman, M., Clark, C. M., McCluskey, L. F., Miller, B. L., Masliah, E., Mackenzie, I. R., Feldman, H., Feiden, W., Kretschmar, H. A., Trojanowski, J. Q., & Lee, V. M. (2006). Ubiquitinated TDP-43 in frontotemporal lobar degeneration and amyotrophic lateral sclerosis. *Science*, 314(5796), 130-133. <https://doi.org/10.1126/science.1134108>
- Ni, L., Llewellyn, R., Kesler, C. T., Kelley, J. B., Spencer, A., Snow, C. J., Shank, L., & Paschal, B. M. (2013). Androgen induces a switch from cytoplasmic retention to nuclear import of the

- androgen receptor. *Mol Cell Biol*, 33(24), 4766-4778. <https://doi.org/10.1128/MCB.00647-13>
- Nicolaou, P., Knöll, R., Haghghi, K., Fan, G. C., Dorn, G. W., Hasenfub, G., & Kranias, E. G. (2008). Human mutation in the anti-apoptotic heat shock protein 20 abrogates its cardioprotective effects. *J Biol Chem*, 283(48), 33465-33471. <https://doi.org/10.1074/jbc.M802307200>
- Nicolau, S., Liewluck, T., Elliott, J. L., Engel, A. G., & Milone, M. (2020). A novel heterozygous mutation in the C-terminal region of HSPB8 leads to limb-girdle rimmed vacuolar myopathy. *Neuromuscul Disord*. <https://doi.org/10.1016/j.nmd.2020.02.005>
- Nikolay, R., Wiederkehr, T., Rist, W., Kramer, G., Mayer, M. P., & Bukau, B. (2004). Dimerization of the human E3 ligase CHIP via a coiled-coil domain is essential for its activity. *J Biol Chem*, 279(4), 2673-2678. <https://doi.org/10.1074/jbc.M311112200>
- Nonaka, T., Arai, T., Buratti, E., Baralle, F. E., Akiyama, H., & Hasegawa, M. (2009). Phosphorylated and ubiquitinated TDP-43 pathological inclusions in ALS and FTL-D-U are recapitulated in SH-SY5Y cells. *FEBS Lett*, 583(2), 394-400. <https://doi.org/10.1016/j.febslet.2008.12.031>
- Norton, N., Li, D., Rieder, M. J., Siegfried, J. D., Rampersaud, E., Züchner, S., Mangos, S., Gonzalez-Quintana, J., Wang, L., McGee, S., Reiser, J., Martin, E., Nickerson, D. A., & Hershberger, R. E. (2011). Genome-wide studies of copy number variation and exome sequencing identify rare variants in BAG3 as a cause of dilated cardiomyopathy. *Am J Hum Genet*, 88(3), 273-282. <https://doi.org/10.1016/j.ajhg.2011.01.016>
- Onesto, E., Rusmini, P., Crippa, V., Ferri, N., Zito, A., Galbiati, M., & Poletti, A. (2011). Muscle cells and motoneurons differentially remove mutant SOD1 causing familial amyotrophic lateral sclerosis. *J Neurochem*, 118(2), 266-280. <https://doi.org/10.1111/j.1471-4159.2011.07298.x>
- Orrell, R. W. (2000). Amyotrophic lateral sclerosis: copper/zinc superoxide dismutase (SOD1) gene mutations. *Neuromuscul Disord*, 10(1), 63-68. [https://doi.org/10.1016/s0960-8966\(99\)00071-1](https://doi.org/10.1016/s0960-8966(99)00071-1)
- Packham, G., Brimmell, M., & Cleveland, J. L. (1997). Mammalian cells express two differently localized Bag-1 isoforms generated by alternative translation initiation. *Biochem J*, 328 (Pt 3), 807-813. <https://doi.org/10.1042/bj3280807>
- Pagliuca, M. G., Leroise, R., Cigliano, S., & Leone, A. (2003). Regulation by heavy metals and temperature of the human BAG-3 gene, a modulator of Hsp70 activity. *FEBS Lett*, 541(1-3), 11-15. [https://doi.org/10.1016/s0014-5793\(03\)00274-6](https://doi.org/10.1016/s0014-5793(03)00274-6)
- Pakdaman, Y., Sanchez-Guixé, M., Kleppe, R., Erdal, S., Bustad, H. J., Bjørkhaug, L., Haugarvoll, K., Tzoulis, C., Heimdal, K., Knappskog, P. M., Johansson, S., & Aukrust, I. (2017). characterization of six. *Biosci Rep*, 37(2). <https://doi.org/10.1042/BSR20170251>
- Palmio, J., & Udd, B. (2016). Myofibrillar and distal myopathies. *Rev Neurol (Paris)*, 172(10), 587-593. <https://doi.org/10.1016/j.neurol.2016.07.019>
- Pandey, P., Farber, R., Nakazawa, A., Kumar, S., Bharti, A., Nalin, C., Weichselbaum, R., Kufe, D., & Kharbanda, S. (2000). Hsp27 functions as a negative regulator of cytochrome c-dependent activation of procaspase-3. *Oncogene*, 19(16), 1975-1981. <https://doi.org/10.1038/sj.onc.1203531>
- Parcellier, A., Brunet, M., Schmitt, E., Col, E., Didelot, C., Hammann, A., Nakayama, K., Nakayama, K. I., Khochbin, S., Solary, E., & Garrido, C. (2006). HSP27 favors ubiquitination and proteasomal degradation of p27Kip1 and helps S-phase re-entry in stressed cells. *FASEB J*, 20(8), 1179-1181. <https://doi.org/10.1096/fj.05-4184fje>
- Parone, P. A., Da Cruz, S., Han, J. S., McAlonis-Downes, M., Vetto, A. P., Lee, S. K., Tseng, E., & Cleveland, D. W. (2013). Enhancing mitochondrial calcium buffering capacity reduces aggregation of misfolded SOD1 and motor neuron cell death without extending survival in mouse models of inherited amyotrophic lateral sclerosis. *J Neurosci*, 33(11), 4657-4671. <https://doi.org/10.1523/JNEUROSCI.1119-12.2013>

- Pasinelli, P., & Brown, R. H. (2006). Molecular biology of amyotrophic lateral sclerosis: insights from genetics. *Nat Rev Neurosci*, 7(9), 710-723. <https://doi.org/10.1038/nrn1971>
- Paul, C., Simon, S., Gibert, B., Viot, S., Manero, F., & Arrigo, A. P. (2010). Dynamic processes that reflect anti-apoptotic strategies set up by HspB1 (Hsp27). *Exp Cell Res*, 316(9), 1535-1552. <https://doi.org/10.1016/j.yexcr.2010.03.006>
- Peeters, K., Chamova, T., & Jordanova, A. (2014). Clinical and genetic diversity of SMN1-negative proximal spinal muscular atrophies. *Brain*, 137(Pt 11), 2879-2896. <https://doi.org/10.1093/brain/awu169>
- Perng, M. D., Cairns, L., van den IJssel, P., Prescott, A., Hutcheson, A. M., & Quinlan, R. A. (1999). Intermediate filament interactions can be altered by HSP27 and alphaB-crystallin. *J Cell Sci*, 112 (Pt 13), 2099-2112.
- Pipkin, W., Johnson, J. A., Creazzo, T. L., Burch, J., Komalavilas, P., & Brophy, C. (2003). Localization, macromolecular associations, and function of the small heat shock-related protein HSP20 in rat heart. *Circulation*, 107(3), 469-476. <https://doi.org/10.1161/01.cir.0000044386.27444.5a>
- Planchamp, V., Bermel, C., Tönges, L., Ostendorf, T., Kügler, S., Reed, J. C., Kermer, P., Bähr, M., & Lingor, P. (2008). BAG1 promotes axonal outgrowth and regeneration in vivo via Raf-1 and reduction of ROCK activity. *Brain*, 131(Pt 10), 2606-2619. <https://doi.org/10.1093/brain/awn196>
- Pras, E., Frydman, M., Levy-Nissenbaum, E., Bakhan, T., Raz, J., Assia, E. I., & Goldman, B. (2000). A nonsense mutation (W9X) in CRYAA causes autosomal recessive cataract in an inbred Jewish Persian family. *Invest Ophthalmol Vis Sci*, 41(11), 3511-3515.
- Pratt, W. B., & Toft, D. O. (1997). Steroid receptor interactions with heat shock protein and immunophilin chaperones. *Endocr Rev*, 18(3), 306-360. <https://doi.org/10.1210/edrv.18.3.0303>
- Pratt, W. B., & Welsh, M. J. (1994). Chaperone functions of the heat shock proteins associated with steroid receptors. *Semin Cell Biol*, 5(2), 83-93. <https://doi.org/10.1006/scel.1994.1012>
- Puls, I., Jonnakuty, C., LaMonte, B. H., Holzbaur, E. L., Tokito, M., Mann, E., Floeter, M. K., Bidus, K., Drayna, D., Oh, S. J., Brown, R. H., Ludlow, C. L., & Fischbeck, K. H. (2003). Mutant dynactin in motor neuron disease. *Nat Genet*, 33(4), 455-456. <https://doi.org/10.1038/ng1123>
- Qi, R., Sarbeng, E. B., Liu, Q., Le, K. Q., Xu, X., Xu, H., Yang, J., Wong, J. L., Vorvis, C., Hendrickson, W. A., & Zhou, L. (2013). Allosteric opening of the polypeptide-binding site when an Hsp70 binds ATP. *Nat Struct Mol Biol*, 20(7), 900-907. <https://doi.org/10.1038/nsmb.2583>
- Qian, J., Ren, X., Wang, X., Zhang, P., Jones, W. K., Molkentin, J. D., Fan, G. C., & Kranias, E. G. (2009). Blockade of Hsp20 phosphorylation exacerbates cardiac ischemia/reperfusion injury by suppressed autophagy and increased cell death. *Circ Res*, 105(12), 1223-1231. <https://doi.org/10.1161/CIRCRESAHA.109.200378>
- Quraishe, S., Asuni, A., Boelens, W. C., O'Connor, V., & Wyttenbach, A. (2008). Expression of the small heat shock protein family in the mouse CNS: differential anatomical and biochemical compartmentalization. *Neuroscience*, 153(2), 483-491. <https://doi.org/10.1016/j.neuroscience.2008.01.058>
- Rajan, R. S., Illing, M. E., Bence, N. F., & Kopito, R. R. (2001). Specificity in intracellular protein aggregation and inclusion body formation. *Proc Natl Acad Sci U S A*, 98(23), 13060-13065. <https://doi.org/10.1073/pnas.181479798>
- Ranganathan, S., Harmison, G. G., Meyertholen, K., Pennuto, M., Burnett, B. G., & Fischbeck, K. H. (2009). Mitochondrial abnormalities in spinal and bulbar muscular atrophy. *Hum Mol Genet*, 18(1), 27-42. <https://doi.org/10.1093/hmg/ddn310>
- Ratti, A., & Buratti, E. (2016). Physiological functions and pathobiology of TDP-43 and FUS/TLS proteins. *J Neurochem*, 138 Suppl 1, 95-111. <https://doi.org/10.1111/jnc.13625>

- Rauch, J. N., & Gestwicki, J. E. (2014). Binding of human nucleotide exchange factors to heat shock protein 70 (Hsp70) generates functionally distinct complexes in vitro. *J Biol Chem*, 289(3), 1402-1414. <https://doi.org/10.1074/jbc.M113.521997>
- Rauch, J. N., Tse, E., Freilich, R., Mok, S. A., Makley, L. N., Southworth, D. R., & Gestwicki, J. E. (2017). BAG3 Is a Modular, Scaffolding Protein that physically Links Heat Shock Protein 70 (Hsp70) to the Small Heat Shock Proteins. *J Mol Biol*, 429(1), 128-141. <https://doi.org/10.1016/j.jmb.2016.11.013>
- Reinhardt, P., Glatza, M., Hemmer, K., Tsytsyura, Y., Thiel, C. S., Höing, S., Moritz, S., Parga, J. A., Wagner, L., Bruder, J. M., Wu, G., Schmid, B., Röpke, A., Klingauf, J., Schwamborn, J. C., Gasser, T., Schöler, H. R., & Sternecker, J. (2013). Derivation and expansion using only small molecules of human neural progenitors for neurodegenerative disease modeling. *PLoS One*, 8(3), e59252. <https://doi.org/10.1371/journal.pone.0059252>
- Renton, A. E., Majounie, E., Waite, A., Simón-Sánchez, J., Rollinson, S., Gibbs, J. R., Schymick, J. C., Laaksovirta, H., van Swieten, J. C., Myllykangas, L., Kalimo, H., Paetau, A., Abramzon, Y., Remes, A. M., Kaganovich, A., Scholz, S. W., Duckworth, J., Ding, J., Harmer, D. W., Hernandez, D. G., Johnson, J. O., Mok, K., Ryten, M., Trabzuni, D., Guerreiro, R. J., Orrell, R. W., Neal, J., Murray, A., Pearson, J., Jansen, I. E., Sondervan, D., Seelaar, H., Blake, D., Young, K., Halliwell, N., Callister, J. B., Toulson, G., Richardson, A., Gerhard, A., Snowden, J., Mann, D., Neary, D., Nalls, M. A., Peuralinna, T., Jansson, L., Isoviita, V. M., Kaivorinne, A. L., Hölttä-Vuori, M., Ikonen, E., Sulkava, R., Benatar, M., Wu, J., Chiò, A., Restagno, G., Borghero, G., Sabatelli, M., Heckerman, D., Rogaeva, E., Zinman, L., Rothstein, J. D., Sendtner, M., Drepper, C., Eichler, E. E., Alkan, C., Abdullaev, Z., Pack, S. D., Dutra, A., Pak, E., Hardy, J., Singleton, A., Williams, N. M., Heutink, P., Pickering-Brown, S., Morris, H. R., Tienari, P. J., Traynor, B. J., & Consortium, I. (2011). A hexanucleotide repeat expansion in C9ORF72 is the cause of chromosome 9p21-linked ALS-FTD. *Neuron*, 72(2), 257-268. <https://doi.org/10.1016/j.neuron.2011.09.010>
- Rhodes, L. E., Freeman, B. K., Auh, S., Kokkinis, A. D., La Pean, A., Chen, C., Lehky, T. J., Shrader, J. A., Levy, E. W., Harris-Love, M., Di Prospero, N. A., & Fischbeck, K. H. (2009). Clinical features of spinal and bulbar muscular atrophy. *Brain*, 132(Pt 12), 3242-3251. <https://doi.org/10.1093/brain/awp258>
- Robertson, R., Conte, T. C., Dicaire, M. J., Rymar, V. V., Sadikot, A. F., Bryson-Richardson, R. J., Lavoie, J. N., O'Ferrall, E., Young, J. C., & Brais, B. (2020). BAG3. *Am J Pathol*, 190(3), 554-562. <https://doi.org/10.1016/j.ajpath.2019.11.005>
- Rodriguez-Muela, N., Litterman, N. K., Norabuena, E. M., Mull, J. L., Galazo, M. J., Sun, C., Ng, S. Y., Makhortova, N. R., White, A., Lynes, M. M., Chung, W. K., Davidow, L. S., Macklis, J. D., & Rubin, L. L. (2017). Single-Cell Analysis of SMN Reveals Its Broader Role in Neuromuscular Disease. *Cell Rep*, 18(6), 1484-1498. <https://doi.org/10.1016/j.celrep.2017.01.035>
- Rosati, A., Ammirante, M., Gentilella, A., Basile, A., Festa, M., Pascale, M., Marzullo, L., Belisario, M. A., Tosco, A., Franceschelli, S., Moltedo, O., Pagliuca, G., Leroise, R., & Turco, M. C. (2007). Apoptosis inhibition in cancer cells: a novel molecular pathway that involves BAG3 protein. *Int J Biochem Cell Biol*, 39(7-8), 1337-1342. <https://doi.org/10.1016/j.biocel.2007.03.007>
- Rosen, D. R. (1993). Mutations in Cu/Zn superoxide dismutase gene are associated with familial amyotrophic lateral sclerosis. *Nature*, 364(6435), 362. <https://doi.org/10.1038/364362c0>
- Rosenbohm, A., Hirsch, S., Volk, A. E., Grehl, T., Grosskreutz, J., Hanisch, F., Herrmann, A., Kollwe, K., Kress, W., Meyer, T., Petri, S., Prudlo, J., Wessig, C., Müller, H. P., Dreyhaupt, J., Weishaupt, J., Kubisch, C., Kassubek, J., Weydt, P., & Ludolph, A. C. (2018). The metabolic and endocrine characteristics in spinal and bulbar muscular atrophy. *J Neurol*, 265(5), 1026-1036. <https://doi.org/10.1007/s00415-018-8790-2>
- Rosenfeld, G. E., Mercer, E. J., Mason, C. E., & Evans, T. (2013). Small heat shock proteins Hspb7 and Hspb12 regulate early steps of cardiac morphogenesis. *Dev Biol*, 381(2), 389-400. <https://doi.org/10.1016/j.ydbio.2013.06.025>

- Rossor, A. M., Kalmar, B., Greensmith, L., & Reilly, M. M. (2012). The distal hereditary motor neuropathies. *J Neurol Neurosurg Psychiatry*, *83*(1), 6-14. <https://doi.org/10.1136/jnnp-2011-300952>
- Rout, A. K., Strub, M. P., Piszczek, G., & Tjandra, N. (2014). Structure of transmembrane domain of lysosome-associated membrane protein type 2a (LAMP-2A) reveals key features for substrate specificity in chaperone-mediated autophagy. *J Biol Chem*, *289*(51), 35111-35123. <https://doi.org/10.1074/jbc.M114.609446>
- Ruparella, A. A., Oorschot, V., Vaz, R., Ramm, G., & Bryson-Richardson, R. J. (2014). Zebrafish models of BAG3 myofibrillar myopathy suggest a toxic gain of function leading to BAG3 insufficiency. *Acta Neuropathol*, *128*(6), 821-833. <https://doi.org/10.1007/s00401-014-1344-5>
- Rusmini, P., Cortese, K., Crippa, V., Cristofani, R., Cicardi, M. E., Ferrari, V., Vezzoli, G., Tedesco, B., Meroni, M., Messi, E., Piccolella, M., Galbiati, M., Garrè, M., Morelli, E., Vaccari, T., & Poletti, A. (2019). Trehalose induces autophagy via lysosomal-mediated TFEB activation in models of motoneuron degeneration. *Autophagy*, *15*(4), 631-651. <https://doi.org/10.1080/15548627.2018.1535292>
- Rusmini, P., Crippa, V., Cristofani, R., Rinaldi, C., Cicardi, M. E., Galbiati, M., Carra, S., Malik, B., Greensmith, L., & Poletti, A. (2016). The Role of the Protein Quality Control System in SBMA. *J Mol Neurosci*, *58*(3), 348-364. <https://doi.org/10.1007/s12031-015-0675-6>
- Rusmini, P., Crippa, V., Giorgetti, E., Boncoraglio, A., Cristofani, R., Carra, S., & Poletti, A. (2013). Clearance of the mutant androgen receptor in motoneuronal models of spinal and bulbar muscular atrophy. *Neurobiol Aging*, *34*(11), 2585-2603. <https://doi.org/10.1016/j.neurobiolaging.2013.05.026>
- Rusmini, P., Cristofani, R., Galbiati, M., Cicardi, M. E., Meroni, M., Ferrari, V., Vezzoli, G., Tedesco, B., Messi, E., Piccolella, M., Carra, S., Crippa, V., & Poletti, A. (2017). The Role of the Heat Shock Protein B8 (HSPB8) in Motoneuron Diseases. *Front Mol Neurosci*, *10*, 176. <https://doi.org/10.3389/fnmol.2017.00176>
- Rüdiger, S., Germeroth, L., Schneider-Mergener, J., & Bukau, B. (1997). Substrate specificity of the DnaK chaperone determined by screening cellulose-bound peptide libraries. *EMBO J*, *16*(7), 1501-1507. <https://doi.org/10.1093/emboj/16.7.1501>
- Sacconi, S., Féasson, L., Antoine, J. C., Pécheux, C., Bernard, R., Cobo, A. M., Casarin, A., Salviati, L., Desnuelle, C., & Urtizberea, A. (2012). A novel CRYAB mutation resulting in multisystemic disease. *Neuromuscul Disord*, *22*(1), 66-72. <https://doi.org/10.1016/j.nmd.2011.07.004>
- Salinas, S., Proukakis, C., Crosby, A., & Warner, T. T. (2008). Hereditary spastic paraplegia: clinical features and pathogenetic mechanisms. *Lancet Neurol*, *7*(12), 1127-1138. [https://doi.org/10.1016/S1474-4422\(08\)70258-8](https://doi.org/10.1016/S1474-4422(08)70258-8)
- Sanbe, A., Marunouchi, T., Abe, T., Tezuka, Y., Okada, M., Aoki, S., Tsumura, H., Yamauchi, J., Tanonaka, K., Nishigori, H., & Tanoue, A. (2013). Phenotype of cardiomyopathy in cardiac-specific heat shock protein B8 K141N transgenic mouse. *J Biol Chem*, *288*(13), 8910-8921. <https://doi.org/10.1074/jbc.M112.368324>
- Sarparanta, J., Jonson, P. H., Golzio, C., Sandell, S., Luque, H., Screen, M., McDonald, K., Stajich, J. M., Mahjneh, I., Vihola, A., Raheem, O., Penttilä, S., Lehtinen, S., Huovinen, S., Palmio, J., Tasca, G., Ricci, E., Hackman, P., Hauser, M., Katsanis, N., & Udd, B. (2012). Mutations affecting the cytoplasmic functions of the co-chaperone DNAJB6 cause limb-girdle muscular dystrophy. *Nat Genet*, *44*(4), 450-455, S451-452. <https://doi.org/10.1038/ng.1103>
- Schneikert, J., Hübner, S., Martin, E., & Cato, A. C. (1999). A nuclear action of the eukaryotic cochaperone RAP46 in downregulation of glucocorticoid receptor activity. *J Cell Biol*, *146*(5), 929-940. <https://doi.org/10.1083/jcb.146.5.929>
- Schrank, B., Götz, R., Gunnensen, J. M., Ure, J. M., Toyka, K. V., Smith, A. G., & Sendtner, M. (1997). Inactivation of the survival motor neuron gene, a candidate gene for human spinal muscular

- atrophy, leads to massive cell death in early mouse embryos. *Proc Natl Acad Sci U S A*, 94(18), 9920-9925. <https://doi.org/10.1073/pnas.94.18.9920>
- Schubert, U., Antón, L. C., Gibbs, J., Norbury, C. C., Yewdell, J. W., & Bennink, J. R. (2000). Rapid degradation of a large fraction of newly synthesized proteins by proteasomes. *Nature*, 404(6779), 770-774. <https://doi.org/10.1038/35008096>
- Selcen, D., Muntoni, F., Burton, B. K., Pegoraro, E., Sewry, C., Bite, A. V., & Engel, A. G. (2009). Mutation in BAG3 causes severe dominant childhood muscular dystrophy. *Ann Neurol*, 65(1), 83-89. <https://doi.org/10.1002/ana.21553>
- Semmler, A. L., Sacconi, S., Bach, J. E., Liebe, C., Bürmann, J., Kley, R. A., Ferbert, A., Anderheiden, R., Van den Bergh, P., Martin, J. J., De Jonghe, P., Neuen-Jacob, E., Müller, O., Deschauer, M., Bergmann, M., Schröder, J. M., Vorgerd, M., Schulz, J. B., Weis, J., Kress, W., & Claeys, K. G. (2014). Unusual multisystemic involvement and a novel BAG3 mutation revealed by NGS screening in a large cohort of myofibrillar myopathies. *Orphanet J Rare Dis*, 9, 121. <https://doi.org/10.1186/s13023-014-0121-9>
- Shama, K. M., Suzuki, A., Harada, K., Fujitani, N., Kimura, H., Ohno, S., & Yoshida, K. (1999). Transient up-regulation of myotonic dystrophy protein kinase-binding protein, MKBP, and HSP27 in the neonatal myocardium. *Cell Struct Funct*, 24(1), 1-4. <https://doi.org/10.1247/csf.24.1>
- Shammas, S. L., Waudby, C. A., Wang, S., Buell, A. K., Knowles, T. P., Ecroyd, H., Welland, M. E., Carver, J. A., Dobson, C. M., & Meehan, S. (2011). Binding of the molecular chaperone α B-crystallin to A β amyloid fibrils inhibits fibril elongation. *Biophys J*, 101(7), 1681-1689. <https://doi.org/10.1016/j.bpj.2011.07.056>
- Shi, Y., Wang, J., Li, J. D., Ren, H., Guan, W., He, M., Yan, W., Zhou, Y., Hu, Z., Zhang, J., Xiao, J., Su, Z., Dai, M., Jiang, H., Guo, J., Zhang, F., Li, N., Du, J., Xu, Q., Hu, Y., Pan, Q., Shen, L., Wang, G., Xia, K., Zhang, Z., & Tang, B. (2013). Identification of CHIP as a novel causative gene for autosomal recessive cerebellar ataxia. *PLoS One*, 8(12), e81884. <https://doi.org/10.1371/journal.pone.0081884>
- Shroff, N. P., Cherian-Shaw, M., Bera, S., & Abraham, E. C. (2000). Mutation of R116C results in highly oligomerized alpha A-crystallin with modified structure and defective chaperone-like function. *Biochemistry*, 39(6), 1420-1426. <https://doi.org/10.1021/bi991656b>
- Shy, M., Rebelo, A. P., Feely, S. M., Abreu, L. A., Tao, F., Swenson, A., Bacon, C., & Zuchner, S. (2018). Mutations in BAG3 cause adult-onset Charcot-Marie-Tooth disease. *J Neurol Neurosurg Psychiatry*, 89(3), 313-315. <https://doi.org/10.1136/jnnp-2017-315929>
- Sim, N. L., Kumar, P., Hu, J., Henikoff, S., Schneider, G., & Ng, P. C. (2012). SIFT web server: predicting effects of amino acid substitutions on proteins. *Nucleic Acids Res*, 40(Web Server issue), W452-457. <https://doi.org/10.1093/nar/gks539>
- Singh, R. N., Howell, M. D., Ottesen, E. W., & Singh, N. N. (2017). Diverse role of survival motor neuron protein. *Biochim Biophys Acta Gene Regul Mech*, 1860(3), 299-315. <https://doi.org/10.1016/j.bbarm.2016.12.008>
- Singh, R. N., & Singh, N. N. (2018). Mechanism of Splicing Regulation of Spinal Muscular Atrophy Genes. *Adv Neurobiol*, 20, 31-61. https://doi.org/10.1007/978-3-319-89689-2_2
- Sondermann, H., Ho, A. K., Listenberger, L. L., Siegers, K., Moarefi, I., Wenthe, S. R., Hartl, F. U., & Young, J. C. (2002). Prediction of novel Bag-1 homologs based on structure/function analysis identifies Snl1p as an Hsp70 co-chaperone in *Saccharomyces cerevisiae*. *J Biol Chem*, 277(36), 33220-33227. <https://doi.org/10.1074/jbc.M204624200>
- Sondermann, H., Scheufler, C., Schneider, C., Hohfeld, J., Hartl, F. U., & Moarefi, I. (2001). Structure of a Bag/Hsc70 complex: convergent functional evolution of Hsp70 nucleotide exchange factors. *Science*, 291(5508), 1553-1557. <https://doi.org/10.1126/science.1057268>
- Song, Z., Xu, S., Song, B., & Zhang, Q. (2015). Bcl-2-associated athanogene 2 prevents the neurotoxicity of MPP+ via interaction with DJ-1. *J Mol Neurosci*, 55(3), 798-802. <https://doi.org/10.1007/s12031-014-0481-6>

- Sorarù, G., D'Ascenzo, C., Polo, A., Palmieri, A., Baggio, L., Vergani, L., Gellera, C., Moretto, G., Pegoraro, E., & Angelini, C. (2008). Spinal and bulbar muscular atrophy: skeletal muscle pathology in male patients and heterozygous females. *J Neurol Sci*, *264*(1-2), 100-105. <https://doi.org/10.1016/j.jns.2007.08.012>
- Sorarù, G., Orsetti, V., Buratti, E., Baralle, F., Cima, V., Volpe, M., D'ascenzo, C., Palmieri, A., Koutsikos, K., Pegoraro, E., & Angelini, C. (2010). TDP-43 in skeletal muscle of patients affected with amyotrophic lateral sclerosis. *Amyotroph Lateral Scler*, *11*(1-2), 240-243. <https://doi.org/10.3109/17482960902810890>
- Sormanni, P., Aprile, F. A., & Vendruscolo, M. (2015). The CamSol method of rational design of protein mutants with enhanced solubility. *J Mol Biol*, *427*(2), 478-490. <https://doi.org/10.1016/j.jmb.2014.09.026>
- Sreedharan, J., Blair, I. P., Tripathi, V. B., Hu, X., Vance, C., Rogelj, B., Ackerley, S., Durnall, J. C., Williams, K. L., Buratti, E., Baralle, F., de Bellerocche, J., Mitchell, J. D., Leigh, P. N., Al-Chalabi, A., Miller, C. C., Nicholson, G., & Shaw, C. E. (2008). TDP-43 mutations in familial and sporadic amyotrophic lateral sclerosis. *Science*, *319*(5870), 1668-1672. <https://doi.org/10.1126/science.1154584>
- Srinivas, P. N., Reddy, P. Y., & Reddy, G. B. (2008). Significance of alpha-crystallin heteropolymer with a 3:1 alphaA/alphaB ratio: chaperone-like activity, structure and hydrophobicity. *Biochem J*, *414*(3), 453-460. <https://doi.org/10.1042/BJ20080544>
- Sroka, K., Voigt, A., Deeg, S., Reed, J. C., Schulz, J. B., Bähr, M., & Kermer, P. (2009). BAG1 modulates huntingtin toxicity, aggregation, degradation, and subcellular distribution. *J Neurochem*, *111*(3), 801-807. <https://doi.org/10.1111/j.1471-4159.2009.06363.x>
- Stenoien, D. L., Cummings, C. J., Adams, H. P., Mancini, M. G., Patel, K., DeMartino, G. N., Marcelli, M., Weigel, N. L., & Mancini, M. A. (1999). Polyglutamine-expanded androgen receptors form aggregates that sequester heat shock proteins, proteasome components and SRC-1, and are suppressed by the HDJ-2 chaperone. *Hum Mol Genet*, *8*(5), 731-741. <https://doi.org/10.1093/hmg/8.5.731>
- Sudria-Lopez, E., Koppers, M., de Wit, M., van der Meer, C., Westeneng, H. J., Zundel, C. A., Youssef, S. A., Harkema, L., de Bruin, A., Veldink, J. H., van den Berg, L. H., & Pasterkamp, R. J. (2016). Full ablation of C9orf72 in mice causes immune system-related pathology and neoplastic events but no motor neuron defects. *Acta Neuropathol*, *132*(1), 145-147. <https://doi.org/10.1007/s00401-016-1581-x>
- Sugiyama, Y., Suzuki, A., Kishikawa, M., Akutsu, R., Hirose, T., Waye, M. M., Tsui, S. K., Yoshida, S., & Ohno, S. (2000). Muscle develops a specific form of small heat shock protein complex composed of MKBP/HSPB2 and HSPB3 during myogenic differentiation. *J Biol Chem*, *275*(2), 1095-1104. <https://doi.org/10.1074/jbc.275.2.1095>
- Sun, X., Fontaine, J. M., Hoppe, A. D., Carra, S., DeGuzman, C., Martin, J. L., Simon, S., Vicart, P., Welsh, M. J., Landry, J., & Benndorf, R. (2010). Abnormal interaction of motor neuropathy-associated mutant HspB8 (Hsp22) forms with the RNA helicase Ddx20 (gemin3). *Cell Stress Chaperones*, *15*(5), 567-582. <https://doi.org/10.1007/s12192-010-0169-y>
- Suzuki, A., Sugiyama, Y., Hayashi, Y., Nyu-i, N., Yoshida, M., Nonaka, I., Ishiura, S., Arahata, K., & Ohno, S. (1998). MKBP, a novel member of the small heat shock protein family, binds and activates the myotonic dystrophy protein kinase. *J Cell Biol*, *140*(5), 1113-1124. <https://doi.org/10.1083/jcb.140.5.1113>
- Takayama, S., Krajewski, S., Krajewska, M., Kitada, S., Zapata, J. M., Kochel, K., Knee, D., Scudiero, D., Tudor, G., Miller, G. J., Miyashita, T., Yamada, M., & Reed, J. C. (1998). Expression and location of Hsp70/Hsc-binding anti-apoptotic protein BAG-1 and its variants in normal tissues and tumor cell lines. *Cancer Res*, *58*(14), 3116-3131.
- Takayama, S., Sato, T., Krajewski, S., Kochel, K., Irie, S., Millan, J. A., & Reed, J. C. (1995). Cloning and functional analysis of BAG-1: a novel Bcl-2-binding protein with anti-cell death activity. *Cell*, *80*(2), 279-284. [https://doi.org/10.1016/0092-8674\(95\)90410-7](https://doi.org/10.1016/0092-8674(95)90410-7)

- Takayama, S., Xie, Z., & Reed, J. C. (1999). An evolutionarily conserved family of Hsp70/Hsc70 molecular chaperone regulators. *J Biol Chem*, 274(2), 781-786. <https://doi.org/10.1074/jbc.274.2.781>
- Tanaka, H., Takahashi, T., Xie, Y., Minami, R., Yanagi, Y., Hayashishita, M., Suzuki, R., Yokota, N., Shimada, M., Mizushima, T., Kuwabara, N., Kato, R., & Kawahara, H. (2016). A conserved island of BAG6/Scythe is related to ubiquitin domains and participates in short hydrophobicity recognition. *FEBS J*, 283(4), 662-677. <https://doi.org/10.1111/febs.13618>
- Tang, M., Ji, C., Pallo, S., Rahman, I., & Johnson, G. V. W. (2018). Nrf2 mediates the expression of BAG3 and autophagy cargo adaptor proteins and tau clearance in an age-dependent manner. *Neurobiol Aging*, 63, 128-139. <https://doi.org/10.1016/j.neurobiolaging.2017.12.001>
- Taylor, J. P., Brown, R. H., & Cleveland, D. W. (2016). Decoding ALS: from genes to mechanism. *Nature*, 539(7628), 197-206. <https://doi.org/10.1038/nature20413>
- Terlecky, S. R., Chiang, H. L., Olson, T. S., & Dice, J. F. (1992). Protein and peptide binding and stimulation of in vitro lysosomal proteolysis by the 73-kDa heat shock cognate protein. *J Biol Chem*, 267(13), 9202-9209.
- Tetzlaff, J. E., Putcha, P., Outeiro, T. F., Ivanov, A., Berezovska, O., Hyman, B. T., & McLean, P. J. (2008). CHIP targets toxic alpha-Synuclein oligomers for degradation. *J Biol Chem*, 283(26), 17962-17968. <https://doi.org/10.1074/jbc.M802283200>
- Thress, K., Song, J., Morimoto, R. I., & Kornbluth, S. (2001). Reversible inhibition of Hsp70 chaperone function by Scythe and Reaper. *EMBO J*, 20(5), 1033-1041. <https://doi.org/10.1093/emboj/20.5.1033>
- Tiryaki, E., & Horak, H. A. (2014). ALS and other motor neuron diseases. *Continuum (Minneapolis, Minn)*, 20(5 Peripheral Nervous System Disorders), 1185-1207. <https://doi.org/10.1212/01.CON.0000455886.14298.a4>
- Treweek, T. M., Meehan, S., Ecroyd, H., & Carver, J. A. (2015). Small heat-shock proteins: important players in regulating cellular proteostasis. *Cell Mol Life Sci*, 72(3), 429-451. <https://doi.org/10.1007/s00018-014-1754-5>
- Tyedmers, J., Mogk, A., & Bukau, B. (2010). Cellular strategies for controlling protein aggregation. *Nat Rev Mol Cell Biol*, 11(11), 777-788. <https://doi.org/10.1038/nrm2993>
- Ulbricht, A., Eppler, F. J., Tapia, V. E., van der Ven, P. F., Hampe, N., Hersch, N., Vakeel, P., Stadel, D., Haas, A., Saftig, P., Behrends, C., Fürst, D. O., Volkmer, R., Hoffmann, B., Kolanus, W., & Höhfeld, J. (2013). Cellular mechanotransduction relies on tension-induced and chaperone-assisted autophagy. *Curr Biol*, 23(5), 430-435. <https://doi.org/10.1016/j.cub.2013.01.064>
- Urushitani, M., Kurisu, J., Tateno, M., Hatakeyama, S., Nakayama, K., Kato, S., & Takahashi, R. (2004). CHIP promotes proteasomal degradation of familial ALS-linked mutant SOD1 by ubiquitinating Hsp/Hsc70. *J Neurochem*, 90(1), 231-244. <https://doi.org/10.1111/j.1471-4159.2004.02486.x>
- Van Montfort, R., Slingsby, C., & Vierling, E. (2001). Structure and function of the small heat shock protein/alpha-crystallin family of molecular chaperones. *Adv Protein Chem*, 59, 105-156. [https://doi.org/10.1016/s0065-3233\(01\)59004-x](https://doi.org/10.1016/s0065-3233(01)59004-x)
- Vance, C., Rogelj, B., Hortobágyi, T., De Vos, K. J., Nishimura, A. L., Sreedharan, J., Hu, X., Smith, B., Ruddy, D., Wright, P., Ganesalingam, J., Williams, K. L., Tripathi, V., Al-Saraj, S., Al-Chalabi, A., Leigh, P. N., Blair, I. P., Nicholson, G., de Belleruche, J., Gallo, J. M., Miller, C. C., & Shaw, C. E. (2009). Mutations in FUS, an RNA processing protein, cause familial amyotrophic lateral sclerosis type 6. *Science*, 323(5918), 1208-1211. <https://doi.org/10.1126/science.1165942>
- Varlet, A. A., Fuchs, M., Luthold, C., Lambert, H., Landry, J., & Lavoie, J. N. (2017). Fine-tuning of actin dynamics by the HSPB8-BAG3 chaperone complex facilitates cytokinesis and contributes to its impact on cell division. *Cell Stress Chaperones*, 22(4), 553-567. <https://doi.org/10.1007/s12192-017-0780-2>

- Verschuure, P., Croes, Y., van den IJssel, P. R., Quinlan, R. A., de Jong, W. W., & Boelens, W. C. (2002). Translocation of small heat shock proteins to the actin cytoskeleton upon proteasomal inhibition. *J Mol Cell Cardiol*, 34(2), 117-128. <https://doi.org/10.1006/jmcc.2001.1493>
- Verschuure, P., Tatard, C., Boelens, W. C., Grongnet, J. F., & David, J. C. (2003). Expression of small heat shock proteins HspB2, HspB8, Hsp20 and cvHsp in different tissues of the perinatal developing pig. *Eur J Cell Biol*, 82(10), 523-530. <https://doi.org/10.1078/0171-9335-00337>
- Vicart, P., Caron, A., Guicheney, P., Li, Z., Prévost, M. C., Faure, A., Chateau, D., Chapon, F., Tomé, F., Dupret, J. M., Paulin, D., & Fardeau, M. (1998). A missense mutation in the alphaB-crystallin chaperone gene causes a desmin-related myopathy. *Nat Genet*, 20(1), 92-95. <https://doi.org/10.1038/1765>
- Villard, E., Perret, C., Gary, F., Proust, C., Dilanian, G., Hengstenberg, C., Ruppert, V., Arbustini, E., Wichter, T., Germain, M., Dubourg, O., Tavazzi, L., Aumont, M. C., DeGroot, P., Fauchier, L., Trochu, J. N., Gibelin, P., Aupetit, J. F., Stark, K., Erdmann, J., Hetzer, R., Roberts, A. M., Barton, P. J., Regitz-Zagrosek, V., Aslam, U., Duboscq-Bidot, L., Meyborg, M., Maisch, B., Madeira, H., Waldenström, A., Galve, E., Cleland, J. G., Dorent, R., Roizes, G., Zeller, T., Blankenberg, S., Goodall, A. H., Cook, S., Tregouet, D. A., Tiret, L., Isnard, R., Komajda, M., Charron, P., Cambien, F., & Consortium, C. (2011). A genome-wide association study identifies two loci associated with heart failure due to dilated cardiomyopathy. *Eur Heart J*, 32(9), 1065-1076. <https://doi.org/10.1093/eurheartj/ehr105>
- Virador, V. M., Davidson, B., Czechowicz, J., Mai, A., Kassis, J., & Kohn, E. C. (2009). The anti-apoptotic activity of BAG3 is restricted by caspases and the proteasome. *PLoS One*, 4(4), e5136. <https://doi.org/10.1371/journal.pone.0005136>
- Vos, M. J., Kanon, B., & Kampinga, H. H. (2009). HSPB7 is a SC35 speckle resident small heat shock protein. *Biochim Biophys Acta*, 1793(8), 1343-1353. <https://doi.org/10.1016/j.bbamcr.2009.05.005>
- Vos, M. J., Zijlstra, M. P., Kanon, B., van Waarde-Verhagen, M. A., Brunt, E. R., Oosterveld-Hut, H. M., Carra, S., Sibon, O. C., & Kampinga, H. H. (2010). HSPB7 is the most potent polyQ aggregation suppressor within the HSPB family of molecular chaperones. *Hum Mol Genet*, 19(23), 4677-4693. <https://doi.org/10.1093/hmg/ddq398>
- Wang, H. Q., Meng, X., Liu, B. Q., Li, C., Gao, Y. Y., Niu, X. F., Li, N., Guan, Y., & Du, Z. X. (2012). Involvement of JNK and NF- κ B pathways in lipopolysaccharide (LPS)-induced BAG3 expression in human monocytic cells. *Exp Cell Res*, 318(1), 16-24. <https://doi.org/10.1016/j.yexcr.2011.10.005>
- Wang, M., Ding, H., Kang, J., Hu, K., Lu, W., Zhou, X., & Xu, L. (2016). Association between polymorphisms of the HSPB7 gene and Cheyne-Stokes respiration with central sleep apnea in patients with dilated cardiomyopathy and congestive heart failure. *Int J Cardiol*, 221, 926-931. <https://doi.org/10.1016/j.ijcard.2016.07.107>
- Wang, X., Guo, J., Fei, E., Mu, Y., He, S., Che, X., Tan, J., Xia, K., Zhang, Z., Wang, G., & Tang, B. (2014). BAG5 protects against mitochondrial oxidative damage through regulating PINK1 degradation. *PLoS One*, 9(1), e86276. <https://doi.org/10.1371/journal.pone.0086276>
- Wang, X., Zingarelli, B., O'Connor, M., Zhang, P., Adeyemo, A., Kranias, E. G., Wang, Y., & Fan, G. C. (2009). Overexpression of Hsp20 prevents endotoxin-induced myocardial dysfunction and apoptosis via inhibition of NF-kappaB activation. *J Mol Cell Cardiol*, 47(3), 382-390. <https://doi.org/10.1016/j.yjmcc.2009.05.016>
- Waudby, C. A., Knowles, T. P., Devlin, G. L., Skepper, J. N., Ecroyd, H., Carver, J. A., Welland, M. E., Christodoulou, J., Dobson, C. M., & Meehan, S. (2010). The interaction of alphaB-crystallin with mature alpha-synuclein amyloid fibrils inhibits their elongation. *Biophys J*, 98(5), 843-851. <https://doi.org/10.1016/j.bpj.2009.10.056>
- Weedon, M. N., Hastings, R., Caswell, R., Xie, W., Paszkiewicz, K., Antoniadis, T., Williams, M., King, C., Greenhalgh, L., Newbury-Ecob, R., & Ellard, S. (2011). Exome sequencing identifies a

- DYNC1H1 mutation in a large pedigree with dominant axonal Charcot-Marie-Tooth disease. *Am J Hum Genet*, 89(2), 308-312. <https://doi.org/10.1016/j.ajhg.2011.07.002>
- Wegele, H., Müller, L., & Buchner, J. (2004). Hsp70 and Hsp90--a relay team for protein folding. *Rev Physiol Biochem Pharmacol*, 151, 1-44. <https://doi.org/10.1007/s10254-003-0021-1>
- Weihl, C. C., Temiz, P., Miller, S. E., Watts, G., Smith, C., Forman, M., Hanson, P. I., Kimonis, V., & Pestronk, A. (2008). TDP-43 accumulation in inclusion body myopathy muscle suggests a common pathogenic mechanism with frontotemporal dementia. *J Neurol Neurosurg Psychiatry*, 79(10), 1186-1189. <https://doi.org/10.1136/jnnp.2007.131334>
- Wettstein, G., Bellaye, P. S., Micheau, O., & Bonniaud, P. (2012). Small heat shock proteins and the cytoskeleton: an essential interplay for cell integrity? *Int J Biochem Cell Biol*, 44(10), 1680-1686. <https://doi.org/10.1016/j.biocel.2012.05.024>
- Whiten, D. R., San Gil, R., McAlary, L., Yerbury, J. J., Ecroyd, H., & Wilson, M. R. (2016). Rapid flow cytometric measurement of protein inclusions and nuclear trafficking. *Sci Rep*, 6, 31138. <https://doi.org/10.1038/srep31138>
- Wickner, S., Maurizi, M. R., & Gottesman, S. (1999). Posttranslational quality control: folding, refolding, and degrading proteins. *Science*, 286(5446), 1888-1893. <https://doi.org/10.1126/science.286.5446.1888>
- Wigley, W. C., Fabunmi, R. P., Lee, M. G., Marino, C. R., Muallem, S., DeMartino, G. N., & Thomas, P. J. (1999). Dynamic association of proteasomal machinery with the centrosome. *J Cell Biol*, 145(3), 481-490. <https://doi.org/10.1083/jcb.145.3.481>
- Wilhelmus, M. M., Boelens, W. C., Otte-Höller, I., Kamps, B., Kusters, B., Maat-Schieman, M. L., de Waal, R. M., & Verbeek, M. M. (2006). Small heat shock protein HspB8: its distribution in Alzheimer's disease brains and its inhibition of amyloid-beta protein aggregation and cerebrovascular amyloid-beta toxicity. *Acta Neuropathol*, 111(2), 139-149. <https://doi.org/10.1007/s00401-005-0030-z>
- Wu, T., Mu, Y., Bogomolovas, J., Fang, X., Veevers, J., Nowak, R. B., Pappas, C. T., Gregorio, C. C., Evans, S. M., Fowler, V. M., & Chen, J. (2017). HSPB7 is indispensable for heart development by modulating actin filament assembly. *Proc Natl Acad Sci U S A*, 114(45), 11956-11961. <https://doi.org/10.1073/pnas.1713763114>
- Wu, X., Dong, H., Ye, X., Zhong, L., Cao, T., Xu, Q., Wang, J., Zhang, Y., Xu, J., Wang, W., Wei, Q., Liu, Y., Wang, S., Shao, Y., & Xing, H. (2018). HIV-1 Tat increases BAG3 via NF-κB signaling to induce autophagy during HIV-associated neurocognitive disorder. *Cell Cycle*, 17(13), 1614-1623. <https://doi.org/10.1080/15384101.2018.1480219>
- Xu, Z., Graham, K., Foote, M., Liang, F., Rizkallah, R., Hurt, M., Wang, Y., Wu, Y., & Zhou, Y. (2013). 14-3-3 protein targets misfolded chaperone-associated proteins to aggresomes. *J Cell Sci*, 126(Pt 18), 4173-4186. <https://doi.org/10.1242/jcs.126102>
- Xu, Z., Page, R. C., Gomes, M. M., Kohli, E., Nix, J. C., Herr, A. B., Patterson, C., & Misra, S. (2008). Structural basis of nucleotide exchange and client binding by the Hsp70 cochaperone Bag2. *Nat Struct Mol Biol*, 15(12), 1309-1317. <https://doi.org/10.1038/nsmb.1518>
- Xun, W., Shi, L., Cao, T., Zhao, C., Yu, P., Wang, D., Hou, G., & Zhou, H. (2015). Dual functions in response to heat stress and spermatogenesis: characterization of expression profile of small heat shock proteins 9 and 10 in goat testis. *Biomed Res Int*, 2015, 686239. <https://doi.org/10.1155/2015/686239>
- Yang, K., Meinhardt, A., Zhang, B., Grzmil, P., Adham, I. M., & Hoyer-Fender, S. (2012). The small heat shock protein ODF1/HSPB10 is essential for tight linkage of sperm head to tail and male fertility in mice. *Mol Cell Biol*, 32(1), 216-225. <https://doi.org/10.1128/MCB.06158-11>
- Yang, X., Chernenko, G., Hao, Y., Ding, Z., Pater, M. M., Pater, A., & Tang, S. C. (1998). Human BAG-1/RAP46 protein is generated as four isoforms by alternative translation initiation and overexpressed in cancer cells. *Oncogene*, 17(8), 981-989. <https://doi.org/10.1038/sj.onc.1202032>

- Yang, X. D., Cen, Z. D., Cheng, H. P., Shi, K., Bai, J., Xie, F., Wu, H. W., Li, B. B., & Luo, W. (2017). L-3-n-Butylphthalide Protects HSPB8 K141N Mutation-Induced Oxidative Stress by Modulating the Mitochondrial Apoptotic and Nrf2 Pathways. *Front Neurosci*, *11*, 402. <https://doi.org/10.3389/fnins.2017.00402>
- Yang, Z., Wang, Y., Lu, Y., & Zhao, X. (2011). Molecular characterization of rat cvHsp/HspB7 in vitro and its dynamic molecular architecture. *Mol Med Rep*, *4*(1), 105-111. <https://doi.org/10.3892/mmr.2010.382>
- Yerbury, J. J., Gower, D., Vanags, L., Roberts, K., Lee, J. A., & Ecroyd, H. (2013). The small heat shock proteins α B-crystallin and Hsp27 suppress SOD1 aggregation in vitro. *Cell Stress Chaperones*, *18*(2), 251-257. <https://doi.org/10.1007/s12192-012-0371-1>
- Yew, E. H., Cheung, N. S., Choy, M. S., Qi, R. Z., Lee, A. Y., Peng, Z. F., Melendez, A. J., Manikandan, J., Koay, E. S., Chiu, L. L., Ng, W. L., Whiteman, M., Kandiah, J., & Halliwell, B. (2005). Proteasome inhibition by lactacystin in primary neuronal cells induces both potentially neuroprotective and pro-apoptotic transcriptional responses: a microarray analysis. *J Neurochem*, *94*(4), 943-956. <https://doi.org/10.1111/j.1471-4159.2005.03220.x>
- Yu, L., Liang, Q., Zhang, W., Liao, M., Wen, M., Zhan, B., Bao, H., & Cheng, X. (2019). HSP22 suppresses diabetes-induced endothelial injury by inhibiting mitochondrial reactive oxygen species formation. *Redox Biol*, *21*, 101095. <https://doi.org/10.1016/j.redox.2018.101095>
- Zeng, L., Tan, J., Hu, Z., Lu, W., & Yang, B. (2010). Hsp20 protects neuroblastoma cells from ischemia/reperfusion injury by inhibition of apoptosis via a mechanism that involves the mitochondrial pathways. *Curr Neurovasc Res*, *7*(4), 281-287. <https://doi.org/10.2174/156720210793180783>
- Zhai, J., Lin, H., Julien, J. P., & Schlaepfer, W. W. (2007). Disruption of neurofilament network with aggregation of light neurofilament protein: a common pathway leading to motor neuron degeneration due to Charcot-Marie-Tooth disease-linked mutations in NFL and HSPB1. *Hum Mol Genet*, *16*(24), 3103-3116. <https://doi.org/10.1093/hmg/ddm272>
- Zhang, H., Rajasekaran, N. S., Orosz, A., Xiao, X., Rechsteiner, M., & Benjamin, I. J. (2010). Selective degradation of aggregate-prone CryAB mutants by HSPB1 is mediated by ubiquitin-proteasome pathways. *J Mol Cell Cardiol*, *49*(6), 918-930. <https://doi.org/10.1016/j.yjmcc.2010.09.004>
- Zhang, Y. J., Xu, Y. F., Dickey, C. A., Buratti, E., Baralle, F., Bailey, R., Pickering-Brown, S., Dickson, D., & Petrucelli, L. (2007). Progranulin mediates caspase-dependent cleavage of TAR DNA binding protein-43. *J Neurosci*, *27*(39), 10530-10534. <https://doi.org/10.1523/JNEUROSCI.3421-07.2007>
- Zheng, Q., Huang, T., Zhang, L., Zhou, Y., Luo, H., Xu, H., & Wang, X. (2016). Dysregulation of Ubiquitin-Proteasome System in Neurodegenerative Diseases. *Front Aging Neurosci*, *8*, 303. <https://doi.org/10.3389/fnagi.2016.00303>
- Zhuravleva, A., & Gierasch, L. M. (2015). Substrate-binding domain conformational dynamics mediate Hsp70 allostery. *Proc Natl Acad Sci U S A*, *112*(22), E2865-2873. <https://doi.org/10.1073/pnas.1506692112>